THE UNIVERSITY *of* EDINBURGH

Remote Community Drinking Water Supply

– Mechanisms of Uranium Retention and Adsorption by Ultrafiltration, Nanofiltration and Reverse Osmosis

Helfrid Maria Albertina Schulte-Herbrüggen

(nee Rossiter)

A thesis submitted for the degree of Doctor of Philosophy

The University of Edinburgh

School of Engineering

2011

Declaration

I declare that the thesis has been composed by myself and the work contained in it is my own, except where stated otherwise. Further, this work has not been submitted for any other degree or professional qualification except as specified.

Helfrid Schulte-Herbrüggen

Supervisors

Prof Andrea I Schäfer, the University of Edinburgh, School of Engineering, Edinburgh, United Kingdom

Dr Margaret C Graham, the University of Edinburgh, School of GeoSciences, Edinburgh, United Kingdom

Examiners

Prof Viatcheslav Freger, Israel Institute of Technology, The Wolfson Department of Chemical Engineering, Israel

Dr Helen Bridle, the University of Edinburgh, School of Engineering, Edinburgh, United Kingdom

Abstract

Worldwide, around 884 million people lack access to safe drinking water. To address this, groundwater sources such as boreholes and wells are often installed in remote locations especially in developing countries. However, the natural chemical composition of groundwater may be a source of toxicity to human health. Uranium is naturally present in the environment, and concentrations above the World Health Organisation (WHO) drinking water guideline (15 μg/L) are found in various parts of the world. Uranium has a complex aqueous chemistry and its speciation, which varies according to pH and available ligands, determines its behaviour (*e.g.* mobility, reactivity or sorption tendency). Nanofiltration and reverse osmosis have proved effective in removing uranium from water, although fundamental removal mechanisms are not well understood. Even the more porous ultrafiltration (UF) has been shown to remove uranium when used in combination with complexation/coagulation methods.

To address the water purification needs of remotely located communities with no or unreliable access to energy, a renewable energy powered membrane system was designed using UF as pre-treatment to remove particles, bacteria and viruses and NF/RO to remove ions. The system was trialled in the Australian outback, using natural groundwater high in uranium (>300 μg/L). Results showed that pH had a large effect on the uranium behaviour in the system and, curiously, interaction by sorption or precipitation to the membranes was observed at certain pH values. However, due to the complexity of the water and the combination of UF and NF/RO membranes, the mechanisms of the uranium retention and interaction with the membrane were not clear. Further systematic study was needed to investigate the uranium behaviour with the membranes.

Laboratory studies were carried out with one membrane type at a time: UF, NF and RO. It was postulated that pH, organic matter and inorganic ions such as calcium have an important influence on uranium retention and interaction with membranes.

Results show that uranium behaviour in the membrane systems was highly pH dependent. During the UF experiments, increased adsorption of uranium occurred in uranium-only solutions at pH 5-7. From the UF experiments with organic matter it could be concluded that organic matter did not increase retention (size exclusion) of uranium, however it did increase the adsorption. Humic acid increased adsorption to 80-95% at pH 3-5, alginic acid at pH 3 while tannic acid caused a nearly 100% adsorption at pH 10-11.

Further investigating uranium behaviour with NF and RO membranes, it was found that uranium showed the same increase in affinity to the membrane at pH 5-7, with about 50% being taken up by NF and 30% by RO membranes. The effect of pressure on uranium-membrane interaction was investigated for NF and RO at pH 6 and 8.5. Pressure and consequent concentration polarisation only increased uranium affinity to the NF membrane at pH 8.5 where the uranium species and MWCO of the membrane were similar. There was no or little effect of pressure on the affinity of uranium to the NF membrane at pH 6 or to the RO membrane.

At pH 6, STEM-EDX results showed that uranium was distributed through-out the polyamide active layer of the NF membrane while FTIR results confirmed that uranium bound to carboxyl groups in the polyamide. At pH 8.5 however, FTIR results showed that uranium did not form chemical bonds with the membrane, but was rather attracted to the surface through hydrogen bonding and loosely forming a layer on top of the membrane visible in SEM. It was concluded that at least three different characteristics of the uranium species and membranes played a role for the interaction: 1) uranium species valency and membrane charge, 2) uranium species size relative to the membrane pore size, and 3) the reactivity of the uranium species towards the membrane functional groups.

The effect of calcium on uranium retention and uranium-membrane interaction in NF and RO was also investigated. Calcium affects uranium speciation by forming a neutral complex with uranium at pH 8-9, causing a decrease in adsorption to the membrane. Calcium also precipitates at pH 10. SEM and TEM images showed that

the precipitation of calcium carbonate ($CaCO_3$) as calcite caused co-precipitation of uranium, trapping it on the surface of the membrane. About 48-55% of the calcium precipitated which caused a 26-35% co-precipitation of uranium, compared to <5% adsorption in the absence of calcium at pH 10.

Finally the chemical drinking water quality of mainly boreholes and wells across a West African country, Ghana, was investigated (199 samples in total from "improved" sources). In addition, the user water costs were documented and the scope for advanced treatment explored. The WHO guidelines for chemical water quality were exceeded in 38% of the samples. The main contaminants were nitrate (21%), managanese (11%) and fluoride (7%), while heavy metals such as lead, arsenic and uranium were localised to mining areas. It was concluded that when taking the cost of unsuccessful borehole development into account, alternative treatment may be a suitable option where inorganic contamination is high.

The findings from this study show the importance of the water quality conditions (pH, organic matter and calcium) on the behaviour of contaminants such as uranium in membrane systems and explain the mechanisms of adsorption and co-precipitation of uranium to the membranes at certain pH values. These are important considerations when selecting appropriate membranes for water treatment and also for the maintenance of membranes. The study also showed that there is need for advanced treatment of drinking water in *e.g.* Ghana, but highlights the importance of strategies on local and national level to ensure long-term sustainability and integration of any such treatment.

Acknowledgements

I have learnt many things during this project and I owe the opportunity to embark on this research experience to my first supervisor, Andrea Schäfer. The challenges have been various, from discovering that there are different types of stainless steel to wrestling with how to structure a paper. Under her supervision these were transformed into functioning systems and published results.

To my second supervisor, Margaret Graham, I am grateful for scientific discussions, her continued encouragement, unfailing support where needed and for taking the time and putting in the effort to make conscientious comments on my work.

My research scholarship was jointly provided by the Economic and Social Research Council (ESRC) and the Engineering and Physical Sciences Research Council (EPSRC). The Mondialogo Engineering Award (DaimlerChrysler/UNESCO) provided inspiration and funding for part of this research project. I am also grateful to the School of Engineering who funded vital equipment and assisted with the continuation fee. The Fund for Women Graduates (FFWG) kindly provided four months additional scholarship, and the University of Edinburgh discretionary fund is acknowledged for some financial assistance. The Royal Academy of Engineering is thanked for a travel grant allowing me to present my work at an international conference.

The membrane manufacturers GE Zenon, Koch Membrane Systems and the Filmtec Corporation (Dow) kindly provided the laboratory scale ultrafiltration membrane modules and nanofiltration and reverse osmosis membrane sheets used in this study. Peter Moss, Koch Membrane Systems also kindly answered questions regarding, amongst other things, the RoPro software.

A big thank you goes to my fellow membrane PhD students: Peta Neale, Laura Banasiak, Andrea Semião, Molly Patrick, Laura Richards, Annalisa De Munari, Ime Akanyeti, Helen Cope, Payam Malek and Than Hieu - for much of the time we learnt and tackled challenges together. I would especially like to thank Annalisa for reading

my manuscripts and providing zeta potential and contact angle measurements, Ime for AFM measurements and Laura for proof-reading the paper version of Chapter 8. Finally I wish to especially thank Andrea with whom I have gone through much of this PhD process together and with whom I did the work in Chapter 5. Andrea also spent a large part of her time re-designing the cross-flow system used in this research and did much of the TOC analysis. Thank you for all your help over the years, for discussing membrane theories (and checking my calculations!) but also for cheery painting sessions and sharing the journey!

I could not have done without the practical help from a number of people. I would like to thank Steve Gourlay for assisting with re-design and construction of the cross-flow system, Alan Simm for help with LabVIEW, Douglas Carmichael and David Archibald for help with electrical connections, Derek Jardine, Bobby Hogg, Bill Lesley and Bob Gusthard all helped with practical issues in the laboratory, especially as it was being set up at the start of this project. John Davey participated in setting up the UF system as part of his MSc project.

Numerous people offered helpful advice along the way, including Angus MacKenzie (SUERC), Gordon Cook (SUERC), John Brennan, John Farmer, Joanna Cloy, Bryne Ngwenya, Polly Arnold, Kathy Moore, José Torero, Martin Crapper, David Ingram and Asif Usmani (all at the University of Edinburgh), Alan Harper (Heriot Watt), Martin McCoustra (Heriot Watt), Menachem Elimelech (Yale University) and Alan MacDonald (British Geological Survey).

Lorna Eades is thanked for advice and assistance with the ICP-MS analysis of an abundance of samples over the years. Peter Anderson and Tanya Peshkur are thanked for assistance with IC analysis, analysis discussions and lending us bits and pieces for the lab when needed. Chris Jeffree is warmly thanked for sample preparation and excellent SEM and TEM analysis for Chapters 6 and 7. Mari Kallioinen (Lappeenranta University of Technology) provided the FTIR analysis, Perrine Chaurand (CEREGE) the m-XRF analysis and Mike Fay (University of Nottingham) STEM-EDX analysis for Chapter 6, while David Scurr (University of Nottingham)

did the ToF-SIMS analysis for Chapter 7. Henri Wong (ANSTO) is thanked for ICP and IC analysis of the samples collected for Chapter 4. Andrea Schäfer, Bryce Richards and accompanying students are thanked for collecting the field trial data which provided the basis for Chapter 4. They, as well as Peter Antwi Owusu and Esi Awuah (Kwame Nkrumah University of Science and Technology) are also thanked for the field samples collected for Chapter 8.

I was especially helped by Ceci (Xiaolu Xu), who, when it was impossible for me to go into the labortatory to perform some additional experiments, gladly and expertly carried out the precipitation experiments needed for Chapter 6. Thank you!

I especially wish to thank my friends and family for their friendship, love and support over the years, and for providing a welcome break from the PhD sphere. My parents, Gordon and Britt-Marie are especially thanked for their continued encouragement. Barbara is thanked for being there over the phone, email and in person when occasion allowed –thank you for entrusting me to become your daughters God mother! Thank you to friends at church for your prayers and for providing a space in where to step back and re-focus. A special thank you to Emily, Monica, Rosie, Katie, Bethan, Nanette and Hamish. Rachel and Matt, Jake and Gabi provided us with a roof over our heads when we needed it and Gabi has been a lovely "first motherhood mentor".

Importantlu, Björn, now my husband, has been my companion over the last 10+ years and I could not have gone through this PhD without his steadfast and wholehearted support. He even contributed directly to this research by providing some samples and the map for the paper-version of Chapter 8. Thank you for your intellectual, practical, emotional, loving and, in the last year, financial, support!

With a delivery date around the same time period as this thesis, and having attended my viva at a very tender age, Tristan Erik deserves a special mention; what an amazing wee boy, full of curiosity and enthusiasm for his new world and who can't help but brightening up ours with his sunny smiles!

Publications related to this PhD research

Accepted

Rossiter HMA, Owusu PA, Awuah E, Macdonald AM, Schäfer AI. Chemical drinking water quality in Ghana: water costs and scope for advanced treatment. Science of the Total Environment 2010; 408: 2378-86.

Rossiter HMA, Graham MC, Schäfer AI. Impact of speciation on behaviour of uranium in a solar powered membrane system for treatment of brackish groundwater. Separation and Purification Technology 2010; 71: 89-96.

Semião AJC, **Rossiter HMA**, Schäfer AI. Impact of organic matter and speciation on the behaviour of uranium in submerged ultrafiltration. Journal of Membrane Science 2010; 348: 174-180.

Schäfer AI, **Rossiter HMA**, Owusu PA, Richards BS, Awuah E. Physico-chemical water quality in Ghana: Prospects for water supply technology implementation. Desalination 2009; 248: 193-203.

Richards LA, Richards BS, **Rossiter HMA**, Schäfer AI. Impact of speciation on fluoride, arsenic and magnesium retention by nanofiltration/reverse osmosis in remote Australian communities. Desalination 2009; 248: 177-183.

Conference proceeding

Rossiter HMA, Semião AJC, Graham MC, Schäfer AI. Importance of pH and organic matter on removal and adsorption of uranium in membrane systems presented at The 13th Nordic Filtration Symposium 2010, Lappeenranta University of Technology, Finland

In preparation

Schulte-Herbrüggen HMA, Graham MC, Jeffree C, Kallioinen M, Chaurand P, Jeffree C Schäfer AI. Importance of charge, size and reactivity for uranium adsorption to NF/RO membranes. In preparation for Journal of Physical Chemistry B

Schulte-Herbrüggen HMA, Graham MC, Jeffree C, Kallioinen M, Schäfer AI. Effect of calcium on uranium adsorption to and precipitation to NF/RO membranes.

Table 1. Contribution to publications by author (Rossiter/Schulte-Herbrüggen)

Publication	Role	Contribution by author
1. Rossiter et al., 2010, STOTEN	Leading	Co-developed initial idea, set-up collaboration with Ghanaian team, secured Mondialogo funding (samples were collected by Schäfer et al), carried out all chemical analysis on water samples, processed and presented data, carried out literature review and analysed findings accordingly. Lead author on paper.
2. Rossiter et al., 2010, SPT	Major	Chemical analysis of remaining samples, analysis and interpretation of raw data, literature review, processing of data and analysis in speciation prediction and membrane soft-ware. Lead author on paper.
3. Semião et al., 2010, JMS	Co-leading	Experimental development, execution of experiments and chemical analysis and interpretation of results was shared with Semião who did paper outline while paper content and literature review were shared equally between Rossiter and Semião.
4. Schäfer et al., 2009 Desalination	Leading	As for (1), except Schäfer wrote the paper outline while Rossiter processed the data, produced the graphs, interpreted results and wrote the paper content.
5. Richards et al., 2009, Desalination	Minor	Provided Minteq in-put data of chemical water quality and helped with speciation analysis and interpretation of results.
6. Rossiter et al., 2010, NFS	Leading	Some results from experiments by Rossiter and Semião were used. New experiments were planned, executed, chemically analysed and interpreted by Rossiter. Lead author and presenter at the conference.
7. Schulte-Herbrüggen in prep JoPC	Leading	Development of idea, experimental design, execution of experiments, main chemical analysis (specialised analysis as acknowedged in chapters and acknowledgements), interpretation of results and literature review. Contributed to cross-flow system design and problem solving.
8. Schulte-Herbrüggen in prep	Leading	As for (7).

Table of contents

List of Figures

List of Tables

1 Introduction

1.1 Drinking water quality in developing countries

Clean, safe drinking water is often taken for granted in developed countries. Water of excellent quality is even used to flush toilets and wash cars, but the situation is very different for poorer developing nations. Out of the 880 million people in the world lacking access to a safe drinking water supply the vast majority live in developing countries. Sub-Saharan Africa is the region with most people lacking access to an improved drinking water source, leaving 40% of the inhabitants without safe water; approximately 53% of these live in rural areas (JMP, 2010) (Figure 1).

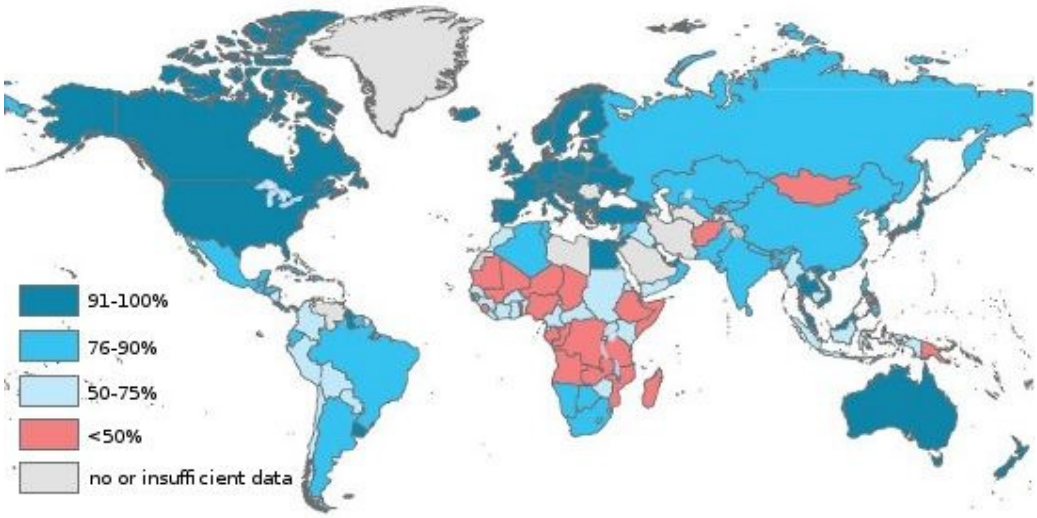

Figure 1. Map showing world-wide use of improved drinking water sources in rural areas (from JMP 2010).

The United Nations Millennium Development Goals (MDGs) were agreed in order to set targets to improve living standards for the world's poorest people. One important target was to reduce by half the proportion of people without access to safe drinking water (*i.e.* protected from faecal contamination by being supplied from an "improved source" (JMP, 2010) and basic sanitation. Access to safe water is also instrumental in achieving a number of other millennium goals, such as MDG 2 "to achieve universal primary education", MDG 3 "to reduce child mortality" and MDG 5 "to improve

maternal health" (Table 15, Appendix). Access to safe pathogen-free water is vital to achieving these goals. For instance, for MDG 2, an important factor in poor school attendance by girls is the need to collect and carry water over long distances (JMP, 2008). A major cause of ill-health among children and women are related to poor sanitation and hygiene and diseases that are water-borne (*e.g.* typhoid and C*ryptosporidium*) or water-related (*e.g.* malaria and schistosomiasis).

Predictions of the achievability of the target for safe drinking water by 2015 are positive for many regions, except sub-Saharan Africa and Oceania. However, it should be pointed out that even if the MDG target for access to safe drinking water is met, it will still leave at least 672 million people without access to an improved water supply (Hunter et al., 2011).

The Joint Monitoring Programme (JMP) categories for what is considered an improved water source are given in Table 2, where piped water is considered to give the greatest health gains and the greatest protection from microbial contamination (JMP, 2010).

Table 2. JMP categories of improved drinking water sources (JMP, 2010)

Unimproved	Other improved	Improved: Piped water
Unprotected well, unprotected spring, cart, tanker, surface water and bottled water	Public taps, tube wells, boreholes, protected dug wells, protected springs and rainwater collection	Piped household water located inside users dwelling, plot or yard.

Due to the relatively low cost, groundwater is often utilised by installing either a well or borehole as a means to provide safe drinking water. In Sub-Saharan Africa, improved access to safe water is mainly through "other improved sources" rather than piped water (JMP, 2010). Wells are generally cheaper than boreholes since they can be manually constructed, while borehole construction requires more advanced drilling equipment (MacDonald et al., 2005). The water quality of hand-dug wells will, however, vary according to nearby sources of pollution (*e.g.* human or animal faeces) and depend on the quality of well construction (MacDonald and Calow, 2009). Since boreholes are deeper than wells, the quality of water from boreholes is

usually good, *i.e.* low likelihood of faecal and microbial contamination; the water may, however, contain high concentrations of inorganic contamination. The inorganic constituents of groundwater depend on the geology from which it springs, as a wide variety of inorganic elements may be leached from surrounding rocks (Plant et al., 2001). The chemical water quality is often paid less attention than microbial water quality (Hunter et al., 2011), possibly due to the less acute effect of chemical contamination and the costs involved in monitoring. Consumption of water with high concentrations of inorganic compounds can, however, have long-lasting and seriously crippling health effects, and the JMP (2010) states that both microbial and chemical quality should be addressed for the next targets, although a cost-effective method would be urgently needed to accomplish this. Probably the most well-known inorganic contaminant is arsenic which tragically caused the chronic poisoning of millions of people in Bangladesh as tube wells were installed to provide safe drinking water (Nordstrom, 2002; Smedley and Kinniburgh, 2002; Bissen and Frimmel, 2003a; Mead, 2005; Ahmed et al., 2006). Arsenic is carcinogenic and affects a number of internal organs such as the liver, bladder and lungs as was well as the skin. Other inorganic elements which commonly cause health problems when present in high concentrations include fluoride, lead, copper and nitrate (World Health Organisation, 2006; Hunter et al., 2011).

Treatment of contaminated water could provide a possible solution to the high levels of inorganic pollution; however the challenge to find appropriate water treatment for developing countries cannot be understated. Not only does the treatment need to effectively remove the relevant contaminant, but just as importantly, it also needs to fulfil economic and social criteria to ensure effective and long-term sustainability. With monetary implications and ease of operation in mind, low-cost low-technological water treatment approaches are often promoted, such as slow sand filtration, aeration, settling, UV-radiation (*e.g.* allowing the sun treat water in PE bottles) and chlorination (Sobsey et al., 2008). Many of these techniques are, however, geared towards the removal of microbial contaminants. One exception is sand filtration which has been shown to remove arsenic (Johnston and Heijnen, 2001), although iron-amended sand filters proved to be in-effective (Chiew et al.,

2009) and further evaluation is needed to establish the effectiveness under different environmental conditions.

There is a rich abundance of studies which have investigated arsenic removal from drinking water (Bissen and Frimmel, 2003b; Malik et al., 2009). Adsorption of especially arsenic but also lead, mercury and zinc to a range of materials such as activated alumina, iron and manganese compounds, zeolites and clays has been investigated by *e.g.* (Celis et al., 2000; Elizalde-Gonzalez et al., 2001; Johnston and Heijnen, 2001; Chakravarty et al., 2002; Buamah et al., 2008). In general, it was found that removal could be very efficient under certain conditions, but factors such as speciation and competition from other ions could decrease adsorption, stressing the need for further understanding of the processes involved. Alternatively, there have been reports suggesting that aquatic plants can be used to remove heavy metals from contaminated waters (Keskinkan et al., 2004; Kara, 2005). In all cases, the challenge is to find a technology which reliably removes inorganic pollutants over a wide range of water conditions (pH, turbidity, competition from other inorganic ions). Removal of inorganic contaminants is often highly influenced by changes in water conditions and by the chemical form and oxidation state (*i.e.* speciation) in which the contaminant is present (Chiew et al., 2009). Thus the optimum removal process is likely to be highly contaminant-specific.

Another water treatment option currently being considered is membrane filtration, which can remove microbial and inorganic contaminants simultaneously. For example Brandhuber and Amy (2001) used negatively charged ultrafiltration membranes and achieved arsenic rejection of 88%. The rejection was highly influenced by operating conditions and water quality. The presence of other inorganic ions decreased the rejection while organic matter increased it. Influencing factors like these make laboratory and also field testing of membranes important in order to determine contaminant removal performance. Several other studies have investigated arsenic removal using nanofiltration (NF) *e.g.* (Van der Bruggen and Vandecasteele, 2003; Ahmed et al., 2010). Oh et al. (2000) even investigated arsenic removal using NF powered with a bike pump. Again they found that removal was

highly speciation-dependent; i.e. dependent on water pH and oxidation state of the arsenic. In this case, higher retention was achieved at pH 8 for oxidised waters as arsenic was present as the neutral As(III) species, H_3AsO_4, rather than the negative As(V) species, $HAsO_4^{2-}$.

In contrast with arsenic, elements such as uranium are generally not part of standard water quality tests after, for example, borehole installation and appropriate treatment options for uranium removal in developing countries have not been extensively investigated. This is because the concentration of uranium in most groundwaters falls below the World Health Organisation (WHO) drinking water guideline of 15 µg/L (World Health Organisation, 2006). However, depending on geological environment, some groundwaters do have concentrations approaching or exceeding this limit. For example, high concentrations of uranium have been documented from groundwaters in both Africa and Asia. These are a result of both natural processes and of mining activities in these areas (Reimann et al., 2003; Winde and van der Walt, 2004; Vasiliev et al., 2005; Kumar et al., 2006; Vandenhove et al., 2006; Granit et al., 2010). Not only are areas in developing countries affected; high uranium concentrations are also found in water in developed countries. In particular, rural areas without access to national water supplies and who source their drinking water from private wells are often affected. In the USA alone, it is estimated that 620,000 residents are exposed to elevated levels of uranium in drinking water (US EPA), while private groundwater supplies in *e.g.* Scandinavia can be subject to high uranium concentrations (> 600 µg/L), depending on the underlying geology and hydrochemistry (Åström et al., 2009).

1.2 Motivation

The motivation for this PhD research was the compelling need to find a solution to providing safe drinking provision in terms of chemical drinking water quality in often remote locations in both developing and developed countries. Membrane filtration was chosen as treatment option due to its effective removal of a wide range of both microbial and inorganic contaminants and due to its increasingly world-wide

use (Van der Bruggen and Vandecasteele, 2003; Tal, 2006). A mobile UF-NF/RO system powered by renewable energy has been developed by Schäfer et al. (2007) for use in remote locations. The analysis of inorganic ion retention results from a field test of this system provided the initial starting point for this study. Uranium was selected as the inorganic contaminant of focus, since, despite its ubiquitous presence and toxicity when present in high concentrations, it is often ignored both in water quality monitoring and treatment considerations, especially in developing countries. The behaviour of uranium varies greatly with speciation, which in turn is influenced by a range of parameters such as available ligands, pH of the water, redox conditions etc (this will be discussed more in-depth in the next chapter). It was quickly realised at the start of this research project that the speciation of uranium also influences the interactions between uranium and the membrane, and moreover, that under certain conditions, uranium was not only retained by the membrane but taken up by the membrane itself. Such uranium-membrane interactions have not been characterised in past studies, and therefore provided a starting point for this research project.

1.3 Aims

There were two overall aims to this research:

1) To investigate the influence of uranium speciation (specifically the variation in pH, presence of other inorganic ions and organic matter) on uranium removal by UF and NF/RO membranes. The aim will be achieved by investigating the effect of:

- pH on uranium removal by and interaction with a UF-NF/RO membrane system (field study results)
- pH and organic matter on uranium removal by and interaction with UF membranes during filtration in a controlled laboratory study
- pH and pressure on uranoim-membrane interaction and uranium removal by a NF and RO membrane in a controlled laboratory study
- calcium on uranium-membrane interaction with and retention by NF and RO in a controlled laboratory study.

2) To investigate the potential for implementation of membrane systems to treat drinking water in remote communities in developing countries. This aim will be achieved by:

- investigating current chemical drinking water problems and drinking water costs in a selected developing country.

An overview of the thesis structure is given in Figure 2. Chapter 2 is a survey of uranium chemistry and distribution, as well as an introduction to UF, NF and RO membrane filtration. Chapter 3 (Materials and Methods) describes the membrane systems used for the laboratory studies as well as the chemical analysis techniques routinely used through-out this study. Materials and analytical techniques specific to an individual chapter are described in the relevant chapter. Chapter 4 gives the starting point for this research project: the analysis of the results from a field study conducted using a mobile UF-NF/RO system powered by renewable energy. UF filtration of aqueous solutions containing uranium with and without different types of organic matter is then investigated in controlled laboratory studies (Chapter 5), while uranium-membrane interaction across the pH range 3-10 with NF and RO membranes is investigated in Chapter 6, both with and without filtration. Chapter 7 investigates the effect of calcium on the uranium-membrane interaction and retention by NF and RO across the pH range 3-10. Finally the research has been concluded by selecting one developing country of interest, Ghana, to investigate the potential for implementation of membrane systems as a drinking water treatment option. This has been done by assessing the current chemical water quality as well as current water pricing (Chapter 8). The main conclusions following this research will be summarised in Chapter 9 along with suggestions for further research.

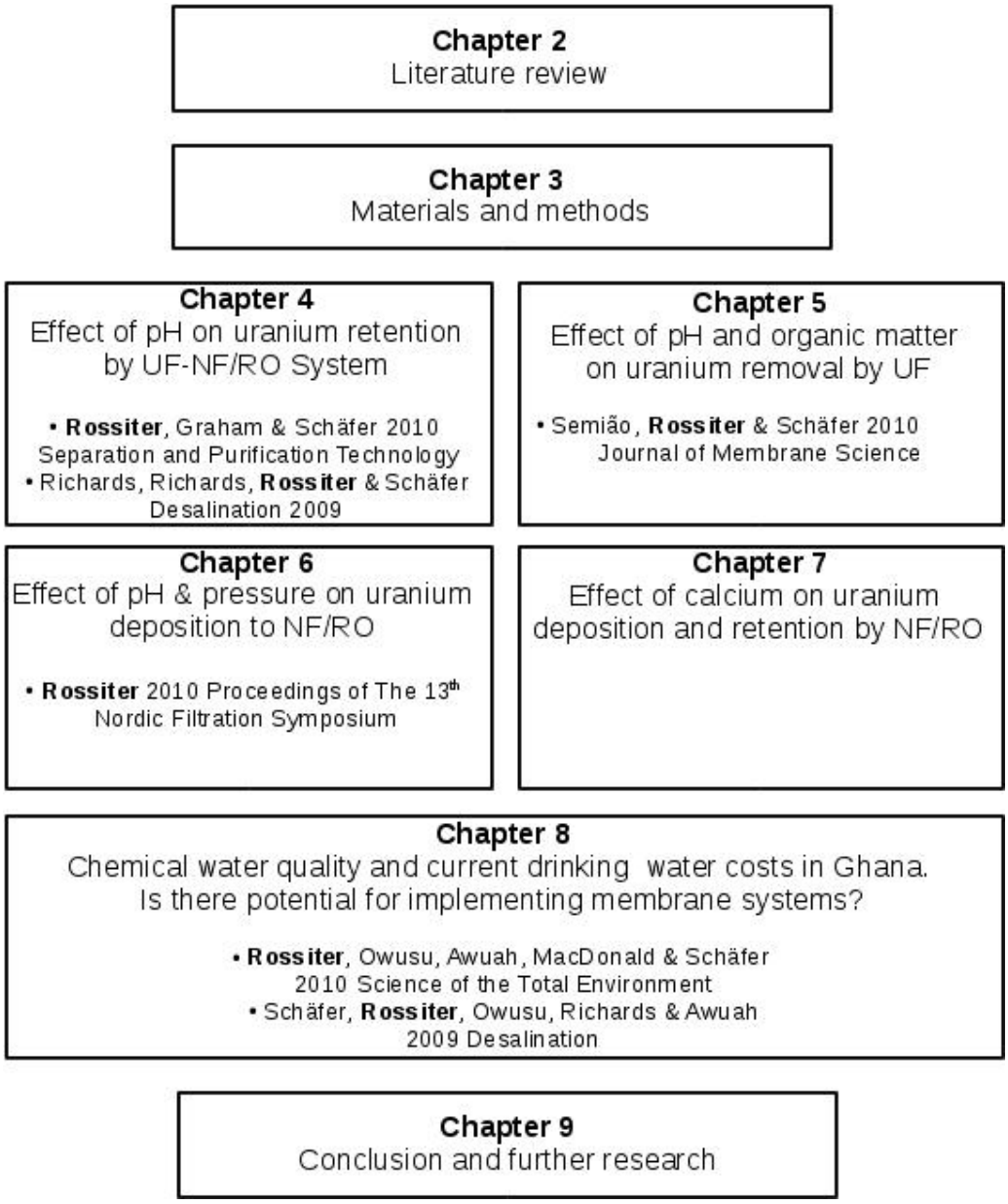

Figure 2. Overview of thesis structure including the publications to which the research presented in each chapter has contributed.

2 Literature review

2.1 The geographical distribution of uranium, its properties and environmental geochemical behaviour

2.1.1 Introduction

Uranium is the heaviest naturally occurring element. It has three main isotopes: ^{238}U, ^{234}U and ^{235}U, out of which ^{238}U is the most common (~99.27%). It is radioactive, the heat emitted during its decay, along with the other radionuclides that are part of the natural decay series, is a likely source of heat in the Earth's mantle (Butcher et al., 1992). ^{238}U emits α-particles and slowly decays with a half-life of 4.6×10^9 years. As well as being naturally radioactive, uranium is above all chemically toxic and may replace calcium in bones and cause kidney damage or even failure when ingested in high concentrations (Miller et al., 2004; 2005). Levels of uranium of 1 mg/kg of kidney have found to cause kidney dysfunction (The Royal Society, 2002) and the LD50[a] of injected uranium is 1 mg/kg body weight (compared with, *e.g.* 6 mg/kg for arsenic) (Alloway and Ayres, 1993). Health effects related to the mainly military use of depleted uranium, a by-product of nuclear fuel production, have also been conducted. Kidney, liver, heart and brain are all organs at risk to be impacted following exposure, although more conclusive studies are needed (Craft et al., 2004). The effects of chronic uranium exposure are also less well established than acute exposure (Kurttio et al., 2006; Vicente-Vicente et al., 2010); however, nephrotoxicity has been found in association with chronic exposure to high levels of uranium in well water (Kurttio et al., 2002), and Kurttio et al. (2005) also suggests uranium replaces calcium in bones. There are also studies suggesting that uranium may affect reproductive health (Raymond-Whish et al., 2007). The WHO provisional drinking water guideline is set to 15 µg/L, based on the tolerable daily uranium intake (World Health Organisation, 2006).

[a]LD50 is a toxicity measure and is the dose that is lethal to 50% of a population of test animals (Baird, 1999).

Uranium is present naturally in the Earth's crust at an average concentration of 2.7 µg/g and in sea water at a concentration of about 3.3 µg/L while higher levels of up to 15 µg/g and 120 µg/g may occur in granite and phosphate rocks, respectively (Langmuir, 1997). Consequently, uranium can also be released into groundwater through weathering of these materials, and so concentrations will vary depending on local geology and water source (Langmuir, 1997; Plant et al., 2001). Anthropogenic activities can also cause increased uranium mobilisation, consequently raising the concentrations found in groundwater (Langmuir, 1997; Myasoedov and Novikov, 1998; Oliver et al., 2008). Outlined in the following sections, is an overview of the processes involved.

2.1.2 Geological occurrence of uranium

Uranium is ubiquitous in the environment and uranium concentrations found in rocks are typically about 1-4 mg/kg, but higher concentrations are found in *e.g.* granite rocks (*e.g.* up to 54 mg/kg in Sweden, up to 20 mg/kg in England), clays, shales, phosphate-rich and iron-rich rocks (Smedley et al., 2006). Organic matter-containing rocks (black shales) have even higher documented uranium concentrations (up to 100-200 mg/kg) (Åstrom 2009).

The vast majority of known uranium deposits occur in Precambrian or Phanerozoic rocks overlying Precambrian basement (Bowie, 1979). Generally, uranium deposits can be classified as vein-type, sandstone, conglomerates and others (*e.g.* lignites, shales, phosphate rocks and calcrete). In areas such as Scandinavia and Australia, vein-type deposits were formed during granite formation while more recent deposits are found in the alpine regions (Bowie, 1979). The more common uranium ores are uraninite (UO_2(c)), pitchblend (UO_2(am)), coffinite ($USiO_4$) and autunite ($Ca(UO_2)_2(PO_4)_2(H_2O)_{11}$) (Langmuir, 1997; Smedley et al., 2006). Uranium containing minerals often occur along fractures, therefore leading to a highly heterogeneous distribution (Smedley et al., 2006). Many of the uranium deposits formed are caused by weathering or erosion such as "roll fronts", where soluble

uranium in the +VI oxidation state is leached and transported by alkaline, oxygenated water, encounters reducing conditions and thereby precipitates as *e.g.* uranitite (Langmuir, 1997). Such roll-fronts can result in economically viable deposits for uranium mining (Smedley et al., 2006). Uranium is often closely associated with iron oxides (*e.g.* goethite, haematite, ferrihydrite and magnetite), phosphates (uranium is part of phosphate-containing minerals like autenite and hydroxapetite), clays and organic matter which can cause its precipitation (Bowie, 1979; Duff et al., 2002; Payne and Airey, 2006; Smedley et al., 2006). Uranium may also be found in association with gold, pyrite, different types of sulphides, chlorites and a range of other metals (such as vanadium, copper, lead and zinc) (Bowie, 1979); extraction of the ores of these other metals may lead to the release of uranium as a by-product.

2.1.3 Aqueous geochemistry of uranium

For certain geologies, uranium concentrations in water are correlated with those found in the underlying rocks. For others, however, uranium dissolution and mobility in water is mainly controlled by hydrochemistry, *e.g.* dissolved calcium and HCO_3^- concentrations, rather than geochemistry *e.g.* uranium abundance in rock type (Åström et al., 2009). The oxidation state often determines an element's chemical behaviour in terms of environmental mobility and bio-availability. Uranium has several oxidation states: +III to +VI, of which +IV (uranous) and +VI (uranyl) are the most common in the natural environment. Under reducing conditions, uranium is present in its +IV oxidation state and is often immobile, while in oxic and acidic conditions it is present as UO_2^{2+} in its +VI oxidation state and is usually highly mobile. A range of U(VI) complexes are formed under neutral and increasingly alkaline conditions (Langmuir, 1997).

In the absence of other ligands, hydrolysis is the main pH-dependent process affecting uranium speciation. Hydrolysis of the uranyl ion starts at pH just greater than 3 and various hydrolysis products are then formed as the pH increases. Figure 3 shows a typical speciation diagram representing the hydrolysis of U(VI) in the absence of any other competing ligands (US EPA, 1999). In waters with uranium

concentrations of up to 10^{-6} M, UO_2OH^+ tends to dominate at pH 5-6, while at higher concentrations (10^{-4} M or 1000 µg/L) polynuclear species start to form (Smedley et al., 2006; Choppin, 2007).

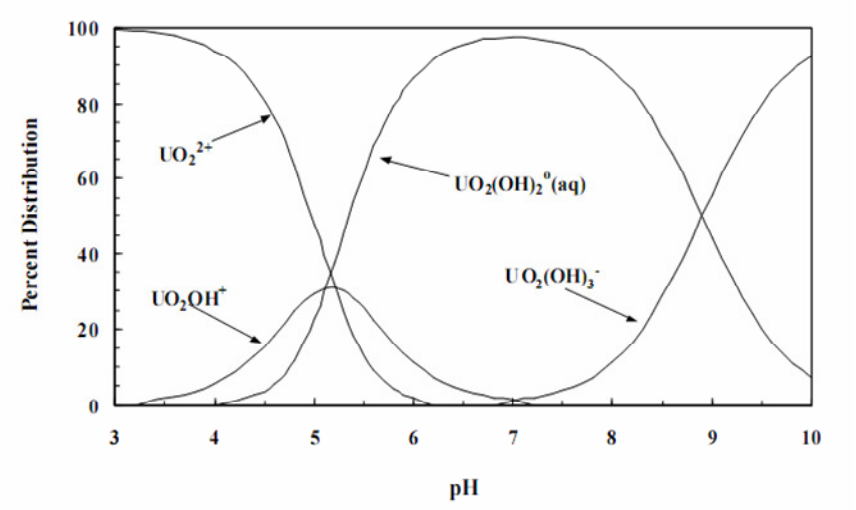

Figure 3. Example of uranium speciation from US EPA (1999) report as a function of pH in absence of any complexing ligands other than OH from water and a uranium concentration of 0.1 µg/L.

Uranium (VI) forms complexes with a wide range of ligands; the most common are carbonate, carboxylate, dissolved organic matter, phosphate, sulphate and calcium ions. Uranium behaves as a hard acid and therefore forms stronger complexes with oxygen-containing ligands compared with sulphur or nitrogen-containing ligands (Shriver and Atkins, 1999). Most natural waters contain dissolved inorganic carbon species as a consequence of CO_2 dissolution from the atmosphere and/or from carbonate minerals. A portion of the dissolved inorganic carbon will be in the form of carbonate ions and these ligands tend to out-compete hydroxide and other ligands with respect to uranium complexation under alkaline aqueous conditions at atmospheric pressure (Langmuir, 1997). Figure 4 shows how carbonate complexation of uranium impacts on the stability fields for the hydrolysis products (Raff and Wilken, 1999). Even dissolved inorganic carbon concentrations of down to ~0.1 mM will significantly influence the uranium chemistry (Konstantinou and Pashalidis, 2004) and carbonate complexes will dominate the speciation above pH 5. Below this pH, the aquated uranyl ion remains dominant (Figure 4).

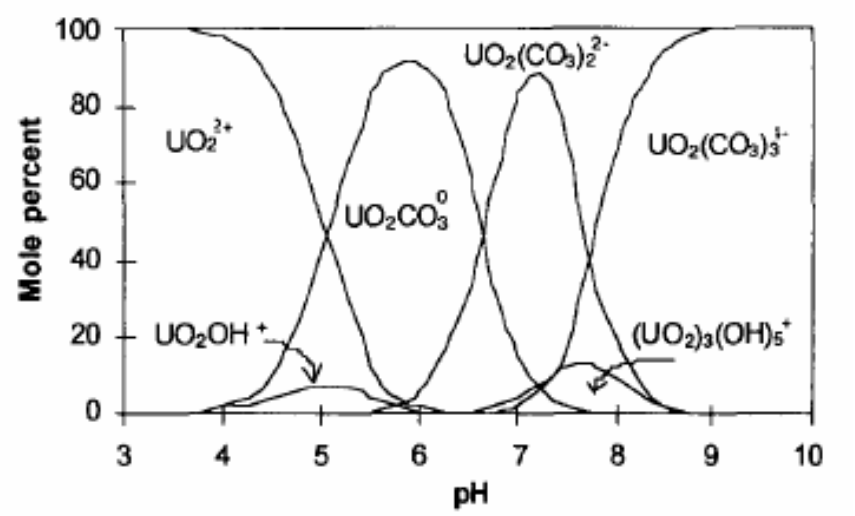

Figure 4. Example of uranium speciation diagram in presence of dissolved organic carbon (from Raff et al. 1999)

In the presence of sulphate, uranyl sulphate species dominate the speciation at acidic pH, up until about pH 5 (Bernhard et al., 1998). An example of a speciation diagram for uranium in sulphate containing water is given in Figure 5. Since the waters in the study of Bernhard et al. (1998) also contained phosphate, the diagram also shows uranium species complexing with phosphate at around pH 4-5. Importantly; carbonate complexation again dominates uranium speciation at alkaline pH (above pH 5). This shows the importance of, not only the elements available for complexation, but also the pH of the water which will determine which complex will dominate the uranium speciation. Not only do carbonate ions have a major impact on uranium speciation, they also increase uranium solubility and mobility at alkaline pH (Figure 6). Sulphate complexes play a similar role at acidic pH (Brugger et al., 2003), while phosphate complexes tend to cause precipitation and immobilisation of uranium (Sowder et al., 2001; Um et al., 2010).

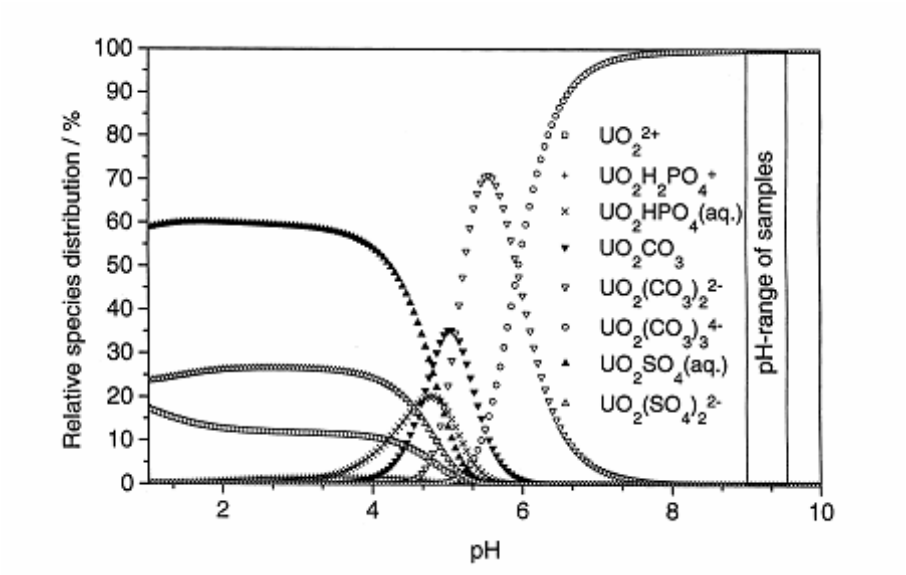

Figure 5. Example of a uranium speciation diagram by Bernard et al. (1998), in the presence of sulphate, phosphate and carbonate ligands.

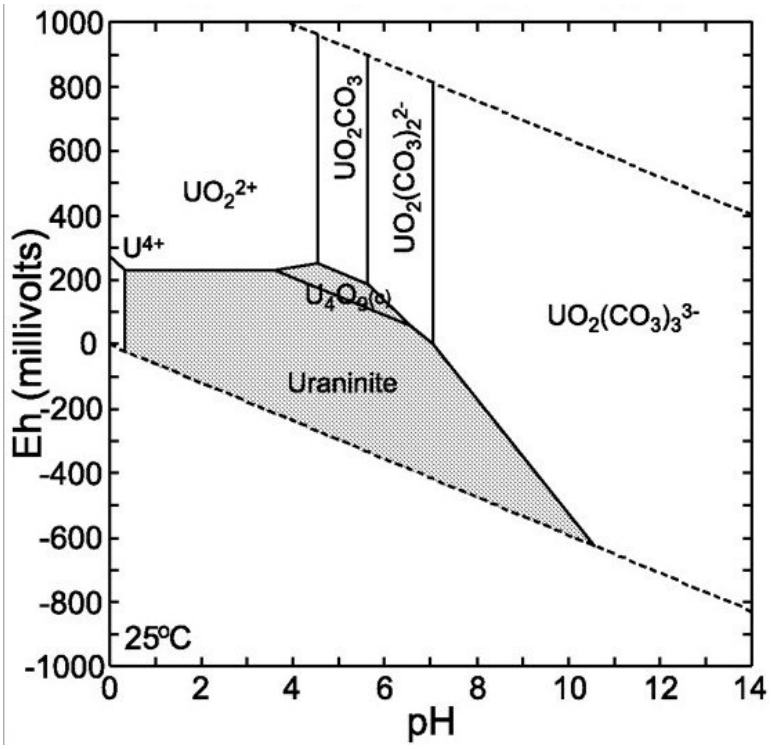

Figure 6. Eh-pH diagram for a U-C-O-H system at 25°C from Pirlo et al. (2004) showing that in oxic conditions at low pH, uranium is present as UO_2^{2+}, while at alkaline pH, uranyl carbonate species dominate. For low oxic or reducing conditions uranium is immobilised in the form of uraninite.

Organic matter acts as a reducing agent and can immobilise uranium by reducing it

to U (IV) (Duff et al., 1997; Langmuir, 1997). However, natural organic matter may form soluble complexes with uranium and has been found to dominate the aqueous speciation of uranium at acidic to neutral pH (Figure 7) (Murphy et al., 1992; Kantar, 2007). Mobility of uranium-organic matter complexes can be limited by deposition to soils and sediments, but, on the other hand, association with small organic colloids (3-30 kDa) can inhibit this deposition process (Graham et al., 2008, 2011).

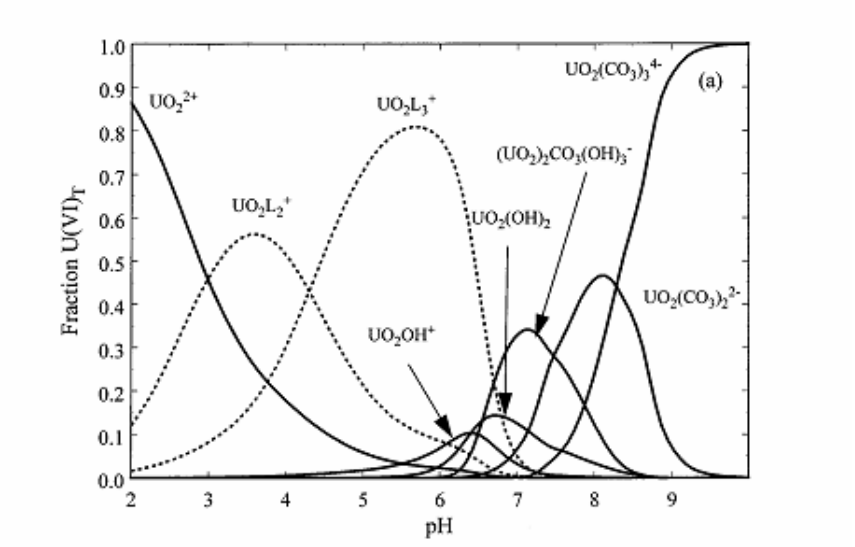

Figure 7. Example of uranium speciation in the presence of organic matter (L) from Murphy et al. (1999). While organic ligands dominate at pH 3.5- 6, carbonate complexes dominate the uranium speciation at pH 7 and above (10^{-6} M U, 10 mg/L OM at atmospheric CO_2 pressure).

2.1.4 Geographical distribution of uranium

World-wide uranium distribution varies greatly according to geology, with certain locations having high enough concentrations to make mining viable, *e.g.* Australia, Canada, Kazakhstan, Namibia, Niger, South Africa, Russia and the USA (Figure 8). Out of these, the first three provide over 60% of the world's uranium production, but uranium is also found in various locations throughout Asia, Africa, North and South America and Europe (see also Figure 9). As a consequence of its near ubiquitous world-wide presence, high uranium levels are often encountered in private wells as groundwater is tapped into (Hakonson-Hayes et al., 2002; Orloff et al., 2004). Some

examples of high uranium concentrations found in waters from different locations in the world are given in Table 3.

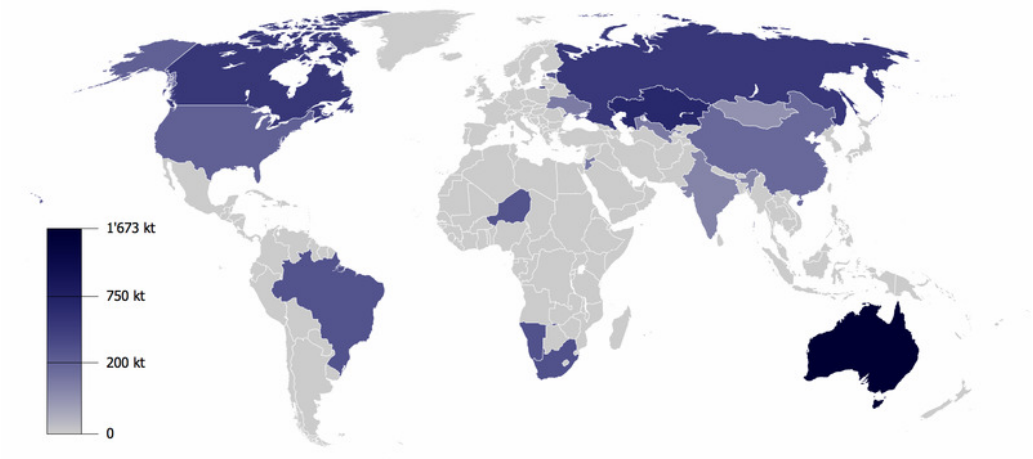

Figure 8. Map from world nuclear association (2010) showing main countries with known recoverable resources of uranium (for mining purposes) highlighted in blue.

Figure 9. Map adapted from Bowie (1979) marking known uranium deposits (note that at the time then communist countries were excluded).

Both studies by Annanmäki et al. (2000) and Plant et al. (2003) give an overview of the geochemical uranium distribution in Europe. Areas where elevated uranium

concentrations can be found are indicated in the map from Annanmäki et al. (2000) (Figure 10).

Table 3. Examples of elevated uranium concentrations from various locations in the world.

Country	Uranium concentrations measured	Reference
Kyrgyz republic	> 20 µg/L	(Vasiliev et al., 2005)
South Africa	< 540 µg/L (groundwater contaminated by gold mining)	(Winde and van der Walt, 2004)
Ethiopia	< 48 µg/L (wells) (47% above 2 µg/L)	(Reimann et al., 2003)
Canada	< 700 µg/L in private wells < 845 µg/L in wells of aboriginal people	(Zamora et al., 2009)
USA	< 620 µg/L in private wells < 1000 µg/L (contaminated groundwater) < 1200 µg/L, 52% of wells > 20 µg/L	(Orloff et al., 2004) (Abdelouas et al., 1998) (Hakonson-Hayes et al., 2002)
Australia	< 2000 µg/L groundwater, S Australia < 440 µg/L groundwater, N Australia	(Pirlo and Giblin, 2004) (Payne et al., 2001)
Germany	14% of bottled mineral water > 2 µg/L	(Birke et al., 2010)
Finland	Median 28 µg/L, max 1920 µg/L in well water < 643 µg/L in bedrock ground water ~80 µg/L in stream water	(Kurttio et al., 2002) (Åström et al., 2009)
Sweden	Median of 39 µg/L in black shale < 122/196 µg/L in bedrock and near-surface groundwater	(Åström et al., 2009)
UK	< 67 µg/L (private wells)	(Smedley et al., 2006)

Plant et al. (2003) found that the concentration for uranium of soils and sediments varied greatly across Europe from below background level to nearly 60 mg/kg. Particularly high levels were found in Brittany, central France, the Black Forest in Germany, the Czech Republic as well as parts of Italy and the Alpine rocks in Slovenia. High background values in stream sediments (10-30 mg/kg) were also found in the Scottish Caledonides and in southern Scandinavia. Generally, uranium was found in association with granite rocks and volcanic areas (Figure 10). Depending on weathering conditions this may result in high uranium concentrations

also leaching into ground and surface water. In fact a study by Birke et al. (2010) conducted on bottled water sourced particularly in Germany but also the whole of Europe found that bottled water contained on average higher uranium concentrations than tap water due to both geological and anthropogenic factors, although only one sample contained levels above the WHO drinking water guideline. However, 14% of the bottled water from Germany exceeded the guideline set for preparation of baby food (2 µg/L). A similar exceedence figure of 15% was found more generally for European bottled water (Birke et al., 2010). A survey of bottled water in the UK also found that concentrations varied from < 0.01 to 13 µg/L (Smedley et al., 2006).

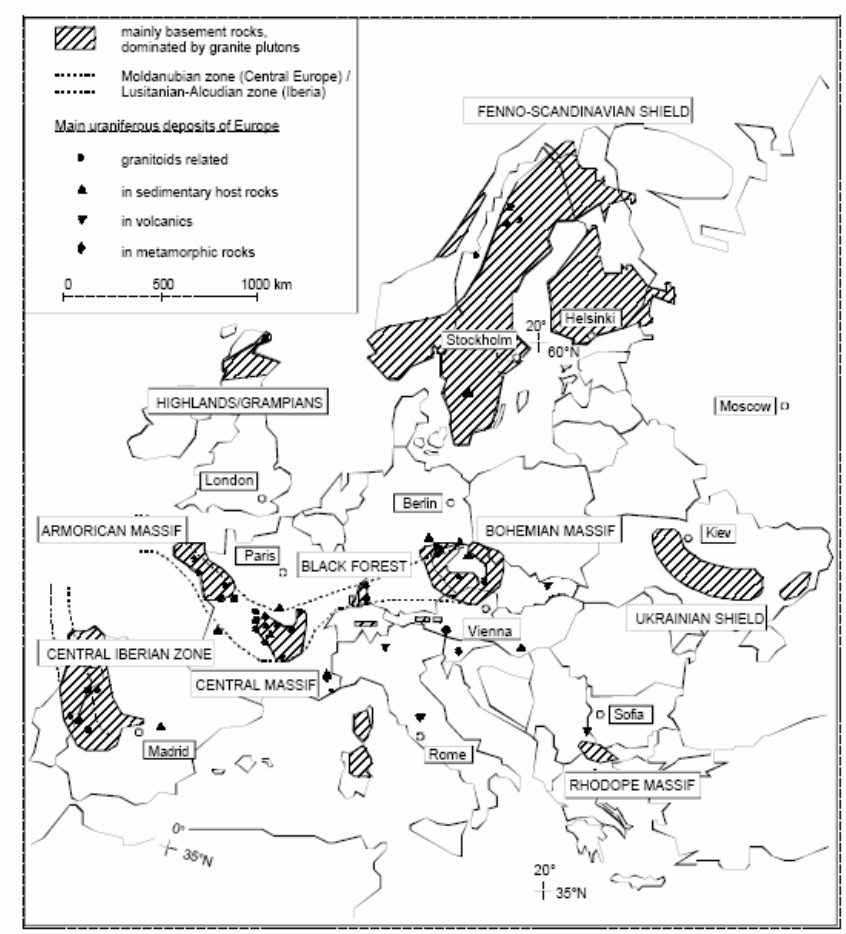

Figure 10. Map from Annanmäki et al. (2000), showing the main uranium deposits in Europe as well as zones dominated by basement rocks with potentially elevated levels of natural radionuclides in ground water.

2.1.5 Anthropological sources of uranium

Uranium is extensively mined, primarily for use as fuel in nuclear power plants and for weapons. Uranium mining will cause an increased risk of high uranium concentrations contaminating the surrounding environment. Even where mines are no longer in use, the dumped tailings still provide sources of contamination as they are subjected to weathering (Vandenhove, 2002; Stone, 2005; Vandenhove et al., 2006). A number of studies have been carried out on contaminated mining sites in for instance Europe, the USA and Australia (Brown et al., 1998; Willett and Bond, 1998; Biehler and Falck, 1999; Zhu and Burden, 2001; Gomez et al., 2008; Hyun et al., 2009). Not only can waters become contaminated, but there is also a risk of radionuclides being taken up by *e.g.* food crops (Hakonson-Hayes et al., 2002; Carvalho et al., 2009). An important factor in the leaching of uranium into water sources is the local and surrounding geology and soil properties, such as pH and organic matter content. Mining of minerals or substances other than uranium may also cause uranium release to the environment. For instance, uranium is found in auriferous sediments in South Africa at concentrations of up to 1000 mg/L. As a by-product of gold-mining, thousands of tonnes of uranium-containg tailings and slimes dams are produced, posing a serious contamination threat to adjacent ground and surface water (Winde and van der Walt, 2004). Tin-mining in Nigeria is also a cause of elevated uranium concentrations in soil and consequently in water and some food (Arogunjo et al., 2009).

Leakage from nuclear power plants and disposal of uranium waste may also pose a source of contamination. It is therefore important to investigate uranium migration at these sites (Toulhoat et al., 1996). In fact numerous studies are being carried out at Hanford, a plutonium production site in Washington State, USA, where there has been uranium contamination of billions of cubic meters of groundwater as a result of leakage from waste storage tanks (Catalano et al., 2006; Arai et al., 2007; Bai et al., 2009; Stubbs et al., 2009; Um et al., 2010). Studies have also been conducted at natural analogues to potential sites of nuclear waste disposal (Suksi et al., 1996; Payne and Airey, 2006) and these have highlighted the complexities involved in understanding uranium transport in natural environments.

There is also increasing concern regarding uranium contamination due to military use of depleted uranium (DU) in both conflict zones such as Kosovo and Iraq (Abu-Qare and Abou-Donia, 2002; Jia et al., 2006). This concern has caused researchers to investigate the mobility and bioavailability of DU in the natural environment (Choy et al., 2006; Oliver et al., 2007, 2008; Graham et al., 2011) and in test-sites in the UK and US. Although fears concerning the health effect related with DU are not always justified (Uijt de Haag et al., 2000) and the definitive health effects not well established, soil has been contaminated from 1000's of kilograms of uranium due to military use, risking contamination of both soil and water (Bem and Bou-Rabee, 2004; Buck et al., 2004; Dong et al., 2006; Oliver et al., 2007).

2.1.6 Methods for the removal of uranium from water

Due to the association of uranium with iron and phosphate materials, these are often explored as potential reduction or adsorption methods (Fuller et al., 2003; Boyanov et al., 2007). Adsorption of uranium onto a range of materials (montmorillonite, titanium dioxide, silicate materials, ferric and aluminium coagulants, hydroxyapetite, aluminosilicate minerals) has been investigated in a number of different studies (Payne and Waite, 1991; Chisholm-Brause et al., 2001; Prikryl et al., 2001; Payne et al., 2004; Simon et al., 2004; Sutton and Burastero, 2004; Baeza et al., 2006; Wazne et al., 2006; Arai et al., 2007). The adsorption was found to be highly pH dependent with effective removal at around pH 4-7, but sharp decreases at alkaline pH. Sorption of uranium to zeolites was investigated by Godelitsas et al. (1996), who found that the effectiveness depended on the starting concentration and was better (~50% sorption) at concentrations lower than 100 mg/L. Uranium adsorption has also been found to be highly dependent on the carbon dioxide pressure (Davis et al., 2004), and thereby sensitive to presence of air.

The TENAWA ("Treatment techniques for removing natural radionuclides from drinking water") project was initiated to find the best method for removal of radioactive contaminants, including uranium, from drinking water (Annanmäki et al., 2000). The techniques investigated included ion exchange resins, adsorption

methods, filtration and techniques already in use for iron and manganese removal (*i.e.* ion exchange and aeration). The efficiency of anion exchange resins depended on the type of resin used, the pH value and presence of competing ions such as chloride, sulphate and organic matter. It was concluded that a strong basic (alkaline) anion exchange resin was the most effective for uranium removal (>95%). Uranium removal using granular activated carbon was investigated, showing that the type of carbon used as well as grain size (smaller being more efficient), pH, water hardness and dissolved organic carbon highly influenced adsorption (~30-97%). Due to the variability it was deemed unsuitable for uranium removal. Moreover they found that removal efficiency was diminished with use. The effectiveness of adsorptive materials such as hydroxyapatite and manganese dioxide was found to be dependent on pH. An advantage of nanofiltration (NF) and reverse osmosis (RO) was that several contaminants could be removed simultaneously (> 95% removal of uranium, polonium, lead and radium). The TENAWA study found that NF and RO removed 95-99.8% of the uranium, although they point out that reverse osmosis permeate requires re-mineralisation prior to consumption (Huikuri et al., 1998; Raff and Wilken, 1999). Only a few pH values, however, were selected for these studies.

Membrane filtration is becoming a more important technology for the purification of drinking water. This is not restricted to large membrane plants in for instance Paris, Spain, the middle East (Cyna et al., 2002; Service, 2006; Al-Amoudi and Lovitt, 2007); in Scandinavia and Scotland, for example, membranes (nanofiltration) are being widely employed since they removes organic matter and, due to the modular configuration, can be installed to purify the water of small remote communities and households (De Munari and Schäfer, 2010b). To increase flexibility for remote locations and reduce dependence on finite energy sources, there is also an interest in using renewable energy to power membrane purification systems (Thomson et al., 2003; Schäfer and Richards, 2005; Coffey, 2008). Since uranium is present in many locations world-wide, in developed and developing countries alike, and has proved a particular problem where groundwater sources are utilised, as is often the case in remote locations, it is important to understand how uranium behaves in membrane systems.

2.2 Uranium and membrane filtration

2.2.1 Introduction to pressure-driven membrane filtration

There are several advantages associated with membrane filtration as a method for water purification, including (i) the small footprint of a membrane plant; (ii) the modular construction of the plant means that it can be relatively easily expanded if necessary; (iii) a variety of contaminants can be removed in one, or a few, steps by a physical barrier; and (iv) the limited use of chemicals in the water treatment. The disadvantages include the uncertainty of membrane lifetime, membrane cost, energy requirements, membrane cleaning procedures and disposal of concentrated waste (Al-Amoudi and Lovitt, 2007; Van der Bruggen et al., 2008).

Membrane filtration describes the process whereby a substance is passed through a selective physical barrier, separating the constituents of the substance according to physico-chemical characteristics such as size and charge (Mulder, 1996). The relevant substance to this study is of course water while, depending on the characteristics of the membrane, its constituents such as organic matter, bacteria, viruses, particles and dissolved ions would be selectively retained by a membrane (Figure 11). There is a range of pore sizes for membranes, from macro-porous to dense membranes. The driving force of interest for this study is pressure; however, several alternative processes exist, *e.g.* concentration gradient (dialysis, pervaporation and forward osmosis), temperature difference (membrane distillation) or electrical potential (*e.g.* electrodialysis) (Mulder, 1996; Strathmann, 1999; McGinnis and Elimelech, 2008). Membrane processes are not limited to water treatment processes but are used for a variety of applications ranging from food and beverage industries, pharmaceutical industry, chemical industry and fuel production (Strathmann, 1999).

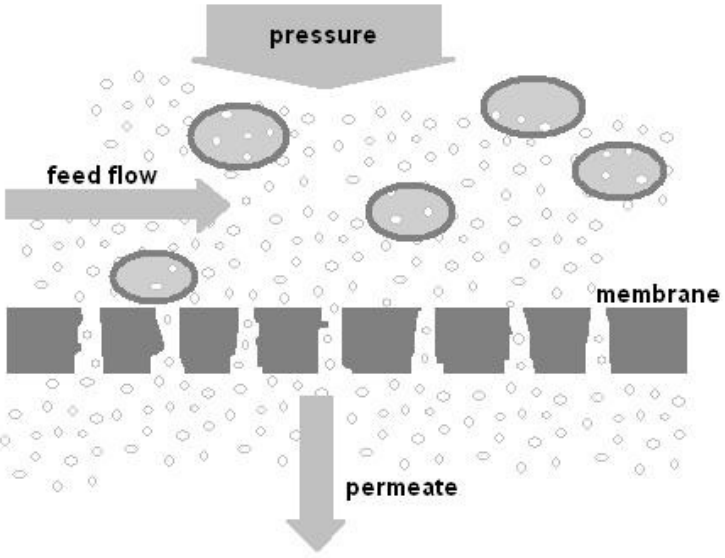

Figure 11. Simple schematic showing how the membrane separates larger particles present in the feed solution (which, in cross-flow systems, flows tangentially to the membrane) from the smaller water molecules which pass into the permeate.

This study will focus on the application of pressure driven UF, NF and RO (Table 4) to remove uranium from drinking water purification. The mechanisms by which solutes are removed vary somewhat between the three membrane types and will be discussed in more detail below. First of all, some basic definitions and equations are introduced.

Table 4. Comparison of UF, NF and RO membranes

	UF	NF	RO
Size ranges removed	1 - 100 nm	0.5 - 5 nm	0.1 - 1 nm
Pressure required[a]	0.5 – 5 bar	2 – 20 bar	10 – 200 bar
Bacteria removal	< 99.99%	< 99%	> 99%
Virus removal	30-99.9999%	99.99-99.9999%	> 99.9999%
$MgSO_4$ removal	-	< 90%	> 99%
NaCl removal	-	< 50%	> 98%

(Mulder, 1996; Van der Bruggen and Vandecasteele, 2003; Sobsey et al., 2008)

Since membrane pores generally have a distribution of sizes, membranes are often compared by measuring their nominal and absolute molecular weight cut-off (MWCO). Nominal MWCO is where a certain percentage of the molecules are retained, while for the absolute MWCO, 100% are retained by the membrane (Mulder, 1996).

The feed concentration represents the concentration in the starting solution (to be treated by the membrane), the permeate concentration is the resulting concentration in the solution passing through the membrane (the product), while the concentrate solution is the resulting solution containing the solutes or particles retained by the membrane (Figure 11). If not separated, the feed and concentrate can be described as bulk solution. Transmembrane pressure is the pressure difference between the pressure exerted on the feed side of the membrane and that of the permeate side.

Membrane retention, given in percent, is calculated using the solute concentration in the permeate and that in the membrane feed (or bulk, if there is not a separate concentrate stream) solution.

$$\mathrm{Re}tention = \left(1 - \frac{C_p}{C_f}\right) \times 100 \qquad \textbf{Equation 1}$$

C_p = solute concentration in permeate, C_f = solute concentration in feed (or bulk).

The permeate (or membrane) flux is given by the volume of permeate obtained over a given time period for a certain membrane area (Equation 2). The pure water flux (using de-ionised water) is often used to characterise membranes and as a starting point to compare the amount of fouling that has occurred to a membrane after exposure to a feed solution.

$$Flux, J = \left(\frac{1}{A}\frac{dV}{dt}\right) \qquad \textbf{Equation 2}$$

V = permeate volume, A = membrane area, t = time.

Permeability is the permeate flux normalised by the transmembrane pressure (Equation 3). This is a useful parameter when comparing membranes operated at different pressures.

$$Permeability, L = \left(\frac{J}{\Delta P} \right)$$ **Equation 3**

J = permeate flux, P = transmembrane pressure.

UF membranes have physical pores of typically between 1-100 nm and will remove large particles, bacteria and many viruses, while molecules and ions are not retained (Table 4). NF membranes are tighter than UF, and while the presence of physical pores is debated and will depend on the tightness of the membrane, NF generally removes viruses, organic matter and divalent ions, while there is only low retention of monovalent ions (Schäfer et al., 2005). RO are dense and remove most ions from solution (although even for RO, retention of low retention of *e.g.* trace organic solutes can be erratic (Schäfer et al., 2011). The two main transport mechanisms in membranes are convective and diffusional flow. For porous UF membranes convective flow is the main transport mechanism, while diffusion can be ignored (Mulder, 1996). The main exclusion mechanism in UF is sieving or size exclusion (Bowen et al., 1997). Higher pressure will lead to higher permeate flux but also increases convection of solutes which leads to decreased retention. For RO membranes, on the other hand, diffusional flow is the main transport mechanism and convection can be ignored (Mulder, 1996). Solutes are transported by dissolving into the membrane and diffusing through it to the permeate side (Figure 12). The exclusion mechanism in RO is thus based on the solution-diffusion model (Wijmans and Baker, 1995). Since the transport of ions is diffusion-dependent, higher pressure which leads to a higher water flux, results in higher retention.

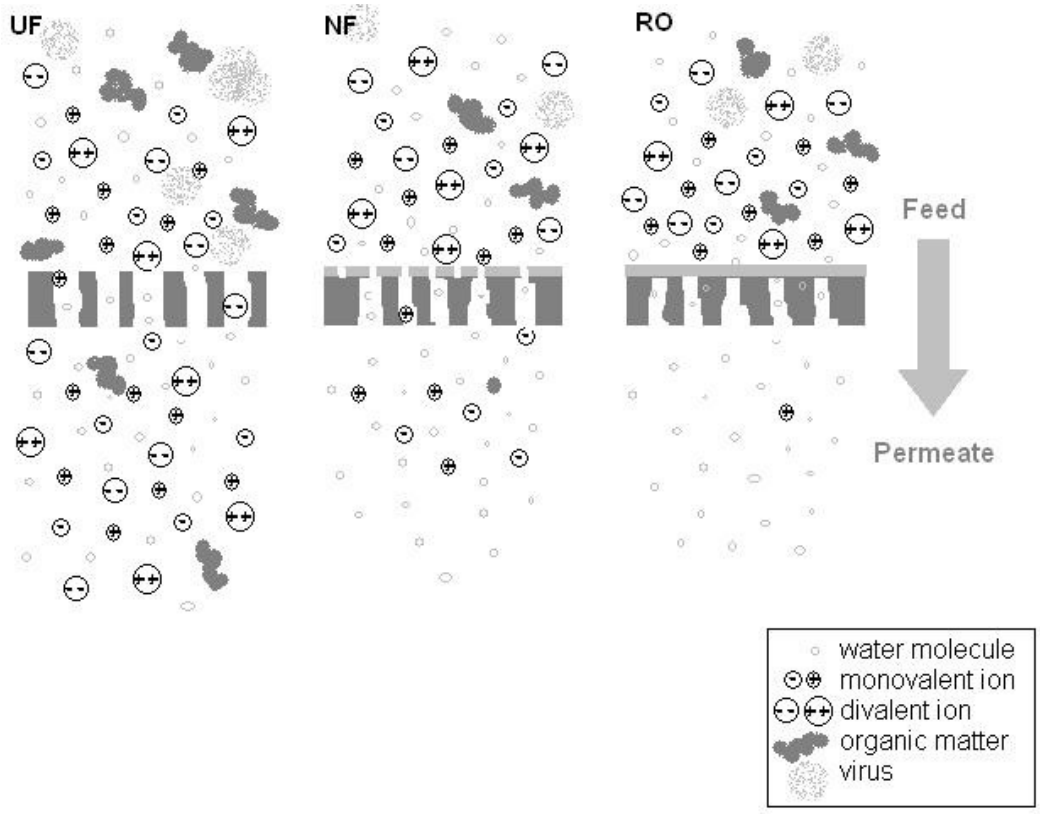

Figure 12. Simple schematic illustrating the retention of monovalent and divalent ions, organic matter and virus by UF, NF and RO. Note that it is not drawn to scale.

NF membranes are considered to lie in between UF and RO in terms of pore-size and consequently transport and retention mechanisms, and are sometimes considered to be tight UF membranes or open RO membranes (Van der Bruggen and Vandecasteele, 2003). The existence of pores is widely debated within the membrane scientific community. However, small pores of around 1 nm can be identified and the transport mechanisms can be influenced by both convection and diffusion while retention mechanisms are a mixture of size exclusion and charge repulsion of ions (Wijmans and Baker, 1995; Schaep et al., 1998). Monovalent ions are generally less well retained than divalent ions by charged NF membranes, both as a consequence of their lower charge as well as smaller hydrated radius of the monovalent ions (Wijmans and Baker, 1995; Van der Bruggen and Vandecasteele, 2003; Schäfer et al., 2005). Where the structure is relatively tight, retention can increase with pressure, as with RO membranes where retention depends on diffusion of ions (constant) and the permeation of water (increases with pressure), whereas for a loose

NF membrane, the retention may be more affected by convection and therefore decrease with pressure (as for UF membranes). A loose NF membrane is also more likely than a RO membrane to be affected by concentration polarisation (more in section 2.2.2), which can also result in decreased retention with pressure. The membrane, and, as a consequence, the retention of charged ions, is also affected by the pH of the solution. Polymeric membranes often have a net positive or neutral charge in acidic solution, while, at more alkaline pH values, a net negative charge of the membrane results (Childress and Elimelech, 1996). As a consequence of the overall reduced charge density of the membranes at acidic pH, monovalent ions are less well retained by NF membranes due to their low charge and small size (Braghetta et al., 1997). On the other hand permeate flux may increase with pH since the increased negative charge causes repulsion within the membrane structure, making the pores more open to permeation of water (Braghetta et al., 1997).

2.2.2 Fouling of membranes

Fouling of membranes occur as substances accumulate at and attach to the membrane surface, attaching to the membrane or blocking the pores, usually resulting in flux decline and lowered productivity of the membrane (amount of permeate produced per membrane area) (Nyström et al., 2004; Van der Bruggen et al., 2008). Often retention is increased as a consequence; this is something which is taken advantage of in, for example, porous membranes such as microfiltration or sandfilters. Alternatively, retention can decrease due to the increased diffusion of accumulated solutes (Lee et al., 2004). In membrane filtration, fouling is generally considered as something to be avoided or controlled as far as possible, since, over time, it will lead to reduced permeate flux, possible degradation of the membrane, increase the energy required, may decrease the quality of the water produced as contaminants diffuse through and will lead to disruptions of the water treatment process due cleaning (Al-Amoudi and Lovitt, 2007; Porcelli and Judd, 2010). Fouling can be categorised into four main types: biofouling (by bacteria), particulate (or colloidal) fouling, inorganic precipitation or scaling and organic fouling (Mulder, 1996; Bartels et al., 2005;

Boussu et al., 2006). In this study, the latter two were investigated since, in groundwater, inorganic scaling is likely to pose a great fouling risk due to potential high concentrations of inorganic ions present, while the presence of organic matter is important for surface water treatment and is likely to affect both uranium speciation due to its metal binding capacity (Zhang et al., 1997; Bryan et al., 1998; de la Rosa et al., 2003; Schwab et al., 2008) as well as membrane performance and characteristics (Ang et al., 2006; Tang et al., 2007).

Organic fouling occurs as organic matter interacts with the membrane through adsorption or by aggregation and the concomitant formation of cake layers (Tang and Leckie, 2007). Natural organic matter is formed from degraded plant remains and is highly heterogenous in composition *i.e.* it may comprise a mixture of hydrophilic, hydrophobic, aromatic and non-aromatic parts. The stable component of natural organic matter is generally classified as humic and fulvic acids, the former being less soluble in acidic solution due to its large molecular weight and relatively lower presence of oxygen (and thus hydrogen bonding capacity) (Baird, 1999). The configuration of organic molecules, especially humic substances, has been found to depend on pH and ionic strength; it is spherical at low pH and high ionic strength while it has a more linear structure at higher pH and low ionic strength (Ghosh and Schnitzer, 1980). Likewise it has been found that low pH and high ionic strength cause increased fouling with organic matter on membranes (Lee and Elimelech, 2006a), showing the impact of the water quality on the filtration process.

Inorganic scaling occurs as inorganic ions accumulate at the membrane surface. Comman scalants are, for instance, SiO_2 and salts of Ca^{2+}, Ba^{2+}, Sr^{2+}, CO_3^{2-}, SO_4^{2-} and PO_4^{2-} (Rahardianto et al., 2007; Tzotzi et al., 2007). The concentration of inorganic ions close to the membrane surface will increase in NF and RO as convection is increased and retention is high. This may result in adsorption of the ions to the membrane surface and, if the solubility limit is exceeded, in precipitation and thereby scaling of the membrane surface. Inorganic scaling can cause drastic flux decline and also damage to the

membrane. Retention can decrease as a consequence of inorganic fouling since, due to the high concentration of ions close the membrane surface, diffusion to the permeate side is enhanced; in NF, masking of the membrane charge by the ions can also decrease charge (Donnan) exclusion (Lee et al., 2004).

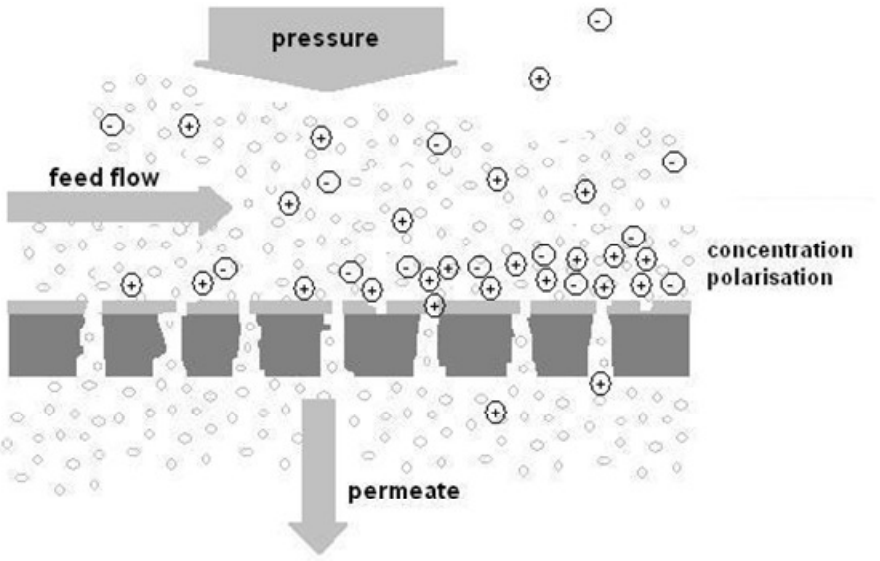

Figure 13. Simple schematic illustrating concentration polarisation; the accumulation of ions close to the membrane surface, a result of the convection of ions towards the membrane due to pressure and the retention of those ions by the membrane.

The increased concentration due to accumulation of (mobile) ions at the membrane surface is known as concentration polarisation (Figure 13) (Potts et al., 1981). A consequence of concentration polarisation can be a decrease in retention due to the increased concentration gradient at the membrane surface. This is generally reversible and can be controlled by, *e.g.* increasing the cross-flow velocity across a membrane surface or by turbulence promoters, to prevent fouling due to adsorption or precipitation. Concentration polarisation does mean, however, that the true or "real" retention of a membrane can not actually be determined by measuring the concentration in the bulk or feed solution, but really by the concentration at the membrane surface. It is difficult to gain accurate quantitative measurements of concentration polarisation (Chen et al., 2004), although there are several models that are used to calculate/predict it (Nghiem et al., 2004; Deon et al., 2007; Geraldes and Afonso, 2007). For

instance, the film model is commonly used to calculate the concentration of solutes at the membrane surface and the resulting real retention (*e.g.* Sutzkover et al., 2000; Tzotzi et al., 2007), which for real retention gives;

$$\frac{1-R_0}{R_0} = \frac{1-R_r}{R_r}\exp\left(\frac{J_v}{k}\right) \qquad \textbf{Equation 4}$$

Where R_0 = observed retention, R_r = real retention, J_v = permeate flux and k = the mass transfer coefficient. R_0 and J_v are determined experimentally and k can either be determined experimentally (Sutzkover et al., 2000) or by use of correlations.

The concentration of solute by the membrane can be estimated by Equation 5 (Sutzcover et al., 2000);

$$\frac{Cm-Cp}{Cb-Cp} = \exp\left(\frac{Jv}{k}\right) \qquad \textbf{Equation 5}$$

where Cm = concentration at membrane surface (mg/L), Cp = concentration in permeate (mg/L), Cb = concentration in feed or bulk solution (mg/L), Jv = permeate flux (m/s) and k = the mass transfer coefficient (m/s).

The level of concentration polarisation experienced by a membrane is reported as the polarisation modulus which gives the ratio of concentration at the membrane surface (Cm) to that in the feed/bulk solution (Cb).

In controlled experiments, the amount of organic or inorganic solutes which has been taken up by the membrane can be calculated by accounting for solute mass at the start and end of the experiment and that in permeate and feed samples (aliquots taken for analysis during an experiment), using mass balance;

$$Mass\ Adsorbed\ (\%) = \frac{V_{b0}C_{b0} - V_{bf}C_{bf} - \sum_{i=1}^{i=n} V_S C_{bi} - \sum_{i=1}^{i=n} V_S C_{pi}}{V_{b0}C_{b0}} \times 100 \quad \textbf{Equation 6}$$

V = volume, C = solute concentration, b = bulk (or feed), p = permeate, S = sample, 0 = initial, f = final. Note that even though this term is described as "Mass adsorbed"; this does *not* reflect the determined membrane up-take mechanism (which may be due to *e.g.* adsorption or precipitation).

2.2.3 Uranium removal from water using UF, NF and RO

Ultrafiltration

Although UF is generally not considered to be able to remove inorganic contaminants due to its large pore size, it has still been found effective in a number of studies, mostly in combination with some form of complexation. As far back as 1982, a method was patented by Stana et al. (1982) using membranes to concentrate uranium from lixiviants used for mining. They suggested the use of either RO membranes or, preferably, more open UF membranes in combination with complexing agents to selectively concentrate uranium. More recently, Kryvoruchko et al. (2004) investigated the uranium removal from water using a UF (UPM-20 polyamide, Vladipor) membrane with an average pore diameter of 20 nm. The concentration of uranium investigated was 10 mg/L over a pH range of 3-9. The retention using only the UF membrane increased linearly from no retention at pH 3 to a maximum of 91% at pH 9. In combination with complexation with polyethylenimine the retention was raised to 98-99% at pH 5-9. Since their starting concentration was so high, the resulting permeate still contained high levels of uranium (100 µg/L) with respect to the WHO drinking water guideline (15 µg/L) even with the highest retention achieved. In terms of treating uranium contamination from *e.g.* mining, it is however a significant and important reduction. They also investigated the effect of applying compressed air rather than nitrogen to the system. This resulted in increased uranium retention for both UF only and UF in combination with polyethylenimine in the pH range 5-9. The authors hypothesise that it might be

due to the formation of a layer of uranium carbonate complexes, but do not substantiate the theory. Kryvoruchko et al. (2007) also investigated the combination of adsorbing materials (a synthetic activated carbon and a natural silicious mineral) with UF and a relatively open NF membrane (pore size range 10-20 nm). They only investigated a pH of 7-8 and used a high concentration of uranium, 5 mg/L. By combining UF with adsorbents they achieved a uranium retention of 87-91%, while combining NF with adsorbents achieved 99% retention –the highest retention still giving a permeate concentration of 50 µg/L.

Enhancement of uranium removal using modified UF membranes, or UF in combination with micelles, has also been studied (Pramauro et al., 1996; Reiller et al., 1996; Roach and Zapien, 2009) and patents using the method of micelles in combination with UF have been developed (Tounissou et al., 2000). In a micelle-UF study by Reiller et al. (1996), only the positively charged uranium species could be associated with the micelles, limiting the application to the acidic pH range. Consequently a retention of >99% was achieved at pH 3 while at pH ~6 the retention had dropped to ~80%. Pramauro et al. (1996) on the other hand found that uranium retention increased from ~20% and >90% (depending on the ligand used) at pH 3 to <90% at pH 4-6, using a hydrophobic ligand in combination with surfactants to form the micelles. Using only UF combined with the surfactant without the hydrophobic ligand gave 3-5% uranium retention. Drawbacks to the micellar-UF technique include the cost especially of organic ligands, surfactant permeation and the need to extract the uranium from the micelles after inclusion. Roach and Zapien (2009) used "inorganic ligand modified, colloid-enhanced ultrafiltration", where, instead of an organic ligand, carbonate was used. Using a 6 kDa equilibrium-dialysis membrane, uranium retention of 99.6% was achieved. In this case the retention of uranium was high (>99%) in the presence of the negative uranyl carbonate species, $UO_2CO_3^{4-}$, while competition from CO_3^{2-} ions and more acidic pH (and thus presence of other uranium species) lowered the retention. The minimum detection limit for the uranium analysis method used was above the WHO drinking water guideline. The authors point out that the method still needs development; *e.g.* the recovery of uranium and the regeneration of the colloids used with the UF need to be addressed.

Although a study not directly involving uranium, Brandhuber and Amy (2001) also used negatively charged ultrafiltration membranes to remove arsenic from water samples and achieved an arsenic rejection of 88%. Importantly, the rejection was highly influenced by operating conditions of the UF system and the water quality. With respect to the latter, the presence of other inorganic ions decreased the rejection while organic matter increased it, probably due to complexation with calcium ions. An important conclusion of relevance to this study of uranium removal is that retention of dissolved inorganic ions during UF tends not to be due to physical size exclusion and is therefore highly dependent on water conditions and, in particular, pH and the presence of competing ions or complexing ligands.

The processes involving UF and complexation are interesting with regards to reducing uranium concentrations in contaminated water; the studies to date do not, however, demonstrate sufficient uranium removal to meet drinking water guidelines. Such high removal would be highly desirable however, due to the low energy required to operate UF systems compared to NF or RO (Table 4). Alternatively, UF can still serve as a valuable pre-treatment to tighter membranes.

Another important point to note is that UF is also used to determine colloidal fractions in natural waters. The rejection of colloidal compared to dissolved uranium was investigated by Guo et al. (2007) using a 1 kDa UF membrane. They found that, in addition to colloidal forms, dissolved uranium was also rejected to a certain extent by the UF membrane; retention of dissolved uranium was attributed of charge repulsion and the authors comment that such retention could lead to erroneous classification as colloidal uranium. This illustrates the importance of fully understanding the uranium behaviour and retention mechanisms during the UF process.

Nanofiltration and reverse osmosis

Favre-Reguillion et al. (2003) investigated the viability of using Osmonics NF membranes (G50, G80, 5DL, G20 and G10) to concentrate uranium from seawater.

Especially G10 was shown to have high selectivity in retaining uranium compared to other ions present (Ca^{2+}, Mg^{2+}, Sr^{2+}, Na^{+} and K^{+}), although it was not deemed economically viable as a uranium concentration process. For uranium removal for the purpose of drinking water production, however, NF has been shown to effectively retain between 80-99% present in the water sample (Raff and Wilken, 1999). Indeed, Favre-Reguillion et al. (2008) investigated the selectivity of NF membranes (DK, DL and G10 Osmonics membranes) and found that high retention of uranium could be achieved while allowing passage of important trace minerals, in this case Ca^{2+}, Mg^{2+}, Na^{+} and K^{+}. Chellam and Clifford (2002) also investigated the removal of uranium and other trace elements from tailings generated during uranium mining and milling using Fe (III) coagulation followed by NF/RO filtration (PAC1, TW30 and TFC-S). They investigated three different pH values and found that removal of uranium by coagulation was poor (<10%). They found that coagulation was less effective in carbonate containing water, but achieved 98-99% removal of uranium at pH 10 due to the membrane filtration. They underscore the importance of ion charge, with the most highly charged species experiencing the highest rejection. As previously mentioned, Huikuri et al. (1998) investigated the removal of natural radionuclides from drinking water in rural Finland by using small RO systems (HR-05). Removal techniques are especially needed for rural settlements outside the communal water supply where drinking water is obtained from privately drilled wells. RO is very effective in removing uranium; Huikuri et al. (1998) did point out that the water is nearly completely de-mineralised when RO is used, necessassitating post-treatment to re-harden the water before consumption. In this respect, NF would be advantageous.

As illustrated above, filtration using NF and RO can achieve very high retention of uranium (Tiepel, 1985; Hsiue et al., 1989). Retention can even be achieved using UF membranes, although this was highly dependent on water conditions and the presence of complexing agents and permeate concentrations below the WHO drinking water guideline were not achieved. However, the pH values of natural waters vary from pH 3-10 (Langmuir, 1997), and uranium speciation and behaviour varies accordingly. Consequently behaviour of uranium in membrane systems should

be thoroughly studied across the pH range –this was lacking in the above NF and RO studies. The effect of potential adsorption of uranium to membranes, as was observed for a variety of materials has also not been studied. Moreover, studies often focus on removal in the presence a few simple mono-or divalent ions, but not more complex combinations of these, making it hard to predict what will happen in a real environment where more complex water chemistry is present.

In summary, studies of uranium removal by UF, NF and RO should consider that: 1) speciation of uranium is influenced by a wide range of factors, as discussed in section 2.1.3, including available ligands (inorganic and organic) and the pH of the water; 2) uranium speciation can affect its retention by membranes, especially UF and NF membranes where exclusion mechanisms are size and charge dependent; and 3) uranium is well-known to adsorb to a variety of materials under specific aqueous conditions, and this should be investigated also for membrane filtration processes.

3 Materials and Methods

This chapter outlines the main filtration systems and membranes used for the laboratory studies carried out as well as the main analysis methods of uranium which was analysed through-out the PhD study. The specific analysis methods and instruments used for individual chapters are detailed within the methods section for the relevant chapters. For instance, analysis methods used for µ-XRF, SEM, TEM and FTIR are detailed in Chapter 6 while ToF-SIMS analysis is detailed in Chapter 7.

3.1 Membranes and filtration equipment

3.1.1 Membranes used

During the course of this PhD work one UF, one NF and one RO membrane was used. The UF membrane module (ZeeWeed hollow fibre, ZW1) was supplied by GE Zenon. The flat sheet NF and RO membranes were supplied by Koch Membrane systems and Dow Filmtec, respectively (Table 5).

Table 5. Overview of membranes used and retention given by manufacturers (PVDF = polyvinylidene fluoride, PA = polyamide, PS = polysulfone)

Type	Name	Manu-facturer	Material	Membrane area (m^2)	$MgSO_4$ retention (%)	NaCl retention (%)	Lp (L/m^2h bar)
UF	ZW1	GE Zenon	PVDF	0.047			128[c]
NF	TFC-SR2	Koch Membrane Systems	PA semi-aromatic active layer on PS support	0.0046	95[a]	10-30[a]	10.97± 1.51[d]
RO	BW30	Dow Filmtec	PA aromatic active layer on PS support	0.0046		99[b]	4.84± 0.15[d]

[a]5000 mg/L $MgSO_4$/2000 mg/L NaCl in DIW, 6.5 bar 25°C, pH 7.5; [b]2000 mg/L NaCl, 15.5 bar, 25°C, pH 8; [c]Typical permeability (Lp) as given by the manufacturer; [d]Permeability (Lp) was measured experimentally using deionised water.

Additionally, the contact angle of TFC-SR2 and BW30 was measured as 61.5 ± 2.5 and 40.3 ± 1.1, respectively (by Annalisa De Munari), while surface roughness (Ra) for TFC-SR2 and BW30 was measured as 17.9 ± 0.6 nm and 67.7 ± 2.4 nm, respectively (by Ime Akanyeti).

The membranes were selected for two reasons:
1) To be able to compare laboratory studies with the field study using the UF-NF/RO system (Chapter 4). This system had used Zenon UF membranes while one of the RO membranes used was BW30.
2) An open NF membrane was of interest in order to explore the effects of the uranium speciation on the uranium behaviour in membrane systems. TFC-SR2 was selected since it is a relatively open NF membrane, which could also be compared to the other NF membranes used in the field study.

3.1.2 Membrane preparation and storage

The UF module was thoroughly washed with DIW before it was first used (as in *e.g.* (Tang and Leckie, 2007). During the experimental period it was cleaned at the end of an experiment (details in section 5.2.2) stored in DIW overnight. The pure water flux was always measured before the start of each new experiment.

The NF and RO membranes were prepared by cutting them to fit the membrane cell of the cross-flow system (0.0046m^2) at least the day before the experiment, swilling them with de-ionised water (DIW) and then soaking them further in de-ionised water over-night at 4ºC. They were then swilled off again with DIW before mounting them in the membrane cell. The membranes were always compacted for an hour (or until permeate flow was stable) before the experiment with DIW at 25 bar and a flow rate of 0.6 L/min.

Depending on the type of analysis to be carried out after the completion of the experiment, the membranes were either allowed to dry and were stored at room temperature (for FTIR and m-XRF), or processed immediately when still wet (as for SEM/TEM and EDX).

3.1.3 Lab-scale UF filtration system

The UF membrane module was placed in a glass beaker and operated by vacuum using "outside-in" configuration (Figure 14). The experimental solution (2.55 L) was stirred using a magnetic stirrer. A peristaltic pump (flow-rate 50 mL/min) re-circulated the solution to the feed beaker in order to keep feed concentration constant. The tubing was stainless steel tubing apart from the Masterflex Norprene L/S 16 tubing with an inner diameter of 3.1 mm. Further equipment consisted of pressure transducer (PX219-30V45G5V) and a thermocouple (TJ2-CPSS-M6OU-200-SB) connected to a datalogger (OMB DAQ 54) for data recording (Omega, UK). Conductivity and pH were measured by using a pH/Cond 340i meter (WTW, Germany). The filtration and cleaning protocol is described in detail in Chapter 5.

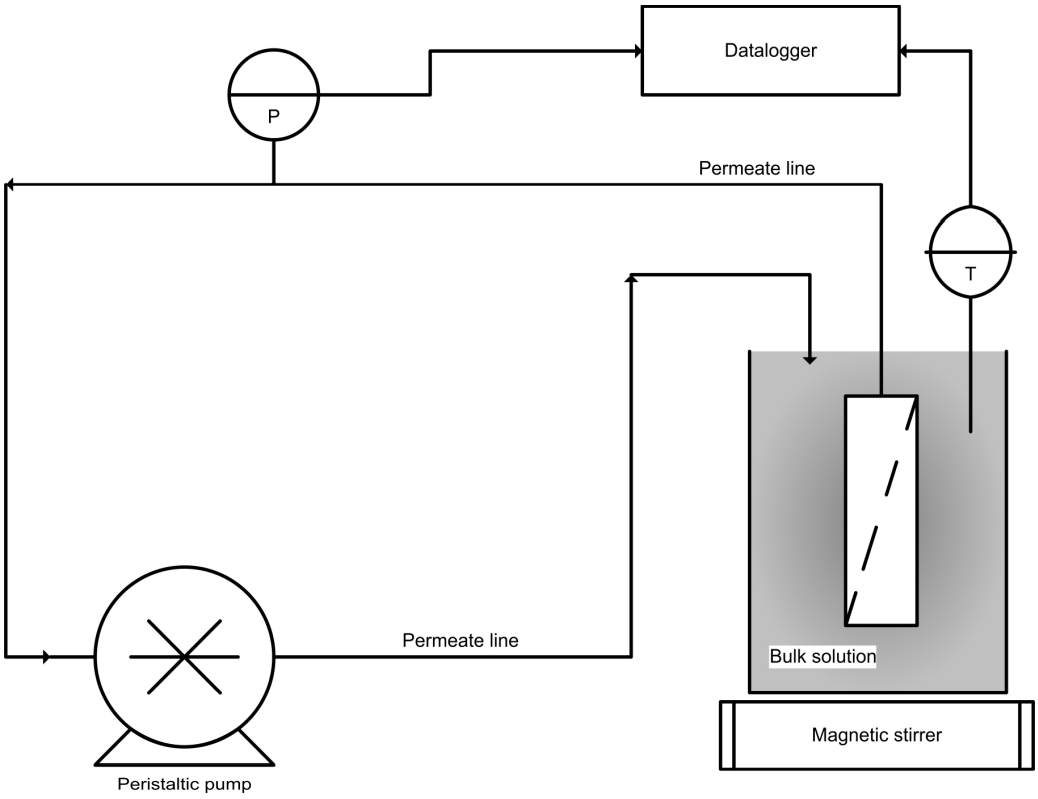

Figure 14. Schematic of UF filtration system, detailing the feed beaker with bulk solution on top of a magnetic stirrer, the submerged UF membrane, the peristaltic pump and the pressure transducer and thermocouple feeding into the datalogger, connected to computer.

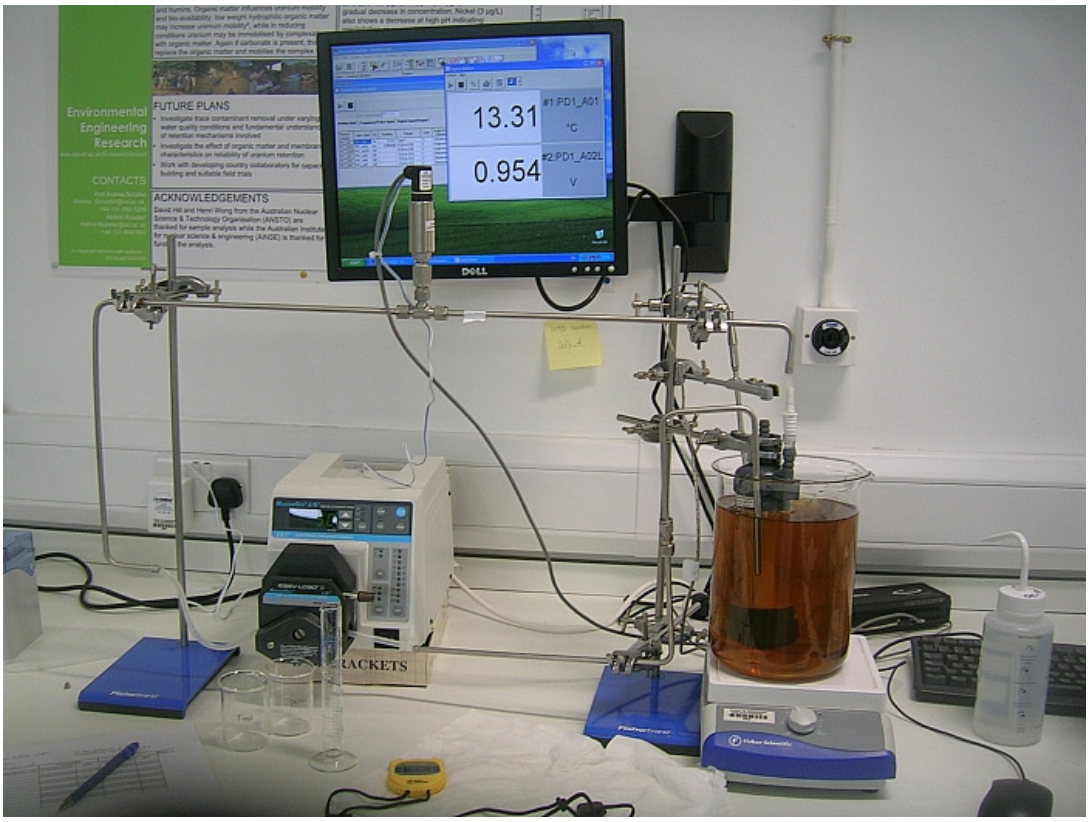

Figure 15. UF system set-up (during an experiment using humic acid which gave the brown colour to the solution).

3.1.4 Lab-scale NF/RO cross-flow system

A stainless steel cross-flow filtration system was built by MMS (Switzerland), incorporating two feed tanks (2.5 L) with cooling jackets connected to a temperature controlled water bath (WK 700, Lauda), a high-pressure pump (Speck, Germany) three flat-sheet membrane cells (0.0046 m^2 and a channel height of 1 mm), a pressure dampener, an in-line temperature indicator (WTM Pt 100-0-6, Condustrie-Metag, Germany) and safety relief valves. Since it was found that the original pump leaked oil and was therefore highly unsuitable for detailed membrane study, the pump had to be replaced. It was replaced by a high pressure pump (P200 from Hydra-Cell, UK), which also required additional optimisation to fully exclude any oil from entering the experimental filtration system and contaminating the solution and membranes being tested. Full details of this process can be found in (Semião, 2011). Three diaphragm materials were available: Viton, Teflon and Buna. Viton

diaphragms were used since these show high chemical resistance but still retain more flexibility compared Teflon diaphragms, and thus are less likely to leak any oil. A back pressure regulator (KPB1N0A415P60000, Swagelok) was added to control the pressure without affecting the flow-rate. Pump speed and thus flow rate was controlled using a drive (Commander SK, Control Techniques). A stainless steel flow-meter (M2SSP1, Hydrasun, UK) was used to measure feed flow-rate prior to the membrane cells. The stainless steel rotors also had to be replaced since it was found that these corroded after little use, contaminating the system with, *e.g.* iron and nickel. This was due to manufacturing process where the rotors had been moulded from stainless steel powder rather than cut out directly from a block of stainless steel. Thus especially cut rotors had to be ordered. Finally, the dampener was removed from the system since it proved to be a source of contamination and was difficult to properly clean. Since the pressures used were relatively low, the dampener was not necessary and pressure variations during an experiment were generally within 5%. Permeate tubing (stainless steel, ss 316) and valves (Swagelock) were added to allow sampling or re-circulation of the permeate solution to the feed tank. Permeate flow-rate was measured by means of a balance (Ohaus) and a stop-watch whenever a permeate sample was taken. The pressure was monitored using two in-line pressure transducers (S-model, Swagelok). Pressure along with temperature, permeate flow (*i.e.* the weight registered by the balance), and flow-rate was logged by a data-logger (DAQ 55, Omega, UK) into LabVIEW (National Instruments). Conductivity and pH measurements of feed and permeate solutions were measured using 340i meter (WTW, Germany).

The details of the NF/RO filtration procedures and cleaning protocol are described in Chapter 6.

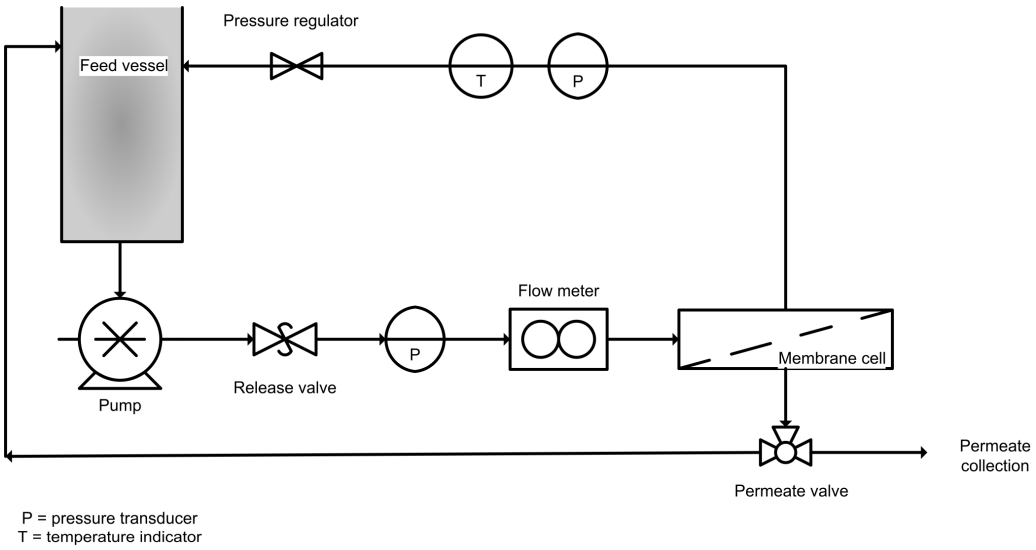

Figure 16. Schematic of the NF/RO cross-flow system entailing feed tank, pressure regulator, temperature probe, membrane cell, permeate line and collection on an Ohaus balance, flow meter, pressure transducers and the Hydra-Cell pump.

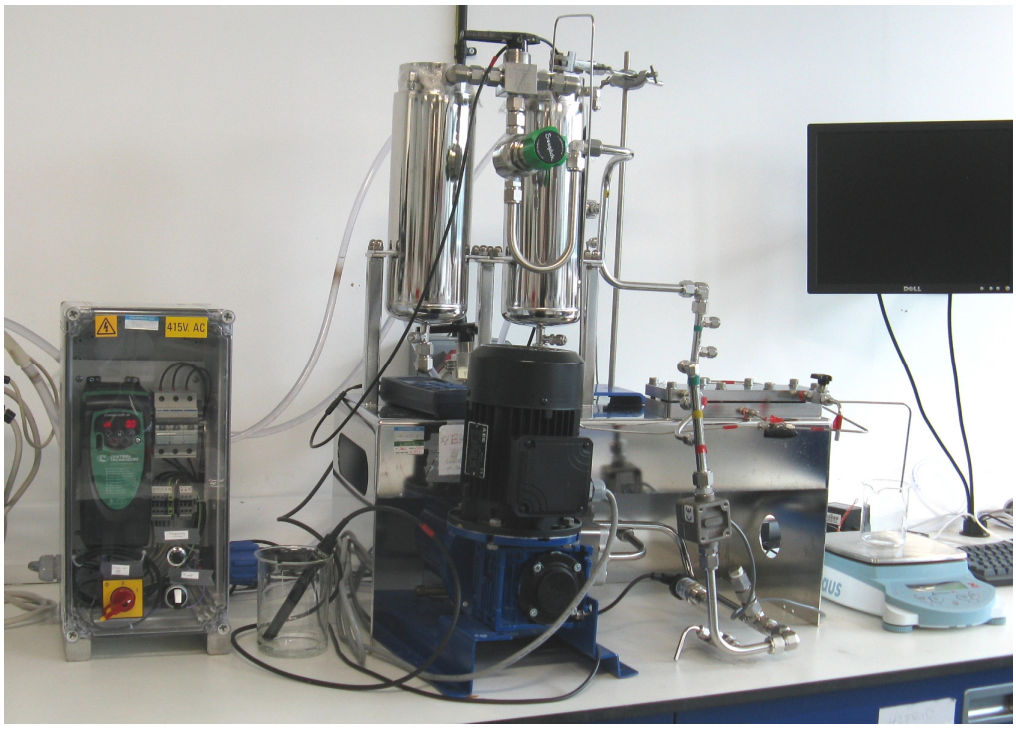

Figure 17. Laboratory NF and RO cross-flow system entailing feed tanks (two were available), pressure regulator, temperature probe, membrane cell, permeate line and collection on an Ohaus balance, flow meter, pressure transducers (two), pH and conductivity meter, the Hydra-Cell pump and a pump frequency control.

3.1.5 Experimental solutions

To mimic natural surface and groundwaters and have a buffer to allow for stable pH values, experiments were performed (unless otherwise stated) using a background electrolyte solution of NaCl (20 mM, Fisher Scientific) and $NaHCO_3$ (1 mM, Fisher Scientific) (Baird 1999). These concentrations allowed comparisons of results with past work as well as the work of PhD colleagues in the group (Banasiak, 2009; Neale, 2009; De Munari and Schäfer, 2010a; Schäfer et al., 2011). The uranium stock solutions were prepared using uranyl nitrate (TAAB, UK) and dilute nitric acid (2.8%, Aristar, VWR International, UK). Unless otherwise stated a concentration of 0.5 mg/L of uranium was prepared for experiments in the background electrolyte solution. This concentration is comparable to concentrations found naturally (Orloff et al., 2004; Seldén et al., 2009), and also allowed feed solution analysis by Inductively Coupled Plasma-Optical Emission Spectroscopy (ICP-OES). Pure de-ionised water (DIW) was used at all times for experiments and was obtained from Elga PURELAB Ultra (High Wycombe, UK). The water quality was < 18.2 Ω/cm. Adjustments to solution pH were done using HNO_3 (0.1-1 M, Aristar, VWR International, UK) or NaOH (0.1-1 M, Fisher Scientific, UK). HNO_3 was used for pH adjustments and sample preservation since it is most suitable for ICP-MS analysis since it gives very few polyatomic ions and little spectral interference compared to other acids (*e.g.* HCl generates chloride-derived polyatmic ions).

3.1.6 Analytical techniques

ICP-OES

Analysis of uranium concentrations in feed solutions was carried out using an Optima 5300 DV ICP-OES (Perkin Elmer, USA). Other major ions such as calcium (Chapter 7), magnesium, aluminium, sulfur and potassium (Chapter 8), were also analysed using ICP-OES (see Table 16 for an overview of the method used for analysis of each inorganic element during the PhD study). A set of uranium (and/or other relevant element) calibration standards spanning the concentration range 0.1-10 mg/L were prepared by dilution of a stock solution (Merck, 1000 mg/L U in dilute nitric acid) using dilute nitric acid (2.8%, Aristar, VWR International, UK). In the

case of calcium, the highest standard used was 100 mg/L. Check standards were inserted approximately every 10 samples to control for instrument drift during analysis and wavelengths were checked and adjusted if necessary. The accuracy of the calibration standard solutions was always determined before sample analysis commenced. This was achieved by analysing a certified reference solution (ICP Multi Element Standards Solution VI, Certipur). Experimental blanks and filtration system cleanliness checks were also analysed. Typical detection limit for uranium in the ICP-OES was 0.03 mg/L. Instrument paramaters and results for the analysis of standard reference materials are detailed in the appendix (section 11.1.2).

ICP-MS

Analysis of uranium concentrations in permeate samples was carried out using Inductively Coupled Plasma – Mass Spectrometry (ICP-MS, Agilent 7500ce), allowing determination of solution concentrations as low as 0.01 µg/L. The concentrations of a wide range of elements in the natural waters in Chapter 8, were also determined with ICP-MS. Calibration standards spanning the concentration range 0.1 -100 µg/L (with more standards in the lower concentration end) were prepared using single and multi-element standards from Merck. Again check standards were inserted at least every 10 samples to control for instrument drift, while accuracy of the calibration was determined by analysing a certified reference solution (ICP Multi Element Standards Solution VI, Certipur) and a reference water (SRM 1640). Instrument settings are detailed in the appendix (section 11.1.3).

3.1.7 Anion determination using IC

Anion concentrations of the water collected during the Ghana field trip (Chapter 8) were analysed using an DX-500 ion chromatograph (DIONEX, USA). Separation was achieved using an IonPac AS4A-5C analytical column and a mobile phase composed of 1.7 mM sodium bicarbonate/1.8 mM sodium carbonate delivered at a flow rate of 2 mL/min. An anion self-regenerating suppressor (ASRS-1) operated at a current of 50 mA was used for post-column eluent suppression. Detection was via an ED40 electrochemical detector set at an output range of 30 µS. PeakNet software was

used to control the instrument and collect the analysis results. Calibration standards were prepared using DIW to concentration of 1, 5, 10 and 25 mg/L. Check standards were inserted approximately every ten samples. Samples were diluted with DIW and re-analysed when necessary.

3.1.8 Speciation Modelling tool –Visual Minteq 2.53

Visual Minteq 2.53 (KTH, Stockholm, Sweden) was used for the speciation predictions for uranium and other relevant elements for Chapters 4, 5, 6 and 7. Visual Minteq 2.53 was updated in October 2007, and includes a major review on thermodynamic data on uranium. This is based on the database used in MinteqA2 (Allison et al., 1991) which incorporated thermodynamic data from Grenthe et al. (Grenthe et al., 1992), but has since been revised by Guillaumont et al. (Guillaumont et al., 2003), and is now the accepted OECD-NEA (Organisation for Economic Development – Nuclear Energy Agency) database. Elemental concentration data for each pH value were entered for an initial model calculation to give the most important species with respect to complexation. Elemental oxidation states of the elements were selected according to general groundwater conditions (Langmuir, 1997) and consultation of phase diagrams. The speciation across pH was then carried out by doing a sweep test on the selected species. The temperature was set to 25°C and the CO_2 pressure was set to atmospheric pressure (partial pressure 3.9×10^{-4} bar) as both the groundwater in Chapter 4 and the experimental solutions in Chapters 5-7 were in contact with air. As explained in the introduction (section 2.1.3), the speciation varies according to solution composition, available ligands, pH etc. The speciation was predicted for each specific solution investigated in each chapter. These will vary according to composition of the water, which is why the groundwater in Chapter 4 will have a different speciation to the experimental uranium solutions prepared in the lab with no additional ions, with OM and with calcium, respectively.

4 Impact of pH on uranium removal from groundwater using a UF-NF/RO system

4.1 Introduction

Groundwater in parts of Australia contains high concentrations of inorganic salts, making it brackish. Moreover uranium concentrations can be high in *e.g.* northern and central Australia, where concentrations of up to 400 µg/L uranium have been measured (Payne et al., 2001; Banasiak and Schäfer, 2009). Many Australian communities and farms are located in remote locations where there is a combination of brackish groundwater, a lack of infrastructure but an abundance of sunlight. For these reasons, a mobile filtration system using UF and NF/RO membranes and powered by solar energy was designed by Schäfer and Richards et al. (2007). This system was trialled in remote locations in the Northern Territory, central Australia for several weeks. One UF and four different NF/RO membranes were tested during the experiments where the pH of the groundwater was varied over the range 3-11. Experiments were also carried out where the energy was allowed to fluctuate according to solar availability, while the pH was not adjusted but remained that of the natural water. Determination of the groundwater composition before filtration as well as analysis of the solutions generated by the filtration process was carried out in Australia by Henri Wong at Australian Nuclear Science and Technology Organisation (ANSTO) and the data provided forms the basis for this chapter of my thesis. My role was to collate and interpret the data, as well as analyse some additional samples that weren't analysed in Australia, with particular focus on the effect of pH on uranium removal from the groundwater by the filtration system. Thus the aim of this analysis was, using a UF-NF/RO system, to 1) determine the effect of pH variation (3-11) on uranium removal and 2) investigate the impact of natural energy variation on uranium removal.

4.2 Materials and methods

During the trials, experiments were conducted at constant energy supply (using a generator) to study the effects caused by varying pH. Since the system is meant to operate using solar energy and does not use batteries for energy storage, any energy fluctuations caused by the variation in the natural energy supply would result in variations in operating flow and pressure. Therefore, solar experiments were also carried out to investigate system behaviour with fluctuating energy.

4.2.1 Solar powered membrane system

Details of the solar-powered hybrid membrane system (submerged UF and NF/RO) have been published by Schäfer et al. (2007); however, a flow diagram of the membrane set-up is shown in Figure 18. The UF modules were immersed in the groundwater to be treated which was contained in a 300 L feed tank. The water was drawn through the UF membranes at a pressure of ~ -0.5 bar, after which it was pressured through the NF/RO modules (four inch). The NF/RO feed pressure was set to 9 bar and the feed flow to 400 L/h. The UF membranes used for both pH and solar experiments were Zenon ZW10 (GE Water and Process Technologies), six modules in parallel with a total surface area of 5.58 m^2 (Schäfer et al., 2007) and a nominal pore size of 0.04 µm in diameter. The NF and RO membranes were exchanged for different experiments, as described in the following sections.

4.2.2 Groundwater chemistry: pH experiments

Experiments to investigate the effect of pH on trace contaminant retention were performed with constant energy supply over the pH range 3-11 The wide pH range was selected to make results relevant to a wider range of water conditions than just the prevailing local ones. In this chapter, the results for five such pH experiments carried out at two locations in the Northern Territory in Australia will be presented: 1) BW30 RO membrane at Ti Tree Farm 2) NF90 NF membrane at Pine Hill 3) ESPA4 RO membrane at Pine Hill 4) TFC-S NF membrane at Pine Hill and 5) BW30 RO membrane at Pine Hill (Table 6).

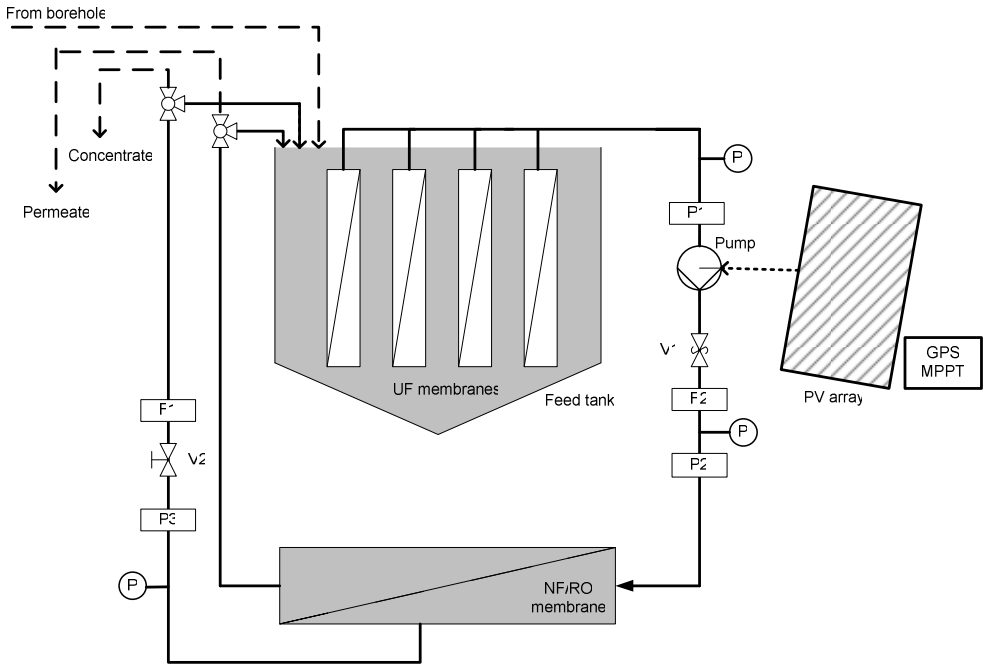

Figure 18. Schematic diagram describing the flow in the membrane system. Large dotted lines represent *continuous* operation, while solid lines represent *batch* operation where water was re-circulated to the feed tank. The schematic shows UF membranes submerged in the feed tank; a positive displacement pump; NF/RO membrane; P = pressure gauges; P1-3 = pressure transducers; F1-2 = flow sensors; V1 = pressure relief valve; V2 = pressure control valve; GPS = solar tracker guided by global positioning system and MPPT = maximum power point tracker. During pH experiments, the pump operated under constant energy supply and the water was re-circulated to the feed tank. During solar experiments the pump was connected to a PV array. During solar *batch* the water was re-circulated, while in the solar *continuous* experiment, the water not re-circulated but the feed tank continuously re-filled from the source (also in Rossiter et al. 2010).

The feed pH was adjusted with NaOH or HCl (analytical grade, Fisher Scientific) to give an incremental pH increase by one unit over the range 3-11 and performance allowed to equilibrate before taking samples (typically 30-60 minutes). Mixing was ensured by air bubbling (Nitto LA80a) for ten minutes before sampling. The temperature remained relatively constant with a variation of between ± 0.3 to 2.5ºC during the individual experiments (Figure 78 in appendix). Samples were taken of the feed, UF permeate, concentrate and NF/RO permeate solutions every 30-60 minutes as parameters such as pH and flow had stabilised. The NF/RO permeate (referred to as "permeate" hereafter) and concentrate solutions were re-circulated back to the feed tank in order to keep a constant feed solution volume and concentration. Conductivity, pH and temperature measurements (Multiline P4

millimetre, WTW) were taken as feed, permeate and concentrate samples were collected.

Table 6. Overview of membrane type, typical retention and test conditions according to manufacturer product information (Dow Product Information, ; Dow Product Information, ; Hydranautics, ; Koch Membrane Systems)

Membrane	Type	NaCl retention	$MgSO_4$ retention	Material[a]	Supplier	Test conditions[b]
Zenon Zw10	UF	-	-	PVDF	GE Water and Process Technologies	
NF90	NF	-	95%	PA TFC	Filmtec	2000 mg/L 4.8 bar
TFC-S	NF	> 80%	99%	PA TFC with PS support	Koch Membrane Systems	1000 mg/L 5.5 bar,
ESPA4	RO	99.2	-	Composite PA	Hydra-nautics	500 mg/L, 6.9 bar,
BW30	RO	> 99.5%	-	PA TFC	Filmtec	2000 mg/L, 15.5 bar,

[a]TFC: thin film composite; PA: polyamide; PS: polysulphone

[b]All at 25°C and 15% recovery

4.2.3 Solar energy experiments

Experiments were conducted as described by Richards et al. (2008) to investigate performance of the system in terms of producing good quality drinking water under natural energy variation. A solar *batch* experiment was conducted at Pine Hill using a BW30 membrane. In *batch* experiments, the permeate and concentrate solutions were re-circulated back to the feed tank for the duration of the experiment (Figure 18). A solar *continuous* experiment was conducted at Pine Hill again using the BW30 membrane. For *continuous* experiments, the water was not re-circulated but the feed tank was instead continuously re-filled from the groundwater source. In both the solar *batch* and *continuous* experiments, the pressure increased with solar radiance, starting at 4 bar and stabilising at ~11 bar once the radiance reached its maximum, while the feed flow stabilised to ~400 L/h (Figure 79 in appendix). Samples were taken at least hourly and the experiment conducted throughout the solar day (12 hours). Conductivity and temperature (WTW Multiline P4) were monitored over 5 second intervals using a datalogger (DataTaker DT500). The

information from flow sensors was also logged although, as the flow surpassed sensor operating range, this had to be done manually using volumetric cylinders (2 L) and stopwatches (as detailed in Schäfer et al. 2007).

4.2.4 Chemical analysis

Samples were filtered and a portion was acidified with HNO_3 (1% v/v, sub-boiled) for cation analysis. A further portion was kept un-acidified for anion analysis. Samples from the pH experiments were analysed by ANSTO and were spiked with cesium (final concentration of 4000 mg/L) to suppress ionisation during analysis by ICP-AES (Varian Vista AX simultaneous CCD). Samples for ICP-MS (Agilent 4500) were spiked with internal standards, indium, yttrium, lithium, scandium, lutetium, bismuth and rhodium, which were used to correct for variations in instrument sensitivity across the mass range of interest. Anions were analysed by IC (Dionex DX-600 with EG40 Eluent Generator) by ANSTO. For the solar experiments the trace elements were analysed at the University of Edinburgh using ICP-MS (Agilent 7500ce) (as described in section 3.1.6).

4.2.5 Speciation modelling of groundwater

Uranium speciation was predicted using the speciation software Visual Minteq 2.53 (as described in section 4.2.5). Elemental oxidation states of the elements were selected according to general groundwater conditions (Langmuir, 1997) and consultation of Pourbaix diagrams. The speciation was then carried out by doing a sweep test on the selected species. The temperature was set to 25°C and the CO_2 pressure was set to atmospheric pressure (partial pressure 3.9×10^{-4} bar) as the groundwater was in contact with air during the experiments. The resulting charge difference in the anion and cation balance was 5.5% for Ti Tree Farm and 3.9% for Pine Hill. Since redox conditions were not measured, the influence of reducing or oxidising conditions based on an expected range of E_h values for these waters, was also tested using Visual Minteq 2.53; there was no change, however, in the predicted uranium speciation as E_h was varied over this range.

4.2.6 Membrane performance modelling

RoPro 7.0 software (Koch Membrane Systems) was used to simulate the effect of dynamic processes occurring in the filtration system on solution speciation and membrane performance under the given experimental conditions for both pH and the solar *continuous* experiments (there was not an option to simulate re-circulating systems). The water quality parameters found for Ti Tree Farm and Pine Hill (Table 7) were entered into the model. The single-pass design option (Figure 19) was selected and the parameters entered were: feed composition, pH, water type (brackish well water), inlet pressure (8.7 bar for pH experiments, while the solar *continuous* experiment varied from 4-11 bar) and membrane information (1 pressure vessel, 1 element). Chemical composition of permeate and concentrate streams, as well as calculation of the saturation index (SI) of five compounds ($CaSO_4$, $BaSO_4$, $SrSO_4$, CaF_2 and SiO_2) were then calculated as a function of flow and pressure. As the software only includes Koch membranes, simulations were performed for the TFC-S NF membrane and TSC-XR (as a proxy for the RO membrane, BW30 as they are both RO membranes and have comparable rejection and permeability).

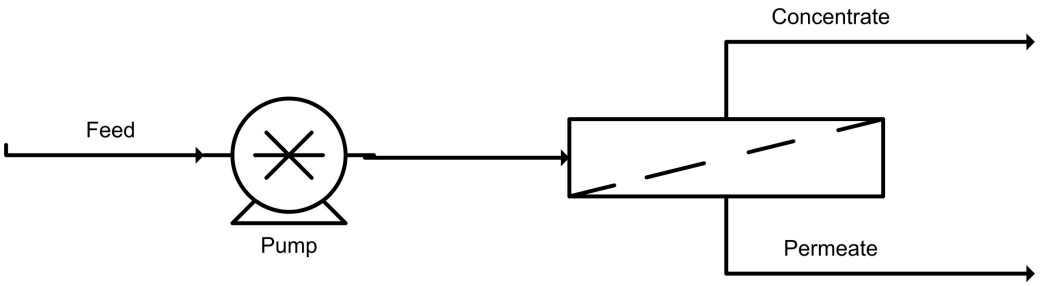

Figure 19. Schematic showing single pass design option in RoPro.

4.3 Results and discussion

For groundwater samples collected at the start of the filtration trials, the concentration of uranium was 25 µg/L for the Ti Tree Farm borehole (only one sample collected) and ~295 µg/L at the Pine Hill station (average of four samples taken on different days with a standard deviation of ± 33 µg/L). These values are both above the Australian Drinking Water Guideline (ADWG) and the WHO

guideline values for uranium, which are 20 and 15 µg/L, respectively, and correspond well with the high uranium concentrations expected in that area.

Table 7. Elemental composition of groundwater in Australian field trial sites.

Element	Unit	Ti Tree Farm	Pine Hill Station	ADWG
Aluminium	mg/L	0.107	< 0.01	0.2[a]
Arsenic	mg/L	0.003	0.005	0.007
Barium	mg/L	0.040	0.016	0.7
Beryllium	mg/L	< 0.001	<0.001	-
Bromide	mg/L	1.000	< 10	-
Calcium	mg/L	30.374	60.09	-
Chloride	mg/L	436.90	1999	250[a]
Chromium	mg/L	< 0.001	< 0.001	0.05
Copper	mg/L	0.0956	0.021	2
Fluoride	mg/L	< 1	< 10	1.5
Iron	mg/L	0.055	0.225	0.3[a]
Lead	mg/L	0.005	0.004	0.01
Lithium	mg/L	0.007	0.060	-
Magnesium	mg/L	38.096	149.4	-
Manganese	mg/L	0.002	0.007	0.5
Molybdenum	mg/L	< 0.001	0.005	0.05
Nickel	mg/L	0.005	0.003	0.02
Nitrate	mg/L	58.428	19.0	50
Nitrite	mg/L	< 1	< 10	3
Phosphate	mg/L	< 1	< 10	-
Potassium	mg/L	26.017	15.39	-
Selenium	mg/L	0.0037	0.015	0.01
Sodium	mg/L	173.297	1651	180[a]
Strontium	mg/L	0.475	1.296	-
Sulfur	mg/L	33.187	271.6	-
Sulphate	mg/L	116.338	889.3	500
Titanium	mg/L	< 0.001	< 0.001	-
Uranium	mg/L	0.0247	0.295	0.02
Vanadium	mg/L	0.0009	0.022	-
Zink	mg/L	0.0008	0.222	3[a]
TDS	mg/L			500[a]
Conductivity (EC)	µS/cm			780

[a]guideline based on aesthetic considerations such as taste or colour.
Note that values listed as "<" are below the detection limit of the technique used.

4.3.1 Retention of monovalent and divalent ions

Due to the brackish nature of the water, there was a relatively high concentration of sodium, chloride and sulphate, especially in the Pine Hill water (Table 7). To get an indication of the performance of the NF/RO membranes, the retention of major ions present in the groundwater (Cl^-, K^+, Na^+, Ca^{2+}, Mg^{2+} and SO_4^{2-}) was calculated according to Equation 1 for each pH value across the experimental range (3-11). As

expected, there were differences between retention of mono (Cl^-, K^+ and Na^+) and divalent (Ca^{2+}, Mg^{2+} and SO_4^{2-}) ions but there were also differences between the results for different membranes (Figure 20).

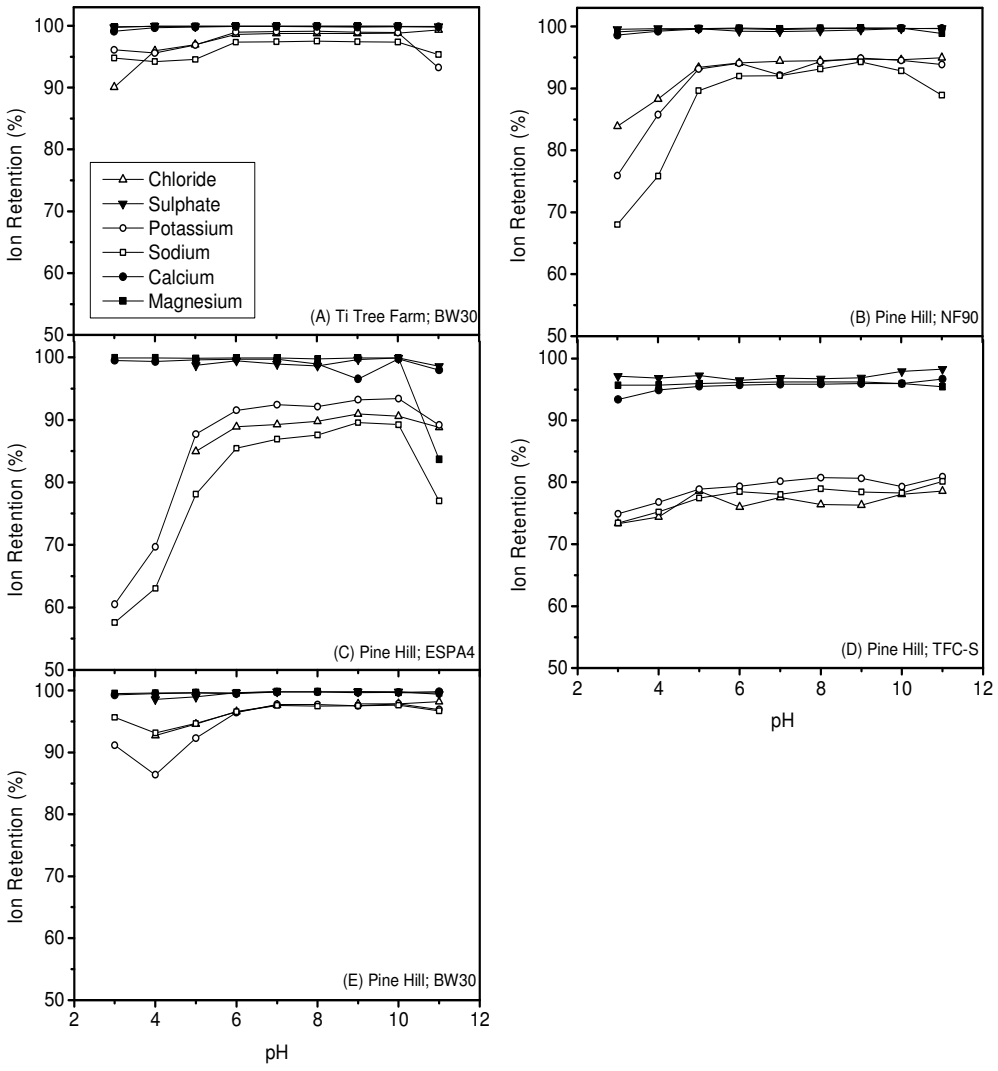

Figure 20. Retention of important salt ions for A) BW30 (Ti Tree Farm), B) NF90, C) ESPA4 D) TFC-S and E) BW30 (all Pine Hill). Full symbols are divalent ions (SO_4^{2-}, Ca^{2+} and Mg^{2+}) while open symbols are monovalent ions (Na^+, K^+ and Cl^-) (adapted from Rossiter et al. 2010).

In general, the lowest retention of both monovalent and divalent ions was obtained for the TFC-S membrane (NF): 73-81% and 93-98% for monovalent and divalent ions, respectively (Figure 20D), while the highest retention was achieved using the

BW30 membrane (RO): 90-99% and >99% for monovalent and divalent ions, respectively (Figure 20A and E). For the operating conditions employed, a Na^+ and Cl^- retention of about 96% would be expected, however, the retention varied between 93-98%. The lower retention is attributed to some deterioration due to age/use of the membrane as noticed also by Park et al. (2011). As discussed in setion 2.2.1, the transition between NF and RO is gradual and, in this case, resulted in ESPA4 (RO) and NF90 (NF) having very similar retention values (Figure 20B and C). The retention of divalent ions (Ca^{2+}, Mg^{2+} and SO_4^{2-}) was fairly consistent across the pH range for all membranes. The retention of monovalent ions (Cl^-, K^+ and Na^+), however, was much lower at acidic pH compared to neutral and alkaline pH. This trend was especially notable for the membranes NF90 and ESPA-4 (Figure 20B and C) where retention increased by about 20-30% from pH 3 to pH 6. This can be explained by the transport mechanisms that operate during NF. The ion transport mechanisms for non-porous RO membranes are described by solution-diffusion processes, while in the looser NF membranes size-exclusion and charge effects play an important role (Wijmans and Baker, 1995; Van der Bruggen and Vandecasteele, 2003; Schäfer et al., 2005). Membrane charge is affected by solution pH (Childress and Elimelech, 1996), where the negative membrane charge and the electrical double layer is reduced at acidic pH, thus allowing easier passage of charged solutes (Braghetta et al., 1997). As well as lower charge, monovalent ions have a smaller hydrated radius compared to divalent ions, and are therefore less well retained. This effect was less pronounced for the tighter RO membrane (BW30) and also the more open NF membrane TFC-S. For the latter, the retention of monovalent ions was only ~75-80% across the entire pH range, presumably since the pore size is significantly different compared to the ion size and therefore the retention is not affected by a change in membrane charge taking place within the membrane pore structure.

In contrast with major cations and anions shown in Figure 20, the results for the retention of uranium by the different membranes were somewhat erratic (Figure 21). There was a decrease in uranium retention at pH 6-7 and 10-11 for BW30 at Ti Tree Farm and a decrease at pH 8 and 10-11 for Pine Hill. This was, however, due to a concentration decrease of uranium in the feed solution rather than an increase in the

permeate solution. Since the retention decrease did not reflect an increase in permeate concentration and as such could be misleading, results will be presented as uranium concentrations of the feed, UF permeate, concentrate and NF/RO solutions as a function of pH (Figure 22). Based on those results, the behaviour of uranium will be explained in more detail.

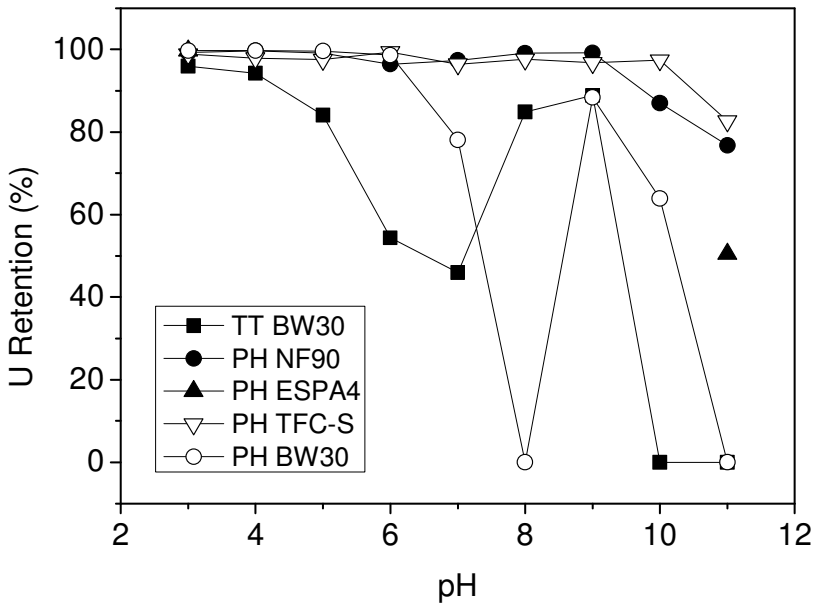

Figure 21. Uranium retention with across the pH range 3-11 for BW30 at Ti Tree Farm (TT) and NF90, ESPA4, TFC-S and BW30 at Pine Hill (PH) (Figure also published in Rossiter et al. (2010a) supporting information).

4.3.2 Impact of pH on uranium concentration in the filtration solutions

First of all it is interesting and important to note that the uranium concentrations decreased after NF/RO filtration from an initial feed concentration of 25 µg/L in Ti Tree Farm and 289-367 µg/L at Pine Hill Station to <1 µg/L in the permeate solutions for all membranes, except for TFC-S where a value of 7 µg/L or less was achieved across the pH range (Figure 22). In all cases the permeate uranium concentrations in the resulting permeate solutions complied with WHO and ADWG drinking water guidelines.

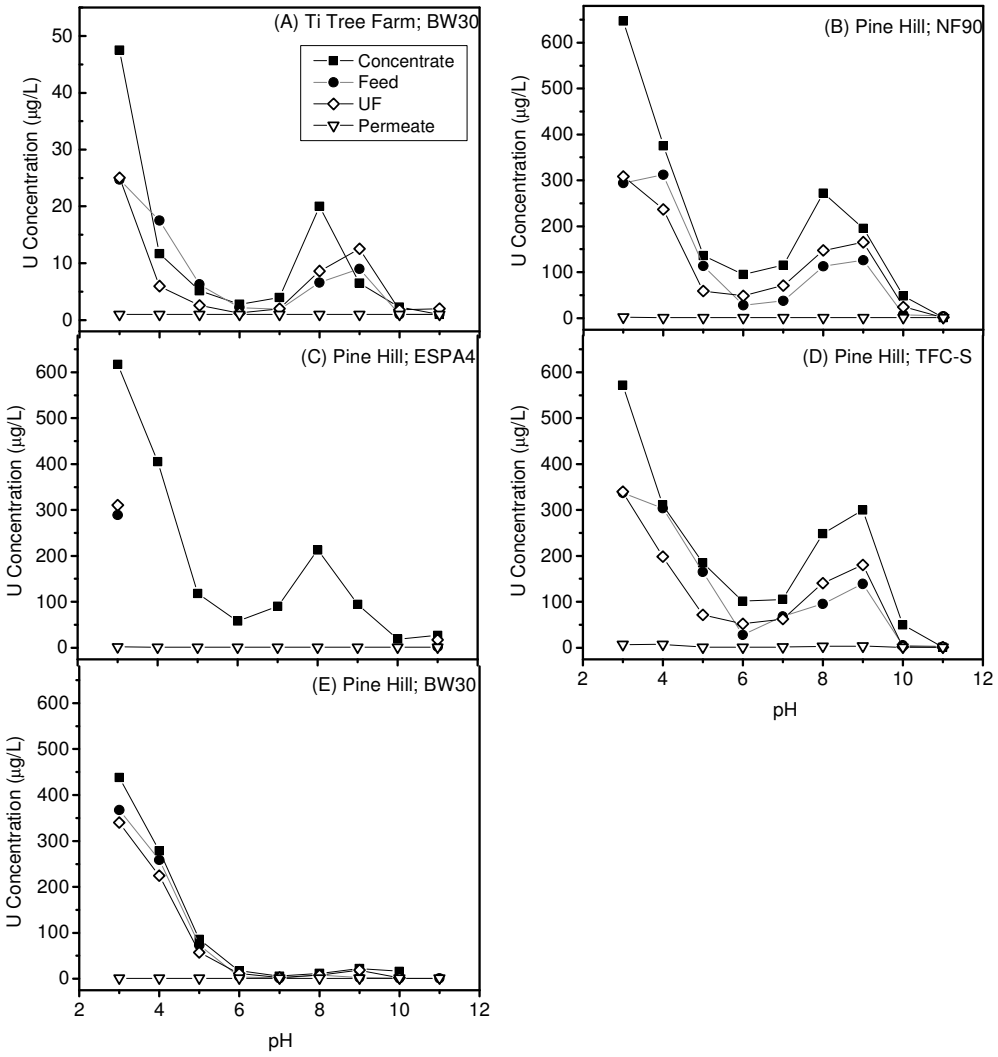

Figure 22. Uranium concentration as a function of pH in feed, UF permeate, NF/RO permeate and concentrate using four different membranes A) BW30 (Ti Tree Farm), B) NF90, C) ESPA4, D) TFC-S and E) BW30 (all Pine Hill). Note the different scale for Ti Tree Farm due to lower uranium concentration (adapted from Rossiter et al. (2010a)).

The feed concentrations were expected to remain constant due to the recirculation of permeate and concentrate solutions. However, uranium behaved very differently to this expectation and the concentration decreased in feed, UF permeate and concentrate at pH 4-7 in all experiments (Figure 22). This surprising behaviour indicated that uranium was either adsorbing or precipitating onto the membrane at these pH values. Note that it is not possible to determine whether the up-take of uranium occurred to the UF or NF/RO membranes or both. Between pH 7-10 the uranium concentration increased again in the feed, concentrate and UF permeate

solutions (except for BW30 at Pine Hill where the concentrations remained low), while at pH 10 and 11 the concentration again decreased markedly. A similar decrease in solution concentration was observed for some other elements such as manganese, vanadium, nickel, zinc, copper and magnesium at pH 10 (published in Richards et al. (2011)). To gain better understanding of the underlying reasons for this behaviour the following section explores the speciation of uranium at different pH.

4.3.3 Speciation of uranium and groundwater chemistry

The results from the speciation calculation for uranium performed using Visual Minteq 2.53 are displayed in Figure 23A and B for Ti Tree Farm and Pine Hill, respectively. The speciation calculation was also performed for calcium and magnesium, the two major divalent cations present in these water samples, and is presented in Figure 23E and F. The uranium mass adsorbed (or taken up by the membrane) during the pH experiments was calculated according to Equation 7. The mass adsorbed, expressed as percentage of the initial feed solution, is given in Figure 23C and D.

$$M_{ads} = V_{f0}C_{f0} - V_{fF}C_{fF} - V_pC_p - V_cC_c \qquad \text{Equation 7}$$

Where M_{ads} is the mass adsorbed (mg), V is the volume (L), C is the element concentration (mg/L), and the subscripts f, c and p stand for feed, concentrate and permeate, respectively. Final and initial values are indicated by subscripts F and 0, respectively.

As the pH increased from 3 to 11, the major species of uranium predicted by Visual Minteq 2.53 were UO_2SO_4, UO_2OH^+, UO_2CO_3, $(UO_2)_2CO_3(OH)_3^-$, $Ca_2UO_2(CO_3)_3$ and $UO_2(CO_3)_3^{4-}$ (Figure 23A and B). To evaluate whether these speciation results could explain the variation in uranium up-take to the membrane, literature data was used to compare species solubilities and stability in aqueous solutions. Then the resulting interpretation was compared with observations about removal of uranium

from solution made in other studies. While relatively few experimental data regarding the solubility products of the above listed species have been published and are hard to determine (Gorman-Lewis et al., 2008), especially as the solubility is highly influenced by any other ions present in the solution, a comparison of log K values (stability constants) could be made (Grenthe et al., 1992; Langmuir, 1997; Payne, 1999).

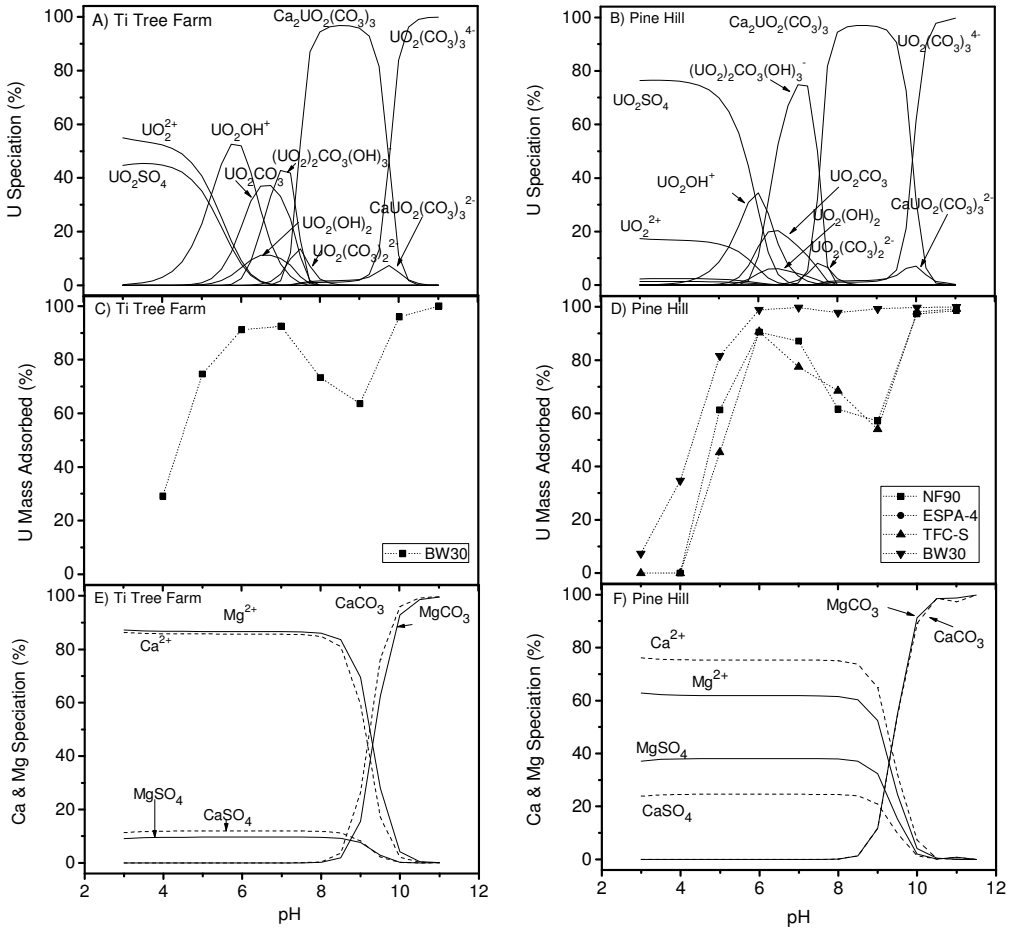

Figure 23. Uranium, magnesium and calcium species (aqueous) predicted using Visual Minteq 2.53 in Ti Tree Farm (A, E) and Pine Hill waters (B, F). Uranium mass adsorbed is displayed in graph C and D (Figure also published in Rossiter et al. (2010a)).

The species are displayed below in increasing order of stability in solution, thus with increased likelihood of remaining in solution rather than forming a complex with another ligand or adsorbing to the membrane:

$UO_2OH^+ < (UO_2)_2CO_3(OH)_3^- < UO_2SO_4 < UO_2CO_3 < UO_2(CO_3)_3^{4-} < Ca_2UO_2(CO_3)_3$

At pH 3, the most acidic in the trial range, uranyl sulphate was predominant at both sites. In the Ti Tree Farm water it constituted about 45% and in the Pine Hill water it was about 78% of the total uranium species. Several other studies have similarly found UO_2SO_4 as the dominant species at low pH in waters with high sulphate content (Winde and van der Walt, 2004; Baeza et al., 2006). Uranyl sulphate complexes are relatively stable in solution, which was reflected in a low mass of uranium adsorbed at pH 3 (Figure 23C and D).

At pH 4.5, the proportion of the uranyl sulphate and of the uranyl ion decreased while that of UO_2OH^+ increased. The latter was predominant between pH 5.5 and 6.5. This falls within the pH range where the first concentration decrease of uranium in the filtration solutions occurred, indicating membrane up-take of uranium. At pH 5, the mass of uranium adsorbed varied amongst the membrane types from 45% mass adsorbed for TFC-S to 82% mass adsorbed for the RO membrane BW30. For all membranes, the mass adsorbed increased to 90%-99% at pH 6. As discussed in section 2.1.6, several other studies have shown that uranium is easily adsorbed onto different materials or immobilised at pH 5-6 (Pabalan and Turner, 1997; Baeza et al., 2006) and some also implicated UO_2OH^+ in the removal processes (Sutton et al., 2003). Since UO_2OH^+ is the least stable of the uranium species, it is not surprising that it shows high mass adsorbed. The adsorption may also be due to charge interactions, as the membranes are known to have a negative charge above pH 5 (Tang et al., 2007), which would attract the positively charged uranium species.

At pH 8-9.5, $Ca_2UO_2(CO_3)_3$ was the dominant uranium species predicted by Visual Minteq 2.53. At this point uranium was again detected in the feed, UF permeate and concentrate solutions, although not to the same extent as in the original solution. The mass adsorbed was calculated to be between 54-68% for all membranes except for BW30 at Pine Hill where it was higher. The lower extent of removal from solution in comparison with that observed at pH 6 can be attributed to some extent to the much

greater stability of $Ca_2UO_2(CO_3)_3$ compared with $UO_2(OH)^+$. The influence of calcium on uranium speciation has also been recognised by other investigators (Tsushima et al., 2002) and uranium is often found in association with calcium in natural waters (Elless and Lee, 1998). In addition, dissolved calcium and magnesium species have been shown to decrease uranium adsorption to minerals at neutral-alkaline pH (Fox et al., 2006). For example, Winde et al. (Winde and van der Walt, 2004) attributed the mobility of uranium in sediments to the presence of negatively charged or neutral calcium uranium carbonate complexes which do not adsorb onto negatively charged sediment surfaces. In this study, it is proposed that as $Ca_2UO_2(CO_3)_3$ is a neutral species, it would not be electrostatically attracted to a negative membrane and this resulted in the lower mass adsorbed at pH 8-9.5 compared with pH 6.

At pH 10, only low concentrations of uranium were detected (<8 mg/L in the feed solutions and <50 mg/L for the concentrate solutions) and the mass balance showed that 95-100% of the uranium was taken up by all membranes (Figure 23C and D). At this pH, the highly soluble and stable $UO_2(CO_3)_3^{4-}$ complex was predicted to dominate the solution phase speciation of uranium (Figure 23A and B). At such a high pH, the membranes possess a strong negative charge and so electrostatic attraction cannot explain the uranium up-take by the membrane. Instead, it was considered that other solution phase components may be involved. For example, it has been found that that $UO_2(CO_3)_3^{4-}$ adsorbed to hydrous ferric oxides at pH 9 under oxic conditions (Giblin et al., 1981). In this study, however, less than 0.2 mg/L of iron was present in Pine Hill and Ti Tree waters, and so it is unlikely that iron oxide coatings/precipitates on the membrane surface could account for the sorption at pH 10. Other solution components included the conservative ions, calcium and magnesium; high concentrations of calcium and magnesium (up to 60 and 150 mg/L, respectively) were found in both water samples and magnesium did show similar removal from solution at pH 11 in the experiments, although only a slight decrease in calcium was observed. Since calcium and magnesium precipitates have been found to remove uranium from solution at pH > 10 it is postulated that this process accounts for the observed experimental results (Chellam and Clifford, 2002; Baeza et

al., 2006)). From the predictive speciation for these two cations in Ti Tree Farm and Pine Hill Station water, aqueous $CaCO_3$ and $MgCO_3$ formed at pH 10, whilst at lower pH, the (soluble) free ions dominated (Figure 23E and F). $CaCO_3$ and $MgCO_3$ have very low solubility (Ksp = 3.36×10^{-9} for calcite and 6.82×10^{-6} respectively) and $CaCO_3$ in the form of calcite is well-known to cause membrane scaling (Schäfer et al., 1998). At the concentrations present in the two groundwaters, calcium and magnesium exceed the saturation limit for $CaCO_3$ and $MgCO_3$, respectively and $UO_2(CO_3)_3^{4-}$ is likely to co-precipitate as a consequence. Indeed many of the minerals predicted using Visual Minteq 2.53 reached their saturation limits at pH 10, in particular carbonates containing calcium, magnesium, copper, vanadium and iron. With respect to the formation of new solid phases, it is considered that precipitation of calcium and magnesium is likely to be of greater significance than that of copper, vanadium and iron since the latter group of ions were present only at very low concentrations (all <0.22 mg/L in Pine Hill compared to 60 and 150 mg/L for calcium and magnesium). Importantly, other studies have also shown that uranium forms co-precipitates with calcite (Suksi et al., 1996; Catalano et al., 2006). A filtration study investigating the use of electrodialysis (ED) to purify the Pine Hill water was performed by Banasiak and Schäfer (2009) and similarly found that scaling by calcium, magnesium, potassium and chloride ions occurred on the ED membrane.

To give an indication of the dependence of membrane performance on feed water quality and operating parameters, RoPro 7.0 was used to evaluate the data for the Ti Tree Farm and Pine Hill groundwater and the TFC-S membrane. The model predicted that, for example, $BaSO_4$ would reach saturation in the concentrate stream of both Pine Hill and Ti Tree Farm (SI of 2.14 and 1.80, respectively) at the natural pH of the water (8.4). The chemical speciation software, Visual Minteq 2.53, only calculates the saturation of a compound based on the feed water concentration, while RoPro takes into account the increased concentration at the membrane surface due to concentration polarization. Thus, Visual Minteq 2.53 did not predict $BaSO_4$ to reach saturation in Ti Tree Farm or Pine Hill water based on their initial elemental compositions; however, when running a concentration sweep, it did reach saturation

(SI = 1.54) after a tenfold concentration increase (independent of pH) was simulated. The SI value was similar to that predicted for $BaSO_4$ by RoPro. While RoPro is a helpful tool in predicting precipitation of a few minerals, the speciation and precipitation of other minerals which may form in natural water are not taken into account. Nevertheless, this illustrates the potential of coupling chemical speciation modelling and process simulation tools.

4.3.4 Uranium retention and specific energy consumption with solar energy

Two experiments to test the impact of using solar energy and the subsequent natural energy variation were performed. In the solar *batch* experiment, permeate and concentrate solutions were re-circulated back into the feed tank, while in the solar *continuous* experiment, the feed tank was continuously filled from the borehole while permeate and concentrate solutions were collected in separate containers. This resulted in a constant flow of inorganic contaminants into the system.

The retention of major cations during the *batch* experiment at Pine Hill was high: >99% for major divalent cations (calcium and magnesium), including uranium, and 95-98% for monovalent cations (*e.g.* potassium and sodium) throughout the experiment. During the *continuous* experiment, the retention of major cations was also high: 94-99% for divalent cations and 87-98% for monovalent cations. A full discussion on the retention of the different ions present in Pine Hill and Ti Tree Farm waters has been published by Richards et al. (2011) and so the focus of the remainder of this chapter will be on uranium and calcium only. The amount of uranium in the concentrate decreased over the course of both experiments to about a third of the original value, indicating up-take of uranium by the membrane. There was also a higher uranium concentration in the permeate solution at the end of the experiment, indicating that uranium may be accumulating on the membrane but eventually permeating. As a consequence, during the *continuous* experiment, permeate samples with concentrations as high as 67 µg/L were measured, which exceeds the WHO drinking water guideline of 15 µg/L. Further fundamental bench-scale studies are needed to elucidate the reasons for these observations.

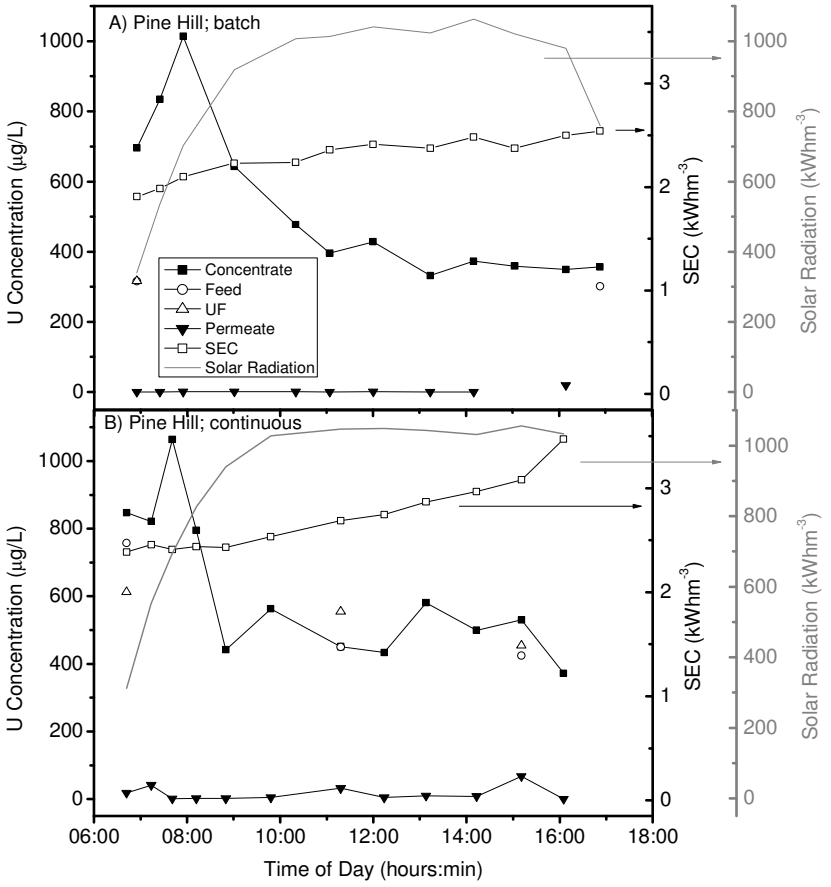

Figure 24. Uranium concentration, specific energy consumption (SEC) and solar radiation for solar *batch* (A) and *continuous* (B) experiments at Pine Hill with BW30 over the course of a day. The pH value of the water during the *batch* experiment was 8.3-8.6, while for the *continuous* experiment it was 7.7-8.2 (Figure also published in Rossiter et al. (2010a)).

The specific energy consumption (SEC) gives a measure of how much energy is needed for the pump to produce the permeate and was calculated from Equation 8 (Schäfer et al., 2007). The less energy required, the more efficient the system.

$$SEC = \frac{I_{pump} U_{pump}}{Q_{permeate}}$$ **Equation 8**

Where I is the current (A), U is the voltage (V) –both of the pump- and Q is permeate flow (L/h). The SEC depends on permeate flow, feed flow (which affects the energy

requirements) pressure and the salinity of the water (which affects the osmotic pressure) (Schäfer et al., 2007). The SEC continuously increased over the course of both the experiments (Figure 24). While pressure and feed flow were relatively constant, the permeate flow decreased towards the end of the experiment. This indicates that the SEC increase was due to fouling of the membrane, as energy demand increased and permeate flow declined (Richards et al., 2008). To determine the amounts of inorganic elements taken up by the membrane for the *batch* and *continuous* experiments, the mass adsorbed by the membrane during the *batch* experiment was calculated using Equation 7. The mass adsorbed during the *continuous* experiment was calculated according to Equation 9, as the sum of each sample set.

$$\mathrm{M}_{\mathrm{ads}} = \sum_{\mathrm{i=1}}^{11} t_i \left(Q_f \cdot c_f - Q_c \cdot c_c - Q_p \cdot c_p\right) \qquad \textbf{Equation 9}$$

Where, t is each time step (1-11) that was sampled (h), Q is flow (L/h), C is the concentration of an element (mg/L), and subscripts as for Equation 7.

The mass balance for calcium in the *batch* experiment showed that a large portion (88%) of calcium had precipitated on the membrane by the end of the experiment, a probable cause of the observed SEC increase. About 2.8 mg (4%) of the uranium originally present in the feed solution had been taken up by the membrane. The mass balance for uranium in the *continuous* experiment showed that the adsorption was higher at about 335 mg or 17% of the total uranium in the feed solution. As mentioned above, the permeate concentration of uranium was also high (up to 67 µg/L) in the *continuous* experiment, indicating that some uranium which had been taken up by the membrane was possibly diffusing through the membrane or being displaced by other ions. The uranium retention decreased over the course of the experiment from 98% to 84%. Concentration polarisation may enhance this effect (Schäfer et al., 2005) due to a concentration gradient at the membrane surface, causing diffusion of ions to the dilute permeate side. It should be pointed out that other ions (including monovalent ones) did not show increased permeation and

therefore it was unlikely to be due to membrane damage. The pH values of the feed water during the *batch* and *continuous* experiments were 8.3-8.6 and 7.7-8.2 respectively. The main uranium species present in this pH range (7.7-8.6) was predicted by Visual Minteq 2.53 to be $Ca_2UO_2(CO_3)_3$ and $(UO_2)_2CO_3(OH)_3^-$ (Figure 23B), and it was shown in the pH experiments that around 60% uranium adsorbed to the membranes at pH 8. This is significantly different to the amount adsorbed during solar experiments and experiments investigating one parameter at a time would be needed to elucidate the reasons for the uranium behaviour. It is possible that more uranium was taken up by the membrane in the solar *continuous* experiments due to slightly lower pH values and consequently the greater proportion of $(UO_2)_2CO_3(OH)_3^-$. Over the course of the experiment some uranium could diffuse through the fouled membrane, leading to the consequent break-through on the permeate side.

4.4 Conclusions

It is difficult to interpret the results and draw definite conclusions based on field experiments using a natural water of such complex chemistry as the one tested in the Australian groundwater. However, several important conclusions could be drawn as a consequence of the work:

1) With respect to uranium removal from groundwater over the pH range 3-11, the system performed well, producing a permeate solution containing uranium concentrations well below the WHO drinking water guideline of 15 µg/L. That is with the exception, however, of the solar *continuous* experiment, where uranium concentrations above the WHO guideline were found in the permeate solution.
2) Depending on pH, uranium was shown to be taken up by the membranes, with high mass adsorbed at pH 5-7 (>90%), somewhat lower at pH 8-9 (>50%) and again high at pH 10-11 (>90%).
3) Visual Minteq 2.53 was a useful tool in predicting the uranium species present across the pH range, leading to explanations for the uranium-membrane interaction occurring at pH 5-7; the behaviour was a consequence

of the low stability of the uranium species as well as charge interactions between the negatively charged membrane and positive uranium species. At pH 8-9 the uranium mass adsorbed was lower due to the stable and neutral $Ca_2UO_2(CO_3)_3$ species.

4) Calcium and magnesium were present in the groundwater as major ions and calcium and magnesium carbonates were predicted using Visual Minteq 2.53 to reach saturation at pH 10-11. This, together with literature-based observations, suggested that the precipitation of calcium and/or magnesium was a likely cause of co-precipitation of uranium at this pH.

There were a number of limitations with the experiments performed and subsequent limitations to interpretation and conclusions, however. These are listed below and should be addressed in controlled laboratory experiments.

1) It was not possible to distinguish whether the up-take of uranium occurred mainly by the UF membrane, the NF/RO membrane or both membrane types. Experiments involving only one membrane type would be needed.
2) It was not possible to definitely determine whether the uranium up-take by the membranes was due solely to uranium-membrane interactions or whether they were a result of the behaviour of other ions (major or minor) present in the solution. To determine this, experiments with only uranium present in solution would be essential.
3) It was also not possible to determine whether the uranium mass adsorbed was due to adsorption through chemical interactions or precipitation due to the accumulation of uranium at the membrane surface as a result of the pressure applied (and resulting concentration polarisation). Experiments without applied pressure compared to experiments over a pressure range would determine this.
4) Also there were substantial differences in the amount of uranium which was taken up by the membrane during the pH experiments and during the solar experiments performed at similar pH value. This could be a consequence of all the pH steps having been performed over the course of one experiment

using the same membrane modules, and thus the uranium mass adsorbed observed at higher pH values may have been an accumulated result from uranium up-take having occurred at lower pH values. It would be important to do separate pH experiments to isolate the effects of individual pH values.

5) Although the retention was generally strong of both mono and multi-valent ions, the retention of Na^+ and Cl^- for BW30 was somewhat lower than expected, which indicates that the membrane may have been aged. This limits the conclusiveness of the results obtained and laboratory experiments using new membrane sheets are needed.
6) Finally, although calcium and/or magnesium were highly likely to cause co-precipitation of uranium at pH 10-11, this could not be conclusively demonstrated from the field trial results and specific experiments are required to prove that this was the case.

5 Impact of pH and organic matter on uranium removal using UF

5.1 Introduction

Ultrafiltration requires less energy compared to NF or RO, making it an attractive process for water treatment in remote locations, especially in developing countries where it is pertinent to keep costs low (Anselme and Jacobs, 1996). As discussed in section 2.2.3, removal of uranium using UF has been demonstrated (Kryvoruchko et al., 2004) and complexation has been shown to increase this removal (Pramauro et al., 1996; Kryvoruchko and Atamanenko, 2007). Natural surface waters often contain dissolved organic matter (OM), and even when present at low concentrations, these tend to dominate the uranium speciation, especially at the acidic to neutral pH range (Kantar, 2007). Considering that OM can be retained by UF to some extent (Anselme and Jacobs, 1996) and has been shown to influence the retention of different metal ions (Sanli and Asman, 2000; Fatin-Rouge et al., 2006), uranium complexed with OM could potentially be retained by UF due to the larger size of U-OM complexes compared to uranium species un-complexed with OM. Moreover, is was demonstrated in Chapter 4 that uranium was removed from solution at certain pH values, although it was not clear whether the decrease in the uranium concentration was due to uranium up-take by the UF membrane or to the NF/RO membranes. The aim of this chapter was therefore to investigate 1) the removal of uranium by UF, 2) the influence of OM complexation with uranium on uranium removal with UF and 3) the occurrence of uranium-membrane interaction with the UF membrane.

For the purpose of this study three types of OM, representative of compounds found in natural waters, were chosen as suitable for further exploration: humic acid (HA), alginic acid (AA) and tannic acid (TA). HA accounts for a large portion of the natural OM extracted from rivers and streams (Bourbonniere and Halderen, 1989). AA was chosen as a representative of polysaccharides present in natural waters (*e.g.* as brown algae (Draget et al., 2002; Davis et al., 2003b)) and wastewater effluents

(Barker and Stuckey, 1999). AA is known to be highly effective in the removal of metals from aqueous solutions (Draget et al., 2002; Davis et al., 2003a; Davis et al., 2003b), including uranium adsorption in waste water treatment (Khani et al., 2006; Khani et al., 2008). In fact the combination of AA with membrane processes has been found to lead to enhanced metal removal (Sanli and Asman, 2000; Fatin-Rouge et al., 2006). TA is a representative of plant polyphenols. Vegetable tannins are plant metabolites readily present in trees (Mueller-Harvey, 2001) and thus found in natural waters. TA is used as a nucleation agent in textiles where it adsorbs/diffuses into the textile and then reduces the metals added, thereby attaching these to the textile structure (Todd, 2000).

5.2 Materials and Methods

5.2.1 UF membrane and set-up

The UF system used was described in detail in section 3.1.3. A GE Zenon ZeeWeed hollow fibre module (ZW1) was used in all the experiments. The nominal pore size of the membrane was 0.04 μm diameter and the membrane surface area was 0.047 m^2. The membrane material is polyvinylidene fluoride (PVDF).

5.2.2 Filtration procedure and cleaning

The feed solution was prepared and pH adjusted 15 to 18 hours prior to the experiment to allow for the uranium and OM to equilibrate. Given that other studies used a much shorter equilibrium time (de la Rosa et al., 2003; Bednar et al., 2007; Khani et al., 2008), this ensured that the solution reached equilibrium well in advance of the experiment. Samples (5 ml) were taken of the feed solution before and after equilibration to confirm that there was no uranium adsorption to the beaker. Conductivity, temperature, pH and trans-membrane pressure were monitored hourly during the experiments, which lasted five hours. The first two parameters remained stable throughout the experiment. When pH changes occurred, online pH adjustments were carried out to keep the pH value within ±0.10 of the selected pH value. Permeate and feed samples (A total of 15 mL for each solution) were collected

hourly for inductively-coupled plasma-optical emission spectroscopy ICP-OES (5 mL) and total organic carbon (TOC) analysis (10 mL). Five pH values were selected for the study, based on initial experiments with both uranium and uranium and OM, showing where the most important changes occurred: pH 3, 5, 7, 10 and 11.

Membrane cleaning was conducted at the end of each experiment. The following protocol was used: DIW backwash (15 min) to remove reversible fouling; nitric acid backwash (0.5% (v/v), 15 min) at pH < 2 to remove any uranium; sodium dodecyl sulfate backwash (15 min, 0.5 g/L, Sigma Aldrich, UK) to remove OM, followed by a commercial bleach backwash (30 min, 1% v/v, Sainsbury's, UK) to further remove OM from the membrane surface. AA was more difficult to remove and a NaOH backwash (20 min, 0.02M) was used in addition to the above. ICP-OES and TOC analysis of the samples collected after the DIW water backwash allowed determination of the mass desposited of uranium and OM corresponding to reversible fouling. The remaining mass adsorbed corresponded to irreversible fouling. The mass adsorbed of uranium and OM to the membrane was quantified by mass balance and was corrected for collected samples as in Equation 6 (section 2.2.2). Representative variation between experiments was calculated by repeating three experiments and taking the standard deviation between them.

5.2.3 Chemicals and reagents

Four different experimental solutions were made (all containing a background electrolyte solution): 1) uranium without OM, 2) uranium with HA, 3) uranium with TA and 4) uranium with AA. The OM was purchased from Sigma Aldrich UK. A concentration of 25 mg C/L was used. The HA had an organic carbon content of 56%, TA of 53.66% and AA of 30%. Uranyl nitrate (TAAB, UK) was added to make up 0.5 mg/L uranium solution. The background electrolyte solution consisted of 1 mM $NaHCO_3$, 0.5 mM $CaCl_2$ and 10 mM NaCl all of analytical grade (Fisher Scientific, UK). To adjust the pH to the required levels 1 M HCl or NaOH were used (analytical grade, Fisher Scientific, UK).

5.2.4 Organic matter properties

The properties of the OM (general overview in Table 8) such as charge, size and functional groups will determine how uranium will form complexes with the OM and what properties the resulting complex would have. As mentioned in 2.2.2, OM properties are highly variable. For instance, HA has an ability to interact with metal ions (Schulten, 1994) as it contains voids which can trap and retain other components (Schulten, 1994). Carboxyl (Schmeide et al., 2003) and phenolic groups (Pompe et al., 2000) present in HA have been found to be important for uranium-HA complexation.

Table 8. Overview of organic matter types used in experiments (Semião et al. 2010)

Compound	Molecular Structure	Molecular Weight (g/mol)	pKa
Alginic Acid (AA)	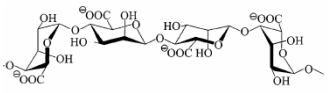	12,000-80,000 (Lee and Elimelech, 2006b)	3.44 (Draget et al., 2002; Davis et al., 2003b)
Humic Acid (HA)	Proposed structure in (Schulten and Schnitzer, 1993)	1000 - >300,000 (Shin et al., 1999)	3.5 - 5.04 (Shin et al., 1999)
Tannic Acid (TA)	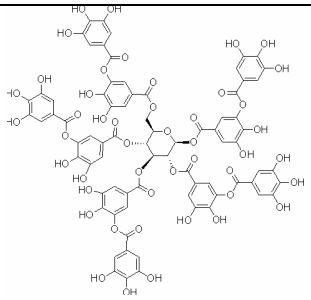	1701	-

AA consists of linear polysaccharides comprising mannuronic and galuronic acid (M and G, respectively) arranged in a non-regular block-wise order (Davis et al., 2003b). M and G block sequences (FMM, FGG and FMG) display different structures and their proportions in the alginate determine the metal binding capacity. The lower the M/G ratio and the higher the FGG content in the alginate, the higher the affinity to bind with metal ions (Davis et al., 2003a; Davis et al., 2003b). TA is a hydrolysable

tannin with a structure consisting of glucose and gallic acid (GA) (Mueller-Harvey, 2001).

5.2.5 Analytical methods

The samples and blanks for uranium analysis were stored in polypropylene centrifuge tubes (15 mL), acidified with nitric acid (Aristar, VWR International, UK) to pH < 2 and analysed with ICP-OES (3.1.6). Samples for TOC determination were stored in capped glass vials (20 mL) at 3-4 °C until they were analysed. TOC was determined using a TOC analyzer (Shimadzu TOC-VCPH, UK) with an ASI autosampler. Analyses were conducted in non-purgeable organic carbon mode (NPOC) used for low concentration samples (see section 11.1.4 for instrument settings).

5.2.6 Solution speciation

Speciation calculations were performed using Visual Minteq 2.53 (as described in 3.1.8). The default database includes a thermodynamic database for uranium and "generic" HA parameters (Gustafsson and van Schaik, 2003). Based on the ion composition of the experimental solutions, the speciation was calculated for each pH value. For HA speciation, the Stockholm Humic Model (SHM) and NICA-Donnan model were both tested and compared to the experimental results showing the HA influence on uranium behaviour. They both predicted HA to dominate the speciation at acidic to neutral pH (also found by (Unsworth et al., 2002)). Based on the correspondence with the experimental results the SHM model was chosen. In general the SHM model assumes that humic acid behaves like gel like spheres with internal charge as well as external. Main binding sites are carboxylic and phenolic groups. There are six parameters for proton binding and equilibrium constants are defined for mono and bi-dentate metal complexation. An overview of the parameters is listed in the Appendix (11.3).

5.3 Results and Discussions

5.3.1 Uranium retention

The filtration of uranium was again investigated over the pH range 3-11 as complex formation between OM and uranium is known to be pH dependent and the resulting changes in uranium speciation will likely affect the interactions between membrane and uranium species. In particular, it was postulated that complex formation would increase retention of uranium by UF. For comparison, the behaviour of uranium in the absence of OM ligand was also investigated. The results showing uranium concentrations in the final feed and permeate solutions by the end of each pH experiment are displayed in Figure 25.

An important finding of this study was that uranium concentration changed in the feed (and permeate) solution with time depending on pH value. For example, at pH 5 and 7 (Figure 25A) uranium feed concentration decreased from 0.5 mg/L to less than 0.1 mg/L at the end of the experiment. This was attributed to membrane deposition or sorption and will be further explained in section 5.3.2.

The results showed that uranium was not retained by the UF membrane (*i.e.* there was no difference between feed and permeate solutions, see Figure 25A) due to the size of uranium species which are much smaller than the membrane pore size (UO_2^{2+} is ~1.8 Å, while the larger $UO_2CO_3^{4-}$ is ~4.5 Å (Duff et al., 2002) (Favre-Reguillion 2003) while the membrane is about 400 Å). The uranium complexes formed with TA and HA were also not retained at any pH value tested (see Figure 25B and D), which indicated that these complexes were smaller than the membrane pore size. An exception was with AA where a difference was observed between the final feed and permeate concentration of uranium (see Figure 26C) and AA. Although AA was not expected to be retained based on its molecular radius of 16.2 nm (Worch, 1993), the final retention of AA ranged from 50 to 80% (data not shown) over the pH range studied. Retention of AA severely affected membrane performance by slowing the pump speed and increasing the transmembrane pressure necessary, which indicated high fouling of the membrane (data not shown) as reported by several authors (Fatin-Rouge et al., 2006; Jermann et al., 2007; Jermann et al., 2009). AA chains can

become interconnected promoting gel network formation (Davis et al., 2003b) thus decreasing membrane flux and effective pore size of the membrane. The high retention of AA was not reflected in the retention of uranium, demonstrating that uranium did not form complexes with AA directly. However the gel network formed by AA may have lead to the smaller increase in uranium retention observed.

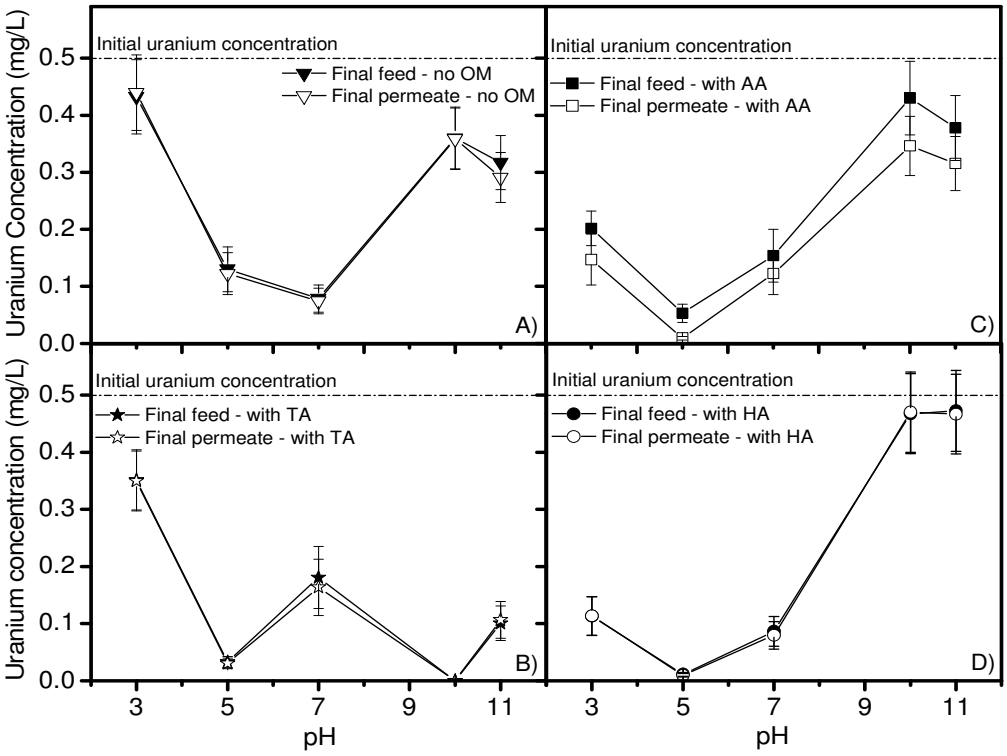

Figure 25. Uranium final feed and permeate concentration with different OM types (at t=5 h). A) without OM, B) TA, C) AA and D) HA. Feed solution: 0.5 mgU/L as $UO_2(NO_3)_2$, 1mM $NaHCO_3$, 0.5 mM $CaCl_2$, 10 mM NaCl, 25 mgC/L OM. All error bars represent the relative error calculated from three repeat experiments (also published in Semião et al. (2010)).

5.3.2 Uranium up-take by the membrane

It was apparent from the concentration results (Figure 25) that uranium was interacting with the membrane during the experiments. The mass adsorbed by the membrane of uranium without the presence of organic matter was calculated and displayed in Figure 26 along with the speciation of uranium for the experimental solution. The uranium speciation is similar to that of the groundwater tested in

Chapter 4, with the main exception of the absence of sulphate complexes. The main uranium species predicted for the experimental solution over the pH range (3-11) were UO_2^{2+}, UO_2OH^+, UO_2CO_3, $Ca_2UO_2(CO_3)_3$ and $UO_2(CO_3)_3^{4-}$ (Figure 26).

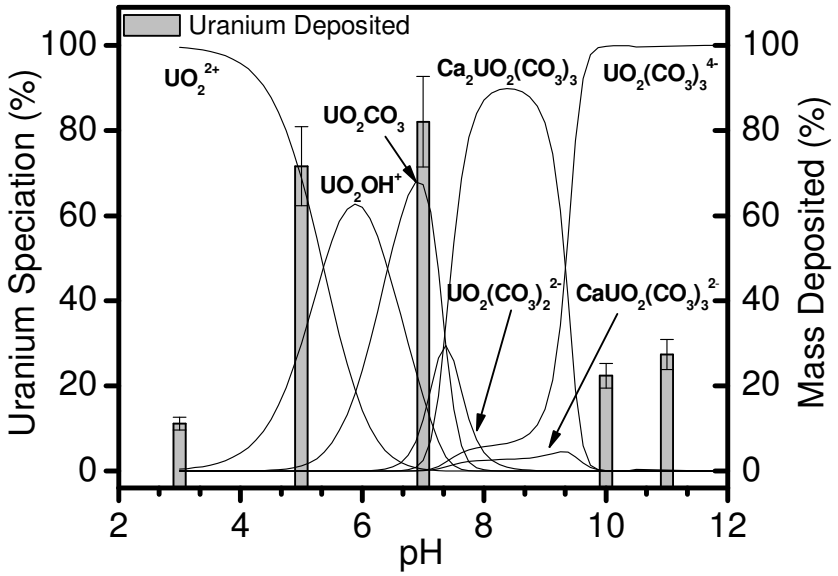

Figure 26 Uranium mass adsorbed to the membrane (at t=5h) and uranium speciation in absence of OM as a function of pH. Feed solution: 0.5 mgU/L as $UO_2(NO_3)_2$, 1mM $NaHCO_3$, 0.5 mM $CaCl_2$, 10 mM NaCl (also published in Semião et al. (2010)).

From the mass balance it was apparent that 70-80% of the uranium was taken up by the membrane at pH 5 and 7 (Figure 26). Uranium up-take to the membrane could be explained by the characteristics of different species formed. While at pH 3-5, UO_2^{2+} is stable in solution, several other studies confirm significant adsorption of uranium around pH 5-7 as UO_2OH^+ starts to dominate, on a variety of media including natural subsurface media (Barnett et al., 2000), polypropylene, Teflon and polycarbonate containers (Payne, 1999) and silica-based materials. The authors explain the sorption mainly through ion exchange of the positive UO_2OH^+ species with a negative surface at pH 5 and below, while at higher pH uranium is likely to sorb through OH-ligand exchange and complex formation (Prikryl et al., 2001; Sutton et al., 2003). Giblin et al. confirmed that adsorption occurred more easily for UO_2OH^+ compared to UO_2^{2+} (Giblin et al., 1981). This was due to surrounding water molecules being less attracted to UO_2OH^+, allowing it to bind to the surface of the studied material (kaolinite).

The log K values (stability constants) also indicate how stable a species is in solution. UO_2OH^+ has the lowest log K value (-5.25), compared to other species predicted. At pH 7 where adsorption to the membrane prevailed, UO_2CO_3 was predicted to dominate. This species is highly polar and the uranium atom possesses a net positive charge (Majumdar et al., 2003), and could thus adsorb to the membrane by electrostatic attraction. At pH 8-11 $Ca_2UO_2(CO_3)_3$ and $UO_2(CO_3)_3^{4-}$ dominated. These are generally soluble in water (Duff and Amrhein, 1996; Langmuir, 1997; Winde and van der Walt, 2004) and therefore only low uranium-membrane interaction was observed at alkaline pH. Although uranium interacted with the membrane over part of the pH range studied this did not appear to affect membrane performance. The uranium species taken up by the membrane were too small to cause any decrease to the permeate flux. The possibility of uranium up-take by the membrane affecting performance over a prolonged period of time was not investigated.

5.3.3 Influence of organic matter on uranium membrane up-take

The results for the mass adsorbed of uranium in the presence of TA, AA and HA are displayed in Figure 27 along with the mass adsorbed for the OM at each pH experiment. The portion of reversible versus irreversible OM is also given.

Uranium mass adsorbed was not significantly affected by TA in the acidic and neutral pH range as confirmed by Li et al. (1980) at acidic pH. The more dramatic effect was observed at pH 10 and 11, where an increase in uranium mass adsorbed from less than 30% up to 100% occurred. This indicated that the presence of TA at high pH had a clear impact on the fate of uranium during the filtration process; this was attributed to complexation between uranium and TA. Similarly, higher adsorption of metals to TA was found by Uçer et al. (Üçer et al., 2006) with increasing pH, possibly due to the dissociation of TA. In the present study, a colour change took place during the alkaline pH adjustment of the TA solutions, from a clear solution to a dark green colour. Such colour change at alkaline pH was reported by Makkar and Becker (Makkar and Becker, 1996). In fact TA is easily degraded to yield glucose and gallic acid (Haslam, 1966; Salunkhe et al., 1990; Mueller-Harvey,

2001). It has been shown that metals attach to the galloyl part of the TA (Ross et al., 2000), which at high pH dissociates into gallic acid. Gallic acid is known to complex with uranium (Domingo et al., 1990), and it is likely that this is what occurred during these experiments. Indeed Shirato and Kamei et al. (1995) used hydrolysable TA at pH 10 to precipitate uranium from solution resulting in <80% adsorption of uranium. Yoon et al. (1989) also described a method for uranium removal using TA extract and $CaCl_2$ at alkaline pH. Uranium was removed by sedimentation. Despite expecting charge repulsion between the negative uranium species at alkaline pH and the negatively charged gallic acid (pKa ~3.13-9.2) the Ca^{2+} ions present in the solution could potentially act as a bridge between gallic acid, the ligands on the uranium ion and the membrane.

Results in Figure 27B show that the presence of AA enhanced the mass adsorbed of uranium at pH <5, whereas at more alkaline pH the mass adsorbed of AA did not affect the mass adsorbed of uranium. Under acidic conditions AA precipitates (Draget et al., 2002) and forms a gel that is compact due to reduced charge repulsion between the neutral AA molecules (Lee and Elimelech, 2006b). Since uranium is positive at this pH range (Figure 26), it is more likely to form complexes with AA as opposed to more alkaline conditions when both uranium and AA are negatively charged. The AA structure determines how well it binds with metals. The affinity increases with G content due to its zig-zag structure which can accommodate the metal ions (Draget et al., 2002; Davis et al., 2003b). This is known as the egg-box model (Draget et al., 2002; Davis et al., 2003a; Davis et al., 2003b). Mycrocystis Pyrifera which is the AA species used in this study has one of the highest M/G ratios: 1.6-1.7 (Draget et al., 2002; Davis et al., 2003a; Lee and Elimelech, 2006b), thus it is less favourable to metal binding compared to other types of alginates available. Having said this, divalent metals have been found to be favoured by AA adsorption (Davis et al., 2003b; Lee and Elimelech, 2006b). At pH 3-5 the divalent species UO_2^{2+} dominates the uranium speciation which would be favourable for complexation by AA and consequent uranium up-take by the membrane. Metal size is also a key variable according to the egg-box model, due to the rigid nature of the GG linkages as well as the steric arrangement of the electronegative ions surrounding

the metal. For instance, Ca^{2+} (1.00 Å) has been found to be selectively favoured by AA over other metal ions (Davis et al., 2003a). Considering that the smallest species of uranium is found in the form of UO_2^{2+} with a radius of 1.8Å (Duff et al., 2002) and that at more alkaline conditions the uranium species are even larger (4.85 Å) (Favre-Reguillon et al., 2003), complexation of uranium with AA would be less favoured in the neutral and alkaline pH range, where in fact the Ca^{2+} present are likely to compete with uranium for binding sites with AA.

The results for mass adsorbed of uranium and HA are displayed in Figure 27C. Uranium complexed with HA had a higher mass adsorbed at the pH range 3-7 compared to alkaline pH. At low pH, HA is by definition insoluble (Ghosh and Schnitzer, 1980; Bourbonniere and Halderen, 1989) and has a more compact configuration due to the reduced charge density at both inter and intramolecular levels (Balnois et al., 1999). Using Visual Minteq 2.53, the complexation of uranium was predicted to be dominated by HA between pH 3-7 (Figure 28), at which stage stable water soluble carbonate complexes become important. These speciation results confirmed experimental results where HA increased adsorption of uranium at pH 3-7 (Figure 27C and Figure 28). This also confirmed results from a variety of studies where HA has been found to be important in uranium complexation in the acidic and neutral pH range and increase uranium adsorption onto different materials (Payne et al., 1996; Lenhart and Honeyman, 1999). Li et al. (1980) also found that uranium-HA complexation was important at low pH. They determined that the uranyl ions in solution decreased at pH 5, but did not study uranium without OM to confirm whether or not this was due to the OM.

This study clearly shows the significant effect of the different types of OM in uranium removal by UF. Solution characteristics such as pH and presence of Ca^{2+} determined whether complexation was favoured, enhancing adsorption of these complexes on the membrane.

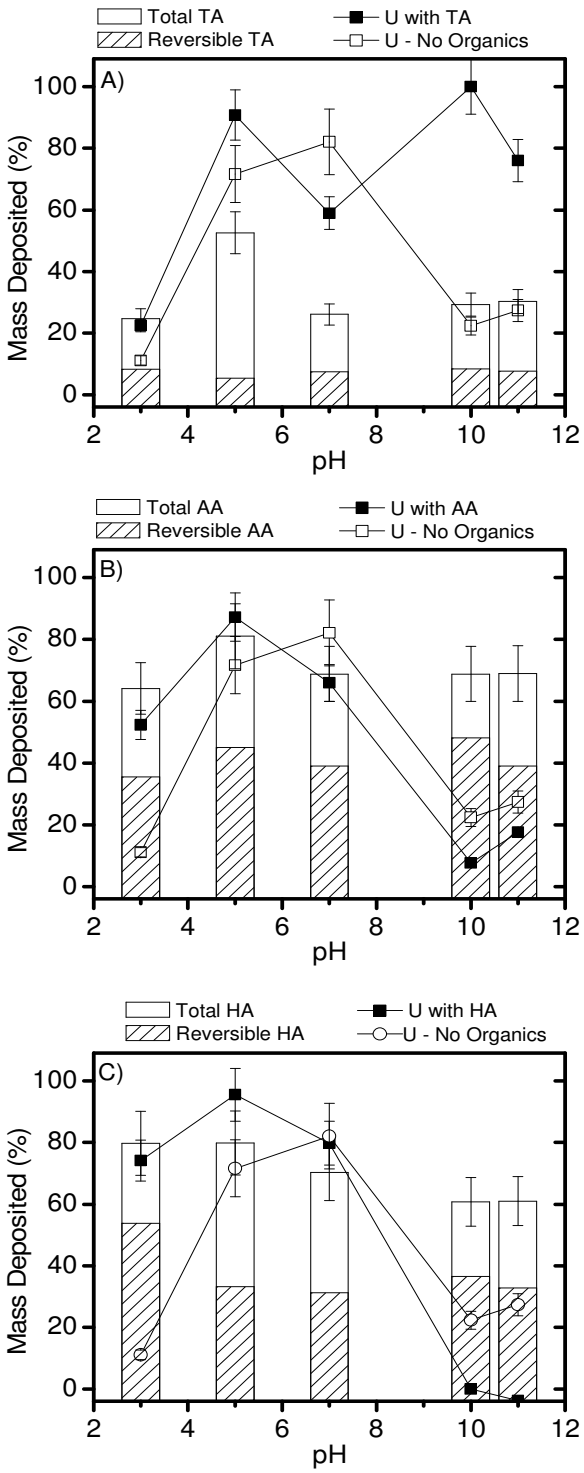

Figure 27. Uranium and organic matter mass adsorbed to the membrane (at t=5h) for A) TA, B) AA and C) HA. Feed solution: 0.5 mgU/L as $UO_2(NO_3)_2$, 1mM $NaHCO_3$, 0.5 mM $CaCl_2$, 10 mM NaCl, 25 mgC/L OM (published in Semião et al. (2010)).

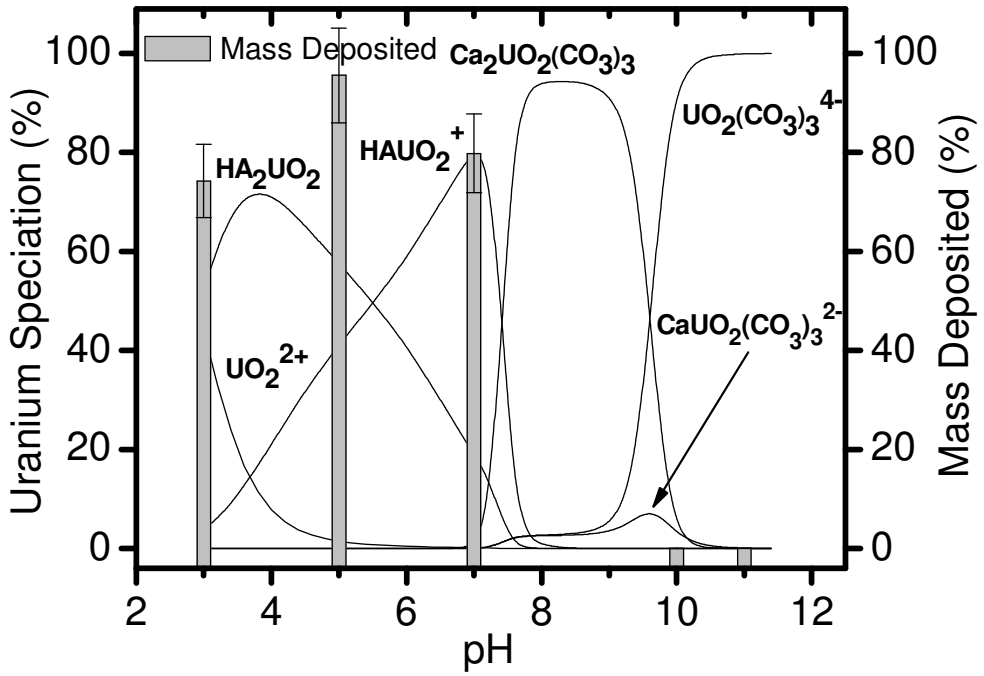

Figure 28. Uranium mass adsorbed to the membrane (at t=5h) and speciation of uranium-HA solution as a function of pH. The solution speciated was 0.5 mgU/L as $UO_2(NO_3)_2$, 1mM $NaHCO_3$, 0.5 mM $CaCl_2$, 10 mM NaCl, 25 mgC/L HA (HA from the Minteq data base) (also published in Semião et al. (2010)).

5.4 Conclusions

The fate of uranium in the UF process was highly dependent on pH and OM type. Retention of uranium was not achieved with this UF membrane irrespective of the presence of OM, with the exception of some retention in the presence of AA.

Significant amounts of uranium were taken up by the UF membrane, however, especially at pH 5-7 in the absence of OM. HA increased this up-take at the pH values 3 and 5 (74 to 96% compared to 11 and 72%), where it was predicted by Visual Minteq 2.53 to dominate uranium speciation. The presence of AA did not affect uranium up-take significantly since the alginate used did not possess the necessary characteristics to bind metals. It only increased the uranium mass adsorbed at pH 3 (52% compared to 11%). The mass adsorbed of uranium was highest (100 and 76% compared to 22 and 27%) in presence of TA at pH 10 and 11 where uranium was postulated to complex with gallic acid, originating from the dissociation

of TA. Speciation calculations of uranium with HA were a useful tool to understand the results that were obtained in regards to the behaviour of uranium in the UF process. Current limitations are the availability of a variety of organic molecules in such databases.

Findings from this study highlight that through pH adjustments to the water and addition of complex forming molecules such as OM, uranium may be removed using UF, however, the complexes would need to have a greater size to be efficiently retained. It could also be concluded that up-take of uranium during the field experiments in Chapter 4 are likely to have occurred by the UF membranes, at least at pH 5-7.

6 Importance of charge, size and affinity for uranium interaction with NF/RO membranes

6.1 Introduction

In Chapter 4 it was shown that uranium present in water samples from Australia was removed from all solutions (feed, UF permeate, concentrate and NF/RO permeate) by a UF-NF/RO system at around pH 5-7 and at pH 10. The natural water matrix was very complicated and it was concluded that controlled laboratory experiments were needed to determine the processes controlling the behaviour of uranium in this system and, in particular, to explain the uranium loss from solution (presumably to the membrane). In Chapter 5 filtration experiments using UF membranes were performed over the pH range 3-10, demonstrating that uranium was removed by the UF membrane at specific pH values. This removal occurred despite the large pore size of the UF membrane (40 nm) and it was concluded that this must be due to adsorption of uranium to the membrane although the mechanisms involved were not elucidated. This chapter aims to investigate the removal of uranium by a NF/RO cross-flow system, and the specific objectives are to explain the interaction of uranium to the membranes and to explore the mechanisms controlling uranium retention.

There are several direct and indirect processes which could lead to removal of uranium from solution onto the membrane, the main ones being direct interactions with the membrane structure, *e.g.* adsorption, and formation of new phases on the membrane surface (and within pores), *e.g.* precipitation. Adsorption describes processes by which atoms or molecules interact with the surface of the sorbent either through physisorption (weak forces such as van der Waals interaction or hydrogen bonding), electrostatic attraction or chemisorption (where ionic or covalent chemical bonding take place) (Shriver and Atkins, 1999). If uranium interacts with the membrane via van der Waals forces or electrostatic attraction, it will only be held very weakly and there should be no chemical change to the membrane structure.

Such interactions are likely to be reversible. In contrast, uranium interactions via chemisorption, a process which involves bond formation between the adsorbate and the substrate, would be expected to change the properties of the membrane in some way since the membrane functional groups would be affected. Interactions via chemisorption are strong (involving ionic or covalent bonds) and accordingly these may be irreversible.

From a natural environmental perspective, surface precipitates can form via a range of mechanisms depending upon the unique characteristics of the interfacial region between a solid and an aqueous phase (Ford et al., 2001). It is unlikely that uranium would be present at sufficiently high concentrations in oxic natural waters such that precipitation of a uranium phase would occur. However, other inorganic species may be present at much higher concentrations and so it is important to consider the effect of co-precipitation of uranium with other major ions present in solution. This scenario also applies to filtration systems where the solid phase is represented by the membrane and the aqueous phase by the solution being filtered. The consequences are, however, often detrimental: uranium deposition via the formation of surface co-precipitates would cause scaling of the membrane, clog the pores and result in flux decline. Unless such a precipitate could be redissolved, this process would be irreversible.

Adsorption as well as precipitation may be enhanced by concentration polarisation, the process by which solutes accumulate close to the membrane surface during transportation across the membrane by convection and diffusion. An increase in convection (as increased pressure is applied) can lead to an increase in concentration polarisation, while an increase in the flow across a membrane will decrease it. Concentration polarisation may lead to reduced permeate flux and also decreased rejection due to the increased concentration gradient between the feed and permeate. The effects of concentration polarisation are by definition considered reversible.

The speciation of uranium will also influence its behaviour in NF/RO systems and indeed its interactions with NF/RO membranes. Influential factors include pH and

chemical composition of the aqueous solution. Importantly, the size and charge of uranium species may vary across the pH range and this will likely result in (i) pH-dependent (sorption) interactions with membrane; (ii) pH-dependent permeation/retention behaviour in the NF/RO system; (iii) differences in behaviour/interactions for different membrane types.

After inclusion of the appropriate experimental parameters, Visual Minteq 2.53 was used to predict the variation in uranium speciation with pH. To determine the influence of membrane pore size on the uranium removal process, one NF and one RO membrane were selected. These were composed of the same materials but had different molecular weight cut-off values. This enabled the variation in species size and valency with pH to be compared with the molecular weight cut-off and charge of the membrane.

To avoid complicating factors such as concentration polarisation, initial experiments to investigate uranium interaction with the two membranes were performed across the pH range 3-10 without applied pressure to investigate how uranium interacts with the membrane. Then two points of interest within this pH range were selected to investigate the effects of pressure on the uranium-membrane interactions: one was the pH value of high uranium-membrane interaction and one was selected to represent low membrane-uranium interaction. Finally, the nature of uranium interactions with the membranes was investigated using a range of spectroscopic and imaging techniques (μ-XRay Fluorescence Spectroscopy (μXRF), Scanning Electron Microscopy (SEM), Transmission Electron Microscopy (TEM), Scanning Transmission Electron Microscopy-Energy Dispersive XRay Spectroscopy (STEM-EDX) and Fourier Transform Infrared Spectroscopy (FTIR)).

6.2 Materials and methods

The cross-flow filtration system was described in section 3.1.4, the experimental solutions prepared in section 3.1.5 and uranium speciation using Visual Minteq 2.53 was described in section 3.1.8. Chemical analysis of the solutions were performed

with ICP-OES and ICP-MS (see section 3.1.6). Descriptions of the membrane characterisation, cross-flow experiments and analysis of the membrane using spectroscopic and microscopic techniques follow below.

6.2.1 Membrane characterisation

Coupons of a NF membrane (TFC-SR2, Koch) and a RO membrane (BW30, Filmtec) were used for all cross-flow experiments. According to manufacturer specifications, both have a dense polyamide active layer on top of a porous polysulfone support layer. Below the polysulfone layer they also have a polyester support web. A simple schematic to illustrate the general membrane composition is shown in Figure 29.

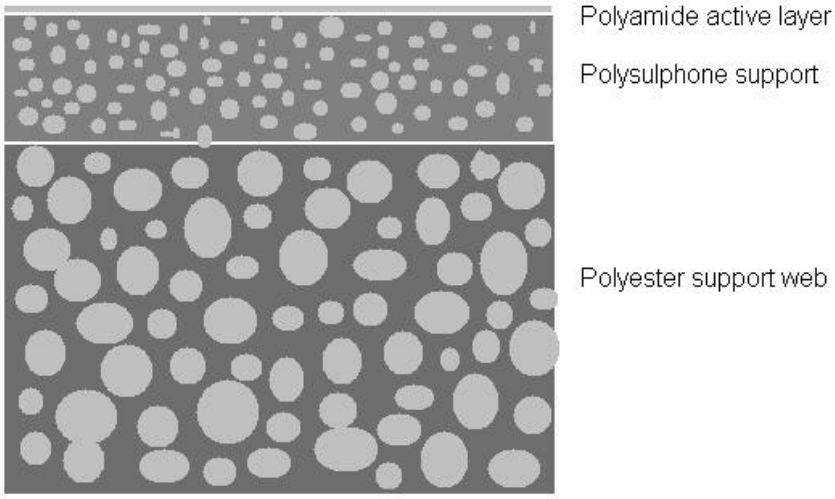

Figure 29. Schematic of a cross section of the TFC-SR2 and BW30 membranes as described by the manufacturer. The active layer is ~0.2 µm thick, the polysulfone support is ~40 µm thick and the polyester support web is ~120 µm thick.

Permeate and salt flux

Baseline permeate and salt flux were measured for both membrane types across the pressure range of 5-15 bar (in steps of 2.5 bar). Membrane wash and compaction was carried out as described in section 6.2.2. A solution containing only background electrolyte (20 mM NaCl and 1 mM $NaHCO_3$) was added to the system and the pressure adjusted accordingly, starting with the lowest pressure. The system was

allowed to equilibrate (30 minutes) and three measurements were then taken of each of the permeate flux, feed and permeate conductivity.

Zeta-potential analysis

For both membrane types, the streaming potential of the membrane sheets was measured using an electrokinetic analyser (EKA), (Anton Paar KG, Gratz, Austria). These measurements were carried out in Imperial College, London by Annalisa De Munari under the direction of Dr Alexander Bismarck and Dr Kingsley Ho. The membranes were rinsed and soaked in DIW for at least 24 hours before the measurements were made. They were then cut into sections of 7.5 cm x 2.5 cm and soaked for 30 minutes in the same background electrolyte as used in the experiments (described in section 3.1.5). The membrane was mounted in the measuring cell of the EKA and flushed with DIW for 3 minutes, followed by a full system flush for 30 minutes with the background electrolyte solution to ensure air removal from the cell. The pH of the background solution was adjusted automatically, in increments of 1 pH unit over the range pH 3 to 10, by an autotitrator (1 M HCl or 1 M KOH, VWR, Germany). Six zeta-potential measurements were taken for each pH value, and the average value was calculated. All measurements were performed at room temperature (~21°C).

Estimation of pore-size and molecular weight cut-off

The pore size of the TFC-SR2 membrane was determined experimentally using a range of neutral organic molecules (dioxane, xylose and dextrose). The method for experimental and theoretical pore radius determination is described in Nghiem et al. (2004). This method was followed, as described in detail in the section 11.4.1 of the appendix, which uses a hydrodynamic model for the calculation of the theoretical pore radius and the ratio of the membrane active layer thickness to porosity. A correlation was used to estimate the mass transfer coefficient (Gekas and Hallström, 1987; van den Berg et al., 1989). The MWCO was measured experimentally using polyethylene glycol (PEG) standards of different molecular weight (200, 400, 600 and 1000 g/mol), as well as dioxane, xylose, dextrose (with a molecular weight of

88, 150 and 180 g/mol, respectively) according to the method described in Hilal et al. (2008). Again this is described in section 11.4.1 of the Appendix. The pore size for the BW30 membrane was determined, using the same methods, membrane sheet and cross-flow system as in this study (except the lower MW solute, methanol was used), by Laura Richards and Andrea Semião and is reported in Richards et al. (2011) and Schäfer et al. (2011).

6.2.2 Investigation of uranium behaviour in a NF/RO system with variation in pH but no applied pressure

Uranium interactions with the NF and RO membrane were investigated in a series of experiments where the pH was varied by increments of 1 unit over the range 3-10. In preparation for each experiment, the protective layer of the membrane was first swilled off with DIW, the membrane was then soaked in DIW at 4ºC overnight and finally swilled once again with DIW. It was subsequently placed in the membrane cell of the cross-flow system and compacted at 25 bar at a flow-rate of 0.6 L/min for one hour, or until the permeate flow was stable. The system was drained of DIW, the experimental solution (see section 3.1.5) added and the flow-rate again set to 0.6 L/min. No pressure was applied in any of these experiments. The pH was monitored throughout and adjusted (using either 0.1 M NaOH or Aristar HNO_3) to remain within 0.1 of the required pH value for each individual experiment. Feed samples were collected hourly over the seven-hour experimental period. After each experiment, the system was drained, the membrane removed, and the system thoroughly washed using dilute HNO_3 (0.35%, wt, Analar) and DIW. Four further washes with DIW followed this procedure. In order to assess the effectiveness of the cleaning procedures, portions of the DIW used during the initial compaction of the membrane and the DIW used for each wash at the end of the experiments were retained for elemental analysis. Membranes from selected experiments were retained for further spectroscopic and microscopic analysis as described in section 6.2.5.

6.2.3 Sorption isotherm and precipitation experiment

Based on the results of the NF/RO experiments described in section 6.2.2, a sorption isotherm experiment was carried out for TFC-SR2 to determine whether an adsorption limit may be reached under the conditions employed. The pH 6 was chosen since most uranium adsorption occurred at this value. The TFC-SR2 membrane was selected because it is the more open membrane, with potential to allow permeation of monovalent ions while uranium is still relatively well retained. The experiments were performed using concentrations of 0.5, 1, 5, 10 and 25 mg/L uranium at pH 6 in the cross-flow system with the TFC-SR2 membrane. The experimental solutions were prepared as in section 3.1.5.

A static precipitation experiment was also carried out where solutions were prepared containing the background buffer solution (section 3.1.5) and varying uranium concentrations (0.5 mg/L, 10 mg/L, 25 mg/L, 50 mg/L and 500 mg/L). The concentration range was chosen to reflect the experimental concentrations used (0.5 mg/L was used for the majority of laboratory experiments and also reflects the concentrations found during the field test in Chapter 4, but 25 and 50 mg/L had to be used for certain visual techniques). The pH was then adjusted using HCl or NaOH as appropriate to cover the pH range 3-10 in steps of 1 pH value. The samples were then measured using a portable turbidity meter (TN-100/T-100 Eutech Instruments/Oakton Instrument), the result taken as the average of five consequetive measurements. Calibration of the instrument was achieved using turbidity standards of 0.02, 20, 100 and 800 NTU.

6.2.4 Investigation of uranium behaviour in a NF/RO system at selected pH values with variation in applied pressure

For the pressure experiments, pH 6 and 8.5 were chosen as points of interest, since, for both membranes, the maximum affinity to the membrane occurred at pH 6 while at pH 8.5 the uranium-membrane interaction was significantly lower. Pressure experiments were then carried out using the same procedures as the experiments without pressure (see section 6.2.2), except that the pressure was adjusted to one set

value (between 5 and 15 bar in steps of 2.5 bar) at the start of the experiment and permeate samples were collected in addition to the feed samples. The experimental solutions were again prepared as in section 3.1.5.

6.2.5 Membrane analysis

Micro-X-Ray fluorescence (μ-XRF) spectroscopy

μ-XRF (Micro X-Ray Fluorescence Spectroscopy) measurements were carried out on a microscope (XGT^{7000}, Horiba JobinYvon) equipped with an X-Ray guide tube producing a finely focused and high-intensity beam with a diameter spot size of 100 μm (for mapping analysis) or 10 μm (for line analysis) (Rh X-Ray tube, accelerating voltage of 50 kV, current of 1 mA). The analysis was carried out by Dr. Perrine Chaurand at CEREGE, France. X-Ray emission from the irradiated sample is detected via an energy-dispersive X-Ray (EDX) spectrometer equipped with a liquid-nitrogen-cooled high purity Si detector. The detector resolution was 145 eV at the Mn Kα emission line. Elements detected by μXRF-EDX ranged from sodium (11) to uranium (92).

Elemental mapping and microanalyses were performed at atmospheric pressure. First the whole TFC-SR2 membrane after a pH 6 experiment was analyzed in mapping mode. The objective was to identify uranium distribution on the membrane surface. An area of ~5×4 cm was selected in the middle of the membrane and then scanned with the 100 μm incident RX beam (total counting time of 15×1000 s). A chemical map of uranium was obtained from the intensity of the U Lα1 emission line (0.0911 nm) after removing background contribution. Because the X-Ray beam penetrates through the membrane, it could not be determined whether uranium was distributed through-out the membrane or in localised areas. To identify the potential uranium penetration within the membrane, cross-sections of the membranes TFC-SR2 and BW30 at pH 6 and 8.5 (strips of 1-2 mm wide and 4-5 cm long were cut using scissors) were examined. To ensure that the cross sections remained perpendicular to the incident X-Ray beam (and avoid shadowing effect), they were mounting end-on in between paperboard support.

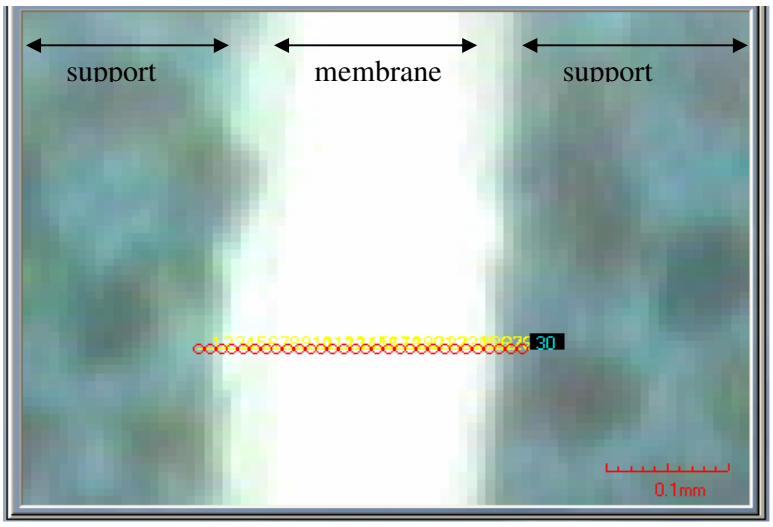

Figure 30. Line-analysis of membrane cross-section was carried out using a counting time of 1000s per spot, each having a spatial resolution of 10 µm due to the X-Ray beam. The membrane section was held in place by a paperboard support (blue).

Line analyses (*i.e.* spot-analyses in a line) were carried out on the cross sections (starting from the top of the membrane surface to the bottom edge), recording a whole XRF-EDX spectrum every 10 µm (counting time 1000s/step, incident X-Ray beam with a diameter of 10 µm) (Figure 30). Cross-section profiles of the uranium distribution, as well as of other membrane elements such as sulfur, could then be plotted. The results from µ-XRF are semi-quantitative and are given as a percentage relative mass of all the elements detected. Light elements such as carbon, nitrogen or oxygen and elements which would indicate the position of the active layer, are not detected. However, the µ-XRF analysis does give a good first idea of the distribution of the elements of interest in the membrane.

Electron microscopy techniques

To gain insight both into the membrane structure and the uranium distribution within this structure, three different microscopy techniques were used: scanning electron microscopy (SEM), transmission electron microscopy (TEM) (by Dr Chris Jeffrey at the University of Edinburgh) and scanning transmission electron microscopy - energy-dispersive X-Ray spectroscopy (STEM-EDX) (by Dr Mike Fay at the

University of Nottingham). Each of the techniques gives different but complementary kinds of information. SEM was useful in examining the surface structure of the membrane. By using the two modes, secondary electron (SE) or yttrium aluminium garnet backscatter electron (YAGBSE) detection, surface topography and regions of higher and lower mean atomic number, respectively, can be distinguished. Elements of higher atomic number give brighter contrast than elements of low atomic number in YAGBSE. Ideal instrument resolution is typically ~1.5 nm in SE mode and 5-50 nm in YAGBSE mode. For TEM, cross-sections of membranes can be examined, and due to the higher contrast and resolution, excellent images of the ultrastructure of the active layer can be obtained, from which the active layer thickness can be determined. Instrument resolution for ideal samples (*e.g.* the graphite lattice) is typically 0.34-1 nm; for non-ideal samples, however, such as the membrane sections where contrast will be lower, resolution will also be lower (2-3 nm at best). Although elements of higher atomic number and electron density give darker contrast in the TEM, identification of the elements is not possible. STEM-EDX enables the provision of information about the elemental distribution.

Scanning electron microscopy (SEM)

Rectangles of freeze-dried or air-dried membranes (from experiments with TFC-SR2 performed with 0.5 mg/L U at pH 6 and 8.5 with no applied pressure, as well as a "blank" membrane washed with DIW) were attached to the surface of an aluminium specimen stub with conductive double-sided adhesive discs (Agar Scientific, Stansted, UK) and rotary coated with about 8 nm of carbon in an Edwards 301 vacuum coating unit. The specimens were examined in a Hitachi 4700II field emission scanning electron microscope (Hitachi High-Technologies Europe GmbH, Maidenhead, UK), at beam accelerating voltages of 5 keV or 10 keV, a beam current of 10 µA and working distances of 8 to 12 mm. Digital images were captured at a resolution of 2,560 by 1,920 pixels by using the signals from the upper (semi-in lens) secondary electron detector and/or the YAG backscattered electron detector.

Transmission electron microscopy (TEM)

Specimens of TFC-SR2 membranes were found to be damaged by the solvents commonly used to dehydrate (*e.g.* ethanol and acetone) and promote infiltration with the resin (*e.g.* acetone and propylene oxide) during specimen preparation for electron microscopy. To minimize ultrastructural damage, losses of uranium from the membrane (by solvent extraction) and to avoid any pH changes from those in the experimental conditions, specimens were dehydrated by freeze-drying.

To avoid preserving and subsequently erroneously analysing a film of fluid on top of the membrane surface, any visible films of fluid were carefully wickened off. Wet specimens of TFC-SR2 membranes were then clamped to a silver specimen carrier and rapidly frozen by plunging into sub-cooled liquid nitrogen at about -210 °C (63 K). The specimen carrier was transferred under reduced pressure (rotary vacuum pumping, pressure not measured) to the cold stage of a Gatan Alto 2500 cryopreparation unit at -130°C (143 K) and warmed to room temperature (~21°C, 294 K) at about 20°C per hour at a pressure of lower than 10^{-7} Pa. As the specimen had reached room temperature, the top filtration layers (the polyamide active layer and the polysulfone support) were stripped from the backing material using tweezers, and rectangles ~1mm square were infiltrated in Agar 100 (Agar Scientific, Stansted, UK) or Durcupan® (Fluka, Switzerland) epoxy resins. Blocks were polymerized for 48 h at 60°C, and sectioned at 90 nm thickness on a Leica Ultracut UCT ultramicrotome (Leica Microsystems (UK) Ltd., Milton Keynes, UK) using a Diatome Ultra diamond knife with 45° angle (DiATOME Histo, Biel, Switzerland). Sections were mounted on open-hole copper grids of 200 mesh or on carbon-coated formvar support films on 2 x 1 mm slot grids. The mounted sections were examined at a beam accelerating voltage of 80 keV in a Philips CM120 Biotwin (FEIand 16-bit images were captured using a Gatan Orius 1000 11 Mpx camera and Gatan Digital Micrograph software. The block surfaces from which the specimens had been cut were also mounted on aluminium specimen stubs, coated with carbon and examined by scanning electron microscopy as described above.

Scanning transmission electron microscopy - Energy-dispersive X-Ray spectroscopy (STEM-EDX)

The amount of uranium present in membranes which had been subjected to the experimental concentrations of 0.5 mg/L was below the EDX detection limit. Therefore a concentration of 50 mg/L (TFC-SR2 at pH 6 and 8.5 at no applied pressure) was used for experiments solely in preparation for STEM-EDX to enable uranium detection.

Samples of membrane cross-sections were prepared as for the TEM. The membrane was examined using the JEOL Digital STEM System operating at 100 kV (typical resolution down to 0.19 nm), while elemental identification of the cross-section was carried out with the Oxford Instruments INCA X-Ray Microanalysis System. Instrument settings are detailed section 11.4.4 in the appendix.

Fourier transform infrared spectroscopy (FTIR)

FTIR spectroscopy can be used to investigate the chemical structure of IR-active inorganic and organic species. It is particularly useful for identifying oxygen-and nitrogen-containing functional groups in the membrane, *e.g.* carboxylic acids, sulphones, amides, but can also detect the presence of the uranyl ion and indeed the carbonate grouping in uranyl carbonate species. As for STEM-EDX, the detection limit for FTIR was above the experimental uranium concentrations used, and therefore solutions containing 25 mg/L of uranium were used to prepare the membranes for FTIR analysis. Experiments performed with TFC-SR2 at pH 6 and 8.5 with no applied pressure were selected for FTIR analysis. Blank membranes were also prepared by mounting them in the cross-flow system and subjecting them to the experimental protocol used for the non-pressure experiments; instead of the experimental solution, pH-adjusted (pH 6 and 8.5) DIW was used. The FTIR analysis was carried out by Dr Mari Kallionen at Lappeenranta University of Technology, Finland. The attenuated total reflectance (ATR) technique was used to obtain the IR spectrum of the membrane surface. The analysis was performed with a Perkin-Elmer 2000 FTIR spectrometer with the wire coil operating at 1350 K as the radiation

source, triglycine sulphate (TGS) as the detector and optical KBr as the beamsplitter. A KRS-5 crystal (thallous bromide iodide) was used as the internal reflection element. The incident angle of IR beam was 45°.

6.3 Results and discussion

Firstly, the results from the membrane characterisation are discussed (section 6.3.1). This will then be followed by 1) the results of "mass adsorbed" of uranium performed across the pH range 3-10 without pressure as well as the adsorption isotherm, precipitation experiment and μ-XRF results (section 6.3.2); 2) the effect of pressure on uranium-membrane interactions at two selected pH-values, pH 6 and 8.5 (section 6.3.3); 3) the spatial distribution of uranium within and on the membrane investigated using microscopy techniques (section 6.3.4), and finally; 4) the FTIR spectroscopy results explaining the nature of the uranium interaction with the membrane (for pH 6 and 8.5) (section 6.3.5).

6.3.1 Membrane characterisation

As described in section 6.1, there are a number of factors which can affect uranium transport through the membranes. Permeability will determine how much convection or diffusion of water towards the permeate side is experienced, pore-size and/or molecular weight cut-off will determine how much of the uranium will be retained by the membrane while the membrane charge (measured by zeta potential) will either attract or repel charged ions to or from the membrane surface and influence the retention. These parameters were therefore characterised for both the TFC-SR2 and BW30 membranes and the results described below.

Permeate and salt flux

From theoretical considerations, permeate flux should increase with increasing pressure for both NF and RO membranes. For RO membranes, salt flux is independent of pressure; salt flux is instead driven by the concentration gradient across the membrane. The amount of salt diffusing across the membrane is therefore unaffected by pressure but the water flux is increase and this leads to dilution of salt

in the permeate. The net effect is increased salt retention with increasing pressure (Wijmans and Baker, 1995). This contrasts with UF membranes, where increased pressure leads to increased convection of ions through the membrane and thus a decrease in solute retention. NF membranes are considered to be in between RO and UF membranes and, with respect to salt flux, can therefore behave like either of them, depending on the tightness of the NF membrane (Section 2.2.1).

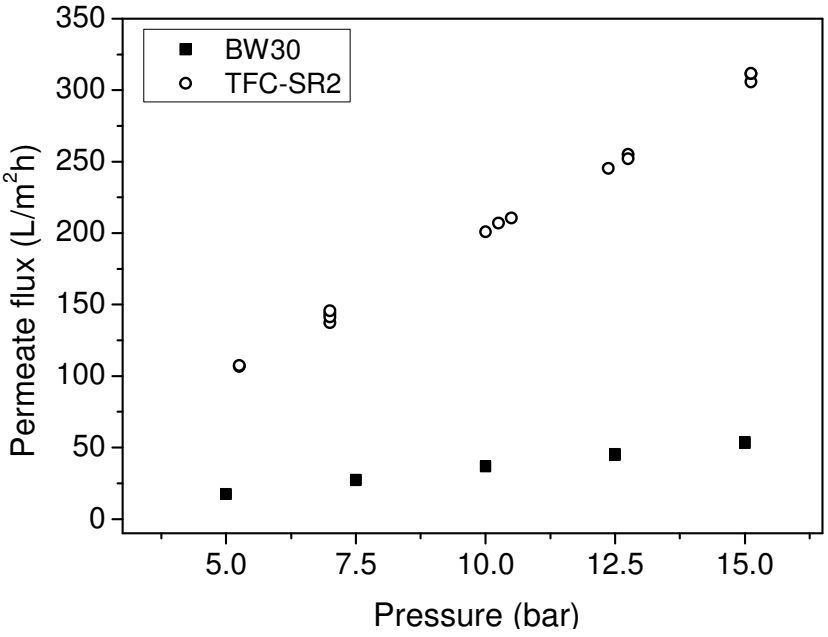

Figure 31. Variation in a) permeate flux with pressure for BW30 and TFC-SR2. Flow-rate = 0.6 L/min, temperature = 25°C.

Figure 31 shows that the baseline permeate flux increased linearly with pressure for both types of membrane used in this study. The more open NF membrane, TFC-SR2, showed a steeper permeate flux increase with increasing pressure than the tighter RO membrane, BW30. The average permeability of TFC-SR2 was 10.97 ± 1.51 L/m^2hbar, while for BW30 it was 4.84 ± 0.15 L/m^2hbar.

The salt retention remained approximately constant for BW30 and was ~97-98%. The salt retention for TFC-SR2 however, decreases from 24.9 ± 2.6% at 5 bar to 14.9 ± 1.9% at 15 bar (Figure 32a). This could be an indication of convection acting as a transport mechanism for this relatively open NF membrane, or and effect of concentration polarisation, or both (Yuan and Kilduff, 2009). The film model was

used for the calculation of real retention by the membranes (described in section 2.2.2).

Calculation of the real retention for TFC-SR2 gave ranges of 30 to 29% or 35 to 44% retention, depending on the Sherwood correlation used (section 6.3.3). BW30 remained unaffected by concentration polarisation and only a marginal difference between observed and real retention was present (Figure 32b).

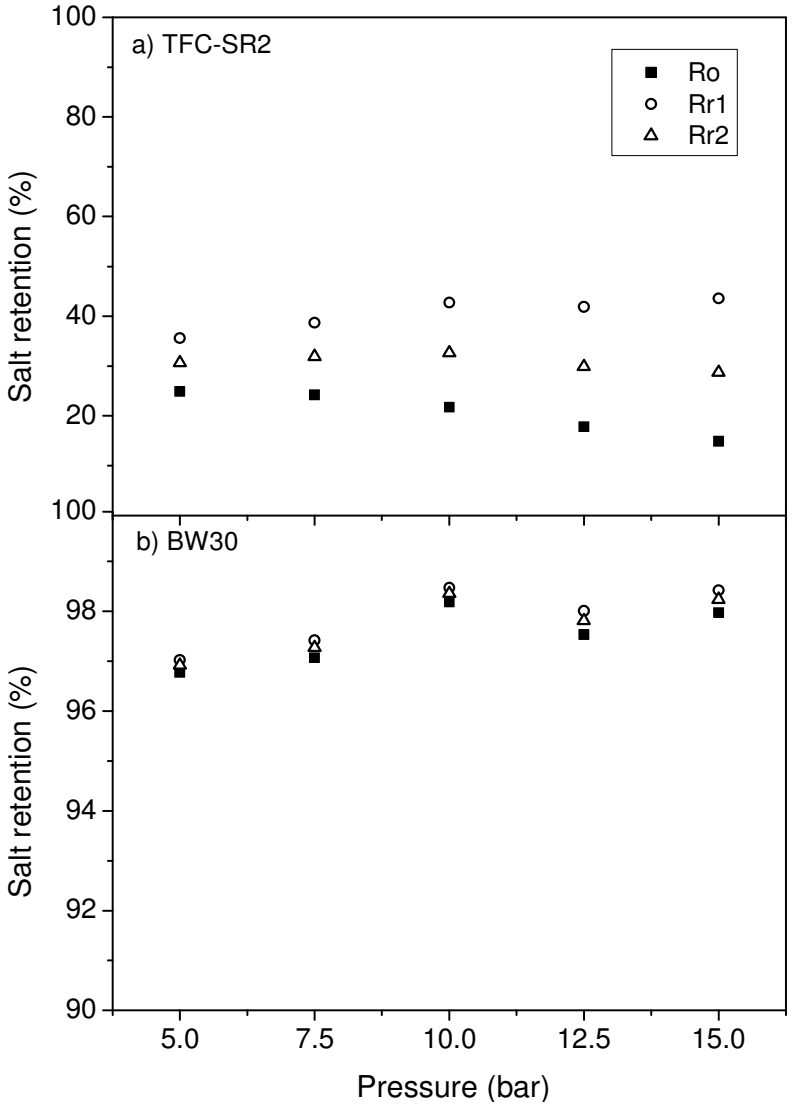

Figure 32. Observed and real salt (conductivity) retention calculated for TFC-SR2 (a) and BW30 (b). Note that the retention scale for BW30 is smaller than for TFC-SR2 to allow comparison of observed and real retention.

Membrane pore size and MWCO

The nominal MWCO (*i.e.* where 90% of greater than a particular molecular weight are retained) for TFC-SR2 and BW30 were determined as 486 g/mol and 88 g/mol, respectively (Table 9). The pore radius was determined as 0.52 ± 0.03 nm while the pore radius for BW30 was given by Richards et al. (2010) and Schäfer et al. (2010) as 0.32 nm, respectively (Table 9).

Table 9. Experimentally determined MWCO and pore radius.

Parameter	TFC-SR2	BW30
Nominal MWCO	486 g/mol	88 g/mol
Pore radius	0.52 ± 0.03 nm	0.32 nm*

*note that RO membranes are considered dense and non-porous and this was determined only as a comparison with the more open structure of TFC-SR2. Absolute (100%) MWCO for TFC-SR2 was 1033 g/mol. Pore radius for BW30 was determined by Laura Richards and Andrea Semião.

Strictly speaking RO membranes are not considered to contain physical pores and so the MWCO is a better measure of the retention of BW30. Nghiem (2005) determined the pore size of TFC-SR2 to be 0.64 nm; slightly greater than the value of 0.52 ± 0.03 nm obtained in this study; however, it is likely that manufacturers have adjusted the structure of this membrane since the measurement was made by Nghiem (2005). Relating to more recent investigations using the same membrane and method but carried out in a stirred cell, DeMunari and Schäfer (2010a) also determined the pore size and MWCO of the TFC-SR2 membrane to be 0.52 nm and 485 g/mol, respectively, *i.e.* identical or very close to the values obtained in this study.

Zeta potential of the membranes

The charge of the membrane is important since it will determine whether ions will be attracted to or repelled by the membrane. Also, as discussed previously (2.2.1) the magnitude charge is an important retention factor in NF, where *e.g.* divalent ions are generally better retained than monovalent ions of opposite charge to the membrane due to higher charge repulsion (Nyström et al., 1995).

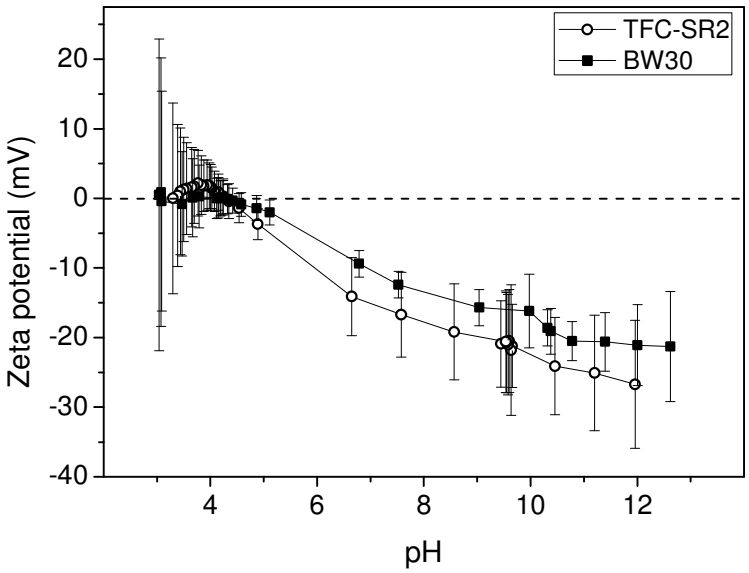

Figure 33. Zeta potential of membranes TFC-SR2 and BW30, measured in background electrolyte (20 mM NaCl and 1 mM $NaHCO_3$).

For a given pH value, the net charge, as indicated by the zeta potential, was similar for both the NF and the RO membrane. The charge varied with pH, changing from slightly positive at acidic pH to negative at pH 5 and becoming increasing negative as pH continued to increase (Figure 33). The iso-electric points for BW30 and TFC-SR2 were determined to be pH 4.19 and 4.25, respectively. For pH 5-12, the values for the NF membrane were always more negative than those for the RO membrane, but at any given pH, the difference was within one standard deviation of the RO membrane values. With respect to uranium interactions with these membranes, it is important to note that zeta potential is a measure of overall surface charge and membranes have been shown to have mixtures of localized positive and negative charged sites (Freger, 2003). A recent study of six membranes with polyamide active layers has also shown that while one pKa value was sufficient to describe the dissociation of amine groups (pKa = 3.6-4.6), two were needed for the carboxylic acid groups (one pKa at around 3.9-5.7 and the next between 5.9 and 9.9) (Coronell et al., 2010). Unfortunately no such detailed studies have been published for the TFC-SR2 membrane

6.3.2 Variation of uranium-membrane affinity with pH and relation to speciation

To investigate the uranium interactions with the membrane, NF/RO experiments were first performed over the pH range 3-10 without applying pressure to avoid conflicting factors, such as concentration polarisation or precipitation, which may increase or otherwise affect the adsorption or precipiatation of uranium. For each membrane, the set of experiments involved solutions containing uranium and background electrolyte varying incrementally by one pH unit over the range 3 to 10 (described in section 6.2.2). The amount of uranium taken up by the membrane by the end of each experiment was calculated using the mass balance shown below (Equation 10) and is presented as the percentage of the initial mass of uranium in solution. The term "mass adsorbed" is used (note that nature of the uranium-membrane interaction has not yet been determined).

$$Mass\ Adsorbed\ (\%) = \frac{V_{b0}C_{b0} - V_{bf}C_{bf} - \sum_{i=0}^{i=8} V_S C_{bi}}{V_{b0}C_{b0}} \times 100 \qquad \textbf{Equation 10}$$

V = volume (L), C = concentration (mg/L), b = bulk (feed + re-circulating concentrate and permeate), 0 = initial, f = final, S = samples (each 0.005 L), i indicates the samples taken during the experiment.

The resulting percentage values of uranium mass adsorbed at each pH value over the pH range 3-10 during the NF/RO experiments are presented in Figure 34 together with the modelled uranium speciation results across the same pH range. The uranium mass adsorbed obtained for the NF and RO membranes ranged between 5.4 – 49.3% and 4.2 - 31.2%, respectively. The percentage uranium mass adsorbed varied with pH but followed the same trend for both TFC-SR2 and BW30 (Figure 34a and b). Minimum uranium-membrane interaction occurred for both membranes at pH 3. The amount of uranium mass adsorbed increased for both membranes towards pH 5-7, while less interaction again took place at pH 8-10.

Although similar pH-dependent adsorption tendencies of uranium have been observed in natural aqueous-solid phase systems (outlined in section 2.1.6), uranium interaction with NF/RO membranes has not been studied before. This interaction may, however, have important implications for membrane filtration of uranium-containing water. To understand the mechanisms of the uranium-membrane interactions, the uranium speciation was modelled using visual Minteq ver 2.53 (described in 3.1.8) and is displayed in Figure 34.

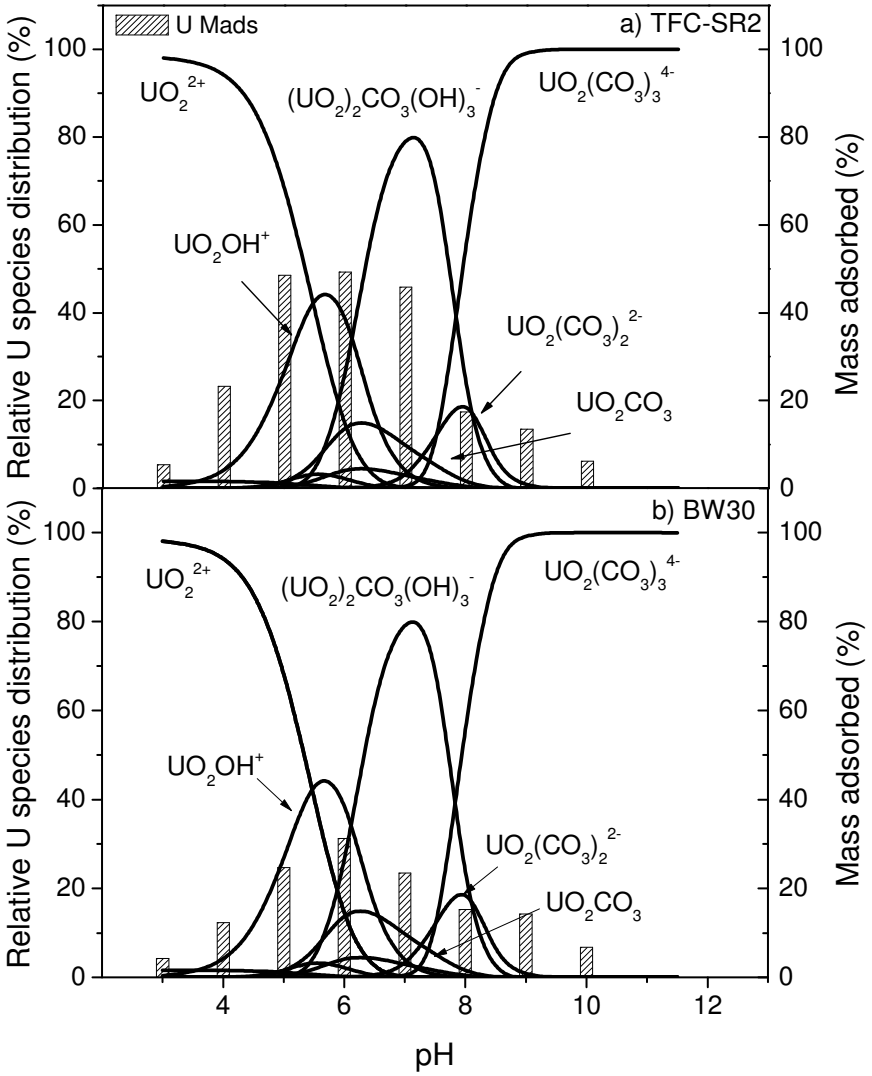

Figure 34. Uranium speciation (lines) and uranium depostion (columns) to a) TFC-SR2 and b) BW30 across the pH range 3-10, at no applied pressure. Experimental solution: 0.5 mg/L uranium and background electrolyte (20 mM NaCl and 1 mM $NaHCO_3$). No applied pressure, flow-rate = 0.6 L/min, temperature = 25°C.

As illustrated in Figure 34, the speciation of uranium (and thereby species charge and size) varies greatly across the pH range. Starting from pH 3, the species are positively charged but they become negatively charged as the pH increases to near-neutral values. The uranyl ion dominates the speciation at pH 5 and below. Thereafter, hydroxyl and carbonate complexes predominate. More specifically, hydroxyl ions are important ligands at pH 5-7, at pH 8 and above carbonate ligands dominate the uranium speciation.

As described in section 6.1, adsorption may involve charge interactions between the adsorbate and the membrane surface, and it is clear from the results of uranium speciation calculations that electrostatic attraction or repulsion between particular uranium species and the membranes can partly explain the uranium-membrane interaction results. At pH 3, both the membrane (see Figure 33) and the main uranium species (UO_2^{2+}), carries a positive charge and it is hypothesised that the <5% mass adsorbed of uranium at this pH is due to repulsion between membrane and uranium species. At pH 5-6, the uranium-membrane interaction was much greater, *i.e.* ~50%, for TFC-SR2 and ~30% for BW30, and could potentially be caused by adsorption to the membrane due to electrostatic attraction between the somewhat negatively charged membrane and the positively charged uranium species, UO_2OH^+. Other species that are also present to a lesser extent at pH 6 are UO_2CO_3 and $(UO_2)_2CO_3(OH)_3^-$. Although a neutral species, UO_2CO_3 is polar (Mujamdar et al. 2003) and may therefore also interact via dipolar interaction of the electropositive part of the molecule with the negative membrane. Surprisingly, the mass adsorbed remained high at pH 7, where both the dominating uranium species, $(UO_2)_2CO_3(OH)_3^-$, and the membrane carry a negative charge. It is conceivable that this uranium species could be attracted to positively charged amine groups present on the active layer of the membrane. However, studies of membranes with polyamide active layers have shown the pKa values of amine groups to be around pH 3-4 (Coronell et al 2010), similar to the value of the iso-electric point of the membranes (just above pH 4 for TFC-SR2 and BW30), so it is unlikely that there are many positively charged sites available at pH 7. Further reasons for the high mass adsorbed at pH 7 will be explored in the sections to follow. At pH 8-10, where both the

membrane and uranium species, $UO_2(CO_3)_3^{4-}$, carry large negative charges, uranium-membrane interaction also decreases rapidly to 5-17% for both BW30 and TFC-SR2. Here, charge repulsion is invoked to explain this decrease. The large size of the tri-carbonate species may also inhibit its ability to enter the membrane pores. Nevertheless, uranium up-take by the membrane of 5-17% is not insignificant. Although negatively charged uranium species would be attracted by any positively charged surface sites that remain at pH 8-10, the pK values for the amine groups strongly suggest that these will almost entirely be present in neutral form.

Uranium isotherm and precipitation

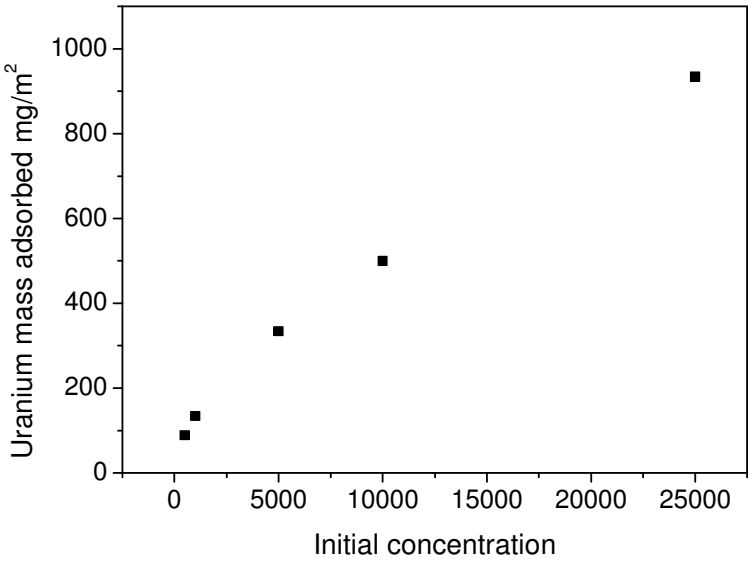

Figure 35. Sorption isotherm for uranium on TFC-SR2 membrane. Background electrolyte: 20 mM NaCl and 1 mM $NaHCO_3$. No applied pressure, flow-rate = 0.6 L/min, temperature = 25°C.

To determine whether uranium adsorption might have been limited by the membrane surface area or by surface site density under the conditions employed in these experiments, a sorption isotherm experiment was carried out using TFC-SR2. This was done for TFC-SR2 at pH 6, since the sorption of uranium had been found to occur to a greater extent with that membrane. Uranium concentrations for the experiments were 0.5 mg/L; thus a range of 0.5 up to 25 mg/L was used for the sorption isotherm. It was concluded that sorption sites were not limited even for

solution uranium concentrations of up to 25 mg/L, since it does not reach a "break-through" concentration (Langmuir 1997). This shows that the sorption capacity for the membrane was not exceeded during the non-pressure and pressure experiments.

Precipitation of uranium was also accounted for, both by using visual Minteq and experimentally. The predicted minerals by visual Minteq were all below saturation across the pH range (SI < 0), for the experimental conditions. Since most interaction between uranium and membrane occurred at pH 6, a concentration sweep was also performed at that pH value. This showed that Schoepite reached saturation only once uranium reached a concentration of 20 times the experimental uranium concentration. Schoepite was, however, not predicted as a major component of the uranium speciation for the experimental water.

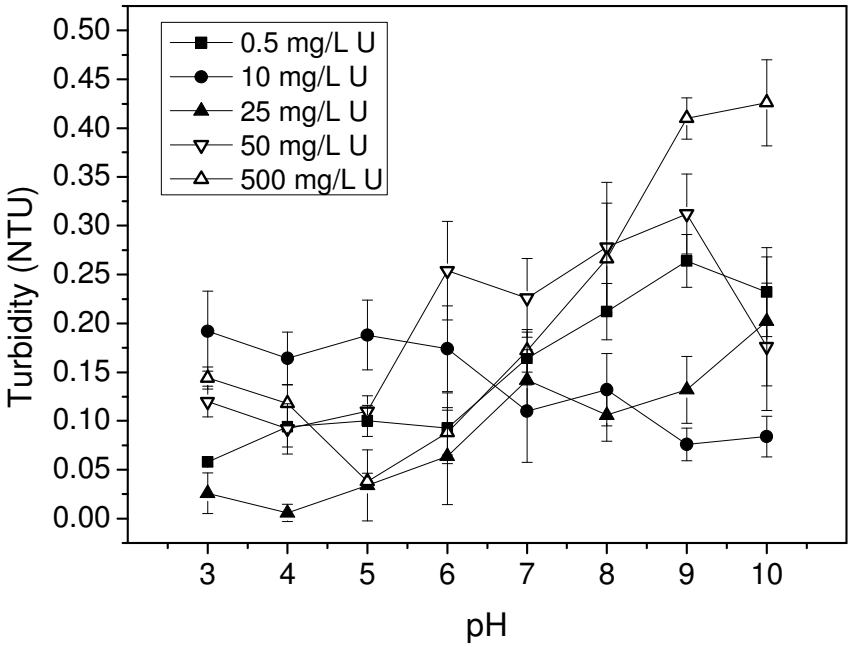

Figure 36. Turbidity results measured for uranium samples containing background solution (20 mM NaCl and 1 mM $NaHCO_3$) and a uranium concentration range of 0.5, 10, 25, 50 and 500 mg/L.

Static precipitation experiments were performed for a range of uranium concentrations between 0.5 mg/L and 500 mg/L. The results showed no visible precipitation of uranium across the pH range 3-10, even for the 500 mg/L uranium sample. The turbidity results (Figure 36) show no significant difference between

samples across the pH range, apart from possibly the 500 mg/L sample at pH 9 and 10 (although precipitation was still not observable visually). This confirmed that for the concentrations relevant for the laboratory experiments (0.5 mg/L), precipitation is unlikely to be an up-take mechanism by the membrane.

Uranium distribution within and on the membrane as determined by μ-XRF spectroscopy

Analysis was performed using μ-XRF spectroscopy in an attempt to see if any differences in spatial distribution of uranium could be observed between pH 6, where maximum uranium-membrane interaction was observed for both membranes, and pH 8.5, where low interaction occurred. As stated above, the uranium species present at these two pH values differed greatly in both size and charge. First of all, analysis of a 4 x 5 cm membrane section was performed for the TFC-SR2 membrane which had resulted from the pH 6 experiment. This showed the homogenous distribution of uranium present in the membrane shown as "dots" across the surface of the membrane viewed from above (Figure 38). Since the X-Ray beam penetrates the membrane, this result showed that uranium was present (Figure 38), but not whether uranium penetrates within the membrane. Therefore, cross-sections were scanned in line analysis mode, with the objective of identifying the uranium profile from top to bottom through the membrane section (Figure 39).

One challenge was to establish the precise position of the borders of the membrane in order to determine the uranium distribution therein. μ-XRF spectroscopy is only sensitive to elements with an atomic number greater than sodium and so, elements present in the active layer of the membrane such as nitrogen, are not detected. Sulfur (S) from the polysulfone support layer is however detected, and can be used to indicate the limits of the polysulfone support layer. Other elements that were detected at low levels were titanium (Ti) and potassium (K). The presence of titanium was not expected and is not a specified component by the manufacturers, although it was noticed in all membrane samples analysed. The approximate location of the top and bottom of the membrane was calculated by plotting the derivative of the fluorescence intensity for the Kα line of the elements present in the membrane (S

and Ti). The membrane thickness could thereby be estimated as between 170 to 210 µm for both TFC-SR2 and BW30. The calcium present in Figure 39 is due to the support material holding the membrane sample in place during analysis, and thus any calcium signals are not from the membrane, giving an additional indication of where the membrane section stops.

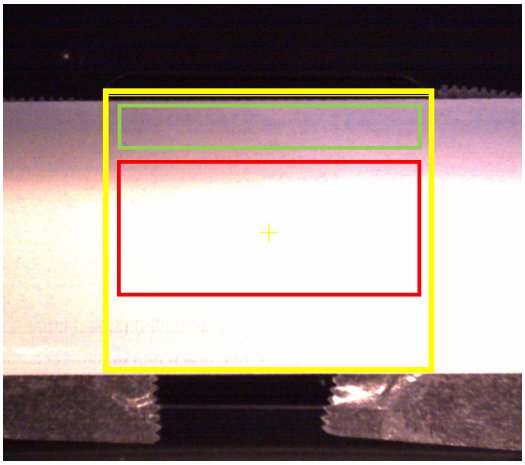

a) Digital image of membrane

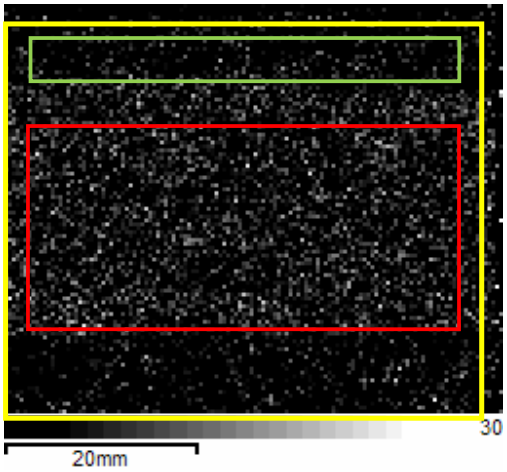

b) U (Lα1 line, 1 px=400 µm, 64 px^2)

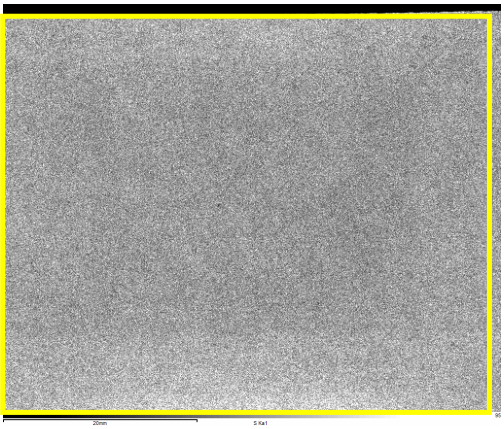

c) S (Kα line, 1 px=100 µm, 256 px^2)

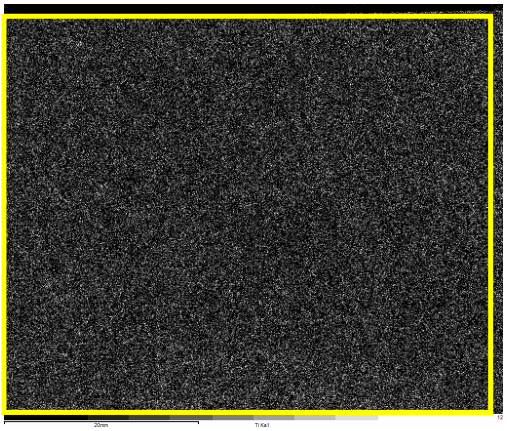

d) Ti (Kα line, 1 px=100 µm, 256 px^2)

Figure 37. Digital image (CCD) of the membrane surface viewed from above (a); uranium (b), sulphur (c) and titanium (d) distribution present in the TFC-SR2 membrane subjected to an experiment with 0,5 mg U/L and background electrolyte (20 mM NaCl and 1 mM $NaHCO_3$) at pH 6 with no applied pressure. The chemical maps were obtained by µ-XRF with a total counting time of 15×1000s, incident X-Ray beam size of 100 µm. ULα1 map resolution was reduced by 4 to improve contrast. On the CCD digital image (a), the yellow square shows the regions scanned by the X-Ray beam during mapping. The spectra from the red and green marked regions are shown in Figure 38.

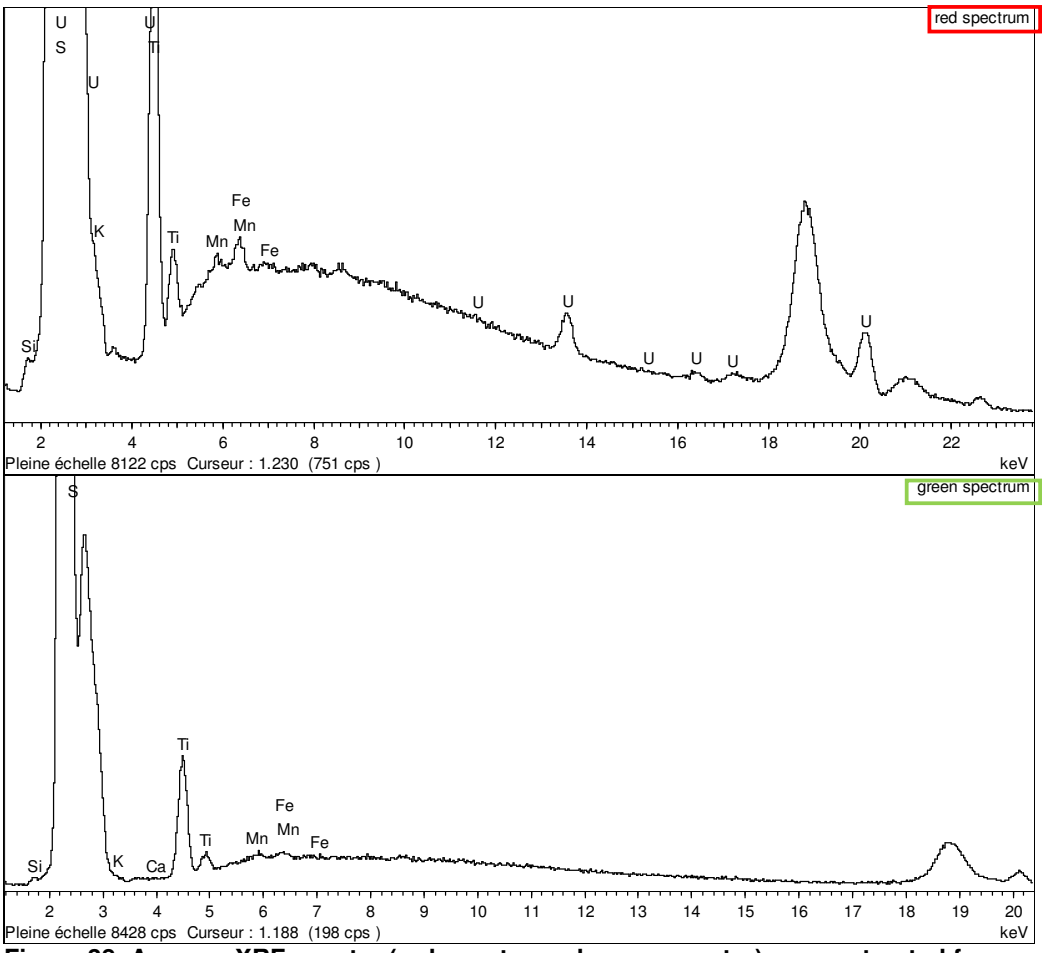

Figure 38. Average XRF spectra (red spectra and green spectra) were extracted from selected pixels (in red or green boxes) of the ULα1 hyperspectral map. The spectra show that uranium was present through-out the main membrane area, marked in red, while the sides of the membrane showed little uranium (which is where the membrane was clamped in the cross-flow system).

The μ-XRF analysis performed on the membrane cross-sections showed interesting differences in uranium distribution within the membrane, both between the membrane types and at the different pH values. From Figure 39 it can be seen that while uranium was detected within the TFC-SR2 membrane at both pH values, there was no uranium signal for the BW30 membrane. This is probably because the uranium taken up by BW30 could not penetrate far into the membrane and thus any amounts were likely to be below the detection limit of the μ-XRF. Uranium-membrane interaction was indeed lower for BW30 (Figure 34) than TFC-SR2 and

the µ-XRF results indicate that the uranium up-take may be mainly at the membrane surface.

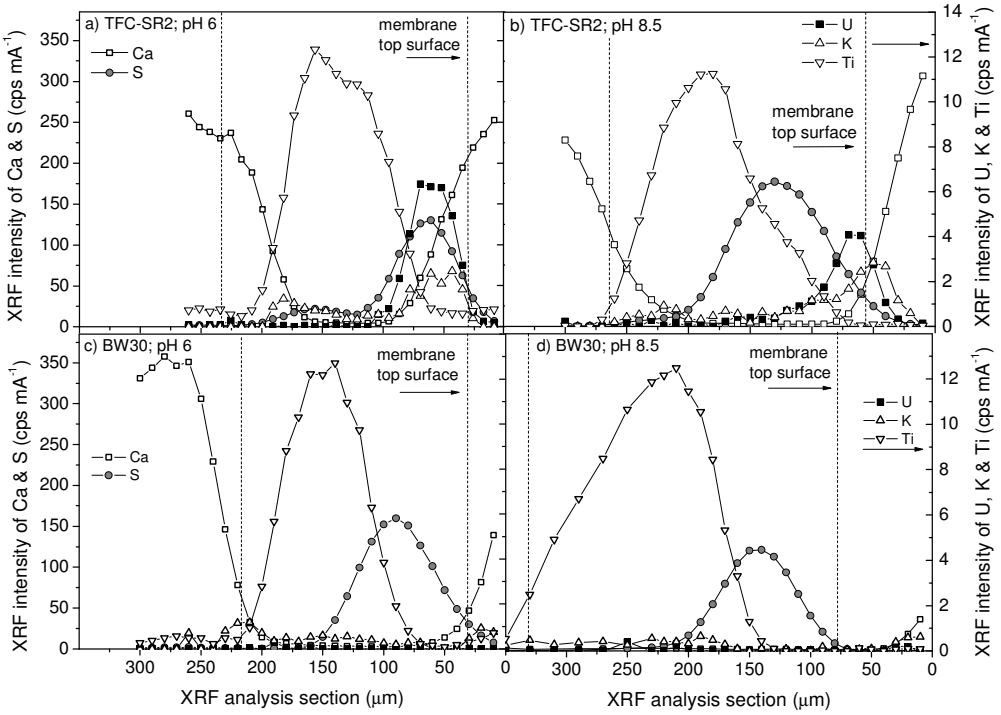

Figure 39. Cross-sections of TFC-SR2 and BW30 showing the elemental distribution of U, S, K, Ti and Ca (Ca due to the sample support) for experiments performed without pressure for TFC-SR2 at pH 6 (a) and pH 8.5 (b) and BW30 at pH 6 (c) and pH 8.5 (d). All experiments performed using 0.5 mg/L uranium with background electrolyte (20 mM NaCl and 1 mM $NaHCO_3$). The S-signal comes from the polysulfone support of the membrane. The approximate top and bottom edge of the membrane is indicated by a dotted line; however it should be kept in mind that the resolution of this technique is only 10 µm. Note the different scales for Ca and S compared to U, K and Ti.

For TFC-SR2, there was also a difference between the uranium distribution at pH 6 and at 8.5. At pH 6, the uranium peak intensity coincided with that of sulfur, indicating that uranium had entered into the membrane. Due to the relatively low resolution of the µ-XRF (10 µm diameter) it is not possible to determine whether the uranium is primarily present in active layer or the support layer of the membrane (or both). The uranium peak at pH 8.5 was of lower intensity than for uranium at pH 6 and did not coincide with that of sulfur. The lower intensity of the uranium peak at pH 8.5 (~4 cps mA^{-1} vs ~7 cps mA^{-1}) was consistent with the lower uranium-membrane interactions shown in Figure 34 (compare with pH 8-9). The position of

the S and U-peak in relation to each other indicates that uranium did not enter into the membrane but remained on the surface –potentially a result of the charge repulsion of the negative species and the negatively charged membrane at alkaline pH. It is important to note, however, that the low resolution of the μ-XRF does not allow for conclusive determination of the uranium distribution in the membrane; higher resolution techniques were therefore employed (see section 6.3.4).

Uranium-membrane interaction over much of the pH range can be explained by the charge of uranium species and the membrane, where oppositely charged uranium species were attracted to the membrane whilst uranium remained in solution when both membrane and species carried similar charge. However, at pH 7, uranium was still found to be interacting with the membrane despite their opposite charges. Chemical bonding may explain the interaction and this will be explored in a later 6.3.5). The relative size of the uranium species compared to membrane pore size may also be important in determining the extent of the interaction and membrane up-take of the uranium. Larger molecules than membrane pore size would be expected to experience higher rejection than smaller molecules, while molecules of similar size to the pore may interact readily with the membrane. The importance of ion size relative to membrane pores is recognised as an important parameter in NF retention (Schaep et al., 1998) and will therefore be discussed further in the next section.

Importance of species size relative to membrane pore size

For the more open TFC-SR2 membrane (MWCO = 486 g/mol), a greater amount of uranium was taken up by the membrane during the adsorption experiments at pH 5-7, compared to the amount taken up by the denser BW30 membrane (MWCO = 88 g/mol) (Figure 34), possibly reflecting the greater membrane surface area (including pore interior) available to uranium in a more open structure such as TFC-SR2 compared to BW30. TFC-SR2 and BW30 are composed of similar material and carry similar charge over the pH range 3 to 12 and so the main difference between them is pore size. Thus the larger amount that was taken up during the adsorption experiments at pH 5-7 for TFC-SR2 (~50%) compared to BW30 (~30%), indicates that membrane pore size could be a limiting factor (Figure 34a compared to b). At

these pH values the uranium species present (UO_2OH^+) is small enough (287 g/mol) to enter the pores of TFC-SR2 (MWCO = 486 g/mol), but is too large for those in the BW30 membrane (Table 9 and Table 10).

Table 10. Dominating uranium species for the pH range 3-10[a]

pH value	Dominating uranium species	Molecular weight[b] (g/mol)
3-4	UO_2^{2+}	270
5-6	UO_2OH^+	287
7	$(UO_2)_2CO_3(OH)_3^-$	651
8-10	$UO_2(CO_3)_3^{4-}$	450

[a] Note that each pH value contains a transition/mixture of several species.

[b] Although molecular weight is not an ideal measure of size, the crystal sizes of all aqueous uranium species have not been determined. As an indication, UO_2^{2+} has a crystal radius determined to 5.4682 Å and a covalent radius of 1.8 Å, whereas $UO_2(CO_3)_3^{4-}$ has a covalent radius of 4.85 Å.

At pH 3, where uranium-membrane interaction is minimal, the resulting mass adsorbed are very similar for both membranes, despite the species, UO_2^{2+}, being small enough to potentially fit through the pores of TFC-SR2. This further supports the hypothesis that the low uranium-membrane interaction observed at those pH values was due to electrostatic repulsion. At pH 8-10, the species, $UO_2(CO_3)_3^{4-}$, is just below the nominal MWCO of TFC-SR2 and much larger than the MWCO for BW30, giving similar low levels of adsorption to both membranes. Again, the relatively high mass adsorbed at pH 7 in TFC-SR2 is not explained by size however, since the dominating species, $(UO_2)_2CO_3(OH)_3^-$, is larger than the nominal MWCO of the membrane.

Initial conclusions following from the experiments with no applied pressure

Maximum uranium up-take by the membrane was observed between pH 5-7 for both TFC-SR2 and BW30, with more up-take occurring onto the TFC-SR2 membrane. At the acidic and alkaline ends of the pH range, mass adsorbed was low and was similar for both membranes. Since the experiments were performed without applied pressure, factors such as concentration polarisation and precipitation were minimised. The main interpretative points are summarised as follows:

- Charge repulsion explained the low interactions of UO_2^{2+} and membrane at pH 3.
- At pH 5-6, the mass adsorbed is high and primarily UO_2OH^+ dominates speciation (there are small amounts of UO_2^{2+}, $(UO_2)_2CO_3(OH)_3^-$ and UO_2CO_3. The observed adsorption behaviour was explained through a combination of charge attraction and small species size. The former is important for both membranes whilst the slightly lower interaction of UO_2OH^+ with the BW30 membrane was attributed to the tightness of the latter.
- The uranium-membrane interaction at pH 7 with TFC-SR2 can not be explained by either charge attraction nor molecular size effects, since both $(UO_2)_2CO_3(OH)_3^-$ and the membrane are negatively charged, and the species is larger than the nominal MWCO of TFC-SR2 the membrane. Nor could precipitation explain the interaction since the solubility of the species is below saturation.
- The low interaction between $UO_2(CO_3)_3^{4-}$ and membrane was attributed to both charge repulsion and its limited ability to enter membrane pores, due to the large size of this complex.

6.3.3 Investigation of uranium behaviour in a NF/RO system at selected pH values with variation in applied pressure

The application of different amounts of pressure to NF and RO membranes influences the retention and could potentially affect the mass adsorbed of solute ions, including uranium. While retention is expected to increase with increased permeate flux for RO, it was demonstrated in Figure 32 that for the NF membrane, salt retention decreased somewhat at higher pressure or only showed a small retention increase. Fouling through concentration polarisation also tends to increase at higher permeate flux so it may be expected that TFC-SR2 would suffer greater concentration polarisation than BW30 at higher pressures, with reversible flux decline as a consequence. The concentration at the membrane surface was calculated using Equation 5 (section 2.2.2). Whereas Cb, Cp and Jv were determined

experimentally, the mass transfer coefficient, k, had to be calculated. A number of Sherwood correlations have been derived, and those relevant for the experimental conditions (i.e. laminar flow and a slit channel) used are;

$$1.85 \times \mathrm{Re}^{0.33} Sc^{0.33} (d_h / L)^{0.33}$$ **Equation 11**

and

$$1.85 \times \mathrm{Re}^{0.43} Sc^{0.32} (d_h / L)^{0.33}$$ **Equation 12**

where Re = the Reynolds number, Sc = the Schmidt number, d_h = channel hydraulic diameter, L = the length of the membrane cell (Semião, 2011). Both correlations were used to estimate the mass correlation coefficient, thus giving two resulting values for Cm and the concentration polarisation modulus. The Reynolds, Schmidt and Sherwood number are, respectively, calculated by;

$$\mathrm{Re} = \frac{\rho v d_h}{\mu},\ Sc = \frac{\mu}{\rho D_{AB}} \text{ and } Sh = \frac{k}{D_{AB}}$$

where ρ = solution density (kg/m^3), μ = solution viscosity (Pa.s), D_{AB} = solute diffusivity in solution (m^2/s) and k = the mass correlation coefficient. Since uranium is taken up by the membrane, thereby decreasing the concentration found in the concentration polarisation layer, the maximum uranium concentration that the membrane would experience during the experiment was calculated by taking Cb as the initial feed concentration during the experiment and Cp = 0 (before any permeation has taken place). The uranyl diffusion coefficient was used (6.52×10^{-9} m^2/s). The resulting polarisation modulus (Cm/Cb) is displayed together with uranium mass adsorbed in Figure 42.

To investigate how pressure affects uranium-membrane interactions and retention by the NF and RO membranes, two pH values were selected: pH 6, where maximum mass adsorbed had occurred and pH 8.5, where lower uranium-membrane interaction

was observed for both membranes when no pressure had been applied. Applied pressures over the range 5-15 bar were investigated.

The pure water flux measured using DIW was measured at the experimental pressure, before and after each pressure experiment to show whether fouling had taken place during the experiment. The pure water flux together with the permeate flux during the experiment are displayed in Figure 40.

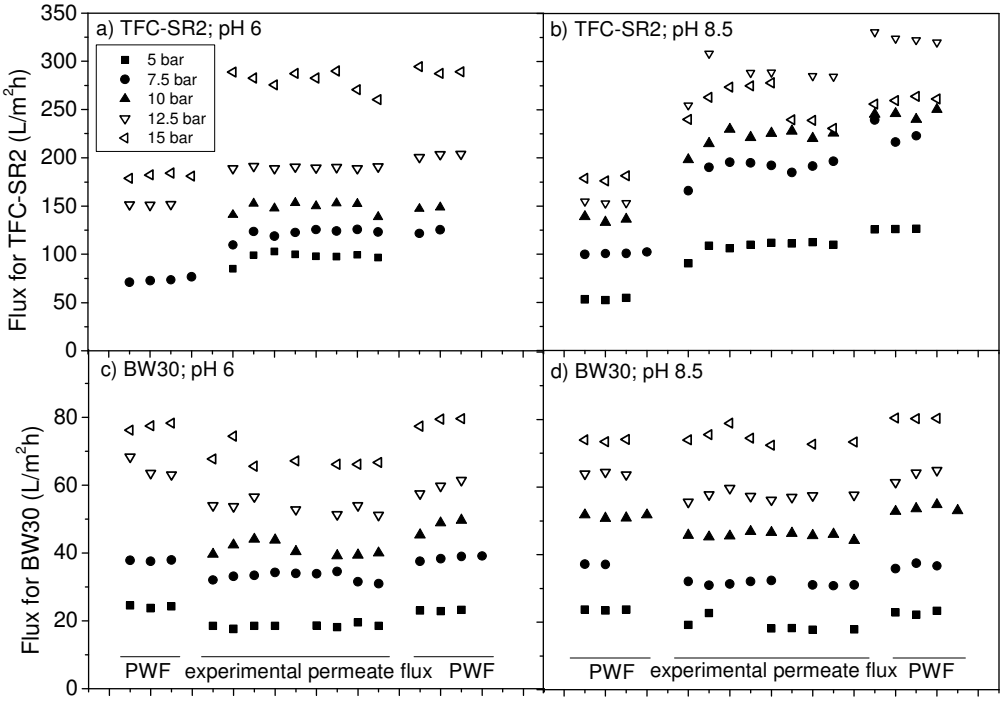

Figure 40. Flux of pure water (PWF) before and after pressure experiments (3-4 readings taken) as well as permeate flux during pressure experiments (5-15 bar) for TFC-SR2 and BW30 at pH 6 and 8.5. Experimental solution: 0.5 mg/L uranium + 20 mM NaCl and 1 mM $NaHCO_3$. Flow-rate = 0.6 L/min, temperature = 25°C. Two readings were taken at the experiment start, then readings were taken ~hourly for a total of seven hours of experiment. Permeability of TFC-SR2 = ± 13% and ± 3% for BW30.

The pure water flux is generally much lower for BW30 than TFC-SR2. For the BW30 membrane, at each selected pressure, the permeate flux obtained for the experimental solutions (containing uranium) was only slightly lower than the pure water flux (Figure 40c and d). Ions in solution often form a concentration polarisation layer which somewhat reduces the permeate flux due to the increased osmotic pressure on the feed side of the membrane. Importantly, this permeate flux

decline was reversible and when the experiments were completed, the pure water flux increased to values similar to those obtained before the experiment, showing that any effect the experimental solution had on flux across BW30 during the experiment was reversible.

For the TFC-SR2 membrane, the changes in permeate flux were quite different. The addition of the experimental solution to the system increased the permeate flux, often nearly doubling the values obtained for pure water (Figure 40a and b). In contrast to the BW30 membrane results, this was not reversible; when pure water was added after the experiment, the flux remained high. Indeed, for the pH 8.5 experiments, the pure water flux even increased somewhat after the experiment (Figure 40b). It is interesting to note that a permeate flux increase occurred for TFC-SR2 compared to DIW flux also with the addition of the background electrolyte only (20 mM NaCl and 1 mM $NaHCO_3$) (Figure 31). This is not really expected behaviour for NF membranes, but has been noted in other studies *e.g.* in a NF study by Nilsson et al., (2006) and Wang et al. (2010). Wang et al. had a 44% permeate flux increase with the addition of 0.002 M NaCl compared to a solution without NaCl, while De Munari and Schäfer (2010a) found that a solution containing Mn and the same background electrolyte as in this study, also increased the permeate flux for TFC-SR2. Nilsson et al. (2006) explain that this behaviour is likely to be caused by swelling or dissociation of the polyamide active layer, which, due to its polyampholytic nature, will be held together by cross-linking between negative and positive charges within the membrane structure. The addition of salt ions will therefore interfere with this cross-linking by interacting with the membrane through electrostatic attraction. In the study of this PhD research, the addition of background electrolyte increased the permeate flux, however, the presence of uranium at *pH 6* reduced this effect, while when uranium was present at *pH 8.5*, the flux remained high. Since the background electrolyte was the same for both pH values, this suggests that at pH 6, uranium interacts with the membrane in a different manner to at pH 8.5.

The resulting mass adsorbed of uranium at the end of each pressure experiment along with uranium retention, overall salt retention (a combination of uranium and

background electrolyte, measured with a conductivity meter) and permeate flux measured at the end of the experiment are displayed in Figure 41. The mass of uranium taken up by the membrane was calculated as before using mass balance, this time also taking into account the permeate samples taken during the experiment, and is given as the percentage of the initial mass of uranium (Equation 13).

$$Mass\ Adsorbed\ (\%) = \frac{V_{b0}C_{b0} - V_{bf}C_{bf} - \sum_{i=0}^{i=8} V_S C_{bi} - \sum_{i=1}^{i=5} V_S C_{pi}}{V_{b0}C_{b0}} \times 100 \qquad \textbf{Equation 13}$$

Symbols as for Equation 10, with the addition of p = permate.

The percentage retention (using the final permeate and bulk concentrations) was calculated as in Equation 1.

For the BW30 membrane, the retention of uranium was >99% for both pH values and across pressure. Salt retention was also >90% for most experiments and this parameter showed a small increase from low to high pressure (as expected for RO). The final permeate flux increased linearly with increasing pressure, although for pH 8.5, the trend was somewhat steeper.

For TFC-SR2, the uranium retention varied from 81 to 94% at pH 6 and 87 to 99% at pH 8.5. Salt retention also varied from 17 to 28% at pH 6 and from 23 to 40% at pH 8.5. The relationship between retention and pressure was somewhat more erratic than it was for BW30, a reflection of the generally more variable permeability of the TFC-SR2 membrane (average permeability of DIW for membranes used in pressure experiments was 10.97 ± 1.51 L/m^2 h bar, giving a 13% variation, compared BW30 which had an average DIW permeability of 4.84 ± 0.15 L/m^2 h bar and a 3% variation). The final experimental permeate flux increased with increasing pressure, but the increase was not linear. In fact for pH 6, the flux increases more steeply at higher pressure, which is contrary to what had been predicted for this membrane, *i.e.* enhanced concentration polarisation effects would be expected to decrease the flux rather than increase it. The permeate flux for the pH 8.5 experiments with TFC-SR2

increased rapidly with pressure, but at higher pressure it evens out. The initial permeability of the membrane was similar to that at lower pressures, so it may be that at the higher pressures, concentration polarisation was reducing the permeability of the membrane somewhat due to the larger uranium species present at pH 8.5.

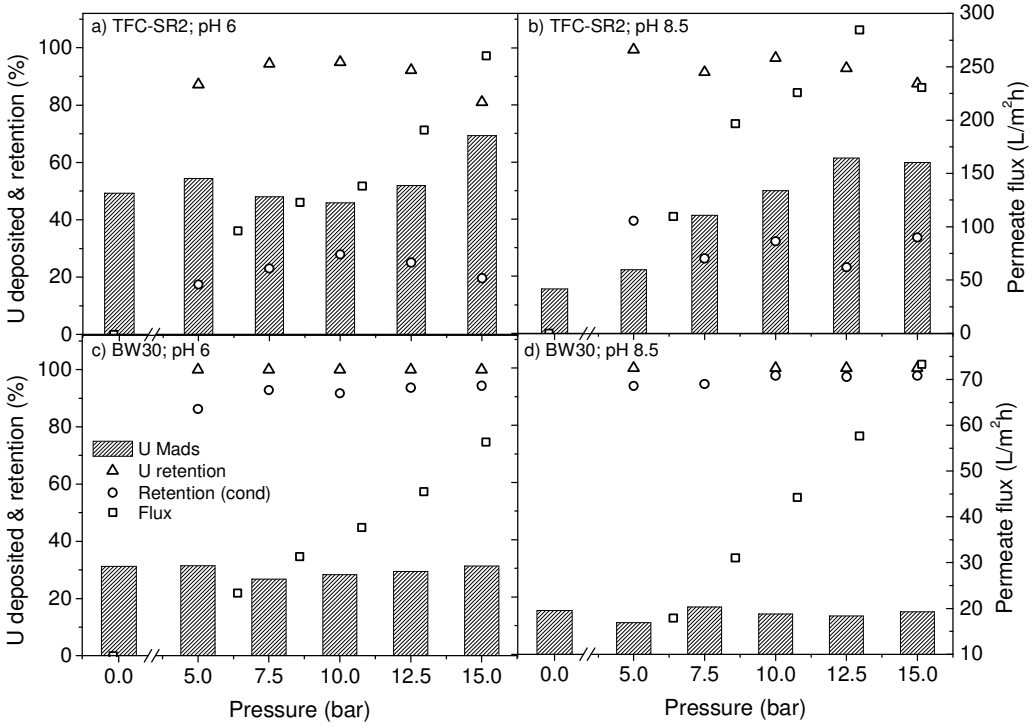

Figure 41. Mass adsorbed of uranium (columns), retention of uranium and salt (triangles and circles) as well as final permeate flux (squares) at the end of each pressure experiment are given for membranes TFC-SR2 (a and b) and BW30 (c and d) for pH values 6 and 8.5. The mass adsorbed of uranium obtained during no-pressure experiments are added for comparision. Experimental solution: 0.5 mg/L uranium + 20 mM NaCl and 1 mM $NaHCO_3$. Flow-rate = 0.6 L/min, temperature = 25°C. The adsorption had a variation of up to ± 10% for TFC-SR2 ± 4.4% for BW30. Retention had a variation of up to 13% for TFC-SR2 and 6% for BW30.

During the experiments with BW30, an increase in pressure did not increase uranium-membrane interactions at either pH 6 (Figure 41c) or 8.5 (Figure 41d) and the mass adsorbed remained at similar levels to that without pressure (~30% at pH 6 and <20% at pH 8.5). This showed that the uranium species were too large to penetrate into the membrane. The molecular weight cut-off of the RO membrane was 88 g/mol, which is significantly lower than that of any of the uranium species (Table 10); consequently none of the uranium species penetrated the membrane even when

pressure was applied. As previously mentioned, the XRF analysis of experiments without pressure showed that any uranium penetrating into the BW30 membrane was below the XRF detection limit (Figure 39c and d). Retention was also not significantly affected by pressure. There was a slight linear increase in Cm/Cb (Figure 42c and d). However, as expected, BW30 did not experience much concentration polarisation due to it's relatively low permeate flux, and Cm/Cb for uranium ranged from 1.02 to 1.10.

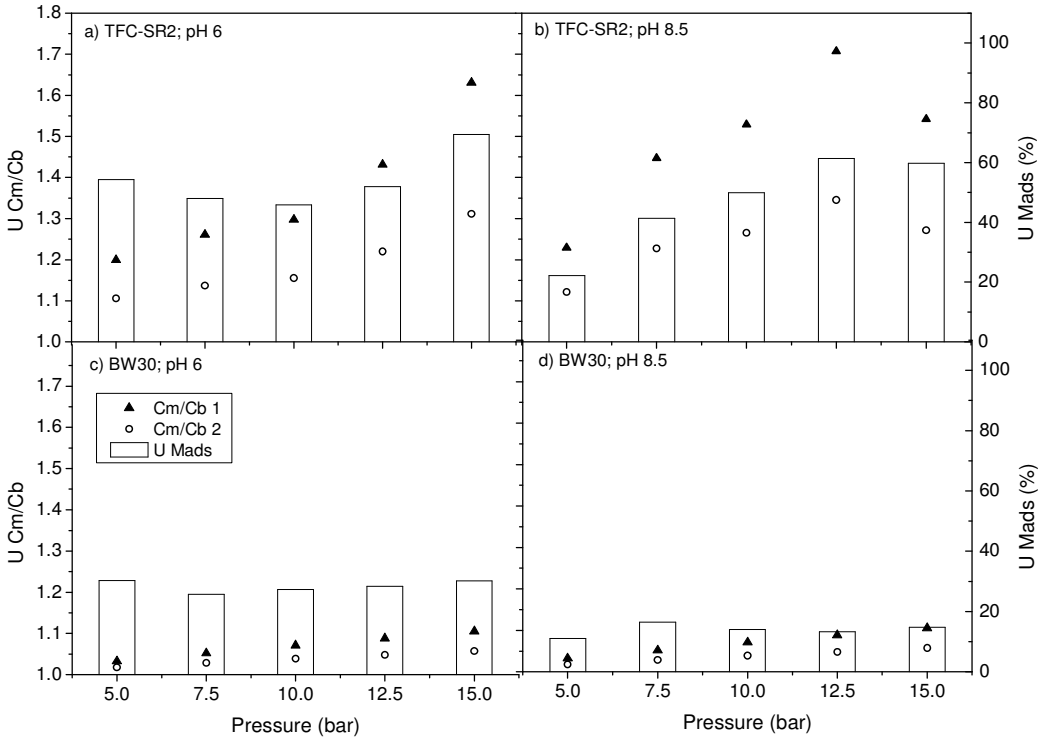

Figure 42. The polarisation modulus (Cm/Cb) for uranium during the experiments. Two values are given, as a result of two correlations used. The mass adsorbed of uranium during the experiments is shown for comparison.

During the experiments with TFC-SR2 at pH 6, pressure did not affect the extent of uranium mass adsorbed (Figure 41a) over the range 5-12.5 bar (within the 6-10% variation). Only at 15 bar did the mass adsorbed of uranium increase from around 50-55% to 70%. This provides further evidence in support of the hypothesis that size was not a limiting factor for uranium-membrane interaction at pH 6 to this membrane since the uranium species were small enough to penetrate and interact with the membrane even when no pressure was applied. At pH 6, the uranium-containing

species are a mixture of mainly UO_2OH^+ and some UO_2^{2+}, UO_2CO_3 and $(UO_2)_2CO_3(OH)_3^-$ with a molecular weight of 287, 270, 330 and 651 g/mol, respectively, while the membrane has a nominal MWCO of 486 g/mol and an absolute MWCO of 1033 g/mol. Indeed, for the situation where no pressure had been applied, XRF analysis of a membrane cross-section confirmed that uranium had penetrated into the membrane (Figure 38a). It is likely that the main uranium-membrane interaction is due to UO_2OH^+ as it is relatively small and also has opposite charge compared to the membrane, which would favour adsorption through charge attraction. Higher adsorption would take place for UO_2OH^+ compared to UO_2^{2+} due to lower aquation of UO_2OH^+ and consequently a lower adsorption energy barrier (Giblin et al., 1981). At 15 bar, uranium mass adsorbed increased, suggesting that penetration increased at the higher pressure, possibly as the higher molecular weight uranium species, $(UO_2)_2CO_3(OH)_3^-$, is forced into the membrane (this would also lead to a higher uranium mass adsorbed per molecule since each contains two rather than one uranyl component).

TFC-SR2 at pH 6 experienced significant concentration polarisation of uranium with Cm/Cb values ranging from 1.10 to 1.60 (Figure 42a). The concentration polarisation increased with increasing pressure and resulting uranium concentrations at the membrane surface were calculated to be a maximum of 0.94 mg/L at 15 bar. This concentration is well below the solubility limit for uranium thus excluding precipitation as an up-take mechanism. Cm/Cb increased with pressure but this was not reflected in the mass adsorbed of uranium. Thus, the high adsorption of uranium at pH 6 (about 60%) appears unrelated to concentration polarisation.

The trend of mass adsorbed to TFC-SR2 with increasing pressure at pH 8.5 was different to that at pH 6. There was only a slight difference between the no pressure and 5 bar pressure results. In both cases only about 20% uranium was taken up by the membrane. The retention was high during the run at 5 bar: >99%, showing that little uranium penetrated through the membrane. The μ-XRF analysis for the experiment without pressure showed that uranium did not penetrate as deeply into the membrane as for pH 6 (Figure 39b). This exclusion is most likely a combination of size and

charge repulsion, since the uranium species, $UO_2(CO_3)_3^{4-}$ (450 g/mol), is very close in size to the nominal MWCO (486 g/mol) of the membrane but smaller than the absolute MWCO (1033 g/mol) and both membrane and uranium species are negatively charged. Increased pressure, however, caused an increase of uranium mass adsorbed of up to 60% at 12.5 and 15 bar (Figure 41b). When comparing Cm/Cb with the mass adsorbed of uranium for pH 8.5, this shows a linear correlation (Figure 42b). It seems that the uranium mass adsorbed at this pH value responds to an increase in concentration polarisation at the membrane surface. The calculated uranium concentration due to concentration polarisation does not exceed 0.97 mg/L, excluding precipitation as a reason for the increased uranium up-take by the membrane. However, the higher concentration of uranium which came in contact with the membrane as a result of increased pressure and concentration polarisation, led to increased adsorption and decreased retention, despite barriers such as charge repulsion.

The results from the pressure experiments above have shown that molecular size and charge play an important role in the membrane up-take of uranium; the negatively charged species at pH 8.5, $UO_2(CO_3)_3^{4-}$, was interacted to a lesser extent than the positively charged species at pH 6, $UO_2(OH)^+$. This is due to the large charge repulsion between the carbonate complex and the negatively charged membrane at pH 8.5, in comparison with charge attraction between the hydroxy complex and the membrane at pH 6. Comparing the results from the RO and NF experiments showed that molecular size of the solute species relative to the pore size of the membrane was a limiting factor. However, when species and membrane pore size where similar as in the case of TFC-SR2 and $UO_2(CO_3)_3^{4-}$ the behaviour of uranium was affected by concentration polarisation (resulting from increased pressure). However, although size may be a limiting factor for certain species (*e.g.* the up-take of UO_2OH^+ at pH 6 was limited for BW30 but not for TFC-SR2), smaller species such as UO_2^{2+} showed only low levels of uranium-membrane interaction with both TFC-SR2 and BW30 at pH 3 (Figure 34a). In addition to charge-repulsion between the positively charged membrane and the positively charged uranium species, the stability of UO_2^{2+} makes it even more unlikely to interact with the membrane.

The mass adsorbed of uranium to TFC-SR2 and BW30 at pH 6 was unaffected by pressure and uranium concentrations remained within the solubility limit. This indicates that mechanisms such as electrostatic interactions or even chemical bonding, are responsible. These may be favoured by the openness of TFC-SR2 which would have an increased membrane area was available compared to BW30. Hence the reactivity of a species is also important in determining its interactions with the NF membrane.

6.3.4 Spatial distribution of uranium within the membrane

To further explore the uranium-membrane interaction, a range of techniques were employed: SEM, TEM and STEM-EDX. The TFC-SR2 membrane was chosen for these experiments since it was made of similar material and had similar charge as BW30, but experienced higher levels of uranium adsorption. Experiments were performed without pressure since these would not be affected by any concentration polarisation or precipitation, the latter being of particular concern for the 50 mg/L uranium solutions.

Firstly TFC-SR2 cross-sections were examined by both the SEM and TEM. The SEM cross-section clearly shows the polysulfone support layer, measuring between 40-60 µm thick on top of the polyester support web (Figure 43). The polyamide active layer can be seen as a brightly contrasting line on top of the polysulfone support layer.

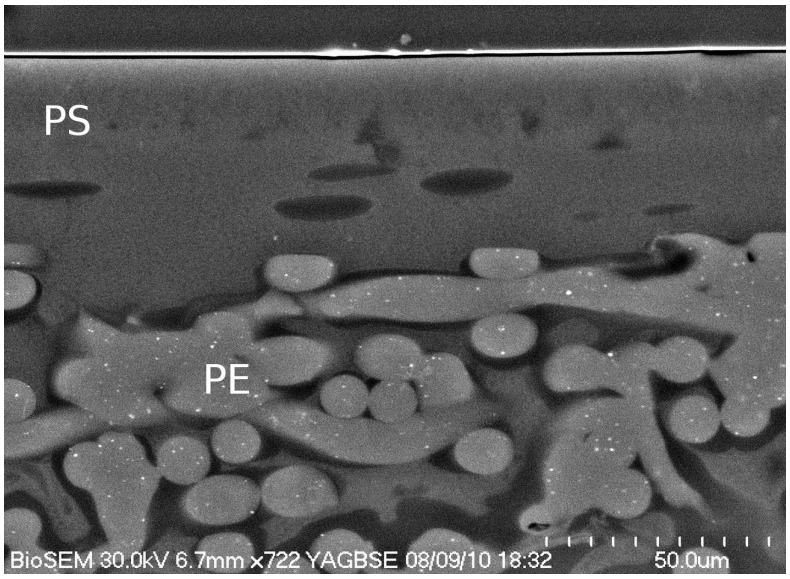

Figure 43. SEM image of cross-section of the TFC-SR2 membrane. The polysulfone (PS) support layer is clearly distinguishable from the underlying polyester (PE) support web and measures between 40-60 µm. The polyamide active layer can be made out as a bright line on top of the polysulfone support layer.

The TEM image gave a more detailed view of the dense polyamide active layer, measuring about 200-250 nm thick, which was separated from the porous polysulfone layer by a bubbly-looking interface (Figure 44).

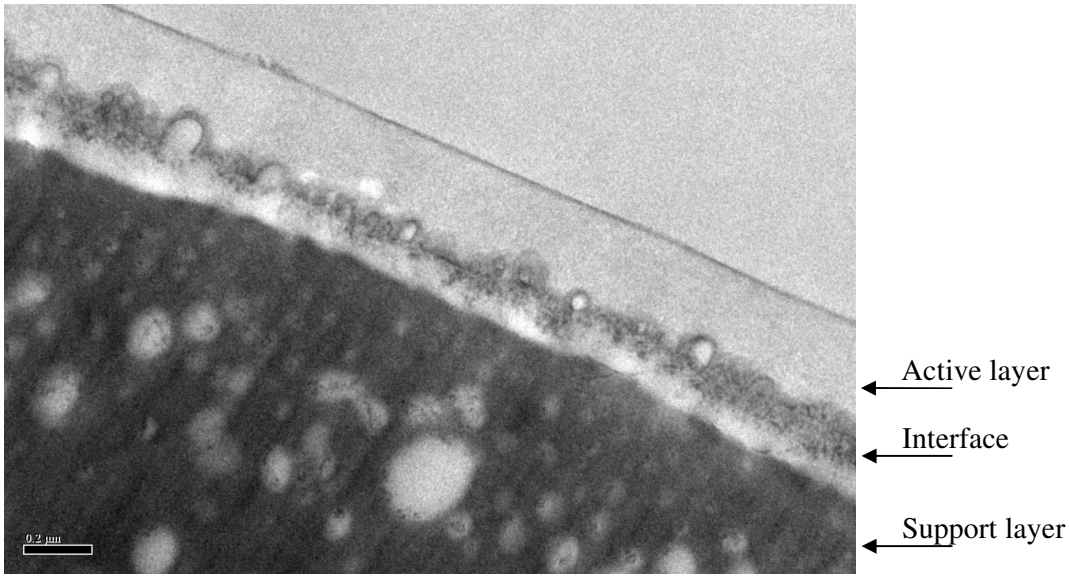

Figure 44. TEM image of cross-section of membrane after a uranium experiment with TFC-SR2 at pH 6. The image shows the polyamide active top layer of the membrane (about 200-400 nm thick), the bubbly looking interface between the polyamide and polysulfone layer and then the dark polysulfone support layer. Darker areas are a result of higher electron density. The scale bar indicates 0.2 µm.

Experiments at pH 6

The SEM images of the TFC-SR2 membrane after an experiment at pH 6 (with a 0.5 mg/L uranium solution) showed the uranium distribution on the membrane, where patches of higher uranium give rise to the brighter contrast (Figure 45b). It should be noted that the SEM beam penetrates some distance into the membrane and certainly the whole active layer is sampled (not just the top surface). Figure 45a shows a clean membrane for comparison.

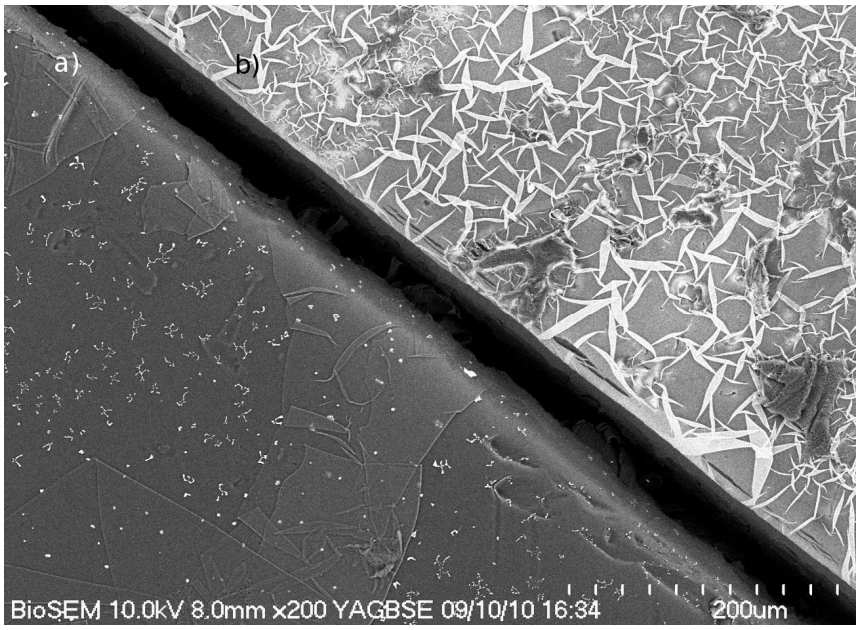

Figure 45. SEM image of a) the clean TFC-SR2 surface compared to b) the TFC-SR2 surface after a pH 6 experiment with 0.5 mg/L U + 20 mM NaCl and 1 mM $NaHCO_3$, no applied pressure, flow-rate = 0.6 L/min, temperature = 25°C. High atomic mass shows up with bright contrast, and it can be seen how uranium has stained the membrane in a net-work like pattern.

Since TEM alone cannot give elemental information, STEM-EDX was needed to confirm uranium presence in the polyamide versus the polysulfone layer. Due to detection limitations of the EDX, experiments had to be performed using a uranium concentration of 50 mg/L to ensure detection. Following the experiment at the higher uranium concentration, the membrane was clearly yellow to the eye and a fine network was visible through an optical microscope. The membrane was also examined in SEM and in the image obtained using the YAGBSE mode, uranium gives a very bright contrast with the otherwise dark background (Figure 46a). Figure

46a shows that, at the high concentrations required for this experiment, the membrane was nearly uniformly covered by uranium (keeping in mind that SEM analysis penetrates into the membrane and does not only measure the surface). The cross-section also analysed with SEM shows that uranium is concentrated in a thin line which denotes the position of the membrane surface (Figure 46), indicating that uranium was mainly present in the polyamide active layer of the membrane.

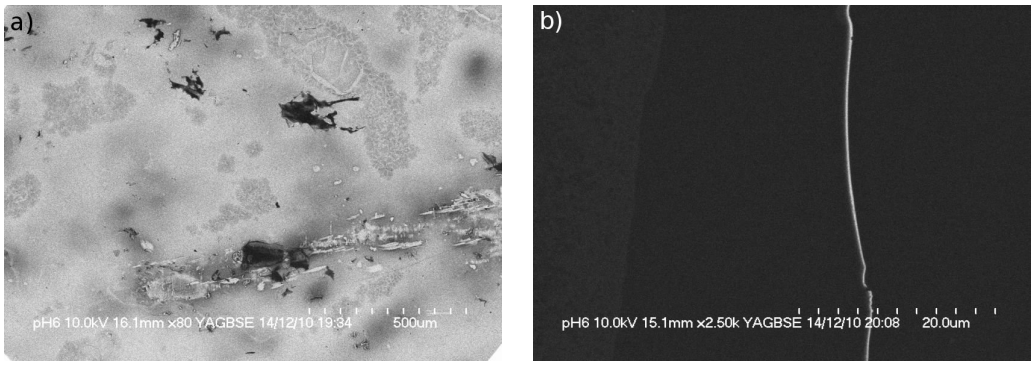

Figure 46. a) SEM of TFC-SR2 after experiment at pH 6 and with a 50 mg/L U solution + 20 mM NaCl and 1 mM $NaHCO_3$, no applied pressure, flow-rate = 0.6 L/min, temperature = 25°C. The surface is covered with uranium, making it appear nearly completely white. b) The SEM image of the membrane cross-section clearly shows a very brightly contrasting line where uranium is present on the membrane surface.

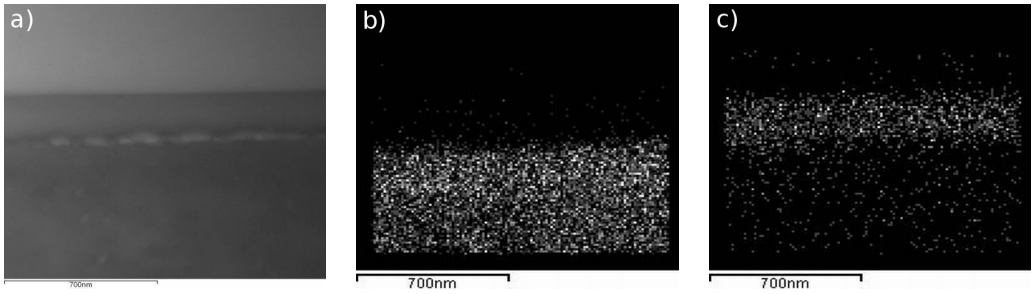

Figure 47. STEM-EDX results of TFC-SR2 membrane after an experiment at pH 6 showing: a) the STEM-EDX reference image b) sulfur distribution c) uranium distribution. Experimental conditions: 50 mg/L U + 20 mM NaCl and 1 mM $NaHCO_3$, no applied pressure, flow-rate = 0.6 L/min, temperature = 25°C. The scale bar shows 700 nm for all three images.

The polyamide and polysulphone layers could be distinguished using STEM-EDX by comparing the reference image (Figure 47a) with the sulphur distribution shown in Figure 47b; sulphur is present in the polysulphone support layer while the polyamide layer is sulphur-free. Additionally, the STEM-EDX results clearly show that the main uranium distribution (Figure 47c) is different to that of sulphur (Figure 47b)

and showed that uranium was present through-out the thickness of the polyamide active layer. The image shows that uranium is evenly adsorbed in the polyamide active layer, and not, for instance, precipitated on top.

Experiments at pH 8.5

The membrane looked somewhat different after the experiments at pH 8.5. Due to the high uranium concentrations, the membrane again appeared yellow to the eye, although with a more matt appearance than for pH 6. Notably it appeared that a layer had formed on top of the membrane which easily peeled off. This layer had high concentrations of uranium, as seen from the YAGBSE image where the bright uranium is contrasted with the membrane, which is dark due to the high contribution of light elements to its structure (Figure 48a). The SEM image of the cross-section of the membrane also shows a bright band on top of the membrane surface (Figure 48b). An additional difference between the pH 6 and pH 8.5 cross-sectional images was that, for the latter, the bright layer appears to be separated from the support material and to fold back on itself whilst, at pH 6, an almost continuous bright line was observed. The STEM-EDX analysis helped to further characterise the pH 8.5 membranes. Figure 49a confirmed that the active surface layer had, in some places, separated from the support material (note the much finer scale in Figure 49a compared with Figure 49b). The sulphur distribution again marked the position of the polysulphone support layer (Figure 49b) while Figure 49c shows that uranium was present in a layer above the membrane surface. The formation of a surface layer by uranyl carbonate complexes leading to increased retention by UF membrane filtration was hypothesised by Kryvoruchko et al. (2004) (using a concentration of 10 mg/L), although not further validated. At higher uranium concentrations, uranium is known to form polynuclear uranyl carbonate species (Schlosser et al., 2010), and it is possible that these could form a loose layer of uranium species as the uranium concentration is increased close to the membrane surface.

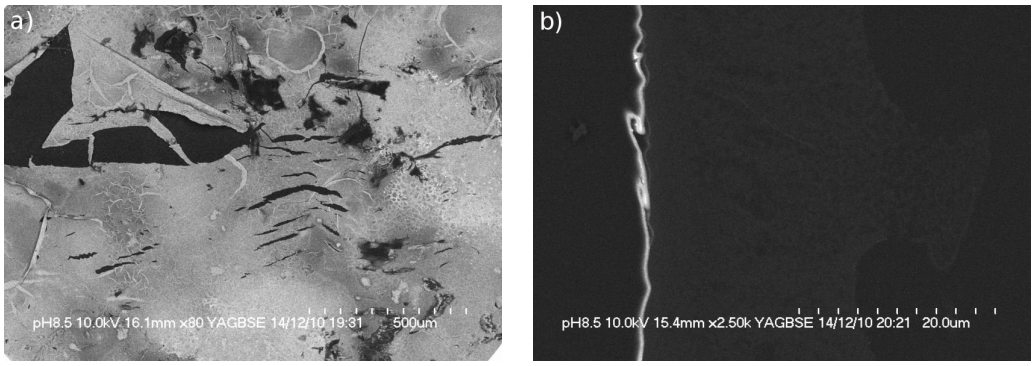

Figure 48. a) SEM image of TFC-SR2 membrane after an experiment at pH 8.5 and b) a cross-section of the same membrane, viewed through SEM, the uranium giving a brightly contrasting band on top of the membrane surface. Experimental conditions: 50 mg/L U + 20 mM NaCl and 1 mM $NaHCO_3$, no applied pressure, flow-rate = 0.6 L/min, temperature = 25°C.

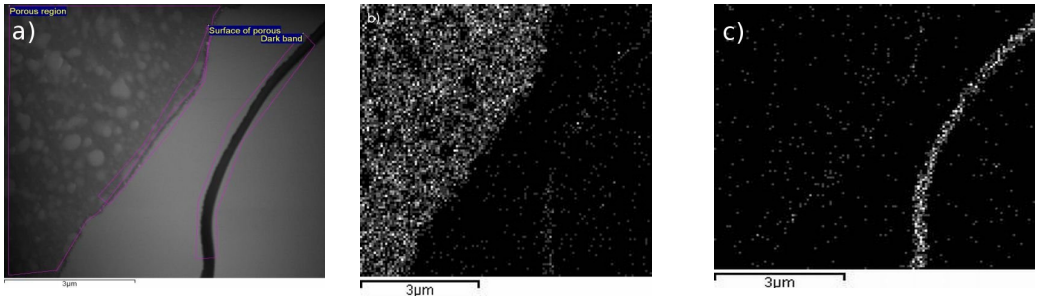

Figure 49. STEM-EDX of membrane after experiment at pH 8.5 showing: a) the reference image, b) sulfur distribution and c) uranium distribution. Experimental conditions: 50 mg/L U + 20 mM NaCl and 1 mM $NaHCO_3$, no applied pressure, flow-rate = 0.6 L/min, temperature = 25°C. Note that the scale bar shows 3 µm for all three images.

Overall, these imaging results show that after experiments performed at pH 6, uranium was evenly distributed through-out the polyamide active layer, while not much uranium detected in the polysulfone support layer. After experiments at pH 8.5, uranium was only loosely covering the surface of the membrane in what appeared to be an easily detachable layer.

6.3.5 Binding of uranium with membrane functional groups

The results from the cross-flow experiments investigating uranium interactions with the NF and RO membranes with and without applied pressure and the images from the spatial distribution of uranium in the membrane strongly suggest that, under

certain pH conditions (in particular, at pH 6), uranium adsorbs to the membrane active layer, either through electrostatic attraction or chemisorption. The latter would involve chemical bond formation and thus membrane functionality would be affected. Above pH 8, uranium showed much lower interaction with the membrane than at pH 6, and did not appear to penetrate as far into the active layer, most likely result of electrostatic repulsion and the large size. A loose uranium layer was still noticeable on top of the membrane however, and thus it was interesting to further explore any changes in membrane functionality.

As described in section 6.2, both BW30 and TFC-SR2 consist of an active layer composed of polyamide on top of a more porous support layer of polysulfone (Figure 44). As can be seen from structures below, the main functional groups of the polymer comprising the active layer would be the carbonyl (-C=O), carboxyl (-COOH), amine (-NH) and amide (-CONH) groups (Figure 50a). Within the polysulfone structure, important groups are the sulfone group ($-SO_2$). Electronegative benzene and methyl groups rings are present in both layers (Figure 50a and b).

a)

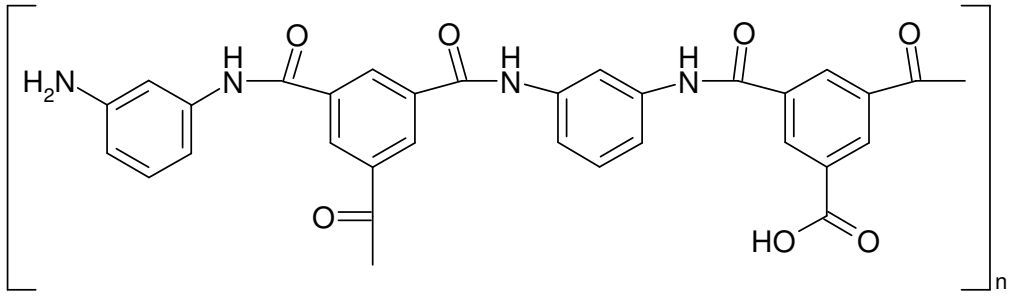

b)

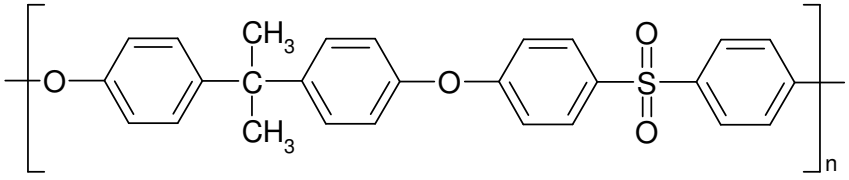

Figure 50. Molecular structure of a) polyamide and b) polysulfone. These are general structures since any modification to chemical structure of the membranes are proprietary to the manufacturing company. Other examples are given in the Appendix (11.4.6)

To investigate if there had been any chemical change in membrane functional groups as a consequence of reactions with uranium species, FTIR analysis was performed for experiments at pH 6 and pH 8.5. FTIR analysis of two clean membranes treated in the cross-flow system with DIW at the experimental pH was performed to identify any changes in the functionality of the membrane that were due to the change in the pH of solution *per se*. Then the FTIR spectra of the two membranes after uranium experiments at pH 6 and 8.5 (25 mg/L uranium, due to detection limitations) were measured. The FTIR spectra for the clean membrane and the membrane after a uranium experiment at pH 6 are presented in Figure 51a, while the respective spectra for the pH 8.5 experiments are presented in Figure 51b.

FTIR of clean membranes at pH 6 and 8.5

The functional groups from the membrane could be identified in the spectra for the clean membranes, *e.g.* there was a large peak at 1722 cm^{-1} from the C=O stretch for carboxylic groups while the C=C from aromatic rings give a peak at 1488 cm^{-1}. There is a clear peak for all membranes at 1240 cm^{-1} from aromatic groups and C-H signals from benzene rings at 852 cm^{-1}. There is also a very broad peak at about 3500-3100 cm^{-1}. This can be assigned to both O-H stretch from hydroxyl groups or N-H stretch from amine groups (Table 11). Since polyamide has both these groups, it is likely to be a combination of both. There is in fact, a shoulder on the peak, indicating that it is a combination of the two. The sulfone groups from polysulfone gave a peak at 1151 cm^{-1}. As measured with the zeta potential (Figure 33), membrane charge changes across the pH range, and from the FTIR spectra it can be seen that functionality also changes somewhat with pH. Comparing the spectra from the two clean membranes, the absorbance from C=O stretch from undissociated carboxylic groups is lower at pH 8.5 compared to pH 6. This is since the number of carboxylic groups present decrease due to deprotonation at alkaline pH (Childress and Elimelech, 1996). There is also an increase in the broad peak at 3500-3100 cm^{-1} at pH 6 compared to pH 8.5. This peak could be due to either amine N-H stretch or hydroxyl O-H stretch or a combination of the two. Since membranes are more protonated at lower pH, it makes sense that there is a stronger absorbance from protonated hydroxyl and/or amine groups at the more acidic pH.

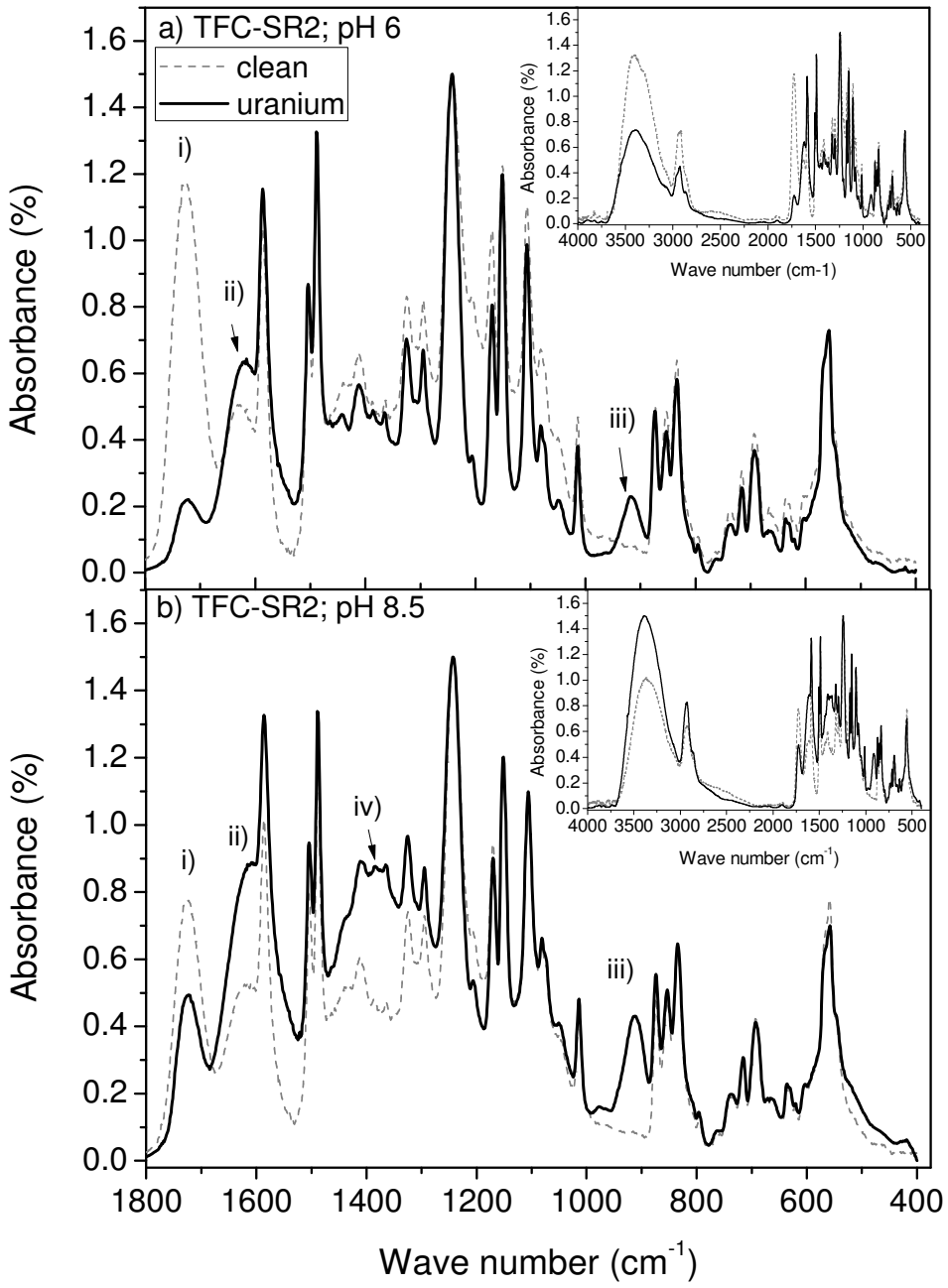

Figure 51. FTIR spectra of the TFC-SR2 membrane at a) pH 6 and b) pH 8.5. The clean membranes at each pH are shown as grey dotted lines, while the membranes after an experiment with uranium (25 mg/L) are shown as black lines. Experimental conditions: 25 mg/L U + 20 mM NaCl and 1 mM $NaHCO_3$, no applied pressure, flow-rate = 0.6 L/min, temperature = 25°C.

Table 11 Relevant FTIR Absorbances and Assignment (Nakamoto, 1997; Coates, 2000)

IR absorbance (cm^{-1})	Assignment
3600-3200	Hydroxyl group, O-H stretch
3510-3460 + 3425-3380	Aromatic primary amine, N-H stretch
~3450	Aromatic secondary amine, N-H stretch
2922	$-CH_3$
2855	$C-O-CH_3$
1722	C=O (carbonyl) from carboxylic acid
1622	C=O stretch (primary amide)
1680-1695 and 1535	-CONH (amide)
1610-1550/1420-1300	$-COO^-$ stretch
1586/1488	C=C vibration (aromatic ring)
1400-1300	C-O stretch from carbonate in $UO_2(CO_3)_3^{4-}$
1385/1365	C-H bending (methyl)
1325/1295 + 1151	SO_2
1240	aromatic
915	UO_2
852	C-H from benzene ring

FTIR of uranium experiment at pH 6

After the uranium experiment at pH 6, there is a peak at 912 cm^{-1}, due to uranyl ion (peak iv, Figure 51a), showing that uranium was present on the membrane at sufficiently high concentrations to be detected by the FTIR. Bond formation is indicated in FTIR by the decrease in absorbance from a specific functional group and a concomitant increase in the absorbance of another group resulting from the new group. The changes in peak absorbances are compared with the aromatic peak at 1240 cm^{-1}, which was 1.5% for all membranes, both before and after an experiment. For the experiment at pH 6, there was a large decrease in the intensity of the -C=O absorbance from carboxylic acid in the active layer of the membrane, where the ratio of carboxylic acid:aromatic peak absorbance changes from 0.8 to 0.13 (peak i, Figure 51a). Taken together, the detection of the uranyl ion on the membrane surface, the loss of carboxylic acid –C=O and –OH and the appearance of $–COO^-$, strongly suggest that uranium binds with the carboxylic acid groups present in the polyamide membrane layer. The theoretical study by Schlosser et al. (2006) shows how both mono and bi-dentate coordination between the uranium atom and the carboxylic acid group would be possible bonding arrangements. The tendency of uranium to bind with carboxylic acid groups below pH 6 is also taken advantage of in cation exchange resins (Konstantinou and Pashalidis, 2004). It should also be noted that

there was a small increase in the intensity the -C=O stretch from amide at 1622 cm^{-1} (peak ii Figure 51a); this suggests a reaction with the amide group, possibly due to hydrogen bonding of $(UO_2)_2CO_3(OH)_3^-$ with N-H (Prudden et al., 2004).

To estimate the binding capacity of uranium to the membrane, information determined by Coronell et al. (2010) on the amount of the available carboxyl groups in membrane active layers was used and compared to the amount of uranium adsorbed by the membranes used in this study. Membrane binding capacity can be calculated by:

$$Q = V_{PA} \times C_{COOH}$$

where Q = binding capacity, V = volume of PA active layer and C = concentration of carboxyl groups. Unfortunately, the concentration of carboxyl groups for TFC-SR2 and BW30 had not been determined, however, the membranes used by Coronells group (ESNA, TFC-S, ESPA 3, FT30 and NF90) also had PA active layers and, at pH 6, contained carboxyl groups ranging from about 0.1 to 0.4 M. The thickness of the TFC-SR2 active layer, as determined by TEM, ranged from 250 to 400 nm, thus the carboxyl group content of the TFC-SR2 could be estimated to between 1.15×10^{-7} to 7×10^{-7} mol. Taking surface roughness into account, which means that actual membrane area is larger than the measured cell area (Schäfer et al., 2010), a range up to 1.6×10^{-6} mol can be estimated. This compares well to the amount of uranium adsorbed to the membrane during the experiments at pH 6: up to 2.6×10^{-6} mol. Considering that BW30 has a thinner active layer (250 nm), and assuming a similar concentration of carboxylic groups in that active layer, the difference observed in uranium mass adsorbed between membranes could be due to the lower availability of carboxylic groups.

FTIR of uranium experiment at pH 8.5

The FTIR spectrum after the uranium experiment at pH 8.5 has some important differences to that of pH 6. Clearly, the change in membrane functional groups is not

so extreme. Again, there was a peak from the uranyl ion at 918 cm^{-1} (peak iii, Figure 51b). An important addition was the broad band around 1400-1300 cm^{-1} (peak iv, Figure 51b) assigned to the carbonate ligands of the uranium species, $UO_2(CO_3)_3^{4-}$ (Bargar et al., 1999). In contrast to the pH 6 spectrum, there was only a small decrease in the 1722 cm^{-1} absorbance (the ratio between carboxyl peak and aromatic peak changed from 0.51 to 0.33) and a slight increase (a shoulder) at 1610-1550 cm^{-1}. This indicates that there might have been some binding with carboxyl groups, although not to the extent observed at pH 6. Importantly, there is an overall increase in absorbance in other peaks related to the polyamide active layer, namely the –NH (or –OH) stretch (3500-3200 cm^{-1}) (Figure 51b, inset) and the amide -C=O stretch (1622 cm^{-1}). This indicates that, rather than reacting with the functional groups and forming a chemical bond with the membrane, the strongly negatively charged $UO_2(CO_3)_3^{4-}$ interacted with the membrane through electrostatic forces with the polyamide causing an enhancement in the absorbances of the membrane functional groups involved. A theoretical study by Tsushima et al. (2002) confirms that the distal oxygens of the $UO_2(CO_3)_3^{4-}$ would interact strongly with ligands through hydrogen bonding, while Prudden et al. (2004) showed that amine groups can provide excellent hydrogen-donors for $UO_2(CO_3)_3^{4-}$ and bind through outer-sphere complexing.

In conclusion, for uranium at pH 6, the results from the spatial distribution images (STEM-EDX, Figure 47) showed that, uranium was present through-out the polyamide active layer while the FTIR analysis showed that uranium interacted with the membrane through chemisorption with the carboxylic acid functional groups. The mol of available carboxyl groups was estimated to be present at a similar amounts as the mol of adsorbed uranium. At pH 6 uranium was present as mainly UO_2OH^+, but also as UO_2^{2+}, UO_2CO_3 and $(UO_2)_2CO_3(OH)_3^-$. There were several factors favouring the uranium-membrane interaction observed at pH 6; 1) the positively charged species (UO_2OH^+ and UO_2^{2+}) and the dipolar UO_2CO_3 were electrostatically attracted to the negatively charged membrane 2) UO_2OH^+ and UO_2^{2+} and UO_2CO_3 were small enough to fit into the pores of TFC-SR2 (while for BW30, size would be

a limitation), 3) the stability of UO_2OH^+ is relatively low making reactivity more likely.

For pH 8.5, the pressure experiments showed that uranium (present as $UO_2(CO_3)_3^{4-}$) did not adsorb or permeate through the membrane at no pressure and 5 bar. It was confirmed by the SEM images that uranium was mainly present as a loose layer on the membrane surface; adsorption was not favourable due to the large species size and the electro-negative repulsion between membrane and uranium. However, due to its tendencies to strongly interact through hydrogen bonding, uranium still loosely attached to the surface of the membrane, most likely interacting with amine groups, as shown by the FTIR analysis. Polynuclear complexes of $UO_2(CO_3)_3^{4-}$ also exist at higher uranium concentrations (Schlosser et al., 2010) and it is possible that, as uranium was concentrated at the membrane surface, these may have formed, forming a loose network (as postulated in Kryvoruchko et al. (2004)).

In the case of the pH 7, where high mass adsorbed was also observed, this could be possible through similar mechanisms as for pH 8.5: hydrogen bonding of $(UO_2)_2CO_3(OH)_3^-$ with the N-H by membrane amide groups. This would be more favourable at pH 7 than at more alkaline pH due to the lower negative charge of both the membrane and uranium species compared to that of $UO_2(CO_3)_3^{4-}$. As discussed previously (*e.g.* 4.3.3), the stability constants (log K) of the uranium species indicate the relative tendency of the species to remain in solution. Compared to *e.g.* the stable complex $UO_2(CO_3)_3^{4-}$, $(UO_2)_2CO_3(OH)_3^-$ is more likely to interact with the membrane surface than remain wholly in solution.

6.4 Conclusions

The following parameters were of importance for the uranium-membrane interaction and uranium retention in NF and RO membranes;

1) Charge interactions between uranium species and membrane determined whether a species was repelled or attracted to the membrane and, as a consequence,

influenced the extent of uranium interaction with the membrane. For example, lowest interaction occurred when the solution phase species were positively charged and the membrane also had net positive charge and when the solution phase species were strongly negatively charged and the membrane also had a net negative charge;

2) Access to functional groups in the membrane was a limiting factor to adsorption; the size of species compared to membrane pore size, determined the extent of penetration, while, taking active layer thickness into account, TFC-SR2 was estimated to contain more carboxyl groups than BW30. For example, ~50% U was adsorbed at pH 6 to the more open TFC-SR2 but only ~30% adsorbed to BW30 at the same pH value;

3) In addition to the importance of charge and size, affinity of the uranium species to membrane functional groups was an additional factor influencing whether or not adsorption to the membrane occurred. For example, it was shown that, at pH 6, uranium reacted with carboxylic acid groups of the polyamide layer, while at pH 8.5 uranium remained on the membrane surface, but interacted through hydrogen bonding with amine groups. It should be noted, that at pH 8.5, this allowed the uranium to be retained at the membrane surface under low pressure conditions, but at higher applied pressure, the sorption of uranium responded to the increasing concentration polarisation which led to an increase in mass adsorbed and also penetration of uranium to the membrane, with lower retention as a consequence.

The results confirm the observations in Chapter 4 and 5 that uranium adsorbs to NF and RO membranes through chemisorption, in particular at pH 5-7. Notably, it was found that at pH 6, uranium reacts with carboxylic acid groups within the polyamide active layer which resulted in about 60% of the uranium being adsorbed, and a lower permeate flux, whereas at pH 8.5, uranium interacts with the membrane through weaker electrostatic forces which only led to about 20% adsorption and no permeate flux decline. The study also confirms that uranium does not adsorb to a large extent at alkaline pH, confirming that additional mechanisms must have been the reason for the high levels of uranium mass adsorbed observed in Chapter 4 at pH 10.

7 Effect of calcium on uranium-membrane interaction during NF/RO filtration

7.1 Introduction

Calcium is a common and important constituent of natural waters. Langmuir (1997) gives median values for calcium in surface water as 15 mg/L, with concentrations ranging from 1 to over 100 mg/L, while for groundwater the median value is 50 mg/L and concentrations range from below 1 mg/L up to 500 mg/L. Most calcium in surface waters arises from the dissolution of calcium carbonate and calcium sulphate, particularly the former where waters flow over limestone-rich areas. When present in the solid phase at more than 1% w/w, calcium-containing minerals tend to dominate soil and groundwater chemistry (Langmuir, 1997). Indeed, calcium ions, along with magnesium and hydrogen carbonate/carbonate ions, are the main contributors to the hardness of water. Levels above 50 mg/L can be problematic due to formation of excess calcium carbonate deposits in plumbing or in decreased cleansing action of soaps. Studies to evaluate the potential of nanofiltration membranes to remove calcium from water have been carried out (Tansel et al., 2006). A further line of research, however, has been calcite membrane-scaling (Sheikholeslami, 2004; Tzotzi et al., 2007; Greenlee et al., 2010). Calcium, along with magnesium, carbonate, sulphate, silica and iron are well known to cause fouling of membranes (Potts et al., 1981). Calcium has also been shown to cause increased membrane fouling when in presence of organic compounds (Nyström et al., 1995; Schäfer et al., 1998; Seidel and Elimelech, 2002; Jarusutthirak et al., 2007).

As a major constituent of many natural waters, calcium can interact with and affect the behaviour of other elements, such as uranium, which are present at lower concentrations, *e.g.* by forming aqueous complexes, incorporating the elements in its crystal structure as it precipitates, or adsorbing the elements onto its surface after precipitation. Researchers have investigated from a theoretical perspective the structure of aqueous calcium-uranium complexes (Tsushima et al., 2002; Kelly et al.,

2007), and from geological (age-dating) and environmental migration viewpoints, calcium-uranium formations in mineral phases (Suksi et al., 1996; Reeder et al., 2004; Valle-Fuentes et al., 2007), adsorption of uranium to calcite (Geipel et al., 1997; Elzinga et al., 2004) and co-precipitation of uranium with calcite or aragonite (Abdelouas et al., 1998; Curti, 1999; Catalano et al., 2006). There has, however, been no published study about the effects of calcium on uranium behaviour during membrane separations.

In Chapter 4 it was postulated that, during the filtration of natural groundwater, calcium and/or magnesium caused co-precipitation of uranium at pH 10 leading to the deposition of uranium on the membrane surface. An initial experiment was performed at pH 10 to investigate if magnesium may cause greater co-precipitation of uranium than calcium. Results showed that only 10% of magnesium precipitated at pH 10, and only 20% of uranium was co-precipitated (result shown in section 11.5.1 in the appendix). In contrast, ~50% of calcium precipitated and so this was considered a more important potential cause of uranium co-precipitation. Consequently, the focus of this chapter is on the effect of calcium on uranium interaction with NF/RO membranes. As mentioned above, to date, the effects of calcium on uranium-membrane interactions have not been systematically investigated across the pH range. In addition to co-precipitation, other possible effects include masking of the negative membrane charge by positive Ca^{2+} ions need to be considered (Bartels et al., 2005). As shown in Chapter 4, calcium also affects uranium speciation by forming complexes such as $Ca_2UO_2(CO_3)_3$ in the pH range 8 to 9.

The structure of the calcium carbonate species is similar to that of the tricarbonate species, but with the inclusion of the two calcium ions in between two of the three carbonate groups (Figure 52). For both the calcium carbonate and the tricarbonate species, it should be noted that there is quite a large first hydration layer (including 10 water molecules for the former). With respect to the NF/RO separations, the formation of the calcium carbonate species may add another interesting aspect to the adsorption and retention mechanisms, since, in contrast with the other uranium

species present across the pH range, $Ca_2UO_2(CO_3)_3$ has a net charge of zero (Tsushima et al., 2002) and its behaviour in an NR/RO system would not be affected by charge interactions with the membrane.

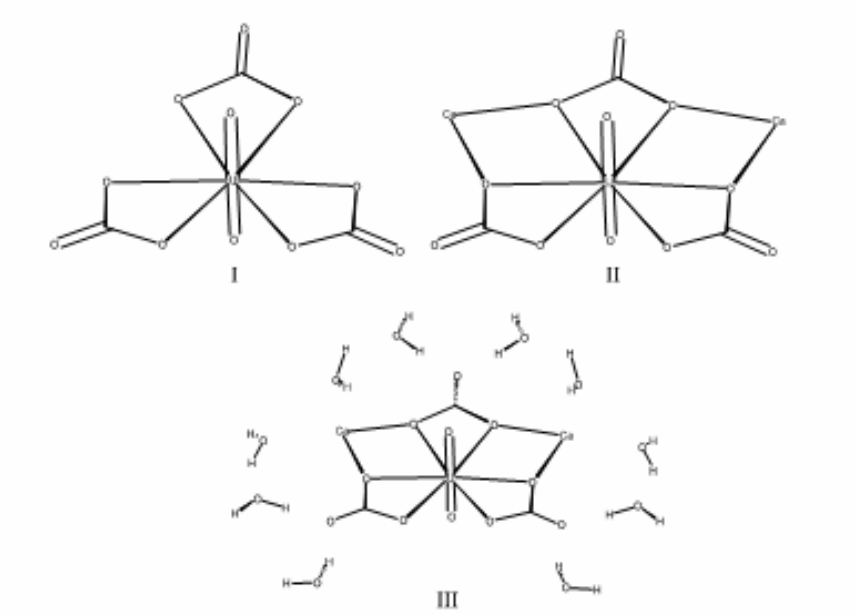

Figure 52. Structure of the tricarbonate (I), calciumcarbonate (II) and hydrated calcium carbonate (III) uranium complexes, $UO_2(CO_3)_3^{4-}$, $Ca_2UO_2(CO_3)_3^0$ and $Ca_2UO_2(CO_3)_3.10H_2O$, respectively. Figure from Tsushima et al. (2002).

The aim of this chapter was therefore to investigate: i) how calcium affects the adsorption of uranium to the membrane (as observed in Chapter 6 in the absence of calcium); ii) how the speciation change due to the presence of calcium affects uranium adsorption and retention; and finally iii) whether calcium carbonate precipitation explains the mass adsorbed of uranium on the membrane at pH 10 observed during the Australian field trial (Chapter 4).

A pressure of 10 bar was selected for comparison with results presented in both Chapters 4 and 6. The filtration experiments were performed with a uranium and calcium containing solution across the pH range 3-10. The characteristics of uranium interaction with the membrane was investigated at selected pH values using SEM, TEM and Time-of-Flight Secondary Ion Mass Spectrometry (ToF-SIMS).

7.2 Materials and methods

The cross-flow filtration system for NF and RO, the chemical analysis using ICP-OES and ICP-MS and the speciation modelling were described in the Chapter 3 (sections 3.1.4, 3.1.6 and 3.1.8, respectively).

7.2.1 Filtration experiments

Filtration experiments for TFC-SR2 and BW30 were carried out at a pressure of 10 bar across the pH range of 3 to 10 for two solution compositions: 1) the same as in section 3.1.5 and 2) as in section 3.1.5 with the addition of calcium (60 mg/L calcium as $CaCl_2$) (See Table 12 for an overview). The calcium concentration used, was the same as the concentration of calcium found in the Australian Pine Hill groundwater described in Chapter 4, and is representative of typical groundwater calcium concentrations (section 7.1).

Table 12. Solution composition for uranium and uranium + calcium experiments

Compound	Supplier	U experiments	U + Ca experiments
NaCl	Fisher	20 mM	20 mM
$NaHCO_3$	Fisher	1 mM	1 mM
$UO_2(NO_3)_2.6H_2O$	TAAB	0.5 mg/L U	0.5 mg/L U
$CaCl_2$	Fisher	-	60 mg/L Ca

Membrane preparation, compaction and cleaning of the system followed the same procedures as described in section 3.1.2. After the addition of the experimental solution, the flow-rate was set to 0.6 L/min and a pressure of 10 ± 0.25 bar was applied. The pH was monitored throughout and adjusted to remain within 0.1 of the required pH value for each individual experiment. The pH range investigated was pH 3-10 at intervals of 1 pH unit; each pH value was investigated in a separate experiment. Feed and permeate samples were collected at the start, 10 minutes from the start and then hourly over the seven-hour experimental period.

7.2.2 Membrane analysis

Membranes from selected experiments were analysed further using SEM and TEM as detailed in section 6.2.5.

Specific experiments were carried out with TFC-SR2 in preparation for analysis with Time-of-Flight Secondary Ion Mass Spectrometry (ToF-SIMS). The experimental procedure outlined in section 6.2.2 was followed. All experiments were conducted using a pH 10 solution. Three membranes were prepared using the following experimental solutions: 1) DIW 2) calcium (60 mg/L Ca as $CaCl_2$) and background electrolyte solution (20 mM NaCl and 1 mM $NaHCO_3$) and 3) uranium (50 mg/L U as uranyl nitrate), calcium (60 mg/L Ca as $CaCl_2$) and background electrolyte solution (20 mM NaCl and 1 mM $NaHCO_3$). The higher concentration of uranium (50 mg/L compared with 0.5 mg/L for the filtration experiments described in section 7.2.1) was required to ensure mass spectrometric detection.

The membrane surface was analysed with a ToF-SIMS IV instrument (ION-TOF, GmbH, Germany) equipped with a liquid metal (Bi^+) ion gun for spectroscopy and imaging with sensitivity down to the 1×10^{-15} molar range. Samples of ~1 cm^2 were cut with scissors from the dry membranes and mounted on the sample holder (the holder was cleaned with chloroform and hexane prior to samples being loaded). Two samples from each membrane were analysed. Spectra were obtained for positive and negative secondary ions, where the count of each ion type was recorded, giving a relative (semi-quantitative) measure of the abundance of certain ions between membrane samples. The data was normalised to total counts. It should be noted that different ion types are detected to varying extent, and direct quantitative comparison between different ions within a sample is therefore not possible. The mass ranges of 0 to ~850 m/z were analysed. Instrument settings are listed in the appendix (section 11.5.3) together with the spectra for the surface for all the negative and positive ion fragments detected.

7.3 Results and discussion

The results and discussion relating to the experiments described above will be structured as follows: the results for average permeability of the membranes used prior to experiments (section 7.3.1) and the permeate flux during the experiments (section 7.3.2) will first be described. The retention of uranium and calcium (section 7.3.3), mass adsorbed of uranium and calcium to the membrane as well as the modelled speciation of uranium and calcium across the pH range for the adopted experimental conditions (section 7.3.4) will then follow. In the light of these results, the effect of calcium on the speciation and interaction of uranium with the membrane across the pH range 3-10 will be discussed (section 7.3.5 to 7.3.7), and finally, the co-precipitation of uranium with calcium at pH 10 will be explored through the use of microscopic and spectrometric techniques.

7.3.1 Permeability of BW30 and TFC-SR2

The permeability of the membranes was calculated based on the pure water flux (DIW) during membrane compaction prior to each experiment. The mean permeability of BW30 for the U only and U + Ca experiment was 4.74 ± 0.41 and 4.55 ± 0.34 L/m^{2}hbar, respectively. The mean permeability was 7.74 ± 0.59 L/m^{2}hbar for the TFC-SR2 membranes used for the U only experiments, whilst the membranes used for the U + Ca experiments had an average permeability was 9.99 ± 0.85 L/m^{2}hbar. The difference in permeability was because two different batches of TFC-SR2 membrane sheet had to be used as the supplier only sent small samples. Although, the variability in permeability would overlap, some care has to be taken when comparing the results.

7.3.2 Permeate flux during U and U + Ca experiments

For BW30, the permeate flux for both solution types was very similar over the pH range 3-8; between 40-50 L/m^{2}h for U experiments and 35-45 L/m^{2}h for U + Ca experiments (Figure 53b). The slightly lower values for the U + Ca experiments may indicate a small decline in flux due to the addition of calcium but the difference between the mean values for the two data sets lies within one standard deviation for

the pure water flux for BW30: ± 8.7 L/m^{2}h (all membrane samples for individual BW30 experiments were cut from the same sheet). At pH 10, the permeate flux decreases by ~40% (from ~35 L/m^{2}h to ~20 L/m^{2}h) over the course of the experiment. Apart from this drastic decrease, no particular trend for permeate flux with pH for BW30 was observed.

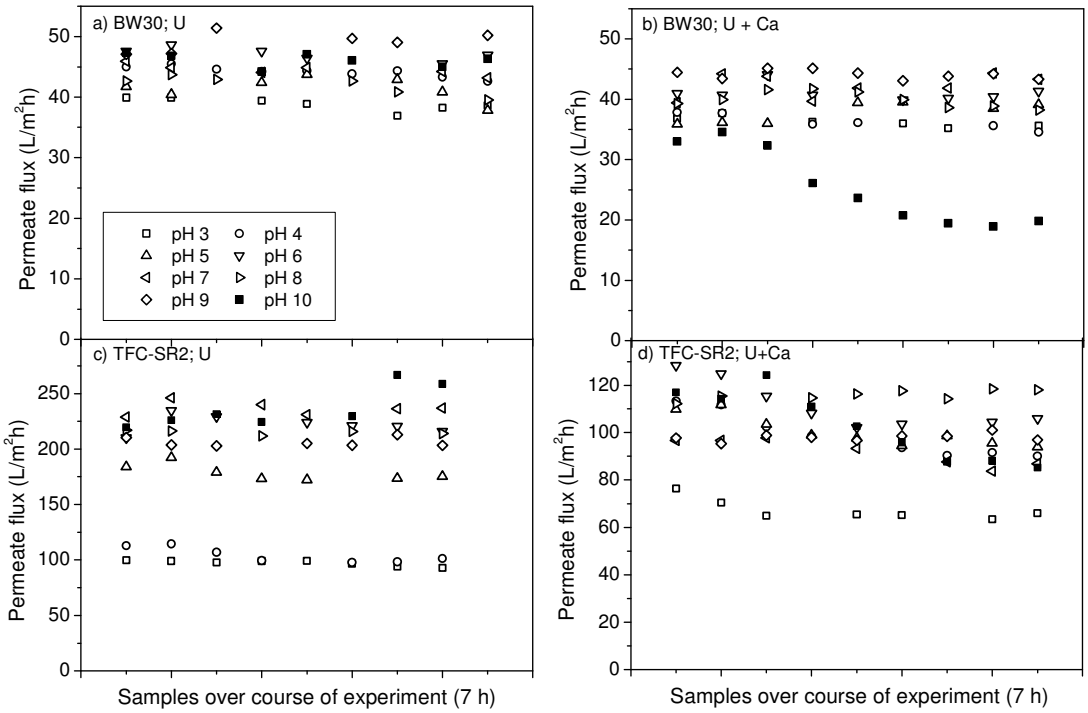

Figure 53. Permeate flux over the course of the experiments (7h. A couple of extra samples were collected at the start of an experiment, after which they were collected hourly). The permeate flux for U + Ca experiments and U experiments for TFC-SR2 are displayed in a) and b), respectively. Note the difference in scale for the TFC-SR2 experiments. The permeate flux for U + Ca experiments and U experiments for BW30 are displayed in c) and d), respectively. Experimental conditions: 0.5 mg/L U, 60 mg/L Ca where applicable + 20 mM NaCl and 1 mM $NaHCO_3$, 10 bar, flow-rate = 0.6 L/min, temperature = 25°C.The standard deviation for permeate flux for TFC-SR2 was ± 39 L/m^{2}h and for BW30 ± 8.7 L/m^{2}h.

For TFC-SR2, permeate flux was lower at pH 3-4 and higher at more alkaline pH, which is something commonly found for NF membranes (Braghetta et al., 1997). There was not a clear trend, however, with increasing pH where much of the permeate flux was within standard deviation of the pure water flux for the respective membrane batches (± 23.4 and ± 32.9 L/m^{2}h for U and U + Ca, respectively) (Figure 53a). As for BW30, the permeate flux for the U+Ca solution decreased at pH 10 over

the course of the experiment; the magnitude of the decrease for the TFC-SR2 membrane was ~30% (from ~120 L/m^{2}h to ~90 L/m^{2}h). Such a decrease was not observed of U only experiments. In addition there is lower permeate flux decline (about 15-20% or 15-23 L/m^{2}h) during the U + Ca experiment at pH values 4-6, also not observed for U only experiments.

In contrast with the results for the BW30 membrane, the permeate flux for the U + Ca experiments was typically much lower than for the U experiments involving the TFC-SR2 membrane, especially in the pH range 5-10; the flux was about 100-130 L/m^{2}h for U + Ca experiments while it was about 180-250 L/m^{2}h for U only experiments. This variation is greater than the standard deviation on the mean pure water flux for those membranes (± 23.4 and ± 32.9 L/m^{2}h for U and U + Ca, respectively), showing that the addition of calcium had significantly reduced the permeate flux in comparison with the solution containing only uranium and background electrolyte.

Wang et al. (2010) also found that an addition 0.002 M calcium solution (*i.e.* similar to the concentration used in this study) caused a permeate flux decrease of 40% compare to that of a dilute salt solution. Braghetta et al. (1997) attributed this effect to the electrical double layer formed by the positive Ca^{2+} ions in the immediate vicinity of the negative membrane surface, thereby neutralising the negative charge within the membrane structure. This would decrease the repulsion within the membrane structure which would lead to a compression of the membrane and the effective membrane pore size and thus a permeate flux decline. During the experiments of this study, the effect from calcium on reducing the permeate was greater at pH 5-10, corresponding to where the membrane carries a negative charge (section 6.3.1) resulting in a layer of positive Ca^{2+} ions as co-ions attracted to the membrane surface.

7.3.3 Retention of uranium and calcium by BW30 and TFC-SR2 membranes

The percentage retention of uranium and calcium was calculated using Equation 1 (section 2.2.1). The retention of uranium by BW30 for both the U and the U + Ca experiments were ~97% at pH 3-4 and >99% at pH 5-10 (Figure 54a). Calcium was similarly well-retained by BW30, with a retention of ~97% at pH 3-5 and >99% at pH 5-10.

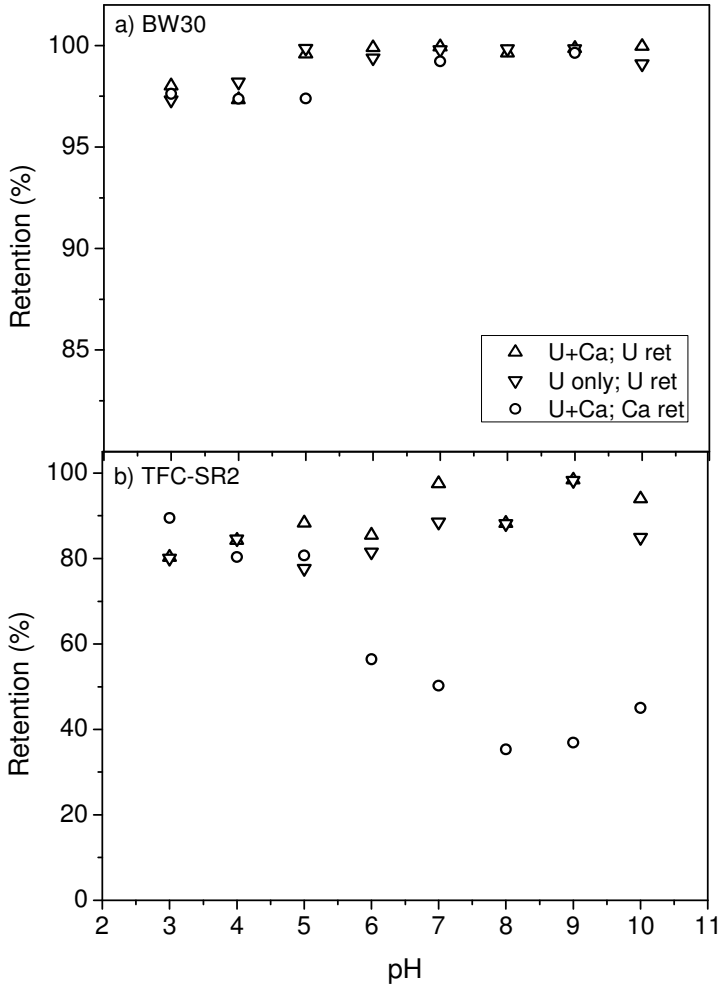

Figure 54. Retention of uranium for the U only and U + Ca experiments and calcium for U + Ca experiment for membranes BW30 (a) and TFC-SR2 (b). The SD for the retention experiments was < 14%. U only experiment: 0.5 mg/L U, 20 mM NaCl and 1 mM $NaHCO_3$ and U + Ca experiment: 0.5 mg/L U, 60 mg Ca, 20 mM NaCl and 1 mM $NaHCO_3$. Experimental conditions: pressure = 10 bar, flow-rate = 0.6 L/min, temperature = 25ºC.

The retention of uranium by TFC-SR2 ranged from ~77 to ~98% for the U only experiment, with higher retentions being obtained at alkaline pH. The trend was not entirely consistent, *e.g.* only ~80% retention at pH 10 but 98% at pH 9. For the U + Ca experiment, the uranium retention varied between ~80 and ~98% across the pH range; again the greatest uranium retention was found at pH 9. In contrast to the fairly consistent uranium retention by TFC-SR2, the calcium retention decreased from ~80% at pH 3-5 down to below ~40% retention at pH 6-10. The reasons for the decrease in calcium retention will be discussed further in section 7.3.6.

7.3.4 Mass adsorbed and speciation of uranium and calcium

The mass adsorbed for each of the uranium and calcium at the end of the experiments was calculated using Equation 13 (6.3.3).

In Figure 55a and b the uranium mass adsorbed to BW30 for the two U only and the U + Ca solutions are compared. In comparison with the U only results, at pH 3-7, the mass of uranium adsorbed during the U + Ca experiments was very similar over the range pH 3-7, significantly lower at pH 8 (5% versus 16%) and markedly higher at pH 10 (27% versus < 2%).

The mass of uranium adsorbed to TFC-SR2 during the U only experiments and U + Ca experiments are displayed in Figure 55c and d, respectively. Over the low pH range (3-6), the mass adsorbed of uranium to the membrane was similar for both experimental solutions. At pH 7-9, however, the uranium mass adsorbed for the U + Ca experiments was very much lower than that for the U experiments (*e.g.* 17% versus 57%) whilst at pH 10 the uranium mass adsorbed was higher for the U + Ca experiment (35% versus 17%).

The uranium speciation for each solution has also been displayed in each of the graphs in Figure 55 so that uranium-membrane interaction can be related to the species present at each pH value. The main difference in the uranium speciation between the U only and the U + Ca experimental solutions occurred at pH 7-10, where, for the U + Ca solutions, uranium formed a neutral complex with calcium,

$Ca_2UO_2(CO_3)_3$, which dominated uranium speciation at pH 8 and 9. The relationship between the speciation and adsorption will be discussed in section 7.3.6.

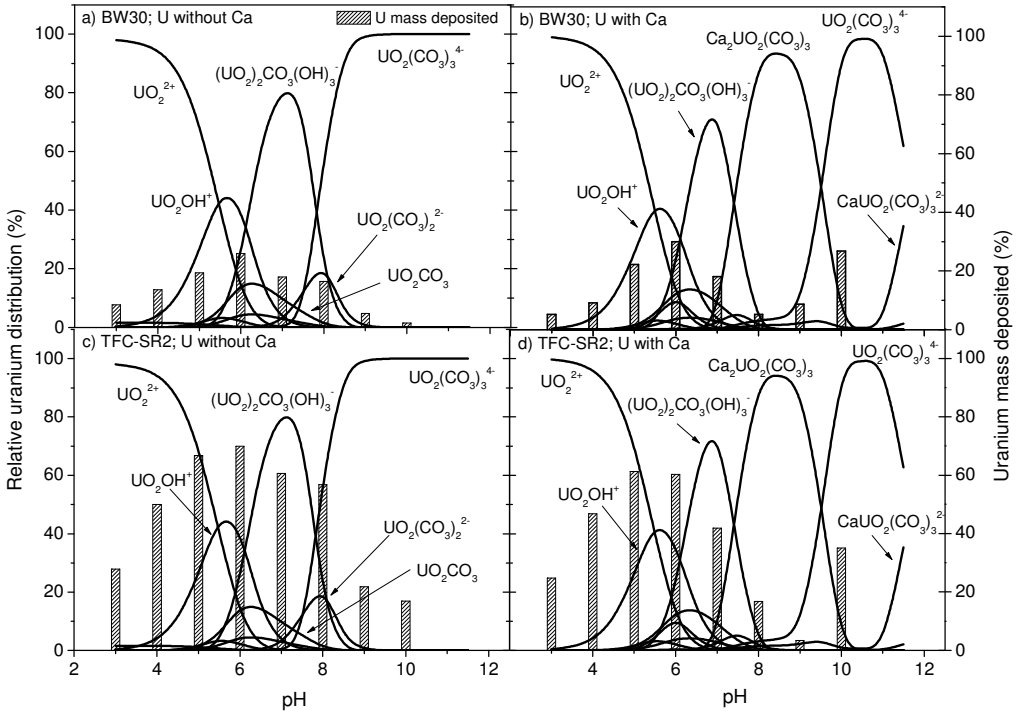

Figure 55. U mass adsorbed (%) over the pH range 3-10 to: a) TFC-SR2 after U+Ca experiment b) TFC-SR2 after U only experiment c) BW30 after U+Ca experiment and d) BW30 after U only experiment. Experimental solutions contained 0.5 mg/L U, 20 mM NaCl and 1 mM NaHCO3 for U only, and for U + Ca experiments 60 mg/L Ca was added. Pressure = 10 bar, flow-rate = 0.6 L/min and temperature 25°C. The relative U species distribution predicted with Visual Minteq 2.53 for the experimental solutions is indicated by the black lines.

The experiments had some concentration polarisation present at the membrane surface. The polarisation modulus for the experiments was calculated as described in section 6.3.3 and the results are shown in Figure 56. The values of the polarisation modulus ranged from 1.04 to 1.09 for BW30 and from 1.1 to 1.5 for TFC-SR2. The mass of uranium adsorbed to the membrane was not affected by a variation in concentration polarisation, however, and the highest uranium concentration calculated by the membrane surface due to concentration polarisation was 0.99 mg/L.

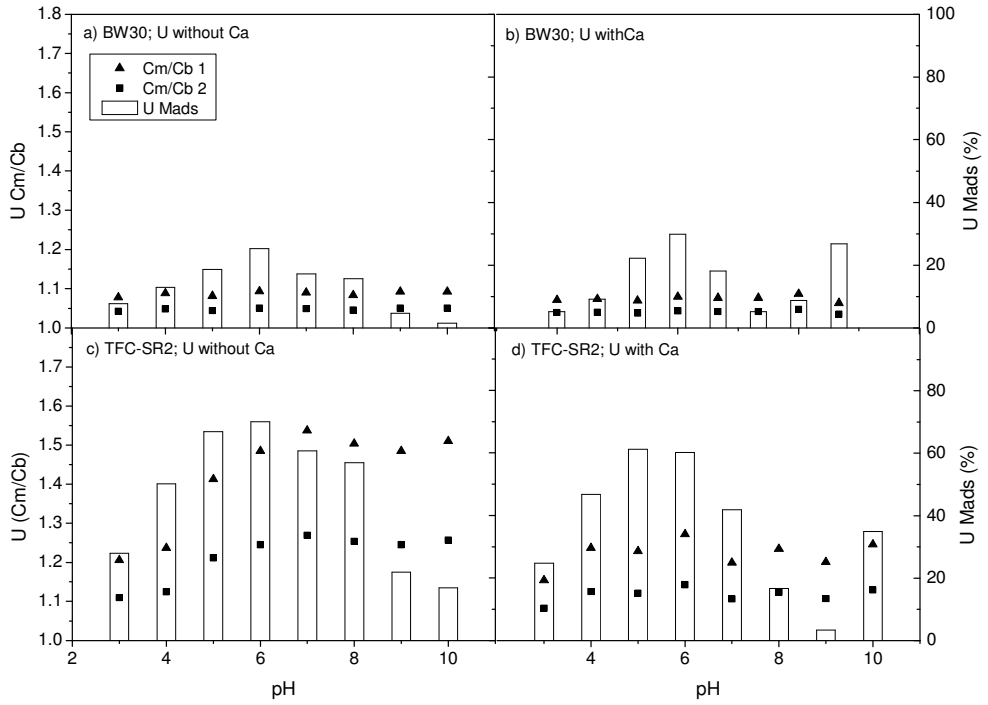

Figure 56. The resulting uranium polarisation modulus (Cm/Cb) is displayed following calculation using two Sherwood correlations. The mass adsorbed of uranium is given as bars for comparison.

The mass of calcium adsorbed to BW30 and TFC-SR2 across the pH range 3-10 is displayed in Figure 57. The calcium mass adsorbed was very similar for both membranes, with significant calcium mass adsorbed only at pH 10. The speciation of calcium is also displayed in Figure 57. The calcium speciation was not as variable with pH as that of uranium; calcium was present as Ca^{2+} from pH 3 up to pH 9 where it starts to form aqueous calcium carbonate ($CaCO_3$).

7.3.5 The effect of calcium on uranium adsorption (pH 3-6)

It was concluded in Chapter 6 that uranium adsorbs to the membrane at pH 5-6, largely through binding of positively charged uranium species with the negatively charged carboxylic groups on the membrane. At pH values greater than iso-electric point (net zero charge) of the membrane, calcium, present mainly as Ca^{2+} (Figure 57) is likely to form a layer of positive counter ions to the negatively charged membrane, known as a Stern layer (Mulder et al., 2005) (Figure 58a). The result of this would be

to decrease the effective negative charge (zeta potential) of the membrane (Childress and Elimelech, 1996) and (Schäfer, 2001). Since Ca^{2+} has been found more effective than other monovalent ions present in solution, such as Na^{+}, in neutralising the effective membrane charge (Braghetta et al. 1997), the presence of calcium might be expected to affect uranium adsorption. Despite this, calcium only caused a very slight decrease in the uranium adsorption at pH 5-6 for TFC-SR2 but had little effect below pH 5 for TFC-SR2 or BW30 membrane at pH 3-6 (Figure 55).

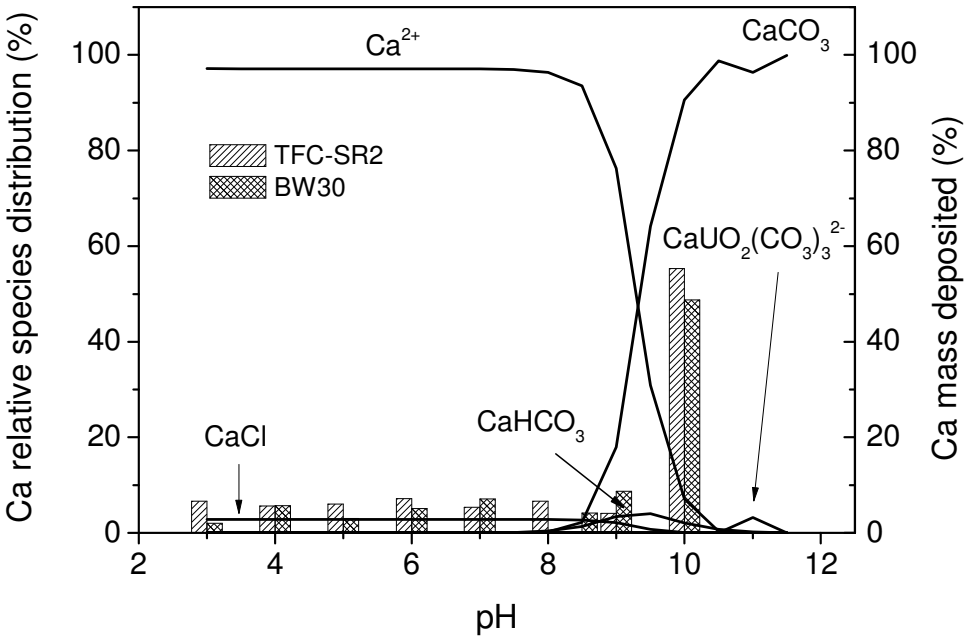

Figure 57. Calcium speciation (lines) for the U + Ca experimental solution across the pH range, as well as mass adsorbed of calcium (bars) to TFC-SR2 and BW30. Experimental solution: 0.5 mg/L U, 60 mg/L Ca, 20 mM NaCl and 1 mM $NaHCO_3$. Experimental conditions: pressure = 10 bar, flow-rate = 0.6 L/min, temperature = 25°C. Note that the U-containing species $Ca_2UO_2(CO_3)_3$, constitutes < 0.3% of the total Ca species and thus does not show up on the scale of this figure.

The adsorption mechanisms between uranium and the membrane carboxylic groups are apparently not affected by the presence of Ca^{2+} ions. Although the uranium adsorption was not affected, the presence of the Ca^{2+} double layer above pH 5 decreased the overall permeate flux of the U + Ca experiments for TFC-SR2 (as discussed in section 7.3.2). The permeate flux did not decrease over the course of the experiments however (except for pH 10), showing that calcium was not fouling the membrane. The flux could, however, be reduced by concentration polarisation,

which tends to occur at the very start of an experiment. Similar decrease of permeate flux caused by calcium has been observed in other studies (Schäfer et al., 1998; Seidel and Elimelech, 2002). At pH 4 and below, the membrane is positively charged, and neither Ca^{2+} ions nor UO_2^{2+} would be electrostatically attracted to the membrane surface (Figure 58b) (Bartels et al., 2005). Consequently, the permeate flux remains similar between the two types of experiments.

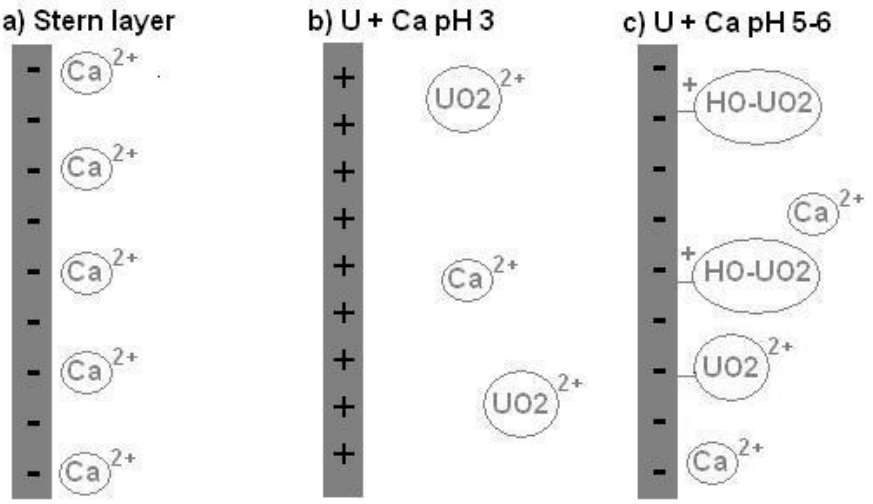

Figure 58. Simple schematic illustrating a) the electrostatic double layer of positive calcium ions attracted to a negative membrane surface (Stern layer) (relevant when the membrane is negative *i.e.* pH 5-10), (note that Na^+ and Cl^- ions would also be present in the water, with Na^+ ions also forming counter ions to the negative membrane) b) at pH 3-4 the TFC-SR2 membrane is positively charged and the positive uranium and calcium ions present are not attracted to the membrane and c) at pH 5-6 the membrane is negatively charged and UO_2OH^+ and UO_2^{2+} bind to the negative carboxyl groups of the membrane. Calcium is positively charged and attracted to the negative membrane.

7.3.6 Effect of calcium on uranium speciation (pH 7-9)

The speciation modelling output showed that the presence of calcium in solution directly affected the speciation of uranium over the pH range 7 to 9. More specifically, at pH 7, uranium starts to form the $Ca_2UO_2(CO_3)_3$ (Figure 55a), which then becomes the dominant uranium-containing species at pH 8-9. The neutral and bulky $Ca_2UO_2(CO_3)_3$ (Figure 52) is less likely than $UO_2(CO_3)_3^{4-}$ to be affected by the charge on the membrane surface. It also has a higher molecular weight (530 g/mol rather than 450 g/mol) and is very stable in solution (Fox et al. 2006). It is important

to note that although $Ca_2UO_2(CO_3)_3$ dominates the uranium species with over 93% of uranium being present as the Ca-complex, this only constitutes about 0.25% of the total calcium species at this pH, due to the much higher concentration of calcium than uranium.

Table 13. Dominant uranium species in Ca-containing solution

pH value	Dominant uranium species	molecular weight* (g/mol)
3	UO_2^{2+}	270
5-6	UO_2OH^+	287
7	$(UO_2)_2CO_3(OH)_3^-$	651
8-9	$Ca_2UO_2(CO_3)_3$	530
10	$UO_2(CO_3)_3^{4-}$	450

*Nominal molecular weight cut-off is 486 g/mol and 88 g/mol for TFC-SR2 and BW30, respectively.

Compared to the adsorption results in absence of calcium, the adsorption of uranium in the presence of calcium at pH 8-9 decreased for both membranes and this is attributable to predominance of the neutral $Ca_2UO_2(CO_3)_3$ species (a simple illustration is presented in Figure 58). For BW30, the adsorption was already low in the absence of calcium at these pH values, and, at pH 8 in the presence of calcium, it decreased even further (Figure 55a and b). For TFC-SR2, the adsorption decreased from about 60% to 17% at pH 8 and from 20% to <5% at pH 9. This decrease in adsorption over the pH range 7-9 did not, however, appear to affect retention of uranium. Decrease of adsorption of uranium to quartz and ferrihydrite due to the presence of calcium was also observed by Fox et al. (2006) who similarly observed a decrease of adsorption of over 30% due to the presence of $Ca_2UO_2(CO_3)_3$.

It could also be concluded that neither the presence of calcium nor the change in uranium speciation due to calcium caused a significant impact on the retention of uranium by either membrane. The calcium retention by TFC-SR2 decreased markedly at pH 6-10, however (Figure 54). This decrease is likely to be due to charge interactions, since the membrane is negatively charged at pH 6 and above, while the calcium ion remains positive and thus is not retained by electrostatic repulsion. The effect is due to the relatively open NF structure of TFC-SR2, where retention mechanisms are a combination of size and charge effects (Van der Bruggen

and Vandecasteele, 2003). Naturally, charge does not make a difference to the calcium retention in the tighter BW30 since retention mechanisms are due to solution-diffusion, and calcium retention is maintained at ~99% across the pH range. The retention by TFC-SR2 of uranium is not decreased by the change in membrane charge since the uranium species is larger than the nominal molecular weight cut-off of the membrane and, importantly, carries a great negative charge at alkaline pH; both contribute to retention mechanisms through size and Donnan exclusion. Selective retention of uranium over calcium by NF membranes was similarly reported by Favre-Reguillion et al (2008), although they only investigated pH 7.

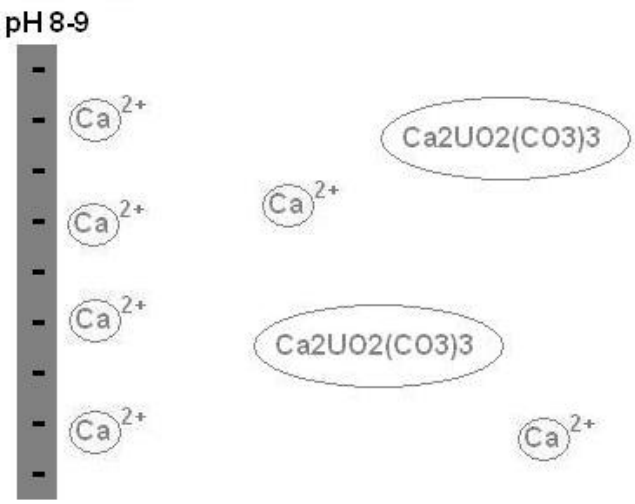

Figure 59. Schematic illustration of the negative membrane with positive calcium ions attracted to it, neutralising the effective charge, while the $Ca_2UO_2(CO_3)_3$ species is not adsorbed or attracted to the membrane due to it's neutral charge.

7.3.7 Co-precipitation of uranium and calcium at pH 10

At pH 10, both the TFC-SR2 and BW30 membrane exhibited a permeate flux decline of between 30-40% over the course of the experiment, showing that the membrane was being fouled. This was most likely due to the formation of $CaCO_3$. At pH 9, $CaCO_3$ starts to form, and at pH 10, 90% of calcium was present as $CaCO_3$ in solution (Figure 57). Solubility of solid phases is controlled by the solubility product, $K_{sp,}$ and in the case if $CaCO_3$, this determines the maximum concentration of calcium

and carbonate ions that can be present in an aqueous solution. The precipitation reaction of calcium carbonate is:

$Ca^{2+} + CO_3^{2-} = CaCO_3(s)$ $\quad\quad$ $K_{sp} = [Ca^{2+}][CO_3^{2-}]$

For $CaCO_3$ to precipitate, the molar concentrations of Ca^{2+} and CO_3^{2-} must be larger than the K_{sp} value ($K_{sp} = 3.311x10^{-9}$ for calcite). pK_{sp} (-log K_{sp}) for well crystallised calcite and aragonite is 8.33-8.48 (Langmuir, 1997). For an open aqueous system the overall reaction for calcite dissolution is written as:

$CaCO_3 + CO_2(g) + H_2O \leftrightarrow Ca^{2+} + 2HCO_3^{2-}$

while in terms of H^+ (acidity), the reaction is:

$CaCO_3 + H^+ \leftrightarrow Ca^{2+} + HCO_3^-$

Dissolved CO_2 is the main source of acidity (H^+) in natural water which increases $CaCO_3$ dissolution by making the reaction shift to the right. Calcite precipitation thereby increases with decreased CO_2 pressure and increased pH. The saturation index (SI) is used to indicate whether a mineral is below or above its saturation or equilibrium point (SI = 0), where SI < 0 indicates undersaturation and SI > 0 indicates supersaturation (Langmuir, 1997). The SI is related to Ksp by:

$$SI = \log \frac{[Ca^{2+}][CO_3^{2-}]}{K_{sp,CaCO_3}}$$

At pH 10, the speciation prediction showed that $CaCO_3$ in the form of calcite and aragonite were above the saturation index (2.41 and 2.27, respectively). This resulted in 48% and 55% of the calcium precipitating onto the BW30 and TFC-SR2 membranes, respectively (Figure 57). This was within the 7% error for mass adsorbed, so does not constitute a significant difference.

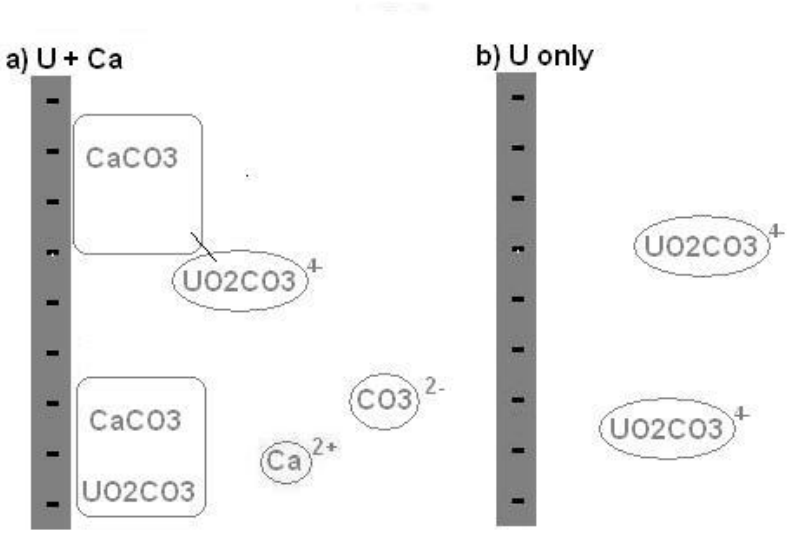

Figure 60. Schematic illustrating a) the co-precipitation of uranium with $CaCO_3$ or possible adsorption of uranium to calcite crystals at pH 10 and b) the negative $UO_2CO_3^{4-}$ which is not attracted to the negative membrane surface in the absence of calcium at pH 10 (only interacts weakly through hydrogen bonding, as discussed in Chapter 6).

Co-precipitation is the inclusion of substances which would normally be soluble into the crystals of a precipitating substance. Sorption may also occur of the minor substance to the crystals of the precipitate. At pH 10, > 99% of uranium is predicted by visual Minteq to be present as $UO_2(CO_3)_3^{4-}$, which is highly soluble, and any uranium-containing minerals predicted to form are well below saturation for both the U only and U + Ca solution (the highest having a SI = -10). In the presence of calcium however, the mass adsorbed of uranium was 35% and 26% (Figure 55b and d) compared to 17% (TFC-SR2) and <5% (BW30) which had adsorbed in the absence of calcium (Figure 55a and c). This shows that the precipitation of $CaCO_3$ caused uranium to co-precipitate at pH 10 for both membranes. The exact coordination of the uranium species within the calcite crystal is harder to determine. Reeder et al. (2001) found $UO_2(CO_3)_3^{4-}$ to be incorporated within the crystal structure of calcite (rather than being present as a second phase). They suggest that one of the carbonate ligands may twist off during the incorporation into calcite, with uranium coordinating with one of the carbonate ligands from the calcite instead. Elzinga et al. (2004) found that only low amounts of $UO_2(CO_3)_3^{4-}$ adsorbed to calcite crystals, indicating that incorporation into the crystal is likely to be the main co-precipitation mechanism.

Analysis of calcium-uranium precipitate to membrane

To visually confirm the effect of calcium on uranium-membrane interaction, SEM analysis of the membrane surface and TEM analysis of membrane cross-sections was performed on TFC-SR2. TFC-SR2 was chosen since this membrane had the higher adsorption of uranium at pH 6, greater co-precipitation of uranium at pH 10 and because this enabled comparison with the microscopic analyses performed in Chapter 6. The membranes selected for characterisation were those from the U + Ca experiments at pH 6 and pH 10.

a) U + Ca at pH 6 b) U + Ca at pH 10

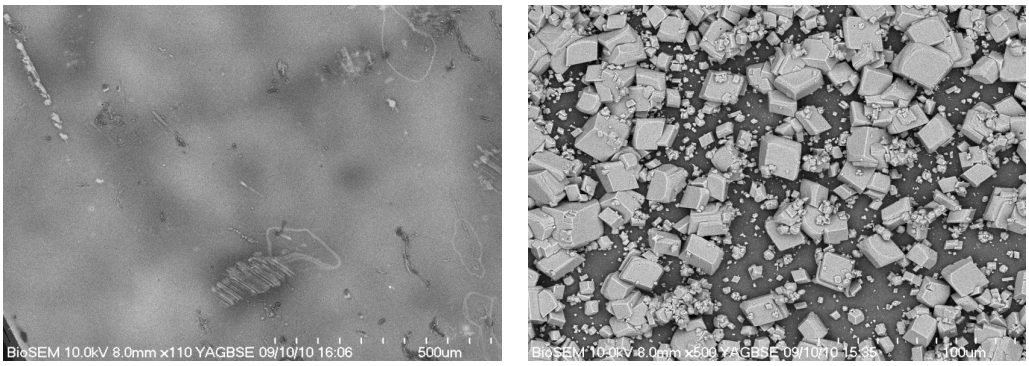

Figure 61. SEM image of membrane surface after experiment with uranium and calcium at pH 6 (a) and after an experiment with uranium and calcium at pH 10 (b). Experimental solution: 0.5 mg/L U, 60 mg/L Ca, 20 mM NaCl and 1 mM $NaHCO_3$. Experimental conditions: pressure = 10 bar, flow-rate = 0.6 L/min, temperature = 25ºC.

The SEM image of the membrane surface after an experiment at pH 6 showed that the membrane surface had a cloudy appearance (Figure 61a). The appearance of the membrane looks different to that at pH 6 after filtration with uranium only in Chapter 6 (Figure 45). This is likely to be due to the presence of calcium ions. After the experiment with U + Ca at pH 10, the precipitated $CaCO_3$ crystals can clearly be seen on top of the membrane surface (Figure 61b). The rhombohedral shape of the crystals showed that the $CaCO_3$ precipitated mainly as calcite (Tzotzi et al., 2007).

The TEM image shows how the uranium can be trapped by co-precipitation with the calcite crystals on top of the membrane active layer (Figure 62). Unfortunately, the large calcite crystals seen with the SEM, fell off as the membrane section was cross-

sectioned for the TEM. This image is compared the TEM image for the membrane after the pH 6 experiment, which shows no similar precipitation (Figure 63).

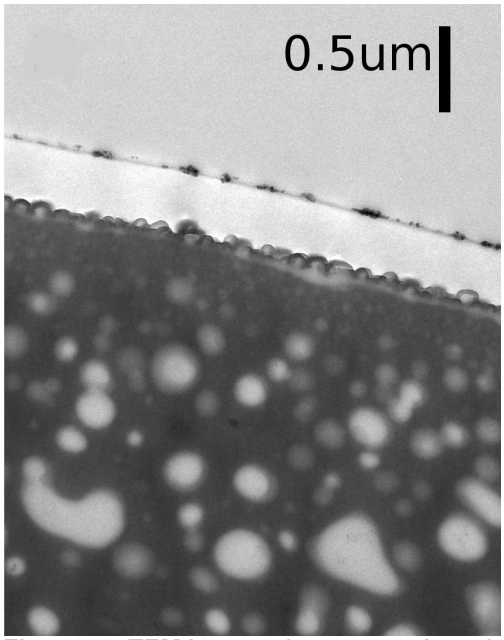

Figure 62. TEM image of cross-section of membrane after an experiment with uranium and calcium at pH 10. The calcium crystals can be seen as dark spots on top of the active layer of the membrane. Experimental solution: 0.5 mg/L U, 60 mg/L Ca, 20 mM NaCl and 1 mM $NaHCO_3$. Experimental conditions: pressure = 10 bar, flow-rate = 0.6 L/min, temperature = 25ºC.

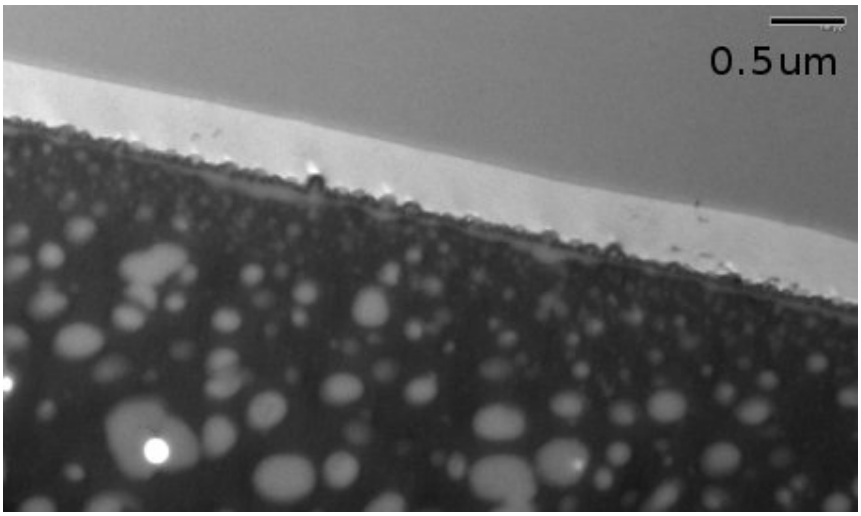

Figure 63. TEM image of cross-section of membrane after experiment with uranium and calcium at pH 6. Experimental solution: 0.5 mg/L U, 60 mg/L Ca, 20 mM NaCl and 1 mM $NaHCO_3$. Experimental conditions: pressure = 10 bar, flow-rate = 0.6 L/min, temperature = 25ºC.

Finally, TOF-SIMS analysis of the membrane surface after an experiment with uranium and calcium at pH 10 was carried out along with a blank membrane treated in the cross-flow system with only DIW at pH 10. The result for a membrane with uranium + background electrolyte at pH 6 is displayed for comparison (Figure 64), showing that in the absence of calcium, uranium is evenly distributed over the membrane surface.

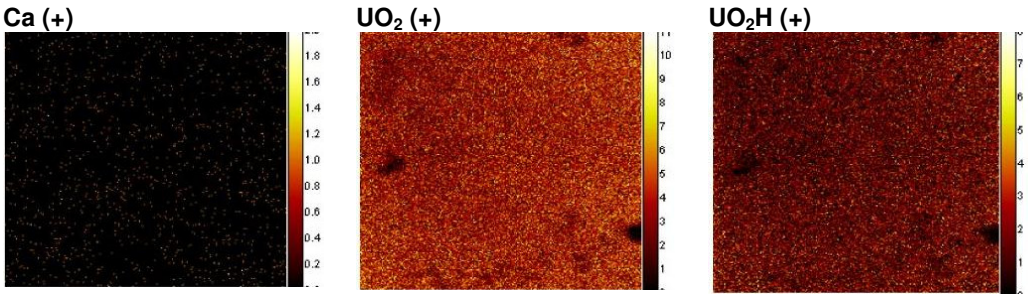

Figure 64. Positive ion intensity maps for selected ions after experiment with 50 mg/L U, 20 mM NaCl and 1 mM $NaHCO_3$ at pH 6, showing a nearly completely even distribution of uranium across the surface of the membrane. Experimental conditions: pressure = none, flow-rate = 0.6 L/min, temperature = 25ºC. The colour gradient indicates higher counts at lighter colours, while black means no counts.

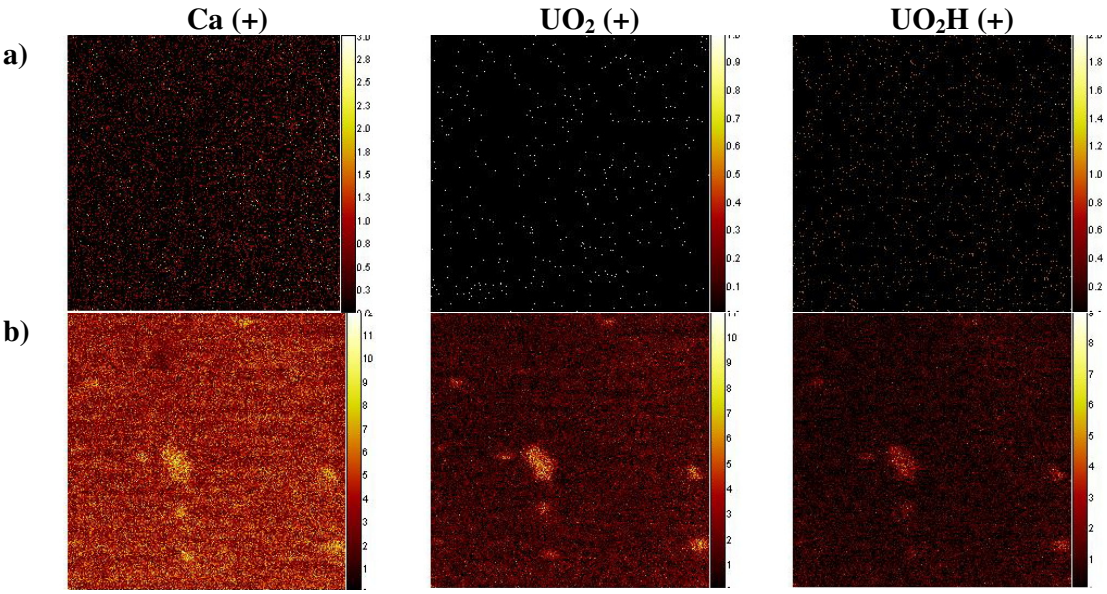

Figure 65. Selected positive ion intensity maps measured with ToF-SIMS for masses found on the surface of membranes treated with the following solutions: a) DIW at pH 10 and b) 50 mg/L U, 60 mg/L Ca, 20 mM NaCl and 1 mM $NaHCO_3$. Experimental conditions: pressure = none, flow-rate = 0.6 L/min, temperature = 25ºC. The colour gradient indicates higher counts at lighter colours, while black means no counts.

Selected results for calcium and uranium ion fragments are presented in Figure 65 whilst those for the complete array of ion fragments detected by the ToF-SIMS are displayed in the Appendix, section 11.5.4.

Due to the high uranium concentration in relation to calcium, the precipitation of $CaCO_3$ was reduced. A similar effect on $CaCO_3$ crystallisation also observed with high zinc concentrations (10 mg/L) (Ghizellaoui and Euvrard, 2008). Importantly, however, the results show that for the U + Ca experiments at pH 10, higher uranium counts are found in areas which contain high calcium counts (Figure 65), while in the absence of calcium, uranium is evenly distributed across the surface. This confirms that the precipitation of calcium as $CaCO_3$ as a cause of co-precipitation of uranium.

7.4 Conclusions

Calcium was found to have a significant impact on the behaviour of uranium at alkaline pH, both for the TFC-SR2 and BW30 membrane. The following conclusions could be drawn from this study:

1) At the pH range 3-6, calcium was present in solution as Ca^{2+} ions, and as such did not affect the uranium adsorption to either the BW30 or TFC-SR2 membrane. Above the iso-electric point of the membrane, the permeate flux was about half of that of uranium only experiments. It is likely that the flux was reduced by the concentration polarisation taking place during the experiment.

2) At pH 8-9, the presence of calcium directly affected the uranium speciation by forming $Ca_2UO_2(CO_3)_3$. This complex is a neutral species and very stable in solution, which lead a much lower adsorption of uranium to both membranes than when calcium was absent.

3) It was also found that that while TFC-SR2 retained > 85% of the uranium at pH 6-10, only ~40 to ~60% calcium was retained. For waters of similar composition, this

is useful for drinking water applications since, as opposed to uranium, calcium is an essential mineral for human health.

4) At pH 10, calcium was shown to cause co-precipitation of uranium at both the NF and RO membrane, where uranium would otherwise have remained in solution. This lead to a higher deposition of uranium on the membrane, as well as 30-40% permeate flux decline caused by the calcite precipitate. The SEM gave visual confirmation of the calcite crystals present on the membrane surface (situated on top of the active layer), while ToF-SIMS gave chemical confirmation that uranium was mainly present in areas of higher calcium loading, confirming that uranium co-precipitated with the $CaCO_3$.

This confirms that the mass adsorbed of uranium to the NF and RO membranes noticed at pH 10 when analysing the results from the natural Australian water described in Chapter 4 can be explained by co-precipitation with calcium.

The resulting precipitation of uranium to the membrane was not as high in the laboratory as during the field experiment, which could be due to a number of reasons, including that a new membrane sheet was used for each pH experiment and there would not be previously adsorbed uranium and/or other ions on the membrane. As mentioned before, other important major ions were magnesium (present at 150 mg/L), and although the initial laboratory experiment involving magnesium and uranium at pH 10 did not show a major effect on uranium, the combined effect of calcium and magnesium, as well as the effect of minor ions, would be worthwhile investigating.

8 Applicability of membrane filtration in remote locations in a developing country

8.1 Introduction

In the past four chapters of this thesis, the impact of varying water quality – pH, organic matter and calcium, on the behaviour of uranium has been determined. It was also found that a variety of these factors will influence the performance of membrane filtration. The membrane system described in Chapter 4 was designed to be mobile, with the aim to implement in locations where treatment is most needed and maybe also more difficult to reach by conventional infrastructure, such as remote locations in developing countries. As outlined in Chapter 1 (section 1.1), it is currently common practice to provide boreholes and wells as a safe drinking water source in developing countries. The questions that arise are 1) whether this water is good enough or needs further treatment and 2) whether a mobile system such as the one described in Chapter 4 could be a viable treatment option. The aim of this chapter was therefore to investigate the current chemical water quality of a West African country, Ghana, and to document present water costs and payment systems in place, in order to make a preliminary assessment as to whether membrane treatment is needed and/or viable.

8.1.1 The current status of Ghanaian water

Ghana, in West Africa, celebrated 50 years of independence from colonial rule in 2008, and is often hailed as an African economic and political success (Naylor, 2003). Yet, Ghana is still struggling to provide safe drinking water and sanitation to all its inhabitancy, especially in rural areas (UNICEF, 2007). Although Ghana is doing better than its immediate neighbours (*e.g.* Côte d'Ivoire and Togo), nearly 12% of Ghanaian children die before they reach the age of five compared to *e.g.* 6% of children in South Africa and 0.6% of children in the UK (UNICEF, 2007). Access to safe water is an important factor to reduce the number of deaths. According to JMP

(2008), 29% of the rural population rely on unimproved water sources. The majority of the improved sources in rural Ghana are boreholes and protected wells.

Ghana has 10 administrative regions: Western Region, Eastern Region, Central Region, Greater Accra, Volta Region, Ashanti Region, Brong-Ahafo, Northern Region, Upper West and Upper East. The population according to the last census (2000) was 18.9 million and with a growth rate of about 2.6% is estimated at 23 million people (UNICEF, 2007). Although most of the population growth is taking part in cities, the majority of Ghana's population still live in rural areas. Ghana's Water Policy expresses the need to both ensure access to enough safe water to meet basic human needs and at the same time ensure the environmental and financial sustainability of the water source (Government of Ghana, 2007). In an attempt to make the water delivery in the country more effective, Ghana's water supply has, amidst much controversy, been made parastatal (Agyeman, 2007). The Ministry of Water Resources, Works and Housing remains the government institution responsible for water resource management and drinking water supply, while the Ghana Water Company Ltd (GWCL) is in charge of urban water provision. The Community Waste and Sanitation Agency (CWSA) is in charge of facilitating safe water provision and providing technical assistance to the District Assemblies, who are responsible for planning and operation of the water supply to rural communities on a local level (Agyeman, 2007). The CWSA standard is one well or borehole per 300 people. The community are responsible for operation and maintenance. Regional progress reports (Government of Ghana, 2007), report 40-80% coverage depending on the region; however some organisations and individuals do not operate through the CWSA and thus the total number of improved sources is not accurately known (Nyarko et al., 2009). As the boreholes are constructed, the chemical water quality should be analysed for fluoride (F^-), manganese (Mn), iron (Fe), magnesium (Mg), calcium (Ca), sulphate (SO_4^{2-}), arsenic (As), lead (Pb), copper (Cu), nitrate (NO_3^-), nitrite (NO_2^-), chloride (Cl^-), phosphate (PO_4^{3-}), aluminium (Al), sodium (Na), zinc (Zn) and alkalinity ($CaCO_3$). Water quality is seldom monitored once a borehole has been established due to financial and logistical constraints.

Studies on the water quality in particular problem areas in Ghana have been conducted, such as the northern parts (Pelig-Ba et al., 1991; Pelig-Ba, 1998; Pelig-Ba et al., 2001, 2004), along the coast (Gill, 1996) and in mining areas (Smedley, 1996; Pelig-Ba et al., 2001; Ahmad et al., 2004; Asante et al., 2007; Buamah et al., 2008; Kortatsi et al., 2008b), and many have identified problem areas, *e.g.* where one or more of the elements listed in the previous paragraph are present at elevated concentrations. For example, in these mining areas, elevated concentrations of Fe, Mn, As, F^-, Pb, Hg and Cr have been found in water sources, soil and air (Kortatsi, 1994; AmonooNeizer et al., 1996; Golow et al., 1996; Obiri et al., 2006; Kortatsi et al., 2008b). Elevated concentrations of NO_3^- have also been found (Kortatsi et al., 2009), but further study is needed to establish the NO_3^- distribution in Ghana (British Geological Survey, 2000). Gill (1996) reported brackish water and high concentrations of Fe, Mn, Cl and NO_3^- in boreholes and wells in the Volta and Upper and Northern regions.

The aim of this study was to gain an overview of the chemical water quality of drinking water sources in the country, particularly of "other improved" sources such as wells and boreholes through a survey of rural water supplies. The potential need for further treatment of the water is discussed in the context of current water prices and how treatment and maintenance costs could be incorporated.

8.2 Materials and methods

8.2.1 Sample collection in Ghana

A total of 230 samples were collected out of which 199 were from improved drinking water sources, mainly boreholes and wells but also some standpipes and trucked water during the 2007 rainy season (July/August) from different regions throughout Ghana. For this study, the samples from the improved drinking water sources were analysed. Where possible the name of the location, age of the water source and pump, funding agency, water charge, money collection system, maintenance arrangements and proximity of other water sources in the area were registered. Difficulties arose when trying to distinguish between boreholes and wells

with hand pumps as information on the depth of the source was usually not available. However, the type of pump installed was used as an indication (see Asklund and Eldvall (2005) for a detailed discussion on this problem). Samples were collected from the source in 500 mL plastic bottles (washed three times with the sample water prior to collection), 20 mL of it filtered through a 0.45 µm syringe filter (Sartorius Minisart, non-pyrogenic CE) and stored in a 20 mL polypropylene vial. The pH of the remaining sample was checked upon collection and measured again at the end of the day as was conductivity (Multiline P4 multimeter, WTW) and turbidity (Turbidimeter TN-100, Eutech Instruments). Drinking water was likely to be exposed to the atmosphere before consumption as it was carried back in open basins and buckets and thus this reflects the pH which would be consumed. Filtered samples were stored at ambient temperature and airlifted to the UK at the completion of the data collection.

8.2.2 Chemical analysis

The samples were kept at 4°C and separated into two portions. One portion was acidified to pH < 2 (concentrated Aristar HNO_3) and left to equilibrate at for at least three days before ICP analysis. The other portion was kept untreated at 4°C for ion chromatography (IC) analysis. Blanks were prepared by using MilliQ water and treating it in the same way as the samples. Major cations (> 0.1 mg/L) were detected by ICP-OES while cations of concentrations as low as 0.01 µg/L were analysed with ICP-MS. Anions were analysed using IC (Dionex, CA, USA) (see section 3.1.6 for more details on analysis).

8.3 Results and discussion

8.3.1 Physico-chemical water quality

The results from the chemical analysis (mean, minimum median, lower inter-quartile range (Q1), median, higher inter-quartile range (Q3) and maximum values) are displayed in Table 14. The number of samples analysed (N), the applicable WHO

Table 14. Mean, minimum, interquartile ranges and maximum values measured for a range of elements in water samples collected. The WHO guideline is also given, as well as the percentage of samples outwith this guideline value (in bold) (Rossiter et al. 2010).

Parameter	Unit	N	Mean	Min	Q1	Median	Q3	Max	WHO guide-line	% outwith guide-line
Al	mg/L	192	**11.87**	<0.020	**3.927**	**8.500**	**14.60**	**66.69**	0.2*	95
As	µg/L	195	1.930	<0.003	<0.003	0.073	0.532	**169.5**	10	0.5
B	µg/L	195	61.11	<2.551	5.820	10.08	27.14	**2034**	500	2.6
Br	mg/L	193	0.029	<0.200	<0.200	<0.200	<0.200	1.116	-	-
Ca	mg/L	192	28.59	0.091	10.411	19.70	39.61	169.4	-	-
Cd	µg/L	195	0.025	<0.001	<0.001	<0.001	0.013	1.755	3	-
Cl^-	mg/L	193	49.44	<0.200	3.711	13.27	41.22	**597.2**	250*	5.7
Co	µg/L	195	0.262	<0.051	<0.051	<0.051	0.077	11.62	-	-
Cr	µg/L	195	0.199	<0.068	<0.068	<0.068	0.151	9.290	50	-
Cu	µg/L	195	2.774	<0.173	<0.173	<0.173	0.715	83.10	2000	-
F^-	mg/L	193	0.470	<0.100	0.044	0.209	0.45	4.238	1.5	6.7
Fe	µg/L	195	84.73	<0.001	5.446	17.78	46.16	**4257**	2000[a] (300*)	1.0 (2.6)
K	mg/L	187	4.382	0.241	1.475	2.564	5.511	29.65	-	-
Mg	mg/L	192	10.52	<0.030	2.586	6.459	14.55	66.20	-	-
Mn	µg/L	195	134.8	0.030	4.447	19.21	117.9	**2051**	400	11
Ni	µg/L	195	0.579	<0.054	<0.054	<0.054	0.436	**29.59**	20	0.5
NO_3^-	mg/L	193	34.01	<0.200	0.514	6.394	31.52	**507.7**	50	21
Pb	µg/L	195	1.526	<0.006	0.489	0.946	1.517	**34.94**	10	1.5
PO_4^{2-}	mg/L	193	0.058	<0.100	<0.10	<0.100	<0.100	1.214	-	-
S	mg/L	192	6.905	<0.200	0.372	1.150	4.091	235.4	-	-
Se	µg/L	195	0.434	<0.306	<0.306	<0.306	0.598	6.175	10	
SO_4^{2-}	mg/L	193	34.69	<0.200	1.648	5.236	23.75	**931.4**	500[b]	1.0
U	µg/L	195	1.988	<0.001	0.049	0.114	0.410	**266.6**	15	1.0
V	µg/L	195	2.380	<0.011	<0.011	<0.011	0.891	45.37	-	-
Zn	µg/L	195	9.305	<1.591	<1.591	<1.591	<1.591	454.8	3000	-
Conduc-tivity	µS/cm	199	457.1	15.00	178.0	314.0	549.0	2280	-	-
TDS	mg/L	198	176.2	4.963	51.77	98.42	178.2	**1454**	1200*	1.0
Turbidity	NTU	199	**14.30**	0	**0.237**	**0.793**	**3.303**	**629.7**	0.1*	90
pH		199	**6.32**	**3.69**	**5.67**	**6.43**	6.98	**8.88**	6.5-8.5*	53

*Recommendation based on aesthetic considerations such as taste and colour.
[a]Taste is often affected before WHO health guideline is reached, which is why many prefer to use the taste guideline value 300 µg/L.
[b]No health based guideline value is set, however values less than 500 mg/L are recommended due to gastrointestinal effects.
Note that any values that occur below the detection limit of the analysis technique (11.1.1) are displayed as "<"

drinking water guidelines and the percentage of samples with concentrations out with the guideline values are also presented.

The following elements do currently not have a WHO guideline value: bromium (Br), calcium (Ca), magnesium (Mg), potassium (K), sulfur (S), vanadium (V) and cobalt (Co). The following elements did not exceed the WHO guideline value in any location: cadmium (Cd), selenium (Se), Copper (Cu), zinc (Zn), cobalt (Co) and chromium (Cr). The following elements exceeded the health-based WHO guideline value in at least one location: boron (B), manganese (Mn), iron (Fe), arsenic (As), lead (Pb), uranium (U), fluoride (F^-), nitrate (NO_3^-), sulphate (SO_4^{2-}) and nickel (Ni). The most widespread parameters exceeding a health based WHO guideline, were NO_3^- (21%), Mn (11%) and F^- (6.7%). Numerous samples exceeded the recommended guidelines based on water treatment considerations or taste for Al (95%) and Cl^- (5.7%). Turbidity and pH were also outside the recommended range for 90% and 53% of the samples, respectively.

Sampling locations which contained parameters exceeding the WHO guideline for chemical quality are shown in Figure 66. Only parameters of greatest concern are shown in this map (Fe, Mn, F^-, B, As, Pb, U, Cl^- and NO_3^-). It is important to note that the concentrations of the analytes are likely to be higher during the dry season (von der Heyden and New, 2004), and hence from a health aspect, the values displayed are conservative since measured during the wet season. As can be seen in Figure 66, several water sources across the country contain concentrations of inorganic contaminants above the WHO drinking water guideline. Many of the water sources along the coast had elevated TDS, due to proximity to the sea. High concentrations of NaCl are expected to some extent due to seawater influence. Other ions such as F^-, Mn, Fe and NO_3^- were also above the WHO guideline along the coast. Further inland, a variety of elements exceeded the guideline value, in particular in the Western, Central, Ashanti and Upper East Regions, where F^- and NO_3^- concentrations exceeded the guideline. Overall 38% of the samples exceeded the health-based WHO drinking water guidelines for a minimum of one parameter.

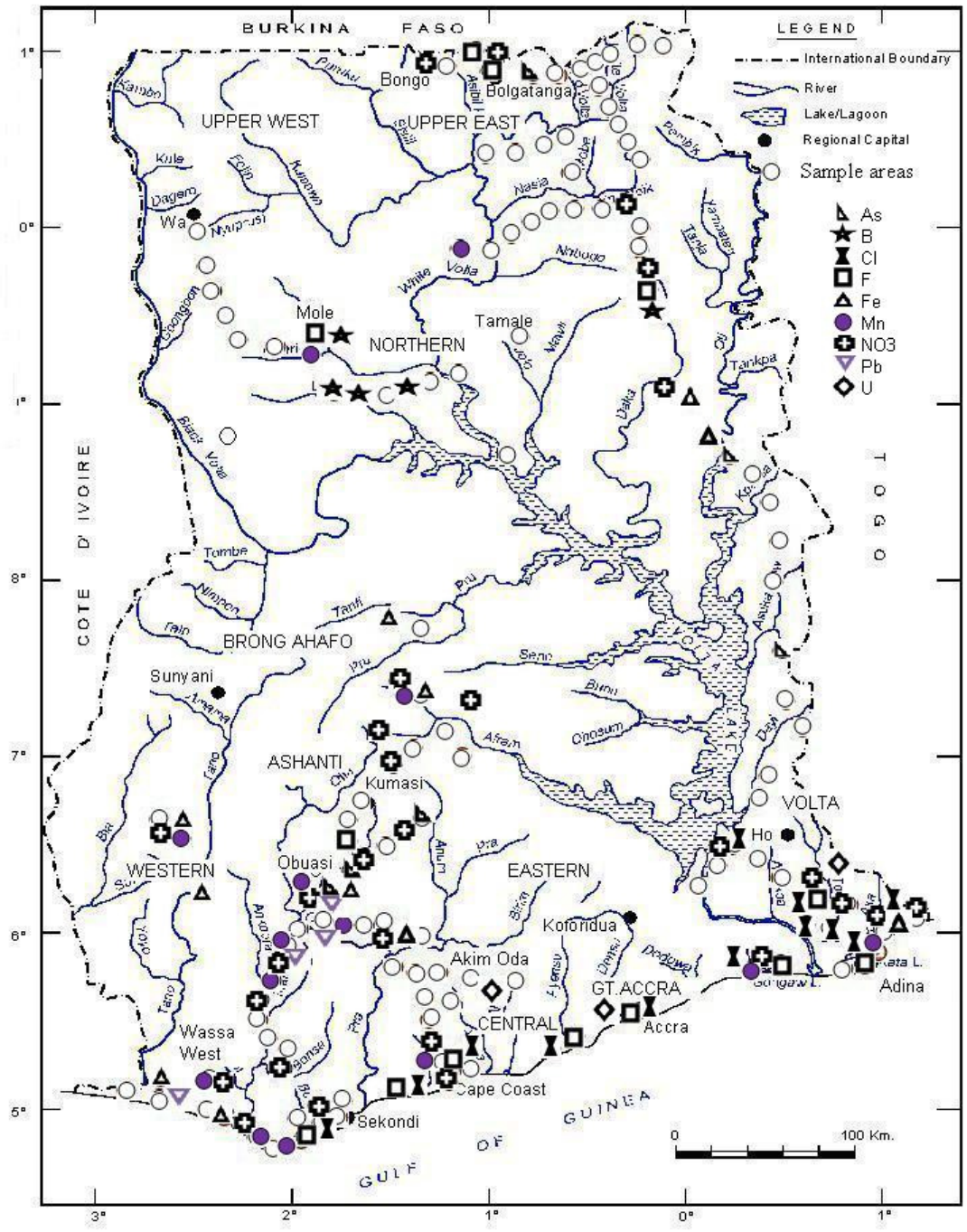

Figure 66. Map of Ghana with regions and sample points marked. Locations tested that did not exceed the WHO guideline value for As, B, Cl^-, F^-, Fe, Mn, NO_3^-, Pb or U were marked with an open circle, locations exceeding the WHO guideline were marked according to the legend in the map (also published in Schäfer et al. 2009)

The graphs of pH, cumulative frequency versus concentration for TDS, conductivity, turbidity and the main inorganic parameters of interest are displayed in Figure 67 to

Figure 70. This shows the range of the concentrations found and the percentage of samples found within a certain concentration. The dotted lines mark the WHO drinking water guidelines, where applicable. A more detailed discussion of the individual contaminants found in the waters sources follows.

pH values

There is no health based guideline for pH, although a range of 6.5-8.5 is often used suggested because aquatic life is negatively affected below pH 6.0 (Mason, 1990). Additionally at low pH, the water is corrosive and can cause wear to equipment. About 50% of the samples fell outside the recommended pH range, with the majority being too acidic (Figure 67).

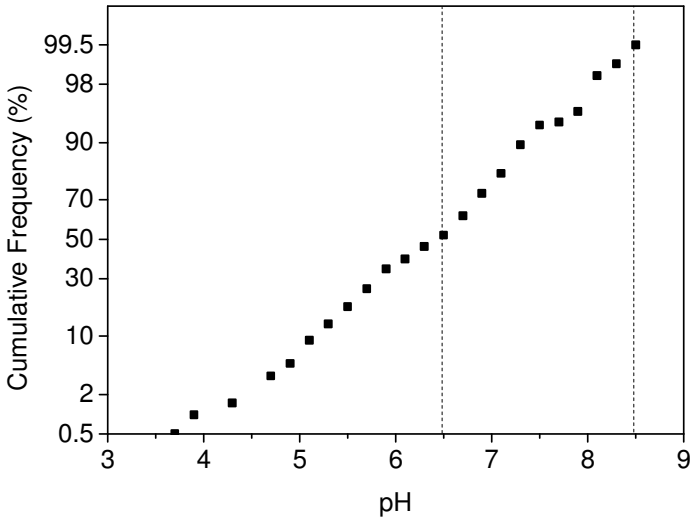

Figure 67. Cumulative frequency (%) versus pH. The dotted lines mark the recommended pH range (Rossiter et al., 2010b).

Acidity is more prominent in environments with granite based rocks with low buffering capacity (Mason, 1990). Of particularly high acidity (pH 3.7) was a borehole close to the mining town Obuasi in the Ashanti Region. The borehole also had high concentrations of Al, Mn, Pb and NO_3^-, indicating contamination from mining. Other acidic waters (pH 4-5.5) were found in the Ashanti, Western and Central Region. Some had high concentrations of Al, Mn or Pb, indicating

contamination from mining. These regions are also subject to much mining on both small and large scale. The Western, Central and Ashanti regions would be naturally more acidic both due to their geology (British Geological Survey, 2000) and due to forest coverage (Gill, 1996). Forests are naturally expected to be somewhat acidic, both due to the organic acids from the breakdown of organic matter and the higher precipitation they receive (Spiro and Stigliani, 1996). This same area also receives the highest rainfall in the country (1500-2200 mm/yr, compared to 700-1000 mm/yr in the northern parts and east coast) (Gill, 1996).

Turbidity and conductivity

Turbidity does not have a health based guideline, but it is recommended that it should ideally be below 0.1 NTU for effective disinfection (World Health Organisation, 2006). Ninety percent of the samples were above this guideline (Figure 68) and the turbidity was generally highest in surface waters, although high values (up to 266 NTU) were also found in boreholes. Ghana has set a guideline for a newly drilled bore holes at 5 NTU; and about 80% of the water sources sampled complied with this value.

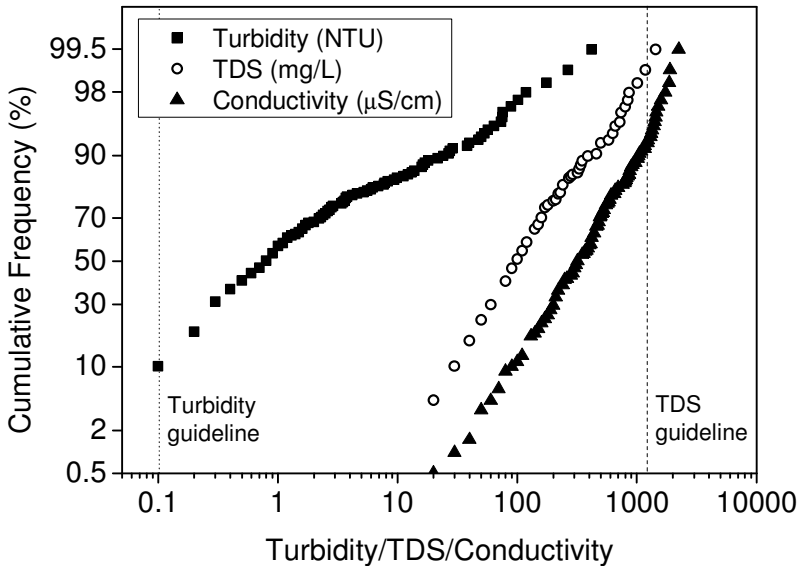

Figure 68. Cumulative frequency (%) versus turbidity (NTU), conductivity (µS/cm) and TDS (mg/L) (Rossiter et al., 2010b).

Conductivity is an indication of the total dissolved solids (TDS), both organic and inorganic found in the water. There is no health-based guideline. The WHO guideline value of 1200 mg/L for TDS is based on taste rather than health. High TDS may cause corrosion of equipment such as hand pumps.

8.3.2 Parameters of health concern

The elements analysed for in this study that exceeded a WHO *health based* guideline value were As, Pb, U, B, F^- and NO_3^-.

Arsenic

The WHO guideline value for arsenic (As) is 10 µg/L. Concentrations exceeding this guideline were found in the Ashanti Region, around Obuasi, in the north of the Volta Region and the Upper East (Figure 69). The highest As concentration was in a borehole in Bolgatanga (170 µg/L). Smedley (1996) and Kinniburgh (Smedley, 1996; Smedley and Kinniburgh, 2002) give a detailed description of As geochemistry and its mobility due to weathering conditions. As can for instance be mobilised by flooding and the reduction and mobilisation of As-containing Fe oxides, or by oxidation of arsenopyrates, which is the case in the gold mining areas of Ghana (Smedley and Kinniburgh, 2002). Similarly high As concentrations were measured by Asante (2007) in the Tarkwa gold mining region (Western Region). Bolgatanga is an active mining area, and may thus release naturally occurring As. Asante et al. (2007) measured As concentrations in human urine samples of inhabitants of Tarkwa, concluding that the concentrations were similar to those of concentrations found in *e.g.* Bangladesh and India, although they could not ascertain a link to drinking water. As concentrations in rivers were higher than boreholes, indicating air-borne contamination (Smedley, 1996). Kortatsi et al. (2008b) found that 21% of the boreholes in the Offin basin (Ashanti Region) contain As concentrations above the WHO guideline. Interestingly, Amonoo-Neizer and Amekor (1993) showed that crops grown close to Obuasi often had double As contents compared to the same crop types grown around Kumasi indicating the release of high concentrations of As in mining areas. Kortatsi (2008a) also identified

a number of samples with As concentrations above the drinking water guideline in the Central, Greater Accra and Volta Region. From the results of this study, it does not appear that As is a widespread problem in Ghana, however, it is still important to monitor and regulate contamination from mining activities as very high localised concentrations occur.

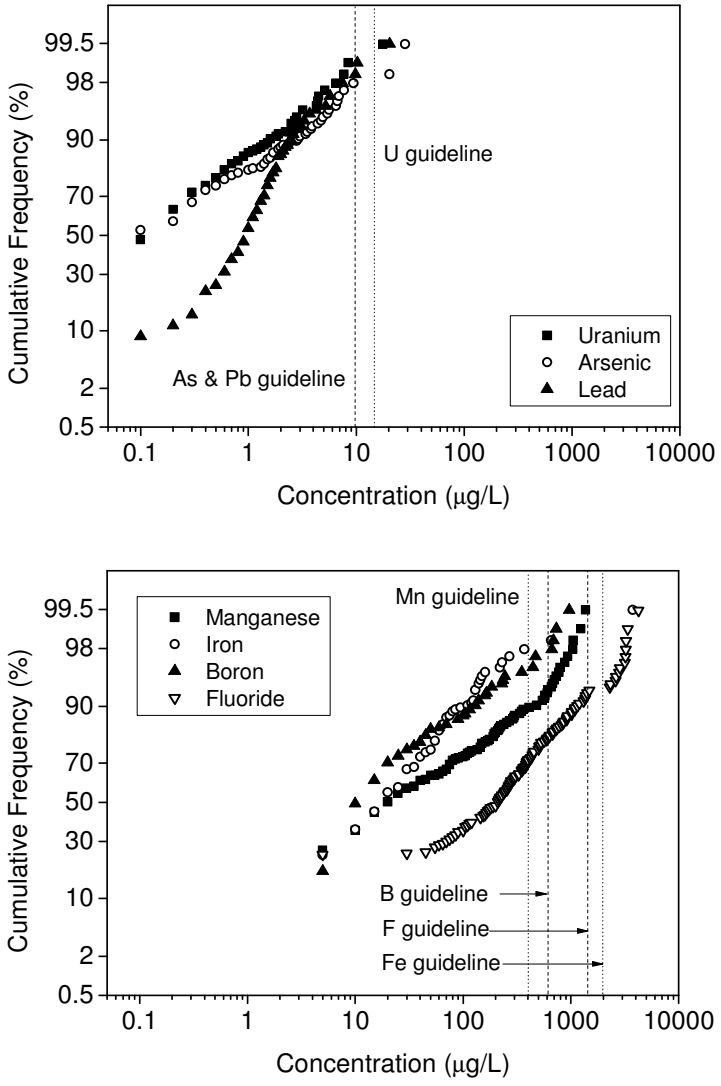

Figure 69. Cumulative frequency (%) versus concentration (µg/L) on log axis for Pb, As and U (top) and Fe, Mn, B and F^- (below). The dotted line indicates the WHO guideline (also in Rossiter et al., 2010b).

Lead

High concentrations of lead (Pb), above the WHO guideline value 10 µg/L, were found in the Ashanti region, as well as on the coast. The highest concentration determined was 35 µg/L. Concentrations of Pb above the WHO guideline in wells and boreholes imply that groundwater sources are not necessarily safe from pollution from industrial activities. The high Pb concentrations found at very low pH, and south of Obuasi, indicating acid mine drainage or other mining contamination as a possible source.

Uranium

Concentrations of uranium (U) above the provisional WHO guideline (15 µg/L) were found in the Central Region and the Volta Region. The Volta Region sample also had high concentrations of NO_3^- (508 mg/L, ten times the WHO guideline value), F^- (4.24 mg/L, nearly three times the guideline value) and Cl^- (500 mg/L, double the taste guideline value). The borehole containing most U (267 µg/L) was in the Central Region. It did not contain other chemical pollutants. Other boreholes in that area also contained U, although below the drinking water guideline value. U was previously found by Dampare (2005). Concentrations below the drinking water guideline were also found in found in the Upper East, indicating that while U might not be a widespread concern, it may be worth monitoring as it is a natural part of the geology. As well as being naturally radioactive, U is chemically toxic and when ingested may target bones or damage the kidney (The Royal Society, 2002; Kurttio et al., 2005).

Boron

Boron (B) was found at levels up to 2034 µg/L (the WHO guideline value is 500 µg/L) in the Northern Region. The highest B concentrations corresponded with alkaline pH. Speciation models of the water (section 11.6), showed B to exist mainly as boric acid (H_3BO_3) over the acidic to neutral pH range, and borate ($H_2BO_3^-$) above pH 8.5. Sources of boron include seawater (unlikely in this situation), coal burning

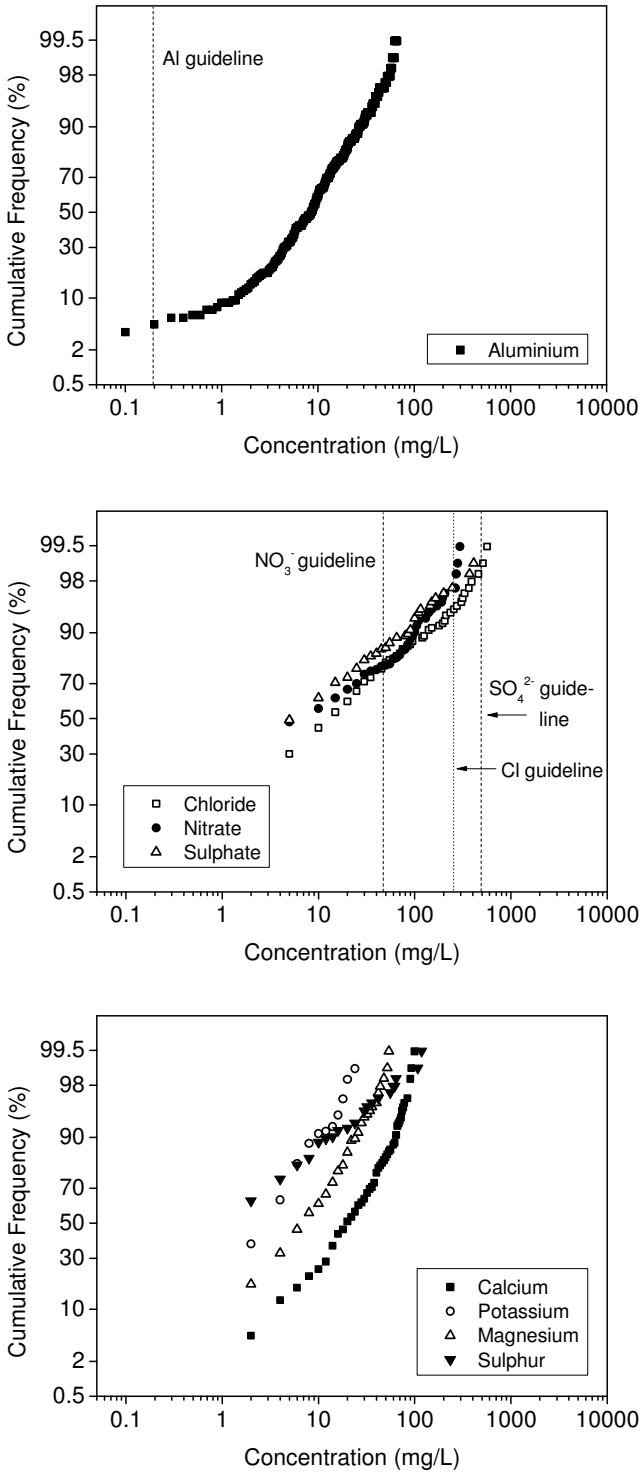

Figure 70. Cumulative frequency (%) versus concentration (mg/L) on log axis for Al (top); then Cl^-, NO_3^- and SO_4^{2-} (middle) and finally Ca, K, Mg and S (bottom). The dotted line indicates the WHO guideline where available (also in Rossiter et al. 2010b).

and industrial sources as well as borate-containing fertilizers, which may be the most likely source in this case as there is agricultural activity in the region.

Fluoride

About 6.7% of the samples contained fluoride (F^-) concentrations above the WHO guideline value (1.5 mg/L) (Figure 69). High concentrations of F^- were found in the north, but also in many locations along the coast, mainly in wells and boreholes. In the Upper East about 17% of the samples contained F^- concentrations above the guideline. Boreholes near the coast in the Volta Region contained F^- concentrations of above 4 mg/L, which can cause skeletal fluorosis. Kortatsi (2008b) also found F^- concentrations of 11 mg/L in the Offin Basin (Ashanti Region).

Nitrate

Nitrate (NO_3^-) has a WHO guideline value of 50 mg/L and exceeded this concentration in 21% of the samples (Figure 70). The highest concentration was 508 mg/L. The locations were widespread but mostly found in the Western, Ashanti, southern Volta, Northern region and Upper East. NO_3^- is regulated as it is one of the causes of methaemoglobinaemia (or "blue-baby syndrome") in infants (Manassaram et al., 2006) as well as a potential risk of stomach cancer (Abrahams, 2002). Forty-seven percent of the well waters had concentrations above the guideline, compared to 16% of the borehole waters (Figure 71). The concentrations of NO_3^- were also higher in wells than in surface water (results not shown). This indicates a widespread problem of elevated NO_3^- in shallow groundwater, probably a result of poor sanitation and latrine construction (MacDonald and Calow, 2009). High levels can also be caused by fertilizer use. The results of Pelig-Ba (2004) confirm those of this study and report a mean of 93.3 mg/L of NO_3^- and a maximum of 511 mg/L in groundwater in the Upper West. The WHO guideline value for nitrite (NO_2^-) is 0.2 mg/L. Because NO_2^- needs to be determined within 48 hours (Clesceri et al., 1998, Rump, 1999), this was not possible during this trial and hence no data is available.

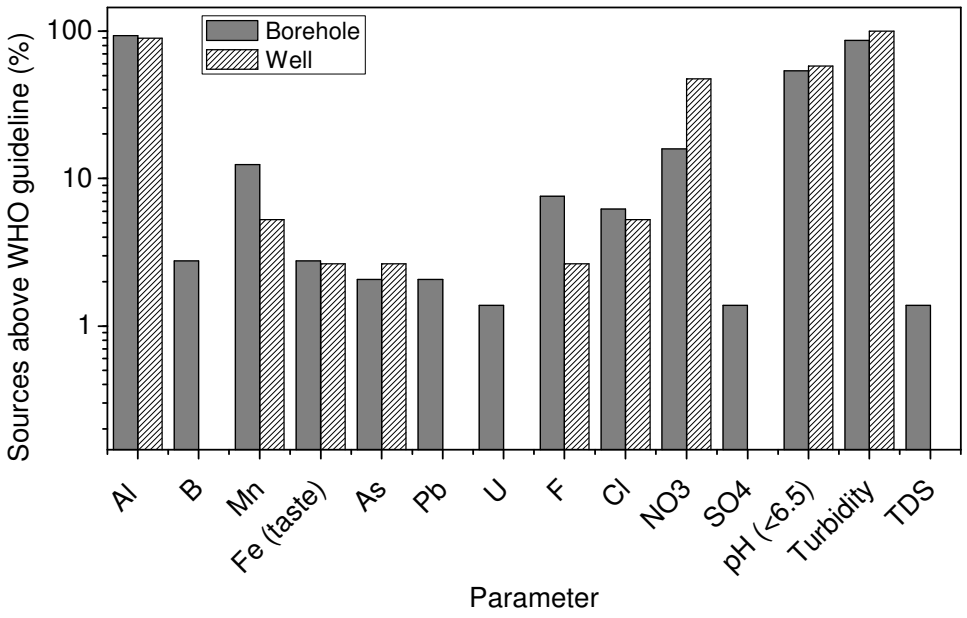

Figure 71. Comparison between boreholes (BH) and wells: percentage of source type with samples above the WHO guideline for Mn, Fe, F^-, Cl, NO_3^- and turbidity (also in Rossiter et al. 2010b).

8.3.3 Aesthetic parameters

Parameters analysed for in this study with non-health based WHO guidelines were Al, Fe, Mn, Cl and SO_4^{2-}. Despite not being a health concern, high concentrations affect the quality of water, leading to bad taste and colouration of cooking utensils and food. This has caused hundreds of wells to be abandoned in favour of surface waters likely contaminated with harmful micro-organisms (Smedley, 1996; Gyau-Boakye and Dapaah-Siakwan, 1999).

The most widespread pollutant was aluminium (Al). The health effects from Al remain unclear, however, Al does have a practicable non-health based WHO guideline value of 0.2 mg/L (stated as an achievable level for small water treatment facilities. This takes into consideration the health concerns but also the benefits from using Al in water treatment (World Health Organisation, 2006)). Ninety-five percent of the samples measured were above the recommended guideline value (Figure 70), several more than ten-fold, with the maximum concentration at 67 mg/L. Areas of particularly high Al concentration were in the Volta Region (regional average of 27

mg/L) where Nkwanta district, Asuogyaman, Hohoe, Keta and Ketu districts had especially high concentrations (average of 30, 42, 28, 55 and 44 mg/L respectively). The Western Region also had locations containing high Al concentrations, with an average of 13 mg/L in the Wassa West district. Al may leach from soils unable to buffer acidic precipitation and from minerals such as kaolinite and gibbsite (Langmuir, 1997). Some researchers find high Al concentrations in association with particles (Reimann et al., 2003), in our study however, Al showed no correlation with turbidity. Al concentrations were found to be highest around neutral pH, where Al normally is less soluble. The high Al in the samples may possibly be associated with colloids smaller than the 0.45 µm filter. Pelig-Ba (2004) also found higher Al concentrations in water at neutral pH and explained it by presence of chelating agents such as soil organic matter raising the Al solubility. In Pelig-Ba's study from the Upper Regions (1998) the Al range was reported as up to 47 mg/L, with a mean of 4.4 mg/L in the Northern Region.

Sulphate

A number of samples had very high sulphate (SO_4^{2-}) concentrations (>500 mg/L) (Figure 70). One was found in a relatively new borehole in the Northern Region, probably due to mudstone geology. In this sample high Mn concentrations were also found. Due to the taste, consumers preferred to drink water from the nearby shallow well, which contained low SO_4^{2-} and Mn concentrations but possible microbiological contamination. This illustrates how poor chemical water quality of new deeper groundwater sources may drive people back to shallow contaminated sources. Another borehole from the same region contained similar SO_4^{2-} and TDS levels, but no Mn, and people were happy to drink the water.

Chloride

Around 5.7% of the waters sampled contain more chloride (Cl^-) than the recommended value (250 mg/L) (Figure 70). This value is based on taste, but waters of these Cl^- concentrations are also more corrosive. As can be seen from the map in Figure 66, much of the high Cl^- concentrations are found in the Volta delta and along

the coast. Gill et al. (1996) also reported high Cl^- concentrations in the Keta district and found similar evidence of seawater intrusion. A study conducted by Kortatsi (2006) in the Accra plains similarly found high concentrations of Cl^- and concluded that 75% of the boreholes in the area were brackish (TDS range 1000-10000 mg/L), with Na and Cl^- as the dominating ions.

Iron

Iron (Fe) concentrations below 2000 µg/L are described as safe by the WHO (Figure 69), although taste is affected above 300 µg/L. This taste based value is used by many studies when reporting Fe. Up to 4257 µg/L was measured. As can be seen from the map (Figure 66), high Fe concentrations were found in a variety of locations along the coast, inland in forested areas and the Northern Region. Most samples (97.4%) fall below 300 µg/L and 99% are below the guideline value 2000 µg/L (Figure 70). Most of the sources containing very high Fe concentrations were found in boreholes. The chemistry of naturally occuring Fe is controlled by the redox conditions of the water (not measured), where Fe is mobilised under reducing conditions, indicating that the environment of these boreholes was reducing.

Manganese

Concentrations of manganese (Mn) above the WHO drinking water guideline value (400 µg/L) were found mainly the Western and Ashanti region and along the coast (Figure 66). The highest concentrations were found in boreholes (Figure 71). Similarly to Fe, Mn chemistry is also redox controlled. High concentrations of Fe and Mn corresponded in some samples, but for the majority of them high Mn concentrations were not accompanied by high Fe concentrations.

Calcium, magnesium and potassium

High concentrations of calcium (Ca), magnesium (Mg) and potassium (K) (Figure 70) are generally not a health concern and thus do not have guideline values set by the WHO, but are important nutrients. Studies have shown an inverse relationship

between cardiovascular disease and water hardness, with increased risk occurring with Ca concentrations <60 mg/L of Ca (Packham, 1990). In fact the water sources in Ghana were relatively soft and the concentrations of the samples in the third percentile were below 15 mg/L for Mg and 40 mg/L for Ca (Figure 70). In large concentrations however, they may affect the taste of the water by contributing to high TDS, which will also affect practical water usage (like washing with soap).

In summary, the water quality from the different sources in Ghana displayed a wide range of chemical water quality, with many sources containing concentrations above the drinking water guidelines. In boreholes high concentrations of NO_3^-, F^-, B, Pb, As, U, Cl^-, Fe, Mn and SO_4^{2-}, and high levels turbidity were found. In wells NO_3^-, Fe and turbidity were common problems, as well as some instances of As, Mn, Cl^- and F^-.

8.3.4 Current rural water sources, costs and ability to pay

The Ghana Water Policy advocates provision of demand driven basic water and sanitation services for communities that contribute towards capital cost, operation, maintenance and repairs (Government of Ghana, 2007). Non-government organisations often support the communities by paying up to 95% of the borehole cost, while the community raises 5% of the borehole cost (Government of Ghana, 2007).

About 25% of the communities visited had an annual user fee per household ranging from 5000 to 40000 cedis (£0.3-£21, August 2007). About 33% of the water supplies had a water collection charge based on quantity of water collected (Figure 72). Surface and many well waters were often free of charge while boreholes, piped and especially truck-delivered water attracted the highest charges. The cost per bucket (18L) for boreholes and piped water ranged from 25 to 250 cedis (£0.07 to £0.7/m^3, based on 62 communities) and the cost per basin (40L) ranged from 50 to 500 cedis (£0.07 to £0.7/m^3, based on 47 communities). Where water was trucked in, the cost was 1000-1200 cedis per bucket (£2.9-3.5/m^3, based on two communities). An appointed water vendor from the WatSan committee was often situated at the water

source to directly collect the payment from the users. Understandably some households choose to use cheaper or free water sources for washing and bathing, increasing the risk of contact with diseases transmitted by surface water. Surface water is often used during the rainy season due to availability while in dry seasons they may be used if borehole re-charge is low (Iten and McCarron, 2006).

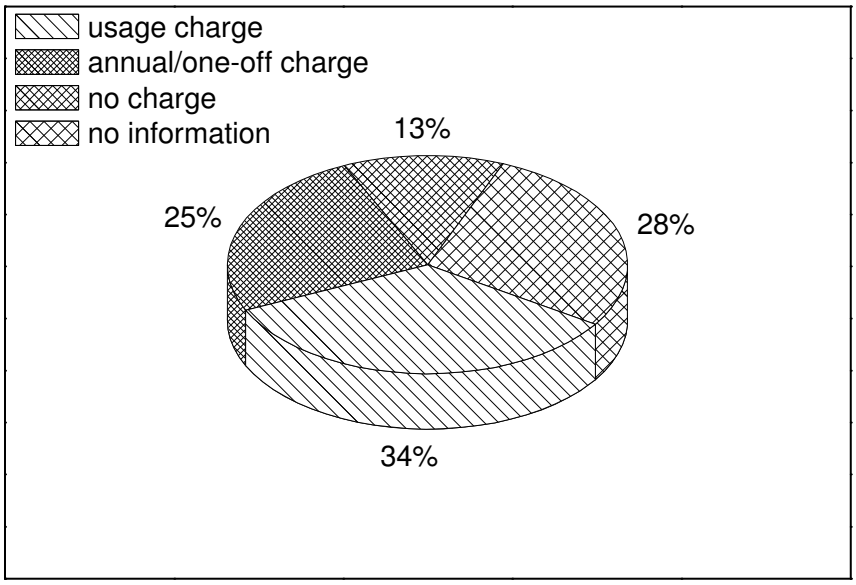

Figure 72. Distribution of water charge systems (charge based on water usage, annual charge, no charge) out of the 220 water sources visited (Also in Rossiter et al. 2010b).

Thirteen percent of the communities visited did not have an operational payment system in place. Many communities were therefore struggling to raise between 1.5-2.5 million cedis (about £80-£130) in order to pay for repairs or spare parts of pumps, broken a couple of years earlier. When this proved to be a major hurdle and pumps would remain disused or even abandoned. Another problem encountered in some communities was that there was no payment system for the trained community members to get paid for maintenance services, which meant that they were unwilling to assist. Organising maintenance and collecting payment for repairs is further complicated by the dynamic movement of people between different communities and even parts of the country (Iten and McCarron, 2006). In some cases pumps were ill designed, causing chronic failure of parts.

8.3.5 Is water treatment a suitable option for sources of poor chemical quality?

The problems encountered in the survey were those of high turbidity, high concentrations of F^-, NO_3^-, Al, Mn, Fe and localised contamination of Pb, As, B and U. Overall, 38% of the sources analysed exceeded a health-based WHO guideline for chemical parameters. Installation costs of boreholes and wells are about £3800 and £1800, respectively. Many boreholes fail due to the high chemical content of for example F^- (Smedley et al., 2002) and up to 64% of the boreholes in the north of Ghana fail based on water flow, re-charge and chemical quality (Iten and McCarron, 2006). Thus for the actual costs of developing ground water the number of unsuccessful boreholes drilled need to be taken into account. To reduce this cost in areas of complex geology, investment in initial hydrogeological investigations is important to improve success (MacDonald and Calow, 2009). An alternative option to capping existing boreholes and drilling new, potentially unsuccessful boreholes would be to treat the water. Suitable treatment options in developing countries can be provided as centralised, community based or point-of-use/household based approaches. For economic and infrastructural reasons, community based or point-of-use treatments are considered preferable to centralised treatment for rural communities (Peter-Varbanets et al., 2009). This also applies to rural areas of Ghana where boreholes or wells may already exist while access to a centralised supply does not. Treatment technologies considered suitable for developing countries, such as sand filtration, UV disinfection (SODIS), ceramic filters and chlorination mainly remove or destroy microbial pathogens and turbidity (Sobsey et al., 2008; Peter-Varbanets et al., 2009) and could potentially be used to disinfect surface waters of good chemical quality, but do not effectively remove chemical contaminants. Importantly, over 90% of the samples had a turbidity of more than 0.1 NTU, which must be reduced before disinfection can be effective.

Treatment methods which target chemical contaminants combine processes such as adsorption or coagulation with ultrafiltration or sandfiltration processes (Brandhuber and Amy, 2001; Johnston and Heijnen, 2001; Chakravarty et al., 2002). Issues of handling, cost of chemicals, sanitation and regeneration of the adsorption materials

are a concern. Ultrafiltration systems are available at an investment cost of about £2000 (20 m^3/day capacity), and are maintained by a daily washing. Low-cost As removal for communities in developing countries have been investigated (Bissen and Frimmel, 2003b; Malik et al., 2009) and wells can even be constructed to allow re-circulation of oxidised water back into the source, thus oxidising and immobilising Fe and As before it is with-drawn (van Halem et al., 2009). This method still requires further development and testing, however, and the resulting concentrations depend on concentrations originally present. The need to remove a variety of chemical contaminants from existing water sources persists and long-term studies are lacking. The issue of F^- removal from drinking water in the northern regions of Ghana, for example, is unresolved (CWSA, 2007). In such situations membrane technologies have unique potential due to their physical separation. Nanofiltration or reverse osmosis are well adapted in developed countries for water desalination, reuse and removal of dissolved contaminants while application in developing countries has not yet widely progressed. Investment cost into single tap reverse osmosis has been estimated to £190-£380 (Peter-Varbanets et al., 2009) which may be an option if it could be developed for boreholes. A solar powered community-based membrane system was field tested by Schäfer et al. (2007) and found to perform well in terms of potable water production. The system had a specific energy consumption of 1.2 kWh/m^3. Investment and maintenance costs into a solar powered electrodialysis systems have been calculated as £0.15-0.28/m^3, with an initial investment of at least £5400 (Ortiz et al., 2008). However, the long-term integration of operation and maintenance of such systems into communities requires solid strategies at a local level.

8.3.6 Sustainability of treatment systems

The effectiveness and sustainability of point-of-use and small-scale water treatment technology remains to be seen as contentious (see for example Hunter (2009), Hunter et al. (2009) and Schmidt and Cairncross (2009)). Three components of sustainability for engineered solutions in developing countries were identified by Montgomery et al. (2009) as 1) effective community demand, 2) local financing and cost recovery, and 3) dynamic operation and maintenance, while Singhirunnusorn and Stenstrom

(2009) identified seven crucial areas when considering technology implementation (in their case waste water treatment). These are listed in order of importance: reliability, efficiency, affordability, social acceptability, sustainability, simplicity and land requirement. The importance of local ownership of both the technology development (local sourcing and production) as well as the resulting systems should be emphasized. Failure to incorporate these components into a water source and potential water treatment reduce the likelihood of its long-term functionality. Cost recovery of five community managed water systems in the Ashanti Region was investigated by Nyarko et al. (2007), who found that neither of the communities recovered their full capital and operational costs, while four out of five recovered their operation and maintenance costs. Interview results showed that there was not an understanding amongst the community members of the full costs involved, while some preferred to use free untreated water sources when the prices were too high. The importance of demand-driven appropriate water treatment was high-lighted in a study by Hoque et al. (2004). They found that household treatment systems often were abandoned after a short period, while community based systems proved more sustainable. For this reason it is important to understand the willingness (and ability) to pay for water provision in such communities as well as elucidating the most suitable treatment option. In conclusion, a number of factors must be taken into consideration when deciding whether to treat a water source. Important considerations include: 1) the water quality (contaminants to be removed, but also how the water quality may affect the effectiveness of the treatment used), 2) alternative water sources, 3) social preferences for *e.g.* community based or household treatment systems, 4) available treatment options, 5) costs and cost-recovery plans, 6) user friendliness or availability of suitable operators 7) supply network of spare parts for maintenance 8) availability of a support network for operational problems and water quality monitoring.

8.4 Conclusions

It was found in this study that 38% of the wells and boreholes in Ghana had high concentrations of inorganic contaminants. Major problems identified were those of

high turbidity, low pH, high concentrations of NO_3^-, F^-, Al and Cl^- and in localised areas As, Pb, B and U. The importance of regular monitoring of groundwater sources is emphasized. While some 'low-cost' treatment technologies to remove, for instance, As and F^- exist, the long-term sustainability and management of such technologies is yet to be proven for a wide range of chemical contaminants. Another problem is how the long-term performance (in particular contaminant breakthrough) of such systems can be monitored. The maintenance costs of systems could potentially be incorporated in the maintenance costs currently paid by community members (up to £0.7/m^3), especially if government and NGO's were willing to invest in the capital costs. This could be worthwhile, considering the cost of unsuccessful boreholes. About 58% of the communities had a payment system in place to recover basic maintenance costs.

In areas of high chemical contamination, more advanced inorganic removal treatment such as nanofiltration and reverse osmosis may be necessary. This would require extensive training of local people in the operation and maintenance of such systems, but while initial investment would increase, it may facilitate maintenance and potentially reduce long-term costs in particular if renewable energy is used as a power supply. Given that renewable energy powered ground water pumps are rapidly penetrating the market and water charges for trucked water is comparable to membrane treatment costs this is a viable option. Any form of improved water supply requires community ownership and commitment by local and national authorities to ensure that long-term needs are met. Research into ensuring long-term sustainability in terms of community demand, cost recovery, failure management, maintenance of water sources and treatment needed is timely and of critical importance.

9 Conclusions and further work

9.1 Summary and conclusions

There were two overall aims to this research: 1) to investigate the influence of speciation across the pH range on uranium removal by and interaction with a UF-NF/RO system, and 2) to investigate the potential for implementation of membrane systems in remote locations in developing countries.

In Chapter 4 the results of a field trial using brackish groundwater were thoroughly analysed and interpreted. Early on during the research it was realised that uranium behaves very differently to all other inorganic ions that were analysed, and was taken up by the membranes at certain pH values. This directed the research towards investigating and explaining the underlying mechanisms behind the uranium-membrane interactions. Other important conclusions drawn from the field trial were that the UF-NF/RO generally showed excellent removal of uranium, producing a permeate with uranium concentrations below WHO drinking water guidelines, with the exception of the experiments conducted with natural energy variation, specifically the solar continuous experiments.

In Chapter 5 the uranium retention by and uranium mass adsorbed to UF membranes was investigated across a wide pH range. The influence of OM on uranium behaviour in the system was explored. The research showed that, although OM clearly influenced the uranium speciation and behaviour and caused uranium to adsorb to the membrane at different pH values, uranium was not well retained, irrespectively of whether OM was present or not. For effective removal of uranium, either a membrane with smaller pore size or complexation with a material of larger size would be necessary. The experiments did, however, provide useful insight to how uranium interacts with a polymeric material under a range of water conditions, however. This will prove especially relevant where membranes are used for surface water treatment, which often contain high concentrations of OM (Scandinavia and the UK are such examples). Specific conclusions from the work in Chapter 5 were:

1) uranium adsorbs to the UF membrane at pH 5-7 even in the absence of OM, 2) humic acid (HA) caused increased in mass adsorbed of uranium at pH 3 and 5, 3) tannic acid (TA) caused a significant increase in uranium mass adsorbed at pH 10 and 11, and 4) alginic acid (AA) had little effect on uranium mass adsorbed apart from at pH 3 where it increased the uranium mass adsorbed. It is worth noting that UF membranes are routinely used in analytical work to determine, for example, the importance of uranium associations with colloids in natural waters (Guo et al., 2007) and so the results of this study will be beneficial in this respect since it is clear from this study that analytical artefacts that can arise during UF. For example, uranium originally present in "truly dissolved" form (<1 kDa) adsorbing to UF membranes could be erroneously assigned as colloidal uranium.

In Chapter 6 the uranium interaction with a NF and a RO membrane was investigated across the pH range 3-10 in a solution containing only background electrolyte and without applied pressure. This was important in order to establish whether the uranium mass adsorbed observed in Chapter 4 was due to uranium-membrane interactions, or whether it was a result of other ions present in the solution or operational parameters causing concentration polarisation and/or precipitation of uranium. Through the experiments, it could be established that uranium does indeed adsorb to the membrane at pH 5-7 (but not at pH 10-11 where major mass adsorbed of uranium to the membranes had been noted in Chapter 4). Importantly, it was discovered that the uranium-membrane interaction was highly speciation-dependent. The spatial (SEM, TEM and STEM-EDX) and FTIR analysis at pH 6 clearly showed that the main adsorption took place in the active layer where the uranium species (mainly UO_2OH^+) reacted with the carboxyl groups of the membrane. At alkaline pH, where $UO_2(CO_3)_3^{4-}$ dominates uranium speciation, a weaker type of interaction occurred through hydrogen bonding between the highly electronegative oxygen atoms on the carbonate ligands with membrane amine groups. The extent of adsorption was limited by membrane pore size: although adsorption was greater at pH 5-7 compared to the other pH values for both the NF and RO membrane, about 20% higher adsorption took place to the NF membrane compared to the RO membrane at pH 6. The application of pressure (5-15 bar) had no effect on the

adsorption to the RO membrane. For the NF membrane the uranium adsorption only increased at 15 bar. The only notable effect of pressure was observed for the NF membrane at pH 8.5 where $UO_2(CO_3)_3^{4-}$ dominated, most likely due to the similarity between species size and molecular weight cut-off of the membrane. Increased pressure caused an increase in the uranium mass adsorbed. This was due to increased concentration polarisation of uranium which also resulted in a decrease of retention from 99% at 5 bar to 87% at 15 bar.

In Chapter 7, the influence of calcium on uranium-membrane interactions and uranium retention was investigated. This was important since calcium is often a major ion in natural waters and was thought to be potential cause of the uranium deposition observed in Chapter 4 at pH 10-11. It was demonstrated that calcium had a marked effect on uranium adsorption at pH values where uranium speciation is altered by the formation of the neutral species, $Ca_2UO_2(CO_3)_3$. This led to a decrease in adsorption by up to 40%. Indeed, the adsorption results obtained for the solar batch and continuous experiments with the RO membrane corresponded well with the laboratory study for the RO membrane at similar pH values. Furthermore, at the same calcium concentrations found in the Australian groundwater, ~50% calcium precipitated at pH 10. This resulted in <35% uranium co-precipitating, as well as a large permeate flux decline due to the calcium scaling of the membrane. Thus the deposition observed in Chapter 4 at pH 10-11 could be explained by co-precipitation of uranium with calcium.

In Chapter 8 the chemical water quality of "improved" water sources in Ghana, mainly wells and boreholes, was investigated. Out of 199 samples from improved sources across the country, 38% exceeded the WHO drinking water guidelines, which could have long-term health consequences for the consumers of that water. Treatment of the water could be a solution to this problem, especially when considering the cost of drilling a new potentially unsuccessful borehole. Household water treatment technologies exist which often address specific contaminants such as arsenic or iron. The effectiveness of these is highly dependent on the individual household members. Membrane filtration could provide a practical community-based

alternative, especially for water sources containing multiple contaminants. This would, however, require extensive training of system operators and a committed support network. About 58% of the communities visited had a payment system in place to recover basic maintenance costs. Many other water sources were dis-used however, due to poor equipment maintenance and a lack of training. These issues would have to be solved before attempting implementation of community membrane systems.

To conclude, this research has demonstrated for the first time that uranium adsorbs to membranes used for drinking water purification. This adsorption was highly dependent on the pH and available ligands (*e.g.* CO_3^{2-}, Ca and OM) which affected the speciation of uranium. It was found that at least three characteristics of the uranium species and membranes determined the uranium-membrane interactions: a) charge of uranium species and membrane, b) uranium species size compared to the relative pore size of the membrane and c) reactivity of uranium with membrane functional groups.

The research shows the importance of understanding the chemistry of the water when selecting a membrane treatment process, as well as deciding how to maintain and clean the systems. There were advantages with NF such as the high retention of uranium (80-98%) compared to the lower retention of calcium (~40-60%) at pH 6-10. This selectivity of uranium over calcium would be advantageous since a certain amount of calcium and other important nutrients are desirable in drinking water. On the other hand, the NF membrane had high uranium adsorption, while only low adsorption was observed for the BW30 membrane.

9.2 Further work

The research presented in this thesis has revealed interesting aspects as to how uranium interacts with membranes used for drinking water purification, and in that process, many more questions have inevitably been raised.

It has been shown that uranium formed bonds with membrane functional groups. Now it would be interesting to investigate what the long-term effect would be on the membrane properties. Potentially these functional groups could be altered, and the effect on membrane performance is unknown. Alternatively, membranes of different material may be chosen to limit adsorption.

The adsorption and precipitation of uranium was shown to be highly dependent on the inorganic and organic ligands available in the water as well as precipitation of major elements. For instance, the combination of calcium and magnesium, as well as the influence of other ions known to affect uranium speciation, such as barium, phosphate, iron and vanadium, are likely to affect uranium interactions with membranes and would be most interesting to investigate further.

Fundamentally, it would also be interesting to establish how uranium binds with the different types of OM tested, and, importantly, how uranium would interact with OM found in natural waters. On the other hand, the tendency of uranium to form complexes with OM and to co-precipitate with calcium could potentially be exploited to further develop and improve uranium water treatment.

From a practical aspect, it would be important to investigate the long-term impact of the uranium adsorption taking place to the NF membrane. Does it build-up and eventually lead to a break-through in the permeate solution? Break-through of uranium was observed for the solar continuous experiments in Chapter 4 using the RO membrane. It could not be , whether this was due to build-up of uranium, the natural energy variation or some other factor such as ageing of the membrane (as implied by the slightly lower-than-expected Na^+ and Cl^- retention). No such break-through was observed during the laboratory studies. This would be of major importance to determine since levels were above drinking water guidelines. Also, adsorbed uranium is likely to desorb under acidic conditions. This is an important consideration for membrane cleaning processes, as de-sorption of uranium may lead to elevated concentrations of uranium in the cleaning solution.

The presence of uranium in drinking water is largely ignored by regulators, possibly due to its localised occurrence and uncertain chronic health effects, although acute effects are well-established. As demonstrated in section 2.1.4, elevated concentrations are found world-wide, however, and are a particular problem in groundwater. These are the sources often employed for drinking water in remote locations both in developed, but especially in developing countries. In fact, during this study, a uranium concentration of 267 µg/L uranium was measured in a community in Ghana (17 times the WHO drinking water guideline). This, as well as the elevated concentrations of many other elements, shows that groundwater cannot necessarily be assumed to be "safe". Regular monitoring is required, as well a treatment, where needed. Unfortunately the cost of both monitoring and treatment is prohibitive for many areas. These are a number of very important aspects that should be addressed in further research: 1) the development of low-cost monitoring techniques and 2) the development of local and regional support networks for effective treatment of contaminated water. 3) Moreover, for the potential implementation of membrane treatment systems, bio-fouling must be taken into account, especially for tropical areas, where biological growth is highly favoured. Extreme caution must also be taken if treating surface waters, since these may contain high levels of pathogens. The disposal of concentrated solutions requires carefull consideration.

Practically, the selection process of a suitable water treatment will have to consider both suitable technical treatment options and local socio-economic circumstances. However, straight forward but still comprehensive overview of treatment options, cost comparisons, technical requirements of users and long-term sustainability would be extremely useful to and appears to be lacking at this point.

10 References

Abdelouas A, Lutze W, Nuttall E. Chemical reactions of uranium in ground water at a mill tailings site. Journal of Contaminant Hydrology 1998; 34: 343-361.

Abrahams PW. Soils: their implications to human health. Science of the Total Environment 2002; 291: 1-32.

Abu-Qare AW, Abou-Donia MB. Depleted uranium - the growing concern. Journal of Applied Toxicology 2002; 22: 149-152.

Agyeman K. Privatization of water in Ghana: stopped in its tracks or a strategic pause? International Journal of Environmental Studies 2007; 64: 525-536.

Ahmad K, Dampare SB, Adomako D, Opata NN, Quagraine RE. The use of neutron activation analysis in gold prospecting in small-scale mining in Ghana. Journal of Radioanalytical and Nuclear Chemistry 2004; 260: 653-658.

Ahmed MF, Ahuja S, Alauddin M, Hung SJ, Lloyd JR, Pfaff A, Pichter T, Saltikov C, Stute M, van Geen A. Ensuring safe drinking water in Bangladesh. Science 2006; 314: 1687-1688.

Ahmed S, Rasul MG, Hasib MA, Watanabe Y. Performance of nanofiltration membrane in a vibrating module (VSEP-NF) for arsenic removal. Desalination 2010; 252: 127-134.

Al-Amoudi A, Lovitt RW. Fouling strategies and the cleaning system of NF membranes and factors affecting cleaning efficiency. Journal of Membrane Science 2007; 303: 6-28.

Allison JD, Brown DS, Novo-Gradac KJ. MinteqA2 / ProdefA2, A geochemical assessment model for environmental systems. US Environmental Protection Agency, Athens, GA, USA, 1991.

Alloway BJ, Ayres DC. Chemical principles of environmental pollution. Glasgow, Blackie Academic & Professional, 1993.

AmonooNeizer EH, Amekor EMK. Determination of total arsenic in environmental samples from Kumasi and Obuasi, Ghana. Environmental Health Perspectives 1993; 101: 46-49.

AmonooNeizer EH, Nyamah D, Bakiamoh SB. Mercury and arsenic pollution in soil and biological samples around the mining town of Obuasi, Ghana. Water Air and Soil Pollution 1996; 91: 363-373.

Ang WS, Lee SY, Elimelech M. Chemical and physical aspects of cleaning of organic-fouled reverse osmosis membranes. Journal of Membrane Science 2006; 272: 198-210.

Annanmäki M, Turtiainen T, Salonen L, Huikuri P, Mehtonen J, Koskela S, Turunen H, Perfler R, Staubmann K, Weingartner A, Haberer K, Wilken R, Raff O, Funk H, Akkermann-Kubillus A, Jungclas H, Weber R, Rausse C, Mjönes L, Hagberg N, Jaakkola T, Lehto J, Vaaramaa K, Kelokaski P, Riekkinen L, Ervanne H, Schönhofer F, Kralik C, Irlweck K, Katzlberger C. Treatment techniques for removing natural radionuclides from drinking water. Oy Edita Ab, Helsinki, Radiation and Nuclear Safety Authority, Finland 2000.

Anselme C, Jacobs EP. Ultrafiltration. In: Water Treatment Membrane Processes Ed: Mallevialle J, Odendaal PE, Wiesner MR. McGraw-Hill, New York, 1996, pp. 10.1-10.88.

Arai Y, Marcus MK, Tamura N, Davis JA, Zachara JM. Spectroscopic evidence for uranium bearing precipitates in vadose zone sediments at the Hanford 300-area site. Environmental Science & Technology 2007; 41: 4633-4639.

Arogunjo AM, Hollriegl V, Giussani A, Leopold K, Gerstmann U, Veronese I, Oeh U. Uranium and thorium in soils, mineral sands, water and food samples in a tin mining area in Nigeria with elevated activity. Journal of Environmental Radioactivity 2009; 100: 232-240.

Asante KA, Agusa T, Subramanian A, Ansa-Asare OD, Biney CA, Tanabe S. Contamination status of arsenic and other trace elements in drinking water and

residents from Tarkwa, a historic mining township in Ghana. Chemosphere 2007; 66: 1513-1522.
Asklund R, Eldvall B. Contamination of water resources in Tarkwa mining area of Ghana. Department of Engineering Geology, Lund University, 2005; M.Sc.: 57.
Åström ME, Peltola P, Rönback P, Lavergren U, Bergbäck B, Tarvainen T, Backman B, Salminen R. Uranium in surface and groundwaters in Boreal Europe. Geochemistry-Exploration Environment Analysis 2009; 9: 51-62.
Baeza A, Fernandez M, Herranz M, Legarda F, Miro C, Salas A. Removing uranium and radium from a natural water. Water, Air and Soil Pollution 2006; 173: 57-69.
Bai J, Liu CX, Ball WP. Study of sorption-retarded U(VI) diffusion in Hanford silt/clay material. Environmental Science & Technology 2009; 43: 7706-7711.
Baird C. Environmental Chemistry New York, W.H. Freeman and Company, 1999, 528.
Balnois E, Wilkinson KJ, Lead JR, Buffle J. Atomic force microscopy of humic substances: effects of pH and ionic strength. Environmental Science and Technology 1999; 33: 3911-3917.
Banasiak LJ. Removal of Inorganic and Trace Organic Contaminants by Electrodialysis. School of Engineering, The University of Edinburgh, 2009; PhD.
Banasiak LJ, Schäfer AI. Removal of inorganic trace contaminants by electrodialysis in a remote Australian community. Desalination 2009; 248: 48-57.
Bargar JR, Reitmeyer R, Davis JA. Spectroscopic confirmation of uranium(VI)-carbonato adsorption complexes on hematite. Environmental Science & Technology 1999; 33: 2481-2484.
Barker DJ, Stuckey DC. A review of soluble microbial products (SMP) in wastewater treatment systems. Water Research 1999; 33: 3063-3082.
Barnett MO, Jardine PM, Brooks SC, Selim HM. Adsorption and transport of uranium(VI) in subsurface media. Soil Science Society of America Journal 2000; 64: 908-917.
Bartels CR, Wilf M, Andes K, long J. Design considerations for wastewater treatment by reverse osmosis. Water Science and Technology 2005; 51: 473-482.
Bednar AJ, Medina VF, Ulmer-Scholle DS, Frey BA, Johnson BL, Brostoff WN, Larson SL. Effects of organic matter on the distribution of uranium in soil and plant matrices. Chemosphere 2007; 70: 237-247.
Bem H, Bou-Rabee F. Environmental and health consequences of depleted uranium use in the 1991 Gulf War. Environment International 2004; 30: 123.
Bernhard G, Geipel G, Brendler V, Nitsche H. Uranium speciation in waters of different uranium mining areas. Journal of Alloys and Compounds 1998; 271-273: 201-205.
Biehler D, Falck WE. Simulation of the effects of geochemical reactions on groundwater quality during planned flooding of the Konigstein uranium mine, Saxony, Germany. Hydrogeology Journal 1999; 7: 284-293.
Birke M, Rauch U, Lorenz H, Kringel R. Distribution of uranium in German bottled and tap water. Journal of Geochemical Exploration 2010; 107: 272-282.
Bissen M, Frimmel FH. Arsenic - a review - Part 1: Occurrence, toxicity, speciation, mobility. Acta Hydrochimica et Hydrobiologica 2003a; 31: 9-18.
Bissen M, Frimmel FH. Arsenic - a review -Part II: Oxidation of arsenic and its removal in water treatment. Acta Hydrochimica et Hydrobiologica 2003b; 31: 97-107.
Bourbonniere, Halderen V. Fractional precipitation of humic acid from coloured natural waters. Water, Air and Soil Pollution 1989; 46: 187-198.
Boussu K, Zhang Y, Cocquyt J, Van der Meeren P, Volodin A, Van Haesendonck C, Martens JA, Van der Bruggen B. Characterization of polymeric nanofiltration membranes for systematic analysis of membrane performance. Journal of Membrane Science 2006; 278: 418-427.
Bowen WR, Mohammad AW, Hilal N. Characterisation of nanofiltration membranes for predictive purposes - use of salts, uncharged solutes and atomic force microscopy. Journal of Membrane Science 1997; 126: 91-105.
Bowie SHU. Mode of occurrence and distribution of uranium deposits. Philosophical transactions of the Royal Society of London series a - Mathematical Physical and Engineering Sciences 1979; 291: 289-300.

Boyanov MI, O'Loughlin EJ, Roden EE, Fein JB, Kemner KM. Adsorption of Fe(II) and U(VI) to carboxyl-functionalized microspheres: the influence of speciation on uranyl reduction studied by titration and XAFS. Geochimica Et Cosmochimica Acta 2007; 71: 1898-1912.

Braghetta A, DiGiano FA, Ball WP. Nanofiltration of natural organic matter: pH and ionic strength effects. Journal of Environmental Engineering-Asce 1997; 123: 628-641.

Brandhuber P, Amy G. Arsenic removal by a charged ultrafiltration membrane-influences of membrane operating conditions and water quality on arsenic rejection. Desalination 2001; 140: 1-14.

British Geological Survey. 2000. Groundwater quality: Ghana. www.bgs.ac.uk/downloads/start.cfm?id=1281, 2009, November

Brown PL, Guerin M, Hankin SI, Lowson RT. Uranium and other contaminant migration in groundwater at a tropical Australian uranium mine. Journal of Contaminant Hydrology 1998; 35: 295-303.

Brugger J, Burns PC, Meisser N. Contribution to the mineralogy of acid drainage of uranium minerals: Marecottite and the zippeite-group. American Mineralogist 2003; 88: 676-685.

Bryan ND, Hesketh N, Livens FR, Tipping E, Jones MN. Metal ion-humic substance interaction - a thermodynamic study. Journal of the Chemical Society - Faraday Transactions 1998; 94: 95-100.

Buamah R, Petrusevski B, Schippers JC. Presence of arsenic, iron and manganese in groundwater within the gold-belt zone of Ghana. Journal of Water Supply Research and Technology-Aqua 2008; 57: 519-529.

Buck BJ, Brock AL, Johnson WH, Ulery AL. Corrosion of depleted uranium in an arid environment: Soil-geomorphology, SEM/EDS, XRD, and electron microprobe analyses. Soil & Sediment Contamination 2004; 13: 545-561.

Butcher SS, Charlson RJ, Orians GH, Wolfe GV. Global Biogeochemical Cycles. London, Academic Press Ltd., 1992.

Carvalho FP, Oliveira JM, Neves MO, Abreu MM, Vicente EM. Soil to plant (Solanum tuberosum L.) radionuclide transfer in the vicinity of an old uranium mine. Geochemistry-Exploration Environment Analysis 2009; 9: 275-278.

Catalano JG, McKinley JP, Zachara JM, Heald SM, Smith SC, Brown GE. Changes in uranium speciation through a depth sequence of contaminated Hanford sediments. Environmental Science and Technology 2006; 40: 2517-2524.

Celis R, Hermosin MC, Cornejo J. Heavy metal adsorption by functionalized clays. Environmental Science and Technology 2000; 34: 4593-4599.

Chakravarty S, Dureja V, Bhattacharyya G, Maity S, Bhattacharjee S. Removal of arsenic from groundwater using low cost ferruginous manganese ore. Water Research 2002; 36: 625-632.

Chellam S, Clifford DA. Physical-chemical treatment of groundwater contaminated by leachate from surface disposal of uranium tailings. Journal of Environmental Engineering-Asce 2002; 128: 942-952.

Chen JC, Li QL, Elimelech M. In situ monitoring techniques for concentration polarization and fouling phenomena in membrane filtration. Advances in Colloid and Interface Science 2004; 107: 83-108.

Chiew H, Sampson ML, Huch S, Ken S, Bostick BC. Effect of groundwater iron and phosphate on the efficacy of arsenic removal by iron-amended bioSand filters. Environmental Science & Technology 2009; 43: 6295-6300.

Childress AE, Elimelech M. Effect of solution chemistry on the surface charge of polymeric reverse osmosis and nanofiltration membranes Journal of Membrane Science 1996; 119: 253-268.

Chisholm-Brause CJ, Berg JM, Matzner RA, Morris DE. Uranium(VI) sorption complexes on montmorillonite as a function of solution chemistry. Journal of Colloid and Interface Science 2001; 233: 38-49.

Choppin GR. Actinide speciation in the environment. Journal of Radioanalytical and Nuclear Chemistry 2007; 273: 695-703.

Choy CC, Korfiatis GP, Meng XG. Removal of depleted uranium from contaminated soils. Journal of Hazardous Materials 2006; 136: 53-60.

Coates J. Interpretation of Infrared Spectra, A Practical Approach. In: Encyclopedia of Analytical Chemistry. Ed: Meyers RA. John Wiley & Sons Ltd, Chichester, 2000, pp. 10815-10837.

Coffey M. Renewable energy: Filtration and the green energy revolution. Filtration and Separation 2008; 45: 24-27.

Coronell O, Gonzalez MI, Marinas BJ, Cahill DG. Ionization behavior, stoichiometry of association, and accessibility of functional groups in the active layers of reverse osmosis and nanofiltration membranes. Environmental Science & Technology 2010; 44: 6808-6814.

Craft ES, Abu-Qare AW, Flaherty MM, Garofolo MC, Rincavage HL, Abou-Donia MB. Depleted and natural uranium: chemistry and toxicological effects. Journal of Toxicology and Environmental Health-Part B-Critical Reviews 2004; 7: 297-317.

Curti E. Coprecipitation of radionuclides with calcite: estimation of partition coefficients based on a review of laboratory investigations and geochemical data. Applied Geochemistry 1999; 14: 433-445.

CWSA. Summary of the fluoride issues in the northern region, 2007.

Cyna B, Chagneau G, Bablon G, Tanghe N. Two years of nanofiltration at the Mery-sur-Oise plant, France. Desalination 2002; 147: 69-75.

Dampare SB, Nyarko BJB, Osae S, Akaho EHK, Asiedu DK, Serfor-Armah Y, Nude P. Simultaneous determination of tantalum, niobium, thorium and uranium in placer columbite-tantalite deposits from the Akim Oda District of Ghana by epithermal instrumental neutron activation analysis. Journal of Radioanalytical and Nuclear Chemistry 2005; 265: 53-59.

Davis JA, Meece DE, Kohler M, Curtis GP. Approaches to surface complexation modeling of uranium(VI) adsorption on aquifer sediments. Geochimica Et Cosmochimica Acta 2004; 68: 3621-3641.

Davis TA, Llanes F, Volesky B, Mucci A. Metal selectivity of Sargassum spp. and their alginates in relation to their a-L-guluronic acid content and conformation. Environmental Science and Technology 2003a; 37: 261-267.

Davis TA, Volesky B, Mucci A. A review of the biochemistry of heavy metal biosorption by brown algae. Water Research 2003b; 37: 4311-4330.

de la Rosa G, Peralta-Videa JR, Gardea-Torresdey JL. Utilization of ICP/OES for the determination of trace metal binding to different humic fractions. Journal of Hazardous Materials 2003; 97: 207-218.

De Munari A, Schäfer AI. Impact of speciation on removal of manganese and organic matter by nanofiltration. Journal of Water Supply Research and Technology-Aqua 2010a; 59: 152-163.

De Munari A, Schäfer AI. Membrane plants for drinking water provision in remote Scottish communities: performance, costs and lessons learnt. Membranes in Drinking and Industrial Water, Trondheim, Norway, 2010b.

Deon S, Dutournie P, Bourseau P. Transfer of monovalent salts through nanofiltration membranes: a model combining transport through pores and the polarization layer. Industrial & Engineering Chemistry Research 2007; 46: 6752-6761.

Domingo JL, Ortega A, Llobet JM, Corbella J. Effectiveness of chelation-therapy with time after acute uranium intoxication. Fundamental and Applied Toxicology 1990; 14: 88-95.

Dong WM, Xie GB, Miller TR, Franklin MP, Oxenberg TP, Bouwer EJ, Ball WP, Halden RU. Sorption and bioreduction of hexavalent uranium at a military facility by the Chesapeake Bay. Environmental Pollution 2006; 142: 132-142.

Dow Product Information. FILMTEC Membranes FILMTEC Fiberglassed Elements for Light Industrial Systems.; http://www.dow.com/PublishedLiterature/dh_0109/0901b80380109c07.pdf?filepath=liquidseps/pdfs/noreg/609-00350.pdf&fromPage=GetDoc, 29 January 2009

Dow Product Information. FILMTEC Membranes FILMTEC NF90 Nanofiltration Elements for Commercial Systems.;

http://www.dow.com/PublishedLiterature/dh_0074/0901b803800749de.pdf?filepath =liquidseps/pdfs/noreg/609-00378.pdf&fromPage=GetDoc, 29 January 2009

Draget KI, Smidsrød O, Skjåk-Bræk G. Alginates from algae. In: Biopolymers; Polysaccharides II: Polysaccharides from Eucaryotes. 6. Ed: De Baets S, Vandamme E, Steinbüchel A. Whiley-VCH Verlag, Weinheim, Germany, 2002, pp. 215-244.

Duff MC, Amrhein C. Uranium(VI) adsorption on goethite and soil in carbonate solutions. Soil Science Society of America Journal 1996; 60: 1393-1400.

Duff MC, Amrhein C, Bertsch PM, Hunter DB. The chemistry of uranium in evaporation pond sediment in the San Joaquin Valley, California, USA, using X-ray fluorescence and XANES techniques. Geochimica Et Cosmochimica Acta 1997; 61: 73-81.

Duff MC, Coughlin JU, Hunter DB. Uranium co-precipitation with iron oxide minerals. Geochimica Et Cosmochimica Acta 2002; 66: 3533-3547.

Elizalde-Gonzalez MP, Mattusch J, Einicke WD, Wennrich R. Sorption on natural solids for arsenic removal. Chemical Engineering Journal 2001; 81: 187-195.

Elless MP, Lee SY. Uranium solubility of carbonate-rich uranium-contaminated soils. Water, Air and Soil Pollution 1998; 107: 147-162.

Elzinga EJ, Tait CD, Reeder RJ, Rector KD, Donohoe RJ, Morris DE. Spectroscopic investigation of U(VI) sorption at the calcite-water interface. Geochimica Et Cosmochimica Acta 2004; 68: 2437-2448.

Fatin-Rouge N, Dupont A, Vidonne A, Dejeu J, Fievet P, Foissy A. Removal of some divalent cations from water by membrane-filtration assisted with alginate. Water Research 2006; 40: 1303-1309.

Favre-Reguillon A, Lebuzit G, Foos J, Guy A, Draye M, Lemaire M. Selective concentration of uranium from seawater by nanofiltration. Industrial and Engineering Chemistry Research 2003; 42: 5900-5904.

Favre-Reguillon A, Lebuzit G, Murat D, Foos J, Mansour C, Draye M. Selective removal of dissolved uranium in drinking water by nanofiltration. Water Research 2008; 42: 1160-6.

Ford RG, Scheinost AC, Sparks DL. Frontiers in metal sorption/precipitation mechanisms on soil mineral surfaces. Advances in Agronomy, Vol 74 2001; 74: 41-62.

Fox PM, Davis JA, Zachara JM. The effect of calcium on aqueous uranium(VI) speciation and adsorption to ferrihydrite and quartz. Geochimica Et Cosmochimica Acta 2006; 70: 1379-1387.

Freger V. Nanoscale heterogeneity of polyamide membranes formed by interfacial polymerization. Langmuir 2003; 19: 4791-4797.

Fuller CC, Bargar JR, Davis JA. Molecular-scale characterization of uranium sorption by bone apatite materials for a permeable reactive barrier demonstration. Environmental Science & Technology 2003; 37: 4642-4649.

Geipel G, Reich T, Brendler V, Bernhard G, Nitsche H. Laser and X-ray spectroscopic studies of uranium-calcite interface phenomena. Journal of Nuclear Materials 1997; 248: 408-411.

Gekas V, Hallström B. Mass transfer in the membrane concentration polarization layer under turbulent cross flow : I. Critical literature review and adaptation of existing sherwood correlations to membrane operations. Journal of Membrane Science 1987; 30: 153-170.

Geraldes V, Afonso MD. Prediction of the concentration polarization in the nanofiltration/reverse osmosis of dilute multi-ionic solutions. Journal of Membrane Science 2007; 300: 20-27.

Ghizellaoui S, Euvrard M. Assessing the effect of zinc on the crystallization of calcium carbonate. Desalination 2008; 220: 394-402.

Ghosh K, Schnitzer M. Macromolecular structures of humic substances. Soil Science 1980; 129: 266-276.

Giblin AM, Batts BD, Swaine DJ. Laboratory simulation studies of uranium mobility in natural waters. Geochimica Et Cosmochimica Acta 1981; 45: 699-709.

Gill HE. A groundwater reconnaissance of the Republic of Ghana, with description of geohydrolic provinces. U.S. Geological Survey Water Supply Paper 1996; 1757-k.
Godelitsas A, Misaelides P, Filippidis A, Charistos D, Anousis I. Uranium sorption from aqueous solutions on sodium-form of HEU-type zeolite crystals. Journal of Radioanalytical and Nuclear Chemistry-Articles 1996; 208: 393-402.
Golow AA, Schlueter A, AmihereMensah S, Granson HLK, Tetteh MS. Distribution of arsenic and sulphate in the vicinity of Ashanti Goldmine at Obuasi, Ghana. Bulletin of Environmental Contamination and Toxicology 1996; 56: 703-710.
Gomez P, Garralon A, Buil B, Turrero MJ, Sanchez L, De la Cruz B. Modeling of geochemical processes related to uranium mobilization in the groundwater of a uranium mine (vol 300, pg 295, 2000). Science of the Total Environment 2008; 390: 579-579.
Gorman-Lewis D, Burns PC, Fein JB. Review of uranyl mineral solubility measurements. Journal of Chemical Thermodynamics 2008; 40: 335-352.
Government of Ghana, National Water Policy, 2007, 70
Graham MC, Oliver IW, MacKenzie AB, Ellam RM, Farmer JG. An integrated colloid fractionation approach applied to the characterisation of porewater uranium-humic interactions at a depleted uranium contaminated site. Science of the Total Environment 2008; 404: 207-217.
Graham MC, Oliver IW, MacKenzie AB, Ellam RM, Farmer JG. Mechanisms controlling lateral and vertical porewater migration of depleted uranium (DU) at two UK weapons testing sites. Science of the Total Environment 2011; 409: 1854-1866.
Granit J, Jägerskog A, Löfgren R, Bullock A, de Gooijer G, Pettigrew S, Lindström A. Regional Water Intelligence Report Central Asia. Stockholm, Stockholm International Water Institute, 2010, 31.
Greenlee LF, Testa F, Lawler DF, Freeman BD, Moulin P. The effect of antiscalant addition on calcium carbonate precipitation for a simplified synthetic brackish water reverse osmosis concentrate. Water Research 2010; 44: 2957-2969.
Grenthe I, Fuger J, Konings RJM, Lemire R, J., Muller AB, Nguyen-Trung Cregu C, Wanner H. Chemical thermodynamics of uranium. Paris, OECD - Nuclear Energy Agency, 1992.
Guillaumont R, Fanghanel T, Fuger J. Update on the chemical thermodynamics of uranium, neptunium, plutonium, americium and technetium, OECD, 2003.
Guo LD, Warnken KW, Santschi PH. Retention behavior of dissolved uranium during ultrafiltration: Implications for colloidal U in surface waters. Marine Chemistry 2007; 107: 156-166.
Gustafsson JP, van Schaik JWJ. Cation binding in a mor layer: batch experiments and modelling. European Journal of Soil Science 2003; 54: 295-310.
Gyau-Boakye P, Dapaah-Siakwan S. Groundwater: solution to Ghana's rural water supply industry? the Ghana Engineer 1999; May.
Hakonson-Hayes AC, Fresquez PR, Whicker FW. Assessing potential risks from exposure to natural uranium in well water. Journal of Environmental Radioactivity 2002; 59: 29-40.
Haslam E. Chemistry of vegetable tannins. London and New York, Academic Press 1966.
Hilal N, Al-Abri M, Al-Hinai H, Abu-Arabi M. Characterization and retention of NF membranes using PEG, HS and polyelectrolytes. Desalination 2008; 221: 284-293.
Hoque BA, Hoque MM, Ahmed T, Islam S, Azad AK, Ali N, Hossain M, Hossain MS. Demand-based water options for arsenic mitigation: an experience from rural Bangladesh. Public Health 2004; 118: 70-77.
Hsiue G-H, Pung L-S, Chu M-L, Shieh M-C. Treatment of uranium effluent by reverse osmosis membrane. Desalination 1989; 71: 35-44.
Huikuiri P, Salonen L, Raff O. Removal of natural radionuclides from drinking water by point entry reverse osmosis. Desalination 1998; 119: 235-239.
Huikuri P, Salonen L, Raff O. Removal of natural radionuclides from drinking water by point of entry reverse osmosis. Desalination 1998; 119: 235-239.

Hunter PR. Household water treatment in developing countries: comparing different intervention types using meta-regression. Environmental Science and Technology 2009; 43: 8991-8997.

Hunter PR, MacDonald AM, Carter RC. Water supply and health. PLoS Medicine 2011; 7.

Hunter PR, Zmirou-Navier D, Hartemann P. Estimating the impact on health of poor reliability of drinking water interventions in developing countries. Science of the Total Environment 2009; 407: 2621-2624.

Hydranautics. Membrane Element ESPA4-4040.; http://www.membranes.com/docs/4inch/ESPA4-4040.pdf, 29 January 2009

Hyun SP, Fox PM, Davis JA, Campbell KM, Hayes KF, Long PE. Surface complexation modeling of U(VI) adsorption by aquifer sediments from a former mill tailings site at rifle, Colorado. Environmental Science & Technology 2009; 43: 9368-9373.

Iten S, McCarron P. Buried in Boreholes. Department of Environment, Technology and Social Studies, Roskilde University, Denmark, 2006; M.Sc. Technological and Socio-Economic Planning: 306.

Jarusutthirak C, Mattaraj S, Jiraratananon R. Influence of inorganic scalants and natural organic matter on nanofiltration membrane fouling. Journal of Membrane Science 2007; 287: 138-145.

Jermann D, Pronk W, Boller M, Schäfer AI. The role of NOM fouling for the retention of estradiol and ibuprofen during ultrafiltration. Journal of Membrane Science 2009; 329: 75-84.

Jermann D, Pronk W, Meylan S, Boller M. Interplay of different NOM fouling mechanisms during ultrafiltration for drinking water production. Water Research 2007; 41: 1713-1722.

Jia GG, Belli M, Sansone U, Rosamilia S, Gaudino S. Concentration and characteristics of depleted uranium in biological and water samples collected in Bosnia and Herzegovina. Journal of Environmental Radioactivity 2006; 89: 172-187.

JMP. Progress on drinking water and sanitation: special focus on sanitation WHO, Geneva and UNICEF, New York, World Health Organisation and United Nations Children's Fund Joint Monitoring Programme for Water Supply and Sanitation (JMP), 2008.

JMP. Progress on Sanitation and Drinking-Water: 2010 Update. WHO, Geneva and UNICEF, New York, WHO/UNICEF Joint Monitoring Programme for Water Supply and Sanitation, 2010.

Johnston R, Heijnen H. Safe water technology for arsenic removal. International workshop on technologies for arsenic removal from drinking water, Bangladesh University of Engineering and Technology, Dhaka, India, 2001.

Kang MJ, Han BE and Hahn PS. Precipitation and adsorption of uranium(VI) under various aqueous conditions. Environmental Engineering Research 2002; 7: 149-157

Kantar C. Heterogeneous processes affecting metal ion transport in the presence of organic ligands: Reactive transport modeling. Earth-Science Reviews 2007; 81: 175-198.

Kara Y. Bioaccumulation of Cu, Zn and Ni from wastewater by treated Nasturtium officinale. International Journal of Enivironmental Science and Technology 2005; 2: 63-67.

Kelly SD, Kemner KM, Brooks SC. X-ray absorption spectroscopy identifies calcium-uranyl-carbonate complexes at environmental concentrations. Geochimica Et Cosmochimica Acta 2007; 71: 821-834.

Keskinkan O, Goksu MZL, Basibuyuk M, Forster CF. Heavy metal adsorption properties of a submerged aquatic plant (Ceratophyllum demersum). Bioresource Technology 2004; 92: 197-200.

Khani MH, Keshtkar AR, Ghannadi M, Pahlavanzadeh H. Equilibrium, kinetic and thermodynamic study of the biosorption of uranium onto Cystoseria indica algae. Journal of Hazardous Materials 2008; 150: 612-618.

Khani MH, Keshtkar AR, Meysami B, Zarea MF, Jalali R. Biosorption of uranium from aqueous solutions bynonliving biomass of marinealgae Cystoseira indica. Electronic Journal of Biotechnology 2006; 9: 100-106.

Koch Membrane Systems. Fluid Systems TFC-S 8" Element.; http://www.pure-aqua.com/pdf_brands/Koch%20TFC-S%208.pdf, 29 January 2009

Konstantinou M, Pashalidis I. Speciation and spectrophotometric determination of uranium in seawater. Mediterranean Marine Science 2004; 5: 55-60.

Kortatsi BK. Groundwater utilization in Ghana. Future Groundwater Resources at Risk 1994: 149-156.

Kortatsi BK. Hydrochemical characterization of groundwater in the Accra plains of Ghana. Environmental Geology 2006; 50: 299-311.

Kortatsi BK, Anku YSA, Anornu GK. Characterization and appraisal of facets influencing geochemistry of groundwater in the Kulpawn sub-basin of the White Volta Basin, Ghana. Environmental Geology 2009; 58: 1349-1359.

Kortatsi BK, Asigbe J, Dartey GA, Tay CK, Anornu G, Hayford E. Reconnaissance survey of arsenic concentration in groundwater in south-eastern Ghana. West African Journal of Applied Ecology 2008a; 13.

Kortatsi BK, Tay CK, Anornu G, Hayford E, Dartey GA. Hydrogeochemical evaluation of groundwater in the lower Offin basin, Ghana. Environmental Geology 2008b; 53: 1651-1662.

Kryvoruchko AP, Atamanenko ID. The effect of dispersed materials on baromembrane treatment of uranium-containing waters. Desalination 2007; 204: 307-315.

Kryvoruchko AP, Yu L, Atamanenko ID, Kornilovich BY. Ultrafiltration removal of U(VI) from contaminated water. Desalination 2004; 162: 229-236.

Kumar M, Singh S, Mahajan R. Trace level determination of U, Zn, Cd, Pb and Cu in drinking water samples. Environmental Monitoring and Assessment 2006; 112: 283-292.

Kurttio P, Auvinen A, Salonen L, Saha H, Pekkanen J, Makelainen I, Vaisanen SB, Penttila IM, Komulainen H. Renal effects of uranium in drinking water. Environmental Health Perspectives 2002; 110: 337-342.

Kurttio P, Harmoinen A, Saha H, Salonen L, Karpas Z, Komulainen H, Auvinen A. Kidney toxicity of ingested uranium from drinking water. American Journal of Kidney Diseases 2006; 47: 972-982.

Kurttio P, Komulainen H, Leino A, Salonen L, Auvinen A, Saha H. Bone as a possible target of chemical toxicity of natural uranium in drinking water. Environmental Health Perspectives 2005; 113: 68-72.

Langmuir D. Aqueous Environmental Geochemistry. Upper Saddle River, Prentice Hall, 1997, 600.

Lee S, Cho J, Elimelech M. Influence of colloidal fouling and feed water recovery on salt rejection of RO and NF membranes. Desalination 2004; 160: 1-12.

Lee S, Elimelech M. Relating organic fouling of reverse osmosis membranes to intermolecular adhesion forces. Environmental Science & Technology 2006a; 40: 980-987.

Lee S, Elimelech M. Relating organic fouling of reverse osmosis membranes to intermolecular adhesion forces. Environmental Science and Technology 2006b; 40: 980-987.

Lenhart JJ, Honeyman BD. Uranium(VI) sorption to hematite in the presence of humic acid. Geochimica Et Cosmochimica Acta 1999; 63: 2891-2901.

Li WC, Victor DM, Chakrabarti CL. Effect of pH and uranium concentration on interaction of uranium(VI) and uranium(IV) with organic-ligands in aqueous-solutions. Journal of Analytical Chemistry 1980; 52: 520-523.

MacDonald A, Davies J, Calow R, Chilton J. Developing Groundwater - A guide for rural water supply, ITDG Publishing, UK, 2005.

MacDonald AM, Calow RC. Developing groundwater for secure rural water supplies in Africa. Desalination 2009; 248: 546-556.

Majumdar D, Roszak S, Balasubramanian K, Nitsche H. Theoretical study of aqueous uranyl carbonate (UO2CO3) and its hydrated complexes: UO2CO3•nH2O (n=1-3). Chemical Physics Letters 2003; 372: 232-241.

Makkar HPS, Becker K. Effect of pH, temperature, and time on inactivation of tannins and possible implications in detannification studies. Journal of Agricultural and Food Chemistry 1996; 44: 1291-1295.

Malik AH, Khan ZM, Mahmood Q, Nasreen S, Bhatti ZA. Perspectives of low cost arsenic remediation of drinking water in Pakistan and other countries. Journal of Hazardous Materials 2009; 168: 1-12.

Manassaram DM, Backer LC, Moll DM. A review of nitrates in drinking water: maternal exposure and adverse reproductive and developmental outcomes. Environmental Health Perspectives 2006; 114: 320-327.

Mason CF. Biological Aspects of Freshwater Pollution. In: Pollution: Causes, Effects and Control. Ed: Harrison RM. The Royal Society of Chemistry, Cambridge, 1990, pp. 108-111.

McGinnis RL, Elimelech M. Global challenges in energy and water supply: the promise of engineered osmosis. Environmental Science and Technology 2008; 42: 8625-8629.

Mead MN. Arsenic: In search of an antidote to a global poison. Environmental Health Perspectives 2005; 113: A378-A386.

Miller AC, Brooks K, Smith J, Page N. Effect of the militarily-relevant heavy metals, depleted uranium and heavy metal tungsten-alloy on gene expression in human liver carcinoma cells (HepG2). Molecular and Cellular Biochemistry 2004; 255: 247-256.

Montgomery MA, Bartram J, Elimelech M. Increasing functional sustainability of water and sanitation supplies in rural sub-saharan Africa. Environmental Engineering Science 2009; 26: 1017-1023.

Mueller-Harvey I. Analysis of hydrolysable tannins. Animal Feed Science and Technology 2001; 91: 3-20.

Mulder M. Basic Principles of Membrane Technology, Kluwer Academic Publishers, 1996, 564.

Mulder MHV, van Voorthuizen EM, Peeters JMM. Membrane Characterisation. In: Nanofiltration: Principles and Applications. Ed: Schäfer AI, Fane A.G., Waite, D.T. . Elsevier Advanced Technology, Oxford, 2005, pp. 90-117.

Murphy JR, Lenhart JJ, Honeyman BD. The sorption of thorium (IV) and uranium (VI) to hematite in the presence of natural organic matter. Colloids and Surfaces A: Physicochemical and Engineering Aspects 1992; 157: 47-62.

Murphy RJ, Lenhart JJ, Honeyman BD. The sorption of thorium (IV) and uranium (VI) to hematite in the presence of natural organic matter. Colloids and Surfaces a-Physicochemical and Engineering Aspects 1999; 157: 47-62.

Myasoedov BF, Novikov AP. Main sources of radioactive contamination in Russia and methods for their determination and speciation. Journal of Radioanalytical and Nuclear Chemistry 1998; 229: 33-38.

Nakamoto K. Infrared and raman spectra of inorganic and coordination compounds. Part B: Applications in coordination, organometallic and bioinorganic chemistry. NY, John Wiley and sons, Inc., 1997, 384.

Naylor R. Ghana, An Oxfam Country Profile. Oxford, Oxfam, 2003.

Neale PA. Influence of Solute-Solute Interactions on Membrane Filtration. School of Engineering, The University of Edinburgh, 2009; PhD.

Nghiem LD. Removal of Emerging Trace Organic Contaminants by Nanofiltration and Reverse Osmosis. Faculty of Engineering, The University of Wollongong, 2005; PhD.

Nghiem LD, Schäfer AI, Elimelech M. Removal of natural hormones by nanofiltration membranes: Measurement, modeling, and mechanisms. Environmental Science & Technology 2004; 38: 1888-1896.

Nilsson M, Trägårdh G and Östergren K. The influence of sodium chloride on mass transfer in a polyamide nanofiltration membrane at elevated temperatures. Journal of Membrane Science 2006; 280: 928-936.

Nordstrom DK. Public health - worldwide occurrences of arsenic in ground water. Science 2002; 296: 2143-2145.

Nyarko KB, Awuah E, Ofori D. Local initiative in community water supply: case study in Ashanti Region, Ghana. Desalination 2009; 248: 650-657.

Nyarko KB, Oduro-Kwarteng S, Adama I. Cost recovery of community-managed piped water systems in Ashanti region, Ghana. Water and Environment Journal 2007; 21: 92-99.

Nyström M, Butylina S, Platt S. NF retention and critical flux of small hydrophilic/hydrophobic molecules. Membrane Technology 2004; 2004: 5-8.

Nyström M, Kaipia L, Luque S. Fouling and retention of nanofiltration membranes. Journal of Membrane Science 1995; 98: 249-262.

Obiri S, Dodoo DK, Okai-Sam F, Essumang DK. Cancer health risk assessment of exposure to arsenic by workers of AngloGold Ashanti-Obuasi gold mine. Bulletin of Environmental Contamination and Toxicology 2006; 76: 195-201.

Oh JI, Yamamoto K, Kitawaki H, Nakao S, Sugawara T, Rahman MM, Rahman MH. Application of low-pressure nanofiltration coupled with a bicycle pump for the treatment of arsenic-contaminated groundwater. Desalination 2000; 132: 307-314.

Oliver IW, Graham MC, MacKenzie AB, Ellam RM, Farmer JG. Assessing depleted uranium (DU) contamination of soil, plants and earthworms at UK weapons testing sites. Journal of Environmental Monitoring 2007; 9: 740-748.

Oliver IW, Graham MC, MacKenzie AB, Ellam RM, Farmer JG. Distribution and partitioning of depleted uranium (DU) in soils at weapons test ranges - investigations combining the BCR extraction scheme and isotopic analysis. Chemosphere 2008; 72: 932-939.

Orloff KG, Mistry K, Charp P, Metcalf S, Marino R, Shelly T, Melaro E, Donohoe AM, Jones RL. Human exposure to uranium in groundwater. Environmental Research 2004; 94: 319-326.

Ortiz JM, Exposito E, Gallud F, Garcia-Garcia V, Montiel V, Aldaz A. Desalination of underground brackish waters using an electrodialysis system powered directly by photovoltaic energy. Solar Energy Materials and Solar Cells 2008; 92: 1677-1688.

Pabalan RT, Turner DR. Uranium(6+) sorption on montmorillonite: experimental and surface complexation modeling study. Aquatic Geochemistry 1997; 2: 203-226.

Packham RF. Water Quality and Health. In: Pollution: Causes, Effects and Control. Ed: Harrison RM. The Royal Society of Chemistry, Cambridge, 1990, pp. 83-97.

Park GL, Schäfer AI and Richards BS. Renewable energy powered membrane technology: The effect of wind speed fluctuations on the performance of a wind-powered membrane system for brackish water desalination. Journal of Membrane Science 2011; 370: 34-44.

Payne TE. Uranium (VI) interactions with mineral surfaces: controlling factors and surface complexation modelling. School of Civil and Environmental Engineering, University of New South Wales, 1999; PhD.

Payne TE, Airey PL. Radionuclide migration at the Koongarra uranium deposit, Northern Australia - Lessons from the Alligator Rivers analogue project. Physics and Chemistry of the Earth 2006; 31: 572-586.

Payne TE, Davis JA, Lumpkin GR, Chisari R, Waite TD. Surface complexation model of uranyl sorption on Georgia kaolinite. Applied Clay Science 2004; 26: 151-162.

Payne TE, Davis JA, Waite TD. Uranium adsorption on ferrihydrate – effects of phosphate and humic acid. Radiochimica Acta 1996; 74: 239-243.

Payne TE, Edis R, Fenton BR, Waite TD. Comparison of laboratory uranium sorption data with 'in situ distribution coefficients' at the Koongarra uranium deposit, Northern Australia. Journal of Environmental Radioactivity 2001; 57: 35-55.

Payne TE, Waite TD. Surface complexation modelling of uranium sorption data obtained by isotope exchange techniques. Radiochimica Acta 1991; 52/53: 487-493.

Pelig-Ba KB. Trace elements in groundwater from some crystalline rocks in the Upper Regions of Ghana. Water, Air and Soil Pollution 1998; 103: 71-89.

Pelig-Ba KB, Biney CA, Antwi LA. Trace-metal concentrations in borehole waters from the Upper Regions and the Accra Plains of Ghana. Water, Air and Soil Pollution 1991; 59: 333-345.

Pelig-Ba KB, Parker A, Price M. Elemental contamination of rainwater by airborne dust in Tamale Township area of the northern region of Ghana. Environmental Geochemistry and Health 2001; 23: 333-346.

Pelig-Ba KB, Parker A, Price M. Trace element geochemistry from the Birrimian metasediments of the Northern Region of Ghana. Water, Air and Soil Pollution 2004; 153: 69-93.

Peter-Varbanets M, Zurbruegg C, Swartz C, Pronk W. Decentralized systems for potable water and the potential of membrane technology. Water Research 2009; 43: 245-265.

Pirlo MC, Giblin AM. Application of groundwater-mineral equilibrium calculations to geochemical exploration for sediment-hosted uranium: observations from the Frome Embayment, South Australia. Geochemistry-Exploration Environment Analysis 2004; 4: 113-127.

Plant J, Smith D, Smith B, Williams L. Environmental geochemistry at the global scale. Applied Geochemistry 2001; 16: 1291-1308.

Plant JA, Reeder S, Salminen R, Smith DB, Tarvainen T, De Vivo B, Petterson MG. The distribution of uranium over Europe: geological and environmental significance. Transactions of the Institution of Mining and Metallurgy Section B-Applied Earth Science 2003; 112: B221-B238.

Pompe S, Schmeide K, Bubner M, Geipel G, Heise KH, Bernhard G, Nitsche H. Investigation of humic acid complexation behavior with uranyl ions using modified synthetic and natural humic acids. Radiochimica Acta 2000; 88: 553-558.

Porcelli N, Judd S. Chemical cleaning of potable water membranes: a review. Separation and Purification Technology 2010; 71: 137-143.

Potts DE, Ahlert RC, Wang SS. A critical review of fouling of reverse-osmosis membranes. Desalination 1981; 36: 235-264.

Pramauro E, Prevot AB, Zelano V, Gulmini M, Viscardi G. Selective recovery of uranium(VI) from aqueous acid solutions using micellar ultrafiltration. Analyst 1996; 121: 1401-1405.

Prikryl JD, Jain A, Turner DR, Pabalan RT. Uranium(VI) sorption behavior on silicate mineral mixtures. Journal of Contaminant Hydrology 2001; 47: 241-253.

Prudden AR, Lien NR, Telford JR. An outer-sphere ligand for uranyl carbonate. Chemical Communications 2004: 172-173.

Raff O, Wilken RD. Removal of dissolved uranium by nanofiltration. Desalination 1999; 122: 147-150.

Rahardianto A, Gao JB, Gabelich CJ, Williams MD, Cohen Y. High recovery membrane desalting of low-salinity brackish water: integration of accelerated precipitation softening with membrane RO. Journal of Membrane Science 2007; 289: 123-137.

Raymond-Whish S, Mayer LP, O'Neal T, Martinez A, Sellers MA, Christian PJ, Marion SL, Begay C, Propper CR, Hoyer PB, Dyer CA. Drinking water with uranium below the US EPA water standard causes estrogen receptor-dependent responses in female mice. Environmental Health Perspectives 2007; 115: 1711-1716.

Reeder RJ, Elzinga EJ, Tait CD, Rector KD, Donohoe RJ, Morris DE. Site-specific incorporation of uranyl carbonate species at the calcite surface. Geochimica Et Cosmochimica Acta 2004; 68: 4799-4808.

Reiller P, Lemordant D, Hafiane A, Moulin C, Beaucaire C. Extraction and release of metal ions by micellar-enhanced ultrafiltration: Influence of complexation and pH. Journal of Colloid and Interface Science 1996; 177: 519-527.

Reimann C, Bjorvatn K, Frengstad B, Melaku Z, Tekle-Haimanot R, Siewers U. Drinking water quality in the Ethiopian section of the East African Rift Valley I - data and health aspects. Science of the Total Environment 2003; 311: 65-80.

Richards BS, Capão DPS, Schäfer AI. Renewable energy powered membrane technology. 2. The effect of energy fluctuations on performance of a photovoltaic hybrid membrane system. Environmental Science and Technology 2008; 42: 4563-4569.

Richards LA, Richards BS, Schäfer AI. Renewable energy powered membrane technology: salt and inorganic contaminant removal by nanofiltration/reverse osmosis. Journal of Membrane Science 2011; 369: 188-195.

Roach JD, Zapien JH. Inorganic ligand-modified, colloid-enhanced ultrafiltration: a novel method for removing uranium from aqueous solution. Water Research 2009; 43: 4751-4759.

Ross ARS, Ikonomou MG, Orians KJ. Characterization of dissolved tannins and their metal-ion complexes by electrospray ionization mass spectrometry. Analytica Chimica Acta 2000; 411: 91-102.

Rossiter HMA, Graham MC, Schäfer AI. Impact of speciation on behaviour of uranium in a solar powered membrane system for treatment of brackish groundwater. Separation and Purification Technology 2010a; 71: 89-96.

Rossiter HMA, Owusu PA, Awuah E, Macdonald AM, Schäfer AI. Chemical drinking water quality in Ghana: water costs and scope for advanced treatment. Science of the Total Environment 2010b; 408: 2378-86.

Salunkhe DK, Chavan JK, Kadam SS. Dietary tannins: consequences and remedies. Boca Raton, CRC Press, 1990.

Sanli O, Asman G. Removal of Fe (III) ions from dilute aqueous solutions by alginic acid-enhanced ultrafiltration. Journal of Applied Polymer Science 2000; 77: 1096-1101.

Schaep J, Van der Bruggen B, Vandecasteele C, Wilms D. Influence of ion size and charge in nanofiltration. Separation and Purification Technology 1998; 14: 155-162.

Schäfer AI. Natural Organics Removal using Membranes: Principles, Performance and Cost. Lancaster, USA, Technomic Publishing Company, 2001, 406.

Schäfer AI, Akanyeti I, Semião AJC. Micropollutant sorption to membrane polymers: a review of mechanisms for estrogens. Advances in Colloid and Interface Science 2011; 164: 100-117.

Schäfer AI, Broeckmann A, Richards BS. Renewable energy powered membrane technology 1. development and characterisation of a photovoltaic hybrid membrane system. Environmental Science and Technology 2007; 41: 998-1003.

Schäfer AI, Fane AG, Waite TD. Nanofiltration of natural organic matter: removal, fouling and the influence of multivalent ions. Desalination 1998; 118: 109-122.

Schäfer AI, Fane AG, Waite TD. Nanofiltration – Principles and Applications, Elsevier, 2005.

Schäfer AI, Richards BS. Testing of a hybrid membrane system for groundwater desalination in an Australian national park. Desalination 2005; 183: 55-62.

Schlosser F, Krüger S, Rösch N. A density functional study of uranyl monocarboxylates. Inorganic Chemistry 2006; 45: 1480-1490.

Schlosser F, Moskaleva LV, Kremleva A, Krüger S, Rösch N. Comparative density functional study of the complexes [UO2(CO3)3]4- and [(UO2)3(CO3)6]6- in aqueous solution. Dalton Trans 2010; 39: 5705-12.

Schmeide K, Sachs S, Bubner M, Reich T, Heise KH, Bernhard G. Interaction of uranium(VI) with various modified and unmodified natural and synthetic humic substances studied by EXAFS and FTIR spectroscopy. Inorganica Chimica Acta 2003; 351: 133-140.

Schmidt W-P, Cairncross S. Household water treatment in poor populations: is there enough evidence for scaling up now? Environmental Science and Technology 2009; 43: 986-992.

Schulten HR. A chemical structure for humic acid. Pyrolysis gas chromatography/mass spectrometry and pyrolysis-soft ionization mass spectrometry evidence. In: Humic substances in the global environment and implications on human health. Ed: Senesi N, Miano TM. Elsevier, Amsterdam, 1994, pp. 43-56.

Schulten HR, Schnitzer N. A state of the art structural concept for humic substances. Naturwissenschaften 1993; 80: 29-30.

Schwab AP, Zhu DS, Banks MK. Influence of organic acids on the transport of heavy metals in soil. Chemosphere 2008; 72: 986-994.

Seidel A, Elimelech M. Coupling between chemical and physical interactions in natural organic matter (NOM) fouling of nanofiltration membranes: implications for fouling control. Journal of Membrane Science 2002; 203: 245-255.

Seldén AI, Lundholm C, Edlund B, Högdahl C, Ek BM, Bergström BE, Ohlson CG. Nephrotoxicity of uranium in drinking water from private drilled wells. Environmental Research 2009; 109: 486-494.

Semião AJC. Removal of Adsorbing Estrogenic Micropollutants by Nanofiltration Membranes in Cross-flow Experiments and Modelling. Institute of Infrastructure of Environment, the University of Edinburgh, 2011; PhD.

Semião AJC, Rossiter HMA, Schäfer AI. Impact of organic matter and speciation on the behaviour of uranium in submerged ultrafiltration. Journal of Membrane Science 2010; 348: 174-180.

Service RF. Desalination freshens up. Science 2006; 313: 1088-1090.

Sheikholeslami R. Assessment of the scaling potential for sparingly soluble salts in RO and NF units. Desalination 2004; 167: 247-256.

Shin H-S, Monsallier JM, Choppin GR. Spectroscopic and chemical characterizations of molecular size fractionated humic acid. Talanta 1999; 50: 641-647.

Shirato W, Kamei Y. Method for adsorbing and separating heavy metal elements by using a tannin adsorbent and method of regenerating the adsorbent, 1995; United States Patent 5,460,791

Shriver DF, Atkins PW. Inorganic Chemistry Oxford University Press, UK, 1999.

Simon FG, Biermann V, Segebade C, Hedrich M. Behaviour of uranium in hydroxyapatite-bearing permeable reactive barriers: investigation using U-237 as a radioindicator. Science of the Total Environment 2004; 326: 249-256.

Singhirunnusorn W and Stenstrom MK. Appropriate wastewater treatment systems for developing countries: criteria and indicator assessment in Thailand. Water Science and Technology 2009; 59: 1873-1884.

Smedley PL. Arsenic in rural groundwater in Ghana. Journal of African Earth Sciences 1996; 22: 459-470.

Smedley PL, Kinniburgh DG. A review of the source, behaviour and distribution of arsenic in natural waters. Applied Geochemistry 2002; 17: 517-568.

Smedley PL, Nkotagu H, Pelig-Ba KB, MacDonald AM, Tyler-Whittle R, Whitehead EJ, Kinniburgh DG. Fluoride in groundwater from high-fluoride areas of Ghana and Tanzania 'Minimising fluoride in drinking water in problem aquifers' R8033. Phase I Final Report. Keyworth, Nottingham, British Geological Survey 2002, 1-72.

Smedley PL, Smith B, Abesser C, Lapworth D. Uranium occurrence and behaviour in British groundwater. Nottingham, British Geological Survey Commissioned Report, 2006, 60.

Sobsey MD, Stauber CE, Casanova LM, Brown JM, Elliott MA. Point of use household drinking water filtration: A practical, effective solution for providing sustained access to safe drinking water in the developing world. Environmental Science and Technology 2008; 42: 4261-4267.

Sowder AG, Clark SB, Fjeld RA. The impact of mineralogy in the U(VI)-Ca-PO4 system on the environmental availability of uranium. Journal of Radioanalytical and Nuclear Chemistry 2001; 248: 517-524.

Spiro TG, Stigliani WM. Chemistry of the Environment. Upper Saddle River, New Jersey, Prentice Hall, 1996.

Stana RR. Recovery of uranium from enriched solution by a membrane seperation process, 1982; UEs Patent 4,316,800

Stone R. Radiation hazards - Kyrgyzstan's race to stabilize buried ponds of uranium waste. Science 2005; 307: 198-200.

Strathmann H. Membrane processes for sustainable industrial growth. Membrane Technology 1999; 1999: 9-11.

Stubbs JE, Veblen LA, Elbert DC, Zachara JM, Davis JA, Veblen DR. Newly recognized hosts for uranium in the Hanford Site vadose zone. Geochimica Et Cosmochimica Acta 2009; 73: 1563-1576.

Suksi J, Ruskeeniemi T, Saarinen L. Selective extractions in uranium migration studies - findings from a natural analogue study at Palmottu, southern Finland. Journal of Contaminant Hydrology 1996; 21: 47-58.

Sutton M, Burastero SR. Uranium(VI) solubility and speciation in simulated elemental human biological fluids. Chemical Research in Toxicology 2004; 17: 1468-1480.

Sutton M, Warwick P, Hall A. Uranium(VI) interactions with OPC/PFA grout. Journal of Environmental Monitoring 2003; 5: 922-928.

Sutzkover I, Hasson D, Semiat R. Simple technique for measuring the concentration polarization level in a reverse osmosis system. Desalination 2000; 131: 117-127.

Tal A. Seeking sustainability: Israel's evolving water management strategy. Science 2006; 313: 1081-1084.

Tang CY, Leckie JO. Membrane independent limiting flux for RO and NF membranes fouled by humic acid. Environmental Science & Technology 2007; 41: 4767-4773.

Tang CYY, Kwon YN, Leckie JO. Characterization of humic acid fouled reverse osmosis and nanofiltration membranes by transmission electron microscopy and streaming potential measurements. Environmental Science and Technology 2007; 41: 942-949.

Tansel B, Sager J, Rector T, Garland J, Strayer RF, Levine LF, Roberts M, Hummerick M, Bauer J. Significance of hydrated radius and hydration shells on ionic permeability during nanofiltration in dead end and cross flow modes. Separation and Purification Technology 2006; 51: 40-47.

The Royal Society. The health effects of depleted uranium munitions: a summary. Journal of Radiological Protection 2002; 22: 131-139.

Thomson M, Miranda MS, Infield D. A small-scale seawater reverse-osmosis system with excellent energy efficiency over a wide operating range. Desalination 2003; 153: 229-236.

Tiepel EW. Application of advanced membrane filtration to industrial wastewater treatment and groundwater clean-up. The International Water Conference 46th Annual Meeting. Engineers Society of Western Pennsylvania Pittsburgh, PA, USA, 1985, pp. 35-43.

Todd WJ. Stable coloring by in-situ formation of micro-particles, 2000; United States Patent 6,136,044

Toulhoat PT, Gallien JP, Louvat D, Moulin V, lHenoret P, Guerin P, Ledoux E, Gurban I, Smellie JAT, Winberg A. Preliminary studies of groundwater flow and migration of uranium isotopes around the Oklo natural reactors (Gabon). Journal of Contaminant Hydrology 1996; 21: 3-17.

Tounissou P, Hebrant M, Rodehuser L, Tondre C. Method for separating metals by micellar ultrafiltration that can be used to process radioactive waste, 2000; United States Patent 6113796

Tsushima S, Uchida Y, Reich T. A theoretical study on the structures of UO2(CO3)(3)(4-), Ca2UO2(CO3)(3)(0), and Ba2UO2(CO3)(3)(0). Chemical Physics Letters 2002; 357: 73-77.

Tzotzi C, Pahiadaki T, Yiantsios SG, Karabelas AJ, Andritsos N. A study of CaCO3 scale formation and inhibition in RO and NF membrane processes. Journal of Membrane Science 2007; 296: 171-184.

Üçer A, Uyanik A, Aygün ŞF. Adsorption of Cu(II), Cd(II), Zn(II), Mn(II) and Fe(III) ions by tannic acid immobilised activated carbon. Separation and Purification Technology 2006; 47: 113-118.

Uijt de Haag PAM, Smetsers RCGM, Witlox HWM, Krus HW, Eisenga AHM. Evaluating the risk from depleted uranium after the Boeing 747-258F crash in Amsterdam, 1992. Journal of Hazardous Materials 2000; 76: 39-58.

Um W, Icenhower JP, Brown CF, Serne RJ, Wang ZM, Dodge CJ, Francis AJ. Characterization of uranium-contaminated sediments from beneath a nuclear waste storage tank from Hanford, Washington: implications for contaminant transport and fate. Geochimica Et Cosmochimica Acta 2010; 74: 1363-1380.

UN. The Millennium Development Goals Report 2010. New York, United Nations, 2010, 80.

UNICEF. The State of the World's Children 2008: Child Survival. New York, USA, 2007.

Unsworth ER, Jones P, Hill SJ. The effect of thermodynamic data on computer model predictions of uranium speciation in natural water systems. Journal of Environmental Monitoring 2002; 4: 528-532.

US EPA. Understanding Variation in Partition Coefficient, Kd, Values; Volume II: Review of geochemistry and available Kd values for cadmium, cesium, chromium,

lead, plutonium, radon, strontium, thorium, tritium (3H), and uranium. Washington DC, United States Environmental Protection Agency, 1999.

Valle-Fuentes FJ, Garcia-Guinea J, Cremades A, Correcher V, Sanchez-Moral S, Gonzalez-Martin R, Sanchez-Munoz L, Lopez-Arce P. Low-magnesium uranium-calcite with high degree of crystallinity and gigantic luminescence emission. Applied Radiation and Isotopes 2007; 65: 147-154.

van den Berg GB, Rácz IG, Smolders CA. Mass transfer coefficients in cross-flow ultrafiltration. Journal of Membrane Science 1989; 47: 25-51.

Van der Bruggen B, Mänttari M, Nyström M. Drawbacks of applying nanofiltration and how to avoid them: A review. Separation and Purification Technology 2008; 63: 251-263.

Van der Bruggen B, Vandecasteele C. Removal of pollutants from surface water and groundwater by nanofiltration: overview of possible applications in the drinking water industry. Environmental Pollution 2003; 122: 435-445.

van Halem D, Heijman SGJ, Amy GL, van Dijk JC. Subsurface arsenic removal for small-scale application in developing countries. Desalination 2009; 248: 241-248.

Vandenhove H. European sites contaminated by residues from the ore-extracting and -processing industries. International Congress Series 2002; 1225: 307-315.

Vandenhove H, Sweeck L, Mallants D, Vanmarcke H, Aitkulov A, Sadyrov O, Savosin M, Tolongutov B, Mirzachev M, Clerc JJ, Quarch H, Aitaliev A. Assessment of radiation exposure in the uranium mining and milling area of Mailuu Suu, Kyrgyzstan. Journal of Environmental Radioactivity 2006; 88: 118-139.

Vasiliev IA, Barber DS, Alekhina VM, Mamatibtaimov S, Betsill D, Passell H. Uranium levels in the Naryn and Mailuu-Suu rivers of Kyrgyz Republic. Journal of Radioanalytical and Nuclear Chemistry 2005; 263: 207-212.

Vicente-Vicente L, Quiros Y, Perez-Barriocanal F, Lopez-Novoa JM, Lopez-Hernandez FJ, Morales AI. Nephrotoxicity of uranium: pathophysiological, diagnostic and therapeutic perspectives. Toxicological Sciences 2010; 118: 324-347.

von der Heyden CJ, New MG. Groundwater pollution on the Zambian Copperbelt: deciphering the source and the risk. Science of the Total Environment 2004; 327: 17-30.

Wang YF, Shu L, Jegatheesan V, Gao BY. Removal and adsorption of diuron through nanofiltration membrane: The effects of ionic environment and operating pressures. Separation and Purification Technology 2010; 74: 236-241.

Wazne M, Meng X, Korfiatis GP, Christodoulatos C. Carbonate effects on hexavalent uranium removal from water by nanocrystalline titanium dioxide. Journal of Hazardous Materials 2006; 136: 47-52.

Wijmans JG, Baker RW. The solution-diffusion model - a review. Journal of Membrane Science 1995; 107: 1-21.

Willett IR, Bond WJ. Fate of manganese and radionuclides applied in uranium mine waste water to a highly weathered soil. Geoderma 1998; 84: 195-211.

Winde F, van der Walt IJ. The significance of groundwater-stream interactions and fluctuating stream chemistry on waterborne uranium contamination of streams - a case study from a gold mining site in South Africa. Journal of Hydrology 2004; 287: 178-196.

Worch E. Eine neue Gleichung zur Berechnung von Diffusionskoeffizienten gelöster Stoffe. Vom Wasser 1993; 81: 289-297.

World Health Organisation. Guidelines for Drinking Water Quality: first addendum to third edition. Geneva, 2006, 515.

Yoon M, Whang S, Insoon C, Han P. Recovery or removal of uranium by the utilization of acorns, 1989; United States Patent 4,871,518

Yuan Y and K. J. Hydrodynamic modeling of NOM transport in UF: effects of charge density and ionic strength on effective size and sieving. Environmental Science and Technology 2009; 43: 5449-5454

Zamora MLL, Zielinski JM, Moodie GB, Falcomer RAF, Hunt WC, Capello K. Uranium in drinking water: renal effects of long-term ingestion by an aboriginal community. Archives of Environmental & Occupational Health 2009; 64: 228-241.

Zhang YJ, Bryan ND, Livens FR, Jones MN. Selectivity in the complexation of actinides by humic substances. Environmental Pollution 1997; 96: 361-367.

Zhu C, Burden DS. Mineralogical compositions of aquifer matrix as necessary initial conditions in reactive contaminant transport models. Journal of Contaminant Hydrology 2001; 51: 145-161.

11 Appendix

Table 15. UN Millennium Development Goals (UN, 2010)

MDG Goal	Target
1. To eradicate extreme poverty	Target 1: Reduce, by one half, the proportion of people whose income is less than one dollar a day. Target 2: Reduce, by one half, the proportion of people who suffer from hunger.
2. To achieve universal primary education	Target 3: Ensure that children, boys and girls alike, will be able to complete a full course of primary schooling.
3. To promote gender equality and to empower women	Target 4: Eliminate gender disparity in primary and secondary education.
4. To reduce child mortality	Reduce, by two thirds, the under-five mortality rate.
5. To improve maternal health	Reduce, by three quarters, the maternal morality rate.
6. To combat HIV/AIDS, malaria and other diseases	Target 7: Have halted by 2015 and begun to reverse the spread of HIV/AIDS. Target 8: Have halted by 2015 and begun to reverse the incidence of malaria and other major diseases.
7. To ensure environmental sustainability	Target 9: Integrate the principles of sustainable development into country policies and programmes and reverse the losses of environmental resources. **Target 10: Reduce, by one half, by 2015 the proportion of people without sustainable access to safe drinking water and basic sanitation.** Target 11: By 2015 to have achieved a significant improvement in the lives of at least 100 million slum dwellers.
8. To develop a global partnership for development	Target 12: Develop further an open, rule-based, predictable, non-discriminatory trading and financial system. Target 13 & 14: Address the special needs of the least developed, land-locked, and small island developing countries. Target 15: Deal comprehensively with debt problems of developing countries through national and international measures in order to make debt sustainable in the long. Target 16: In cooperation with developing countries, develop and implement strategies for decent and productive work for youth. Target 17: In cooperation w0ith pharmaceutical companies, provide access to affordable essential drugs in developing countries Target 18: In cooperation with the private sector, make achievable the benefits of new technologies, especially information and communications technologies.

11.1 Materials and methods

11.1.1 Inorganic analysis

Elemental concentrations were determined using ICP-OES, ICP-MS or IC, according to what was appropriate for the element of interest. Typical detection limits are tabulated in Table 16. Calibration standards were freshly prepared on the day of analysis using dilute nitric acid for ICP-OES and ICP-MS, while those for IC (made up with DIW) were able to be stored for longer periods. The certified standard solutions used for preparing the calibration standards are listed in Table 17.

Table 16. Minimum detection limits for analysis using ICP-OES, ICP-MS and IC.

Element	Method	Unit	Limit of detection
Aluminium	ICP-OES	mg/L	0.02
Arsenic	ICP-MS	µg/L	0.003
Barium	ICP-OES	mg/L	0.1
Boron	ICP-MS	µg/L	2.551
Bromide	IC	mg/L	0.2
Cadmium	ICP-MS	µg/L	0.001
Calcium	ICP-OES	mg/L	0.02
Chloride	IC	mg/L	0.2
Chromium	ICP-MS	µg/L	0.068
Cobalt	ICP-MS	µg/L	0.051
Copper	ICP-MS	µg/L	0.173
Fluoride	IC	mg/L	0.1
Iron	ICP-MS	µg/L	0.001
Lead	ICP-MS	µg/L	0.006
Magnesium	ICP-OES	mg/L	0.03
Manganese	ICP-MS	µg/L	0.057
Nickel	ICP-MS	µg/L	0.054
Nitrate	IC	mg/L	0.2
Phosphate	IC	mg/L	0.1
Potassium	ICP-OES	mg/L	0.03
Selenium	ICP-MS	µg/L	0.306
Sulphate	IC	mg/L	0.2
Sulphur	ICP-OES	mg/L	0.1
Uranium	ICP-OES	mg/L	0.03
	ICP-MS	µg/L	0.001
Vanadium	ICP-MS	µg/L	0.011
Zink	ICP-MS	µg/L	1.591

Table 17. Calibration standards used for inorganic determination

Company	Type	Analysis type
Spex certiprep, Merck	Single element (U, As, Ca) (1000 mg/L in 2% nitric acid)	ICP-OES ICP-MS
Merck	Certipur IV ICP multi-element standard solution IV (Ag, Al, B, Ba, Bi, Ca, Cd, Co, Cr, Cu, Fe, Ga, In, K, Li, Mg, Mn, Na, Ni, Pb, Sr, Tl, Zn in dilute nitric acid)	ICP-OES ICP-MS
BDH Laboratory supplies	Single element (F^-, Cl^-, NO_3^-, NO_2^-, Br^-, PO_4^{2-}) (1000 mg/L in DIW)	IC

11.1.2 Element determination using ICP-OES

The concentrations of multiple elements can be determined simultaneously by ICP-OES. The sample is dissociated into atoms or ions, whose electrons are excited and emit light at a characteristic wavelength, proportional to the concentration in the sample.

Elemental concentrations within the range of 0.1-100 mg/L of primarily uranium, but also aluminium, barium, calcium, magnesium, potassium and sulfur were determined using a Perkin Elmer Optima 5300 DV ICP-OES (Perkin Elmer, USA), equipped with a Gem-cone cross-flow nebuliser, Scott spray chamber and AS 93 plus autosampler. The operating conditions, as recommended by the manufacturer for aqueous analysis, of the instrument are displayed in Table 18. Axial view is generally used for concentrations below 100 mg/L.

Figure 73, Optima 5300 DV ICP-OES instrument used during this study.

Table 18. Instrument settings for ICP-OES

Parameter	Setting
RF Power (kW)	1400
Plasma gas (Ar) flow (L/min)	15
Auxillary gas (Ar) flow (L/min)	0.20
Nebuliser gas (Ar) flow (L/min)	0.80
Sample flow rate (ml/min)	1.50
Sample delay (sec)	30
wash time (sec)	30
Extra wash time (if sample above 40 mg/L) (sec)	10
Replicates	3
Replicate time (sec)	60
Stabilisation time (sec)	15
Viewing position	Axial

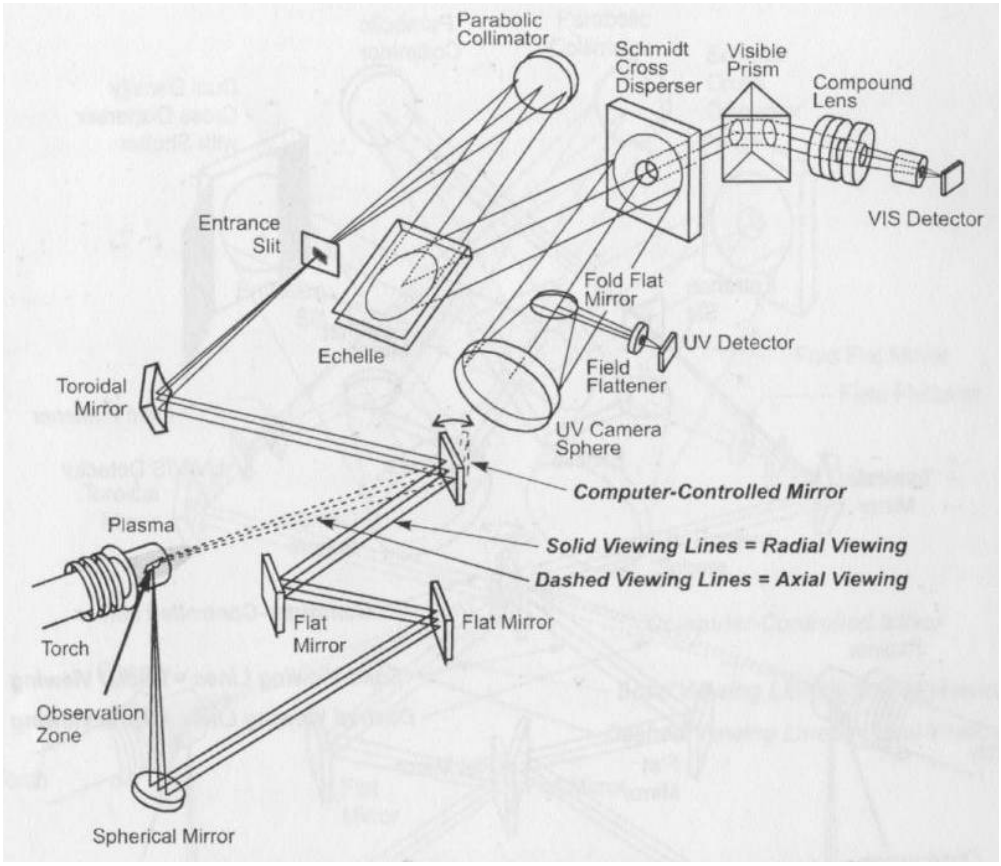

Figure 74. Schematic showing the optics system of the ICP-OES Optima 5300 DV. Axial viewing was used for the analysis (from instrument hardware manual).

The instrument was calibrated using standards made up on the day of analysis. The appropriate calibration standard was diluted using 2.8% (wt.) Aristar nitric acid. The following concentrations were prepared: 0.1, 0.5, 1, 5 and 10 mg/L. If the concentration range was expected to be higher solutions of 30, 50 and 100 mg/L were also prepared. Calibration curves were generated with the instrument software for each emission line. Calibrations curves with a correlation coefficient (r^2) of 0.999 or better were used. When a wide range of concentrations were analysed (*i.e.* 0.1 to 100 mg/L), samples of lower concentrations were re-processed against a calibration curve using only the lower concentration range standards (*i.e.* 0.1 to 10 mg/L). This was the case for instance when analysing samples containing uranium (below 0.5 mg/L) and calcium (around 60 mg/L). Prior to the analysis of the samples, the calibration of the instrument was approved by analysing a certified reference solution (ICP Multi Element Standards Solution VI, Certipur) (Diluted ten times using 2.8%

(wt.) Aristar nitric acid). Typical internal analytical precision (1 SD) for uranium concentrations was 0.014 mg/L or ≤ 1.5 % (n = 45), based on the standard deviation of the mean value for three consecutive measurements of the standard reference solution (Generally the reference solution was inserted at least twice during an analysis). Mean external analytical precision (1 SD) of uranium concentrations, as determined by repeated analysis (n = 45) of the certified reference solution was ± 0.140 or ≤ 14.36%. The average value obtained for this solution over the course of the research project was 0.978 ± 0.140 (n = 45). The expected value is 1.0 ± 0.05 for MVI solutions diluted ten times.

One of the standard solutions was re-analysed about every 10 samples in order to control for any drift during analysis. Sample blanks were also analysed, and the concentrations of the samples were blank corrected, if any uranium concentrations were detected. Several emission lines were analysed for each element; the results of the best one were then used, based on sensitivity, absence of spectral interference, consistency over the course of a run and accuracy of the standard reference solution measurement. The alignment of element emission lines could be controlled using the instrument soft-ware, and re-aligned if necessary. For uranium, line 367.007 nm was mostly used and sometimes 385.958 nm. For calcium, the lines 317.933 and 315.887 nm were used.

11.1.3 Element determination using ICP-MS

ICP-MS uses a high energy source to excite and eject an electron from the atoms in a sample, producing a positively charged ion. These ions are extracted and measured according to their mass/charge ratio in the spectrometer.

Figure 75. Agilent 7500ce ICP-MS instrument used during this study.

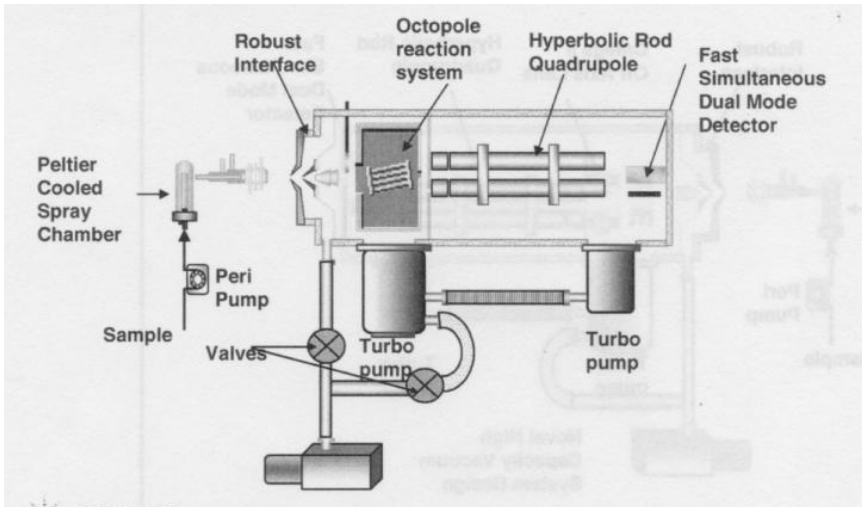

Figure 76. Schematic giving an overview of Agilent 7500c collision cell ICP-MS (from Agilent Technologies).

Elemental concentrations within the range of 0.1-100 µg/L were determined using an Agilent 7500ce ICP-MS with an octopole reaction system, peristaltic pump and autosampler, Mira mist nebuliser, nickel skimmer and sample cones.

To ensure good crossover between pulse counting (P) and analogue counting (A) mode, a P/A factor was determined using a tuning solution (consisting of lithium, magnesium, yttrium, cesium, thallium and cobalt from Agilent Technologies) across the entire mass range at the start of each analysis day. Instrument settings are given in Table 19. For multi-element analysis the instrument was operated in spectrum (multi tune) acquisition mode, where each element was analysed using the relevant mode as listed in Table 20. When only uranium or uranium with a few other elements (usually calcium) were analysed the instrument was operated in spectrum acquisition mode, again with gas choice according to Table 20. When there was uncertainty as to which gas mode was best, an element would be analysed in several and the best one selected based on the standard reference results.

Table 19. Intrument settings used during ICP-MS analysis.

Parameter	Setting
RF forward power (W)	1540
Reflected power (W)	1
Argon gas carrier flow (L/min)	0.82
Argon gas make-up flow (L/min)	0.21
Nebuliser up-take rate (ml/min)	0.2 (0.06 rps)
Analyser pressure (vacuum) (Pa)	3×10^{-6}
IF/BK pressure (vacuum) (Pa)	8.5×10^{-1}
Sample depth (mm)	8.4
Rinse speed (rinse port) (rps)	0.3
Between sample rinse time, rinse vial (sec)	40
Rinse speed (rinse vial) (rps)	0.1
Between sample rinse time, rinse port (sec)	10

Each mass in all three steps was analysed in fully quant mode (*i.e.* three points per unit mass) and was integrated for 0.1 s per point, giving a total integration time of 0.3 s per unit mass. When the instrument was operated in spectrum/multitune acquisition mode, three replicate runs per sample were employed, while in spectrum mode, five replicate samples were employed. The total integration time per sample for a

multitune mode was typically between 50 to 124 seconds, while in spectrum mode between 1.9 to 8.5 seconds.

Table 20. Acquisition modes chosen for the elements analysed as well as stabilisation time and gas flow settings for each mode.

Acquisition modes	Relevant for elements:	Stabilisation time (sec)	Gas flow (L/min)
H_2 mode	^{74}Se, ^{77}Se, ^{78}Se ^{82}Se	5	4.0
He mode	^{42}Ca, ^{43}Ca*, ^{7}Li, ^{10}B, ^{11}B, ^{27}Al, ^{55}Mn, ^{56}Fe, ^{57}Fe, ^{60}Ni, ^{62}Ni, ^{63}Cu, ^{65}Cu, ^{64}Zn, ^{66}Zn, ^{75}As, ^{51}V, ^{52}Cr, ^{53}Cr	30	6.5
No-gas mode	^{238}U, ^{48}Ca, ^{24}Mg, ^{7}Li, ^{10}B, ^{11}B, ^{55}Mn, ^{60}Ni, ^{62}Ni, ^{63}Cu, ^{64}Zn, ^{65}Cu, ^{66}Zn, ^{68}Zn, ^{106}Cd, ^{111}Cd, ^{114}Cd, ^{135}Ba, ^{137}Ba, ^{206}Pb, ^{207}Pb, ^{208}Pb, ^{59}Co, ^{202}Hg	30	

*The results for ^{43}Ca were used.

The instrument was calibrated using standards made up on the day of analysis. The calibration standard was diluted to the appropriate concentration using 2.8% (wt.) Aristar nitric acid. The following concentrations were prepared: 0.25, 0.5, 1, 2.5, 5, 10 and 100 µg/L. There were more standards in the lower concentration range since the majority of the samples had concentrations below 10 µg/L. Linear regression ($y = ax + b$) was used for the calibration curve. Prior to the analysis of the samples, the accuracy of the calibration was determined by analysing a certified reference solution (ICP Multi Element Standards Solution VI, Certipur) and a certified reference water (SRM 1640 or 1643E). Typical internal analytical precision (1 SD) for uranium concentrations was ± 0.16 µg/L or ≤ 1.6%, based on the standard deviation of the mean value for three consecutive measurements of the standard reference solution. The mean value obtained for uranium for the MVI solution was 9.79 ± 0.59 µg/L, based on the standard deviation of the average value determined for MVI over the

course of the research project (n = 17), giving an external precision of ≤ 6 %. The certified value expected for the MVI solution is 10.0 ± 0.5 µg/L.

There are a number of interferences in ICP-MS analysis that one should be aware of, including 1) high amounts of total dissolved solids 2) high mass elements may affect the signals of low mass elements and 3) formations of polyatomic masses (*e.g.* ArO^+ will have the same mass as Fe^+). Matrix effects are reduced by appropriate dilutrions if, for instance, high NaCl amounts are present. Polyatomic argides and oxides can be reduced by appropriate tuning and by using the collision or reaction gas mode options. The mass/charge ratio of common interfering oxides (such as ArO and ClO) is monitored before analysis commences to ensure that these are low. Isotopes chosen for detection during analysis should be selected, taking into consideration that the mass is not the same as an isotope of a different element present in the sample.

11.1.4 Organic carbon analysis

The total organic matter present in the UF feed and permeate samples were analysed using a total organic carbon analyser (TOC-V_{CPH}) (Shimadzu, UK). As part of the method (non-purgable-organic-carbon or NPOC), the samples were acidified using HCl (2 M, Fisher) and sparged for 1.5 minutes with nitrogen gas to remove any inorganic carbon.

Potassium hydrogen phthalate was prepared by drying it at 120°C for one hour in an oven and allowed to cool in a dessicator. This was then used to prepare a 1000 mg/L C stock solution from which a 10 mg/L C standard was diluted, while the instrument made dilutions for standards between 1-10 mg/L C. The 10 mg/L C standard was inserted as a control check through-out the run, along with blank samples. The average value obtained for the 10 mg/L standard was 9.15 ± 0.31 mg/L when using the regular catalyst, giving a variation of 3.4%. The average value obtained when using the high sensitivity catalyst was 9.74 ± 0.27 mg/L giving a variation of 2.7%. Blank samples were used to control for any carry-over or build-up of carbon during the analysis. The regular catalyst was used for samples from the UF experiments

(Chapter 5), while the high sensitivity catalyst was used for the samples from the membrane characterisation experiments (Chapter 6).

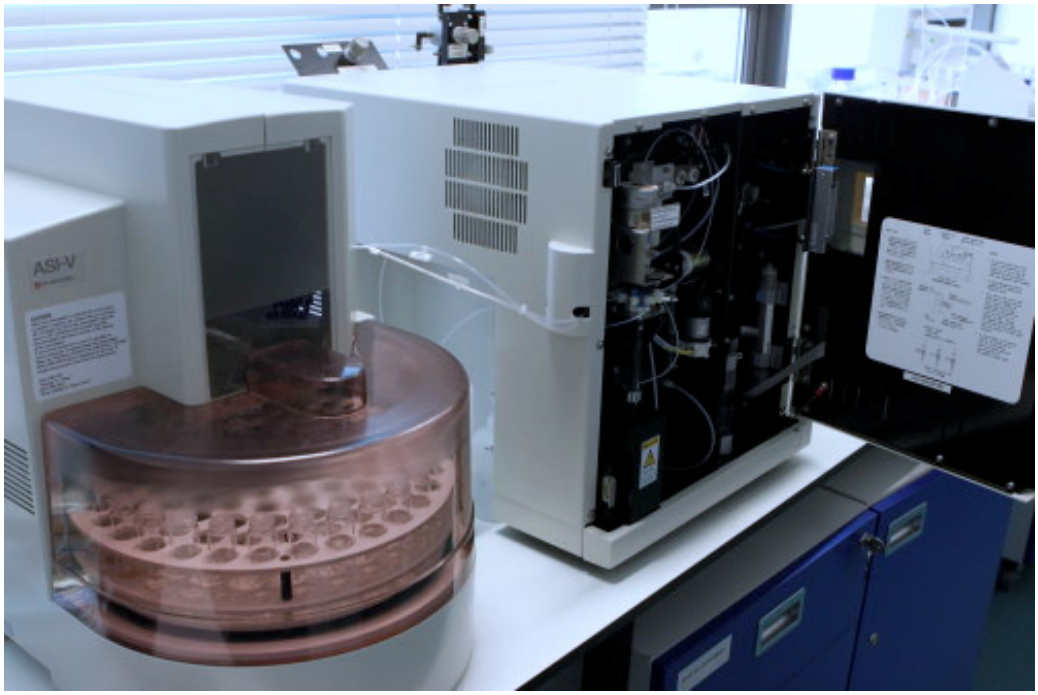

Figure 77. Shimadzu TOC analyser

Table 21. Parameters used for sample analysis

Parameter	Value
Injection volume (µl)	50
HCl (2 M) addition, volume (%)	2
Sparge time (min)	2
Number of needle washes with sample	2
Sample replicates	3/4
Maximum standard deviation (S.D.)	0.1000
Maximum coefficient of variation (C.V.) (%)	2.00

Table 22. Parameters used for calibration curve

Parameter	Value
Injection volume (µl) (UF/characterisation)	50/800
HCl (2 M) addition, volume (%)	1.5
Sparge time (min)	1.30
Number of needle washes with sample	2
Sample replicates	3/4
Maximum standard deviation (S.D.)	0.1000
Maximum coefficient of variation (C.V.) (%)	2.00
Lower limit of r^2 for calibration curve*	0.995

*An r^2 value of 0.9995 was achieved for both calibration curves constructed

11.2 Appendix to Chapter 4

11.2.1 Experimental conditions for pH experiments

The average temperatures were 31.27±1.03°C, 24.90±0.30 °C, 28.16±0.7°C, 25.74±0.9°C and 24.73±2.4°C for the experiments with BW30 at Ti Tree and NF90, ESPA4, TFC-S and BW30 at Pine Hill, respectively. See graphs below for overview of the temperature and feed flow variation throughout the experiment. It can be concluded that both flow and temperature were fairly constant through-out the individual experiments, except for BW30 in Pine Hill, where the temperature decreased by about 2.5°C.

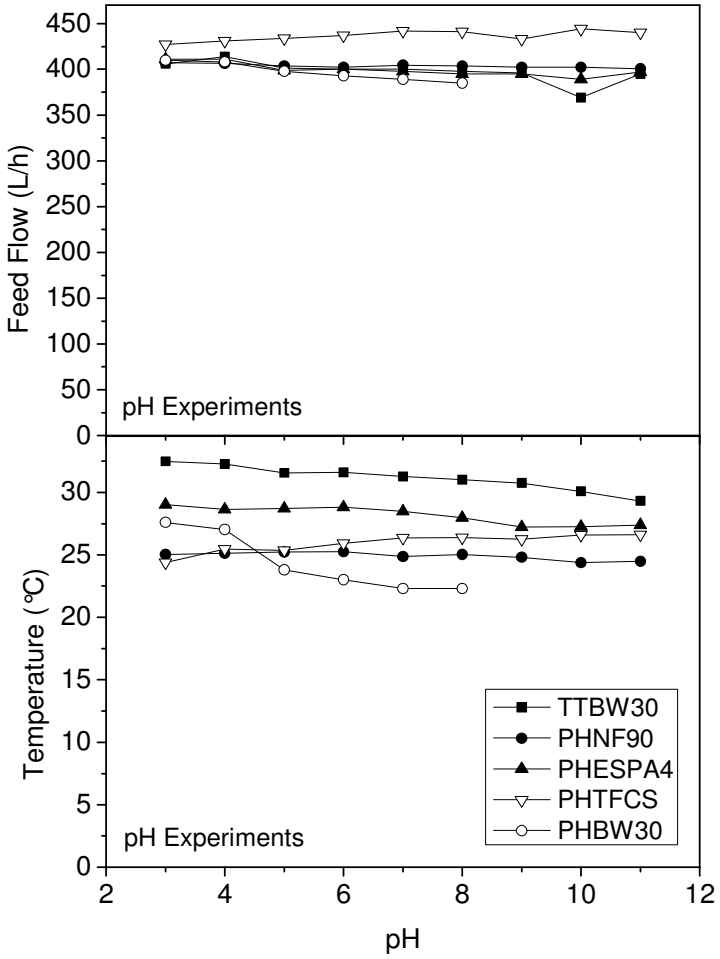

Figure 78. Feed flow and temperature as a function of pH (TT: Ti Tree Farm, PH: Pine Hill Station).

11.2.2 Experimental conditions for solar experiments

The Pressure increased with solar radiance from 4 bar at the start and stabilised at about 11 bar (Figure 79) for both the solar *batch* and solar *continuous* experiment. At the end of the day the pressure dropped to 8-9 bar for the solar *batch* experiment. The feed flow was about 400 L/h. The temperature increased from 25 to about 32°C for the solar *batch* experiment while for the solar *continuous* experiment the temperature increased from 19 to 30°C.

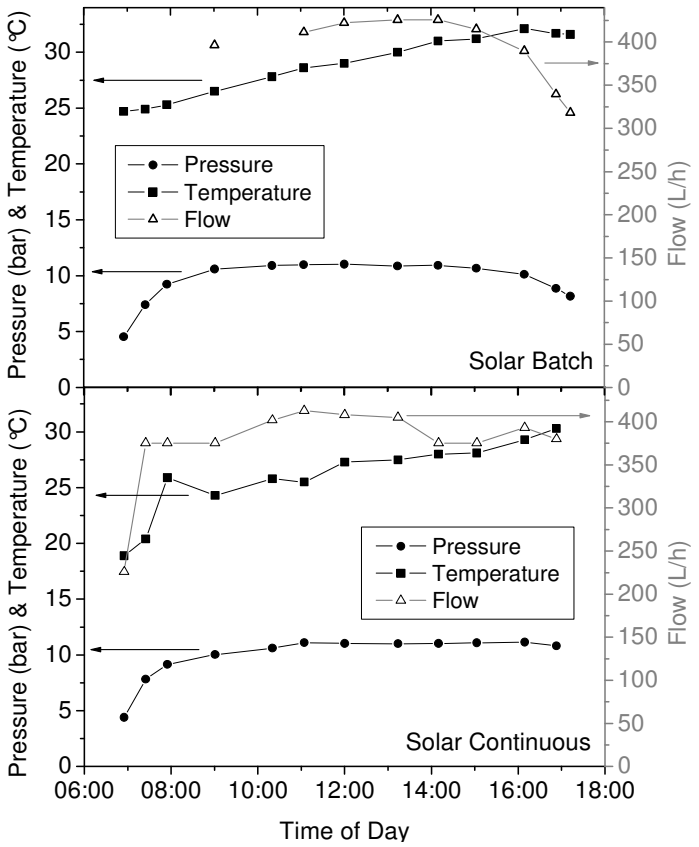

Figure 79. Pressure, temperature and feed flow (L/h) over the course of the solar day for the solar *batch* and solar *continuous* experiments.

11.3 Appendix to Chapter 5

The parameters used for the SHM in Visual Minteq are listed in the below table, adapted from Gustafsson 2001.

Table 23. Parameters used in the Stockholm Humic Model, Visual Minteq.

Parameter	Description
n	Amount of proton-dissociating sites (mol g^{-1})
n_B	Amount of type B sites (mol g^{-1})
Log K_A	Intrinsic proton dissociation constant for type A sites
Log K_B	Intrinsic proton dissociation constant for type B sites
$\Delta p K_A$	Distribution term that modifies log K_A
$\Delta p K_B$	Distribution term that modifies log K_B
Log K_{Mm}	Intrinsic equilibrium constant for monodentate complexation of metal *M*
Log K_{Mb}	Intrinsic equilibrium constant for bidentate complexation of metal *M*
Δ L K_2	Distribution term that modifies the strengths of complexation sites
R	Radius of humic or fulvic acid (Set at 0.75 nm for fulvic acid and 2.0 nm for humic acid)
C	Stern layer capitance (Set at 2 Fm^{-2} through-out)
N_s	Site density of HS functional groups (Fixed at 1.2 sites nm^{-2})
A_s	Specific surface area of HS (Calculated using r and N_S)
G_f	Gel fraction parameters (Varies from 0 to 1 for dissolved humics, with an average of 0.78)
K_C	Intrinsic equilibrium constant for the accumulation of screening counterions (Set at 0.8)

11.4 Appendix to Chapter 6

11.4.1 Pore size and molecular weight cut-off calculations

Pore radius estimation

The method described by Nghiem in his thesis (Nghiem, 2005) and paper (Nghiem et al., 2004) to calculate the pore radius experimentally and theoretically was followed.

Three solutions containing neutral organic molecules (dioxane, xylose and dextrose) were prepared (10 g C/L in DIW). The same membrane was used for the whole series of experiments performed, to avoid between-membrane sample variation.

Before starting the experiment, the membrane was compacted at 25 bar for an hour. The permeability of pure water was then measured for the whole pressure range (5, 7.5, 10, 12.5 and 15 bar). The system was then drained of DIW and the first solute added. The flow-rate was set to 2 L/min and the pressure was adjusted. The system was allowed to stabilise for an hour after adjusting the pressure before sampling. Three feed and permeate samples (with five minutes in between samples) were taken for each measurement. After completing the experiment for one solute, the system was drained and swilled with DIW and washed with DIW for an hour. The permeate flux was then measured and a sample of the DIW collected for analysis. Again, before starting an experiment with the next solute, the system was washed with DIW for 40-60 minutes before starting the experiment and a sample of the DIW was collected.

Samples of the solutes and the DIW system blanks were analysed in the TOC (NPOC method, high sensitivity catalyst). The standard deviation for dioxane, xylose and dextrose were ± 10.5%, ± 5.5% and ± 2.5%, respectively, the higher SD for the compounds retained to a lesser extent. The average permeate flux and observed retention for each solute at each pressure were then used to calculate the real retention as described below.

Using film theory, the real retention is related to the observed retention and permeate flux through the equation:

$$\ln = \frac{1-R_r}{R_r} = \ln\frac{1-R_o}{R_o} - \frac{Jv}{kf} \qquad \textbf{Equation 14}$$

R_r = real retention, R_o = observed retention, J_v = permeate flux (volumetric) and k_f = mass transfer coefficient.

The method of measuring the mass transfer coefficient experimentally (as in Sutzkover et al. 2000) was attempted. This was not successful, however, since the method is based on permeate flux decline following salt addition compared to

permeate flux with pure water (DIW). For TFC-SR2 the permeate flux increases as salt is added to the system.

Instead a correlation had to be used. The mass transfer coefficient is related to the Sherwood number (Sh) through the density, D and the channel length (dh):

$$k = \frac{Sh \times D}{dh} \qquad \textbf{Equation 15}$$

The Sherwood number can be calculated for each solution according to the Deissler relationship for a cross-flow system (Gekas and Hallstrom 1987, van den Berg 1989):

$$Sh = 0.023\,\mathrm{Re}^{0.875}\,Sc^{0.25} \qquad \textbf{Equation 16}$$

Re is the Reynolds number for the system while Sc is the Schmidt number, calculated for each solution (DIW, dioxane, xylose and dextrose).

$$Sc = \frac{v}{Dl \times d} \qquad \textbf{Equation 17}$$

v = dynamic viscosity, Dl = diffusivity of solute, d = feed density.
The diffusion coefficient for dioxane, xylose and dextrose can be calculated using the Stokes-Einstein equation in Worch 2004. The values calculated by Long et al. (2004), were used for these calculations.

$$\mathrm{Re} = \frac{V d_h d}{v} \qquad \textbf{Equation 18}$$

V = fluid velocity, d_h = length of channel, d = feed density and v = dynamic viscosity.

By calculating the Schmidt and Sherwood numbers for each solution, using the above equations, the mass transfer coefficient for each solution could also be calculated using Equation 15 and the real retention could be calculated as in Equation 14 using the experimental parameters measured.

Theoretical pore radius calculation

The theoretical retention can be calculated for NF membranes by using the hydrodynamic model for solute transport. This model assumes that the pores are cylindrical and of equal pore radius, that the solutes are spherical and that retention occurs through size exclusion. The pore radius and the ratio between active membrane layer thickness and porosity can then be determined by curve fitting between experimental results and the theoretical calculations.

First the hydrodynamic hindrance coefficients, K_c and K_d must be determined.

$$K_c = \frac{(2-\Phi)K_s}{2K_t} \qquad \textbf{Equation 19}$$

$$K_d = \frac{6\pi}{K_t} \qquad \textbf{Equation 20}$$

Where K_t and K_s are:

$$Kt = \frac{9}{4}\pi^2\sqrt{2}(1-\lambda)^{-5/2}\left[1+\sum_{n=1}^{2}a_n(1-\lambda)^n\right]+\sum_{n=0}^{4}a_{n+3}\lambda^n \qquad \textbf{Equation 21}$$

$$Ks = \frac{9}{4}\pi^2\sqrt{2}(1-\lambda)^{-5/2}\left[1+\sum_{n=1}^{2}b_n(1-\lambda)^n\right]+\sum_{n=0}^{4}b_{n+3}\lambda^n \qquad \textbf{Equation 22}$$

The coefficients a and b given in Nghiem (2006) were used and are listed below in Table 24:

Table 24. Coefficients for K_t and K_s from Nghiem (2005)

N	a_n	b_n
1	-73/60	7/60
2	77293/50400	-2227/50400
3	-22.5083	4.0180
4	-5.6177	-3.9788
5	-0.3363	-1.9215
6	-1.216	4.392
7	1.647	5.006

K_t and K_s was calculated for each of the solutes, from which K_d is calculated.

$$\phi = (1-\lambda)^2 \qquad \textbf{Equation 23}$$

This depends on λ which is the ratio of solute radius to pore radius = r_s/r_p.

The radius of the solute was calculated using Stokes Einstein equation:

$$D = \frac{kT}{6\pi\eta R} \qquad \textbf{Equation 24}$$

D = diffusivity in dilute solution, k = Boltzmanns constant, T = temperature, η = solvent viscosity and R is the solute radius.

The solute radius was calculated to be 0.235, 0.289 and 0.324 nm for dioxane, xylose and dextrose, respectively.

Using the volumetric permeate flux (J_v), the solute diffusivity (D_∞), the results for K_d and K_c and the ratio between membrane thickness (L) and porosity (ε), the membrane Peclet number (Pe) can be calculated:

$$Pe = \frac{K_c(J_v)L}{K_d \varepsilon D_\infty}$$ **Equation 25**

The theoretical retention, R_r, is then calculated by

$$Rr = 1 - \frac{\phi K_c}{1 - [1 - \phi Kc]\exp(-Pe)}$$ **Equation 26**

The pore radius and the ratio between active membrane layer thickness and porosity can then be determined by curve fitting between experimental retention results and the theoretical retention calculations (Figure 81). The results for the pore radius and active layer thickness to porosity ratio are given in Table 25. The average value for the pore ratio was determined to 0.52 nm.

Table 25. Solute radius, Pore radius (Rp) determined using each solute, as well as the ratio of the membrane active layer to porosity (L/ε).

	R_s (nm)	**R_p (nm)**	**L/ε**
Dioxane	0.235	0.5498	2.28×10^{-6}
Xylose	0.289	0.5178	2.58×10^{-6}
Dextrose	0.324	0.4866	3.79×10^{-6}
Average		**0.518 ± 0.03**	**2.88×10^{-6}**

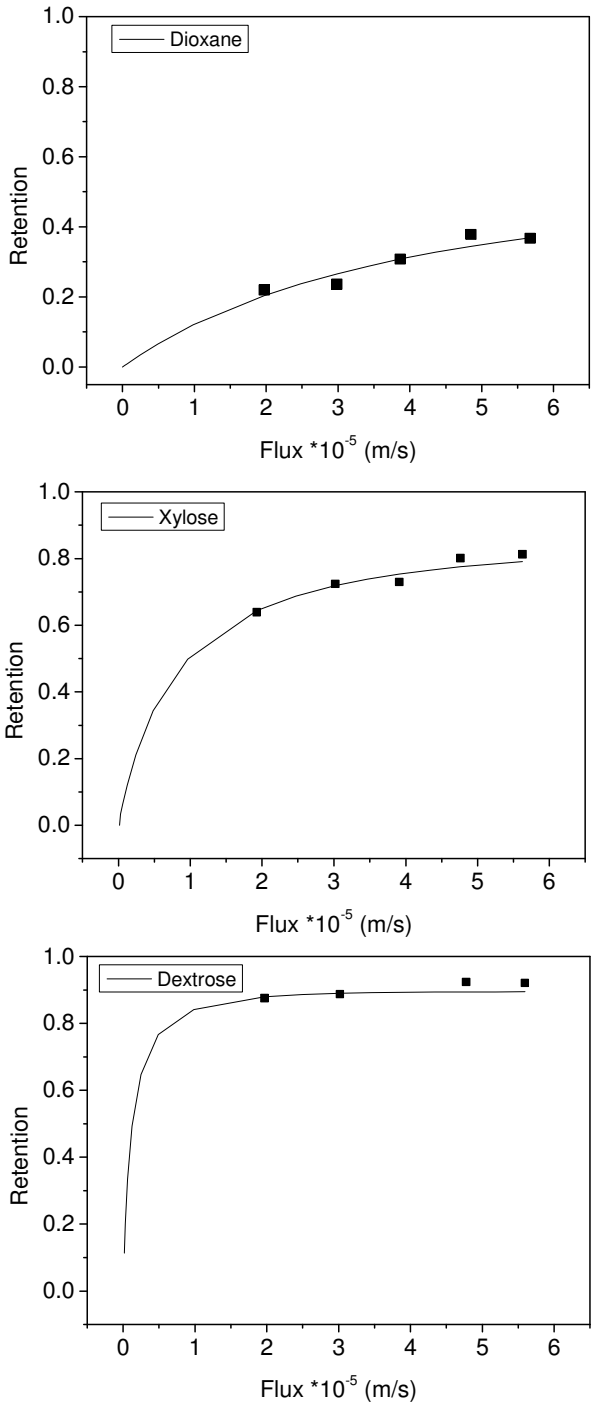

Figure 80. Retention of dioxane, xylose and dextrose as a function of permeate flux for TFC-SR2. The symbols represent the experimental retention results, while the lines represent the result for theoretical retention calculated with the pore transport model using the optimised parameters (r_s, λ and r_p).

Molecular weight cut-off (MWCO)

Four solutions of polyethylene glycol (PEG) (200, 400, 600 and 1000 g/mol) were prepared (10 g C/L) in DIW. Prior to commencing the experiment, the membrane was compacted at 25 bar for an hour. The pure water flux was then measured at 10 bar (169 ± 0.85 L/m^{2}hbar). The system was drained of DIW and the PEG solution added. The flow was set to 2 L/min and pressure to 10 bar and the system was allowed to stabilise for an hour before sampling (three samples taken for each PEG solution, with about five minutes in between each sample). The system was washed with DIW for 30 minutes between PEG solutions. A blank sample was taken of the DIW wash and permeate flux was measured. The standard deviation for the retention measurements for all PEG solutions was ± 1%. The final pure water flux at the end of the experiments was 162 L/m^{2}hbar.

The MWCO was determined by plotting the retention for dioxane, xylose, dextrose (at 10 bar) and the PEG solutions against molecular weight cut-off. Linear regression was used to determine the MWCO (90% retention) as well as the absolute MWCO (100%). The nominal MWCO was calculated as 486 g/mol. This was similar to the nominal MWCO of 485 g/mol for TFC-SR2 obtained by De Munari et al. (2010) using the same experimental method but in a stirred-cell system. The absolute MWCO was calculated as 1033 g/mol.

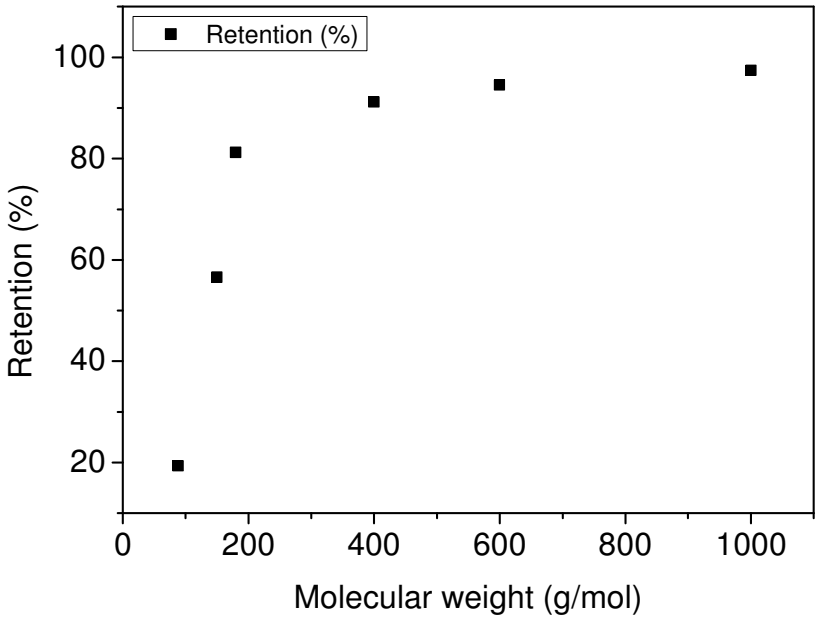

Figure 81. Retention of dioxane, xylose, dextrose, PEG 400, 600 and 1000 plotted against molecular weight.

Non-buffer experiments for TFC-SR2 without applied pressure

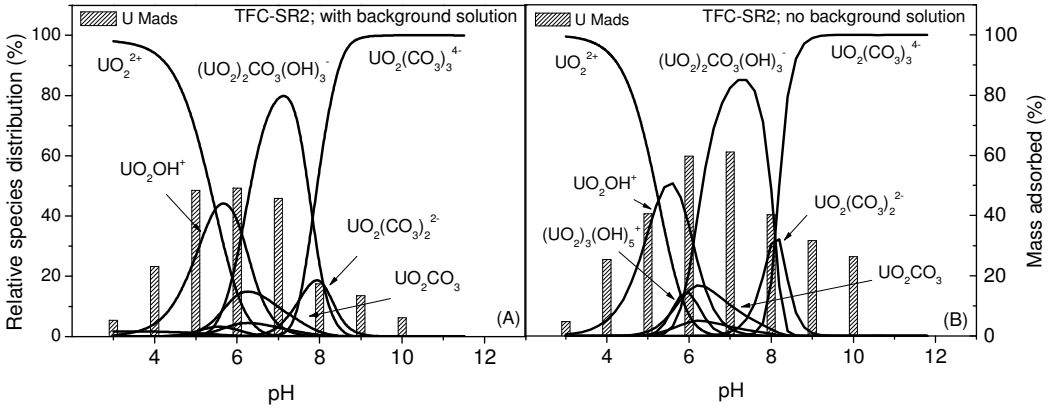

Figure 82. Mass adsorbed of uranium across the pH range 3-10 for solutions (A) containing uranium (0.5 mg/L) and background solution (20 mM NaCl and 1 mM NaHCO3) and for (B) uranium solution (0.5 mg/L) only. The experiments were performed without applied pressure.

Experiments were performed across the pH range without the background solution (normally 20 mM NaCl and 1 mM $NaHCO_3$) and without applied pressure. The results (Figure 82) show that increased uranium-membrane interaction occurred in solutions without background solution compared to background-containing solutions as carbonate became more important for uranium speciation, i.e. at pH 6-10. The

uranium-membrane interaction increased with about 10%. The precise reason is not known, but it is hypothesised that the absence of background solution may decrease the stability of the uranium species in solution and consequently a higher uranium amount was held by the membrane.

11.4.2 µ-XRF instrument settings and analysis

TFC-SR2 and BW30 were analysed after experiments using 0.5 mg/L uranium with µ-XRF.

Analysis mode : MAP								
File name	X-Ray beam size (µm)	X-Ray tube voltage (kV)	Counting time (s)	Pixels size (µm)	Pixels	Processing time (detector)	X/Y (mm)	Comments
Map1 0,5 ppm 251109	100	50	15×1000	100	512	P3	51,2/42,0	VAC P

a)

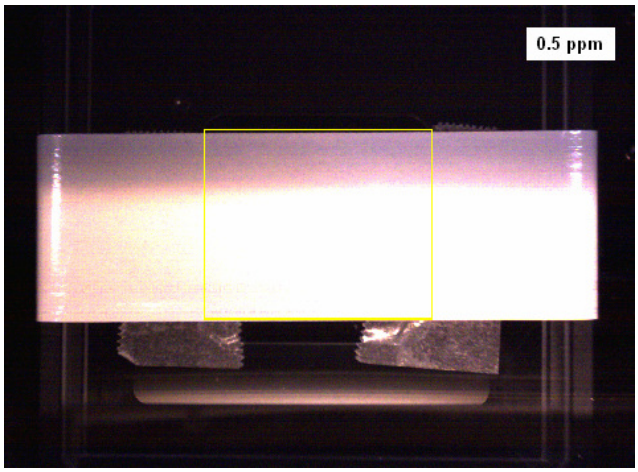

b)

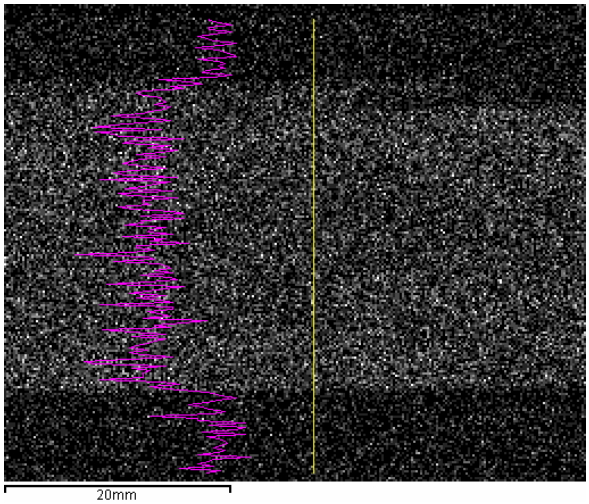

Figure 83. a) shows the membrane flatly mounted in the sample holder, the membrane active layer facing upwards b) shows the scan of uranium across the surface of the membrane.

An area of about 5 x 4 cm was mapped in the μ-XRF for uranium, showing an even distribution across the membrane surface. At the edges the uranium amount decreases since this is where the membrane was clamped in the membrane cell.

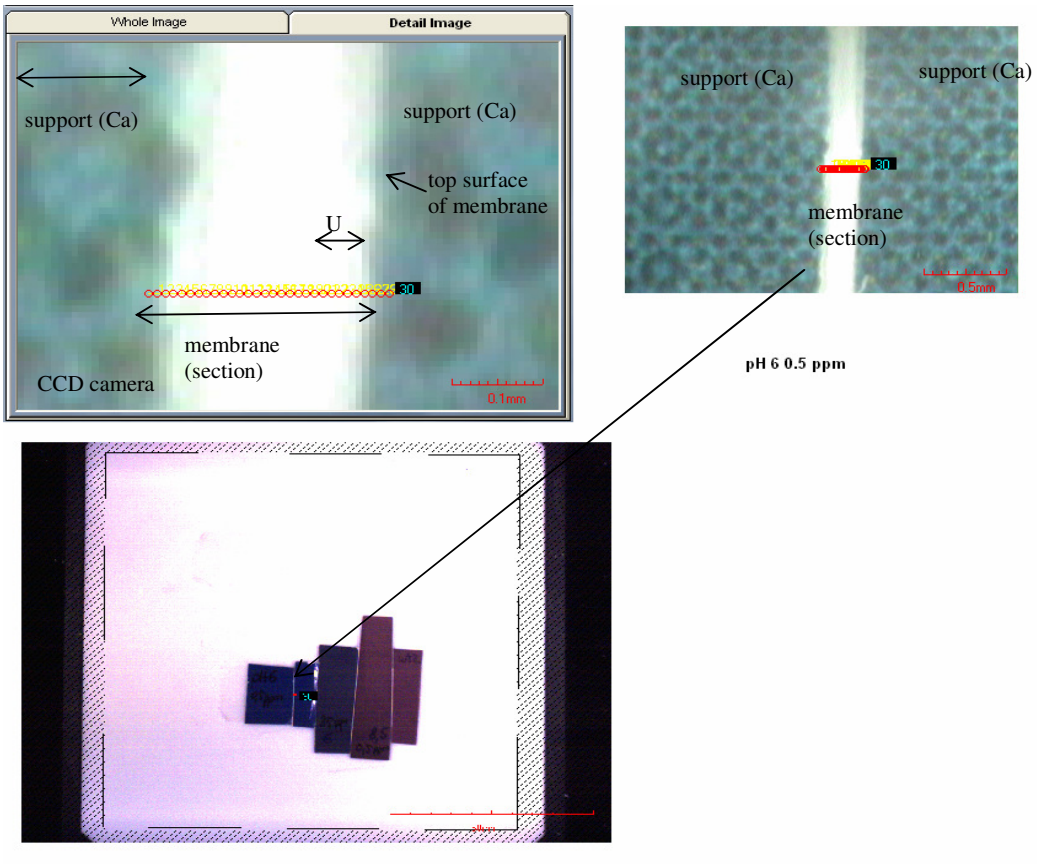

Figure 84. Shows the mounting of the membrane cross-sections in the µ-XRF. The strips were held in place by calcium-containing support.

Cross-sections of the membranes where prepared by cutting the membrane in thin sections with scissors and placing them between paperboard support, rich in calcium. The cross-section was analysed in points, where the X-Ray beam (50 kV) was pointed for 1000s/point. Size of incident X-Ray beam = 10 µm.

11.4.3 TEM images of TFC-SR2 membrane

Several images were taken of TFC-SR2 with the TEM to develop the best analysis method and to identify the active layer of the membrane. Some examples are given in Figure 85. To obtain images of the membrane structure, osmium was used to stain the membrane for images in Figure 85a-c. The membranes in Figure 85d-g were stained by soaking in uranyl nitrate. Importantly, using both of these methods the active layer of the membrane can be distinguished and shown to be ca 400 nm thick. TEM analysis of the membranes from the experiment at pH 6 was performed without

additional staining and by using freeze-drying in order to keep experimental conditions (such as pH) as constant as possible (Figure 86). Again the active layer can be clearly identified. It was, however, not possible to conclusively distinguish the uranium distribution within the membrane from those images.

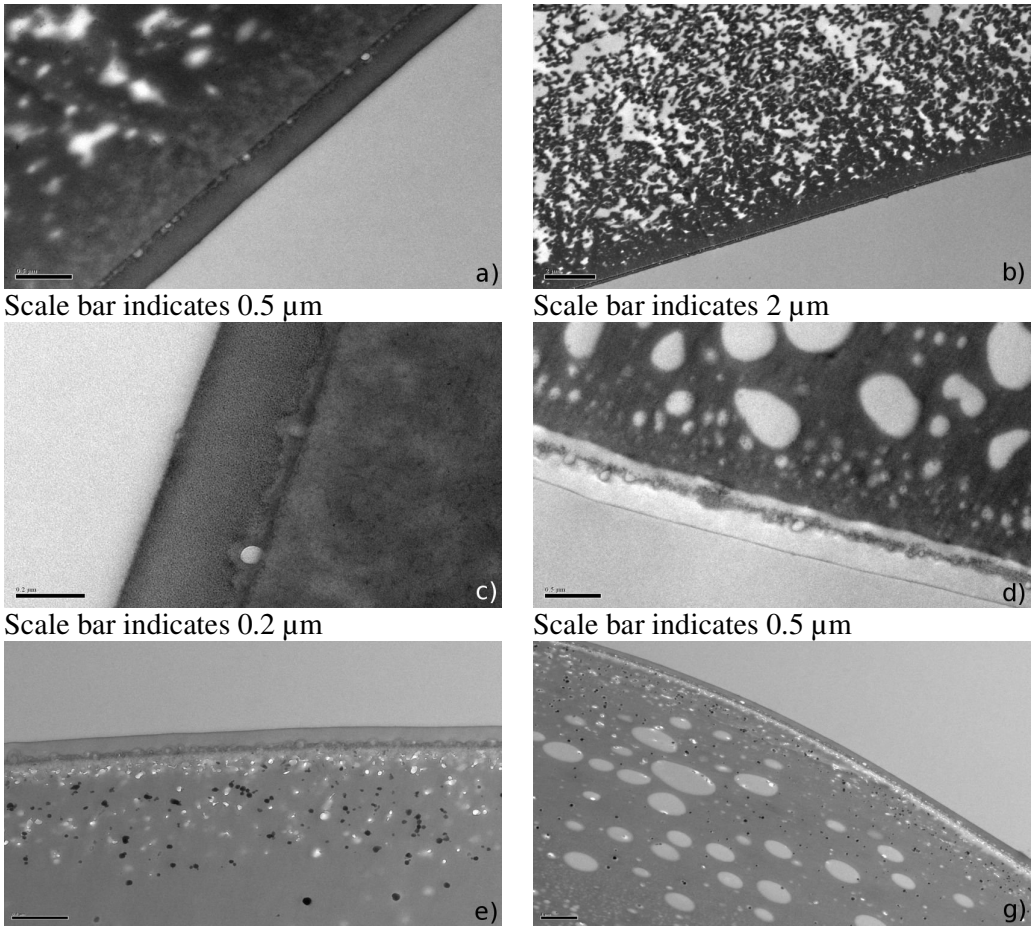

Scale bar indicates 0.5 µm | Scale bar indicates 2 µm

Scale bar indicates 0.2 µm | Scale bar indicates 0.5 µm

Scale bar indicates 0.5 µm | Scale bar indicates 1 µm

Figure 85. TEM images of cross-section of TFC-SR2 membrane. Membranes for Images a-c were stained with osmium and araldite was used rather than freeze-drying. Images a and c show a close-up of the active layer. Image b) has the active layer of the membrane facing down and shows how the polysulfone support becomes gradually more porous. Images d-g were stained with uranyl nitrate.

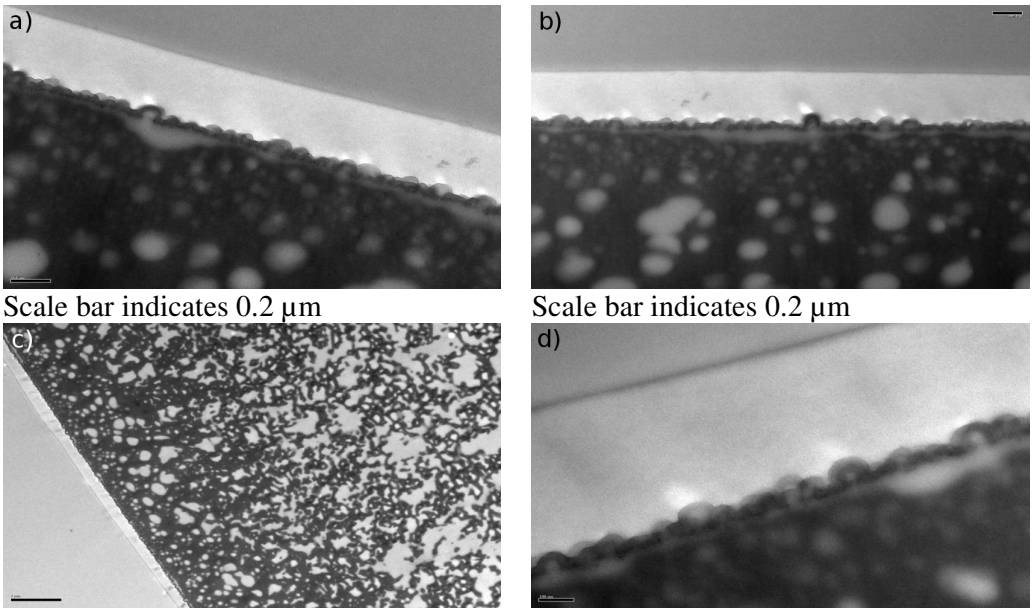

Scale bar indicates 0.2 µm Scale bar indicates 0.2 µm

Scale bar indicates 2 µm Scale bar indicates 100 nm

Figure 86. TEM images of TFC-SR2 after an experiment with 0.5 mg/L U, 20 mM NaCl, 1 mM $NaHCO_3$ at pH 6 and no applied pressure. The active layer is clearly shown and is between 200-400 nm thick.

SEM analysis was performed of the membranes used for the uranium experiments (0.5 mg/L U) at pH 6 and 8.5 and are displayed in Figure 87. The images from both the SE and YAGBSE mode are shown, the former giving and idea of topography and the latter of elemental distribution (elements of higher atomic number give the brighter contrast). All images display a clean membrane surface washed with de-ionised water (bottom left hand corners) as comparison to the membranes after an experiment (top right hand corners). The surface of the membrane after an experiment at pH 8.5 looked very different; while the SE mode of the membrane after a pH 6 experiment indicated that the surface was relatively smooth, the surface after a pH 8.5 experiments appeared to contain a layer on top of the membrane surface (Figure 88).

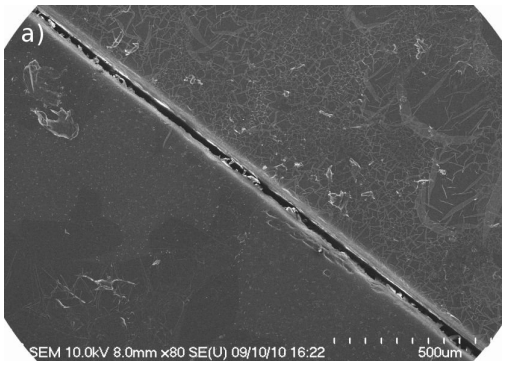

a) SE mode of clean + membrane after pH 6 experiment

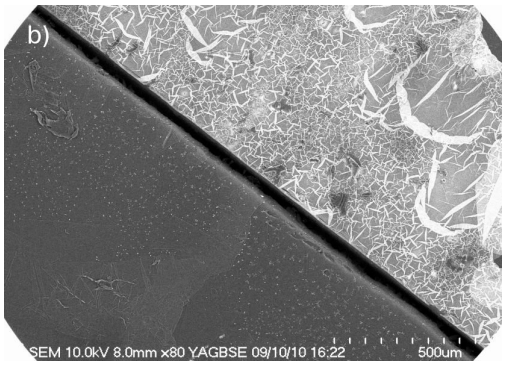

b) YAGBSE mode of clean + membrane after pH 6 experiment

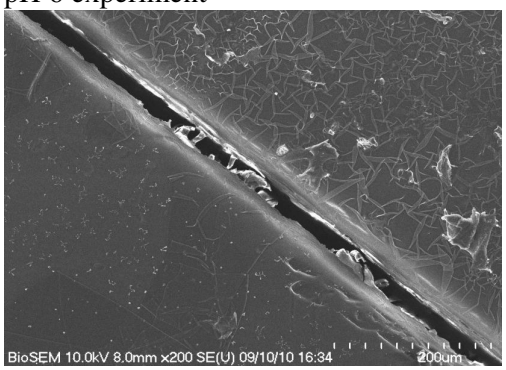

c) SE mode of clean + membrane after pH 6 experiment

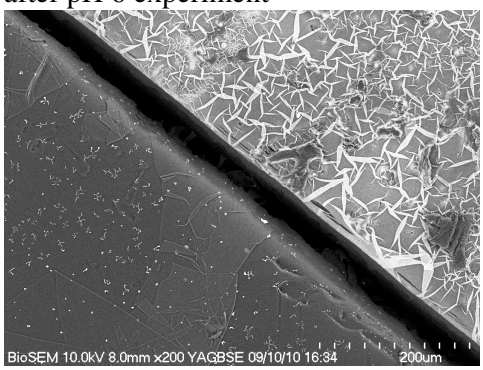

d) YAGBSE mode of clean + membrane after pH 6 experiment

Figure 87. SEM images comparing two sections of a clean membrane surface (washed with DIW) with two sections after an experiment with uranium at pH 6 (0.5 mg/L U + 20 mM NaCl and 1 mM $NaHCO_3$). The bright contrast shown in the YAGBSE setting (b and d) shows that uranium is present. In the SE setting (a and c), brighter contrast springs from topography differences.

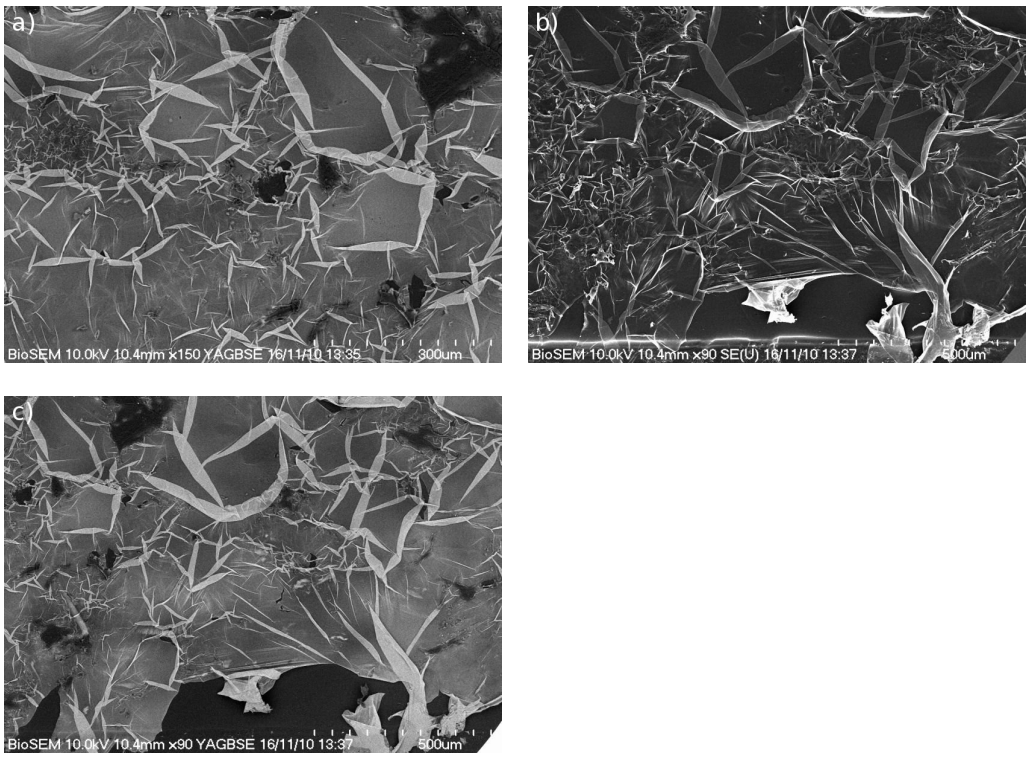

Figure 88. SEM images showing the membrane after an experiment with uranium at pH 8.5 (0.5 mg/L U + 20 mM NaCl and 1 mM $NaHCO_3$). Again the YAGBSE setting shows a lighter contrast due to uranium (a and c), while the image from the SE setting (b) indicates that there is an uneven layer on the membrane.

11.4.4 STEM-EDX instrument settings

Instrument settings:

- 100kV
- 0.7 nm spot size
- Operating in HAADF mode (images are z-contrast, rather than strain/diffraction contrast mode)
- Hard X-Ray aperture in
- Images for EDX acquired at 1024 x 960 frame, 10 sec per frame
- EDX maps at 512x480 resolution unbinned
- 500µs dwell time
- Process time 2
- Spectra recorded with 1k channels

The EDX hardware is an Oxford Instruments INCA X Ray Microanalysis System (TEM 250). STEM hardware is a JEOL Digital STEM System

11.4.5 EDX images

Several images were taken of the membrane samples in STEM-EDX after experiments at pH 6 and 8.5, specifically with an uranium concentration of 50 mg/L to enable detection. It was not always easy to locate the active layer of the membrane, and there were also problems with the stability of the membrane during the EDX measurements, which is why there are less images for pH 8.5. The images where the membrane was destroyed are not included here. The images after the pH 8.5 show that uranium is not close to the support layer of the membrane, but appears to be present in a loose layer detatched from the membrane (Figure 89). The images for pH 6, show the uranium to be present in the active layer, clearly distinctive from the of sulphur distribution (which is indicates the polysulfone support layer) (Figure 90).

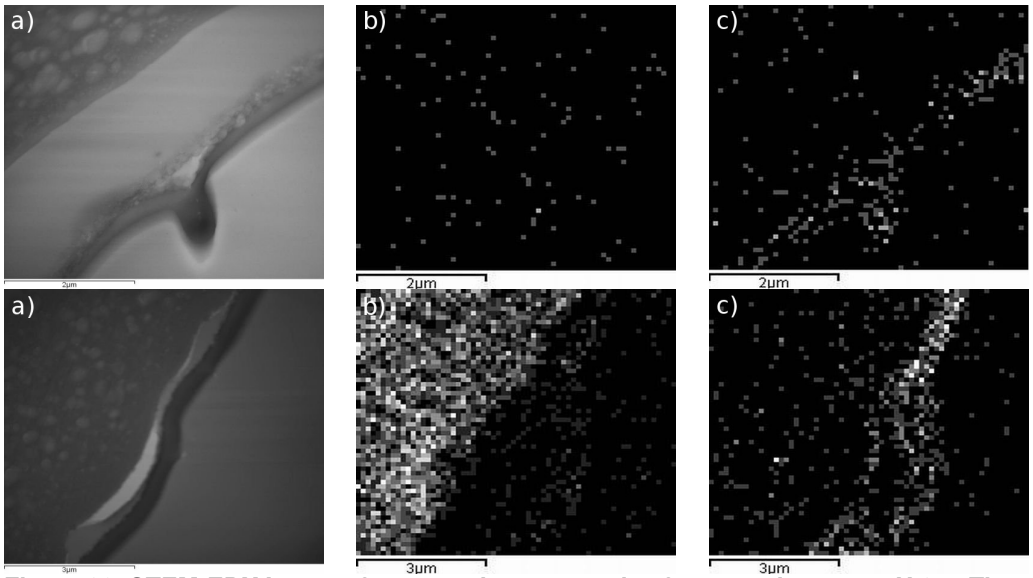

Figure 89. STEM-EDX Images from membrane sample after experiment at pH 8.5. The SEM reference image is given in images a), while b) shows the sulphur distribution and c) the uranium disitribution.

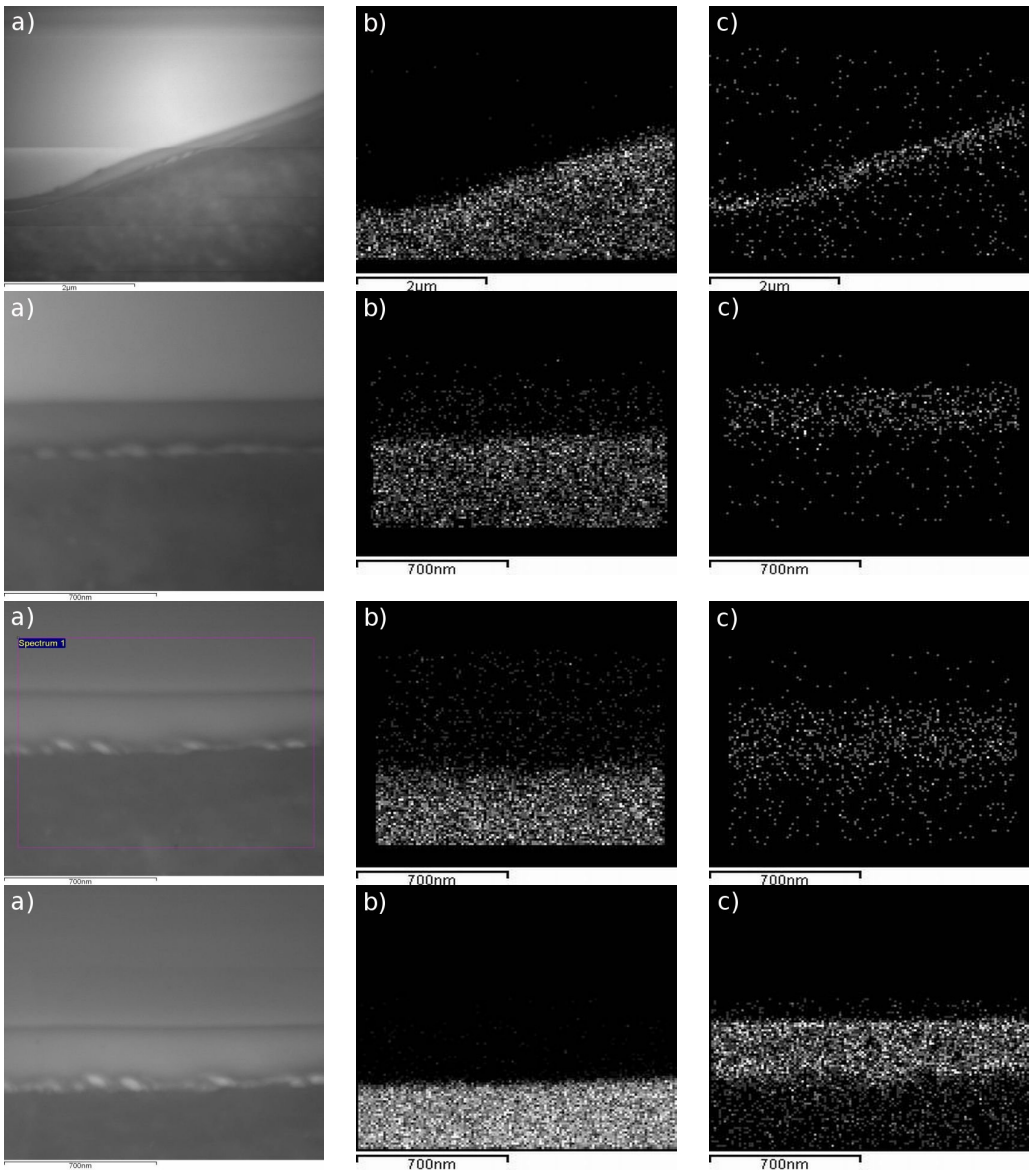

Figure 90. STEM-EDX Images from membrane sample after experiment at pH 6, showing a) the reference image, b) the sulfur distribution and c) the uranium disitribution.

11.4.6 Membrane structures

The exact chemical structures of the membranes are unfortunately not available, since this is proprietary information of the manufacturers. BW30 is described by Tang et al. (2009) as a "coated fully aromatic membrane", whereas according to the manufacturer, TFC-SR2, is a "modified polypiperazinamide membrane". The FTIR spectra compares to that of semi-aromatic membranes in Tang et al. (2009).

Tang et al. (2009) give the following examples of chemical structures of fully aromatic polyamide and of the polypiperazinamide, shown in Figure 91 and Figure 92.

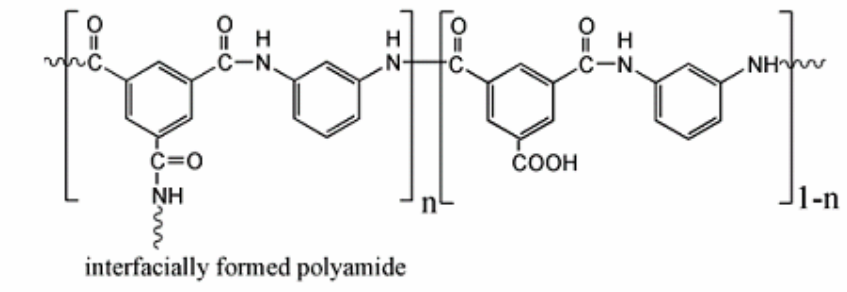

Figure 91. Example of the chemical structure of a fully aromatic polyamide membrane, such as BW30. From Tang et al. (2009).

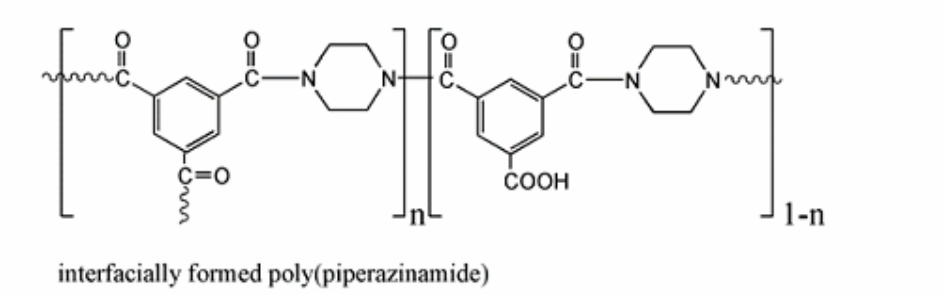

Figure 92. Example of the chemical structure of a semi-aromatic polypiperazinamide membrane, as for TFC-SR2. From Tang et al. (2009).

Tang et al. (2009) also give a very useful overview of the FTIR absorbances associated with membrane functional groups of different layers and chemical structure.

11.5 Appendix to Chapter 7

11.5.1 Precipitation of magnesium

An experiment was performed to investigate whether precipitation of magnesium could be the major cause of uranium co-precipitation at pH 10. The same experimental set-up and procedure was used as for 7.2.1, except that 150 mg/L magnesium was used (MgCl, Fisher Scientific) instead of calcium. The concentration

was selected based on the concentrations measured in the Australian groundwater at Pine Hill (Table 7). The BW30 membrane was used. The samples were analysed using ICP-OES as described in sections 3.1.6 and 11.1.2. Only 10% of the magnesium precipitated and therefore it was concluded that calcium precipitation was likely to be more important, since > 50% deposited to the membrane. On the other hand even the 10% precipitation of magnesium caused a 23% co-precipitation of uranium where it would otherwise have been < 5% and may be interesting for further studies of the complex interactions caused by multiple ions in solution.

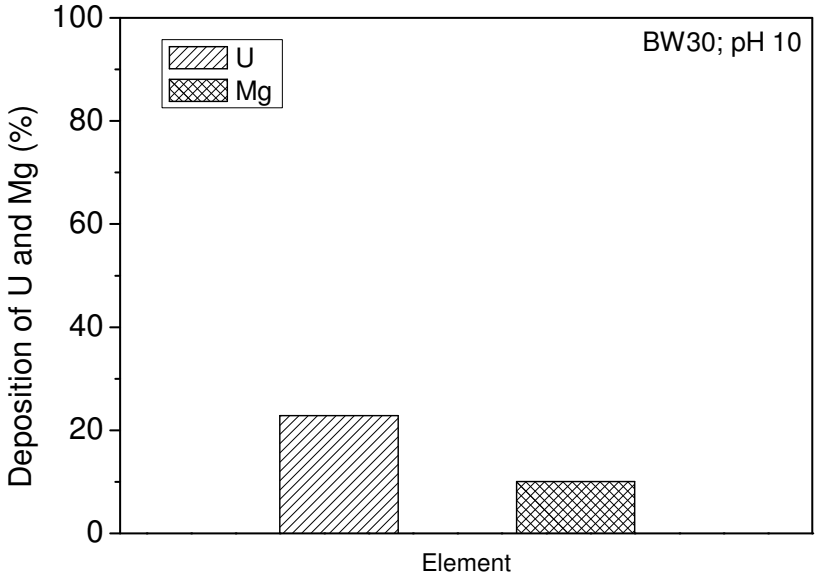

Figure 93. Mass adsorbed of uranium and magnesium to BW30 membrane. Experimental solution: 0.5 mg/L U, 150 mg Mg, 20 mM NaCl and 1 mM $NaHCO_3$. Experimental conditions: pressure = 10 bar, flow-rate = 0.6 L/min, temperature = 25ºC.

11.5.2 SEM images of U+Ca membrane surface

Figure 94 shows the SEM images of the membrane surface after an experiment with uranium (0.5 mg/L) and calcium (60 mg/L) solution. The images clearly show the rhombohedra-shaped calcite crystals on top of the membrane surface.

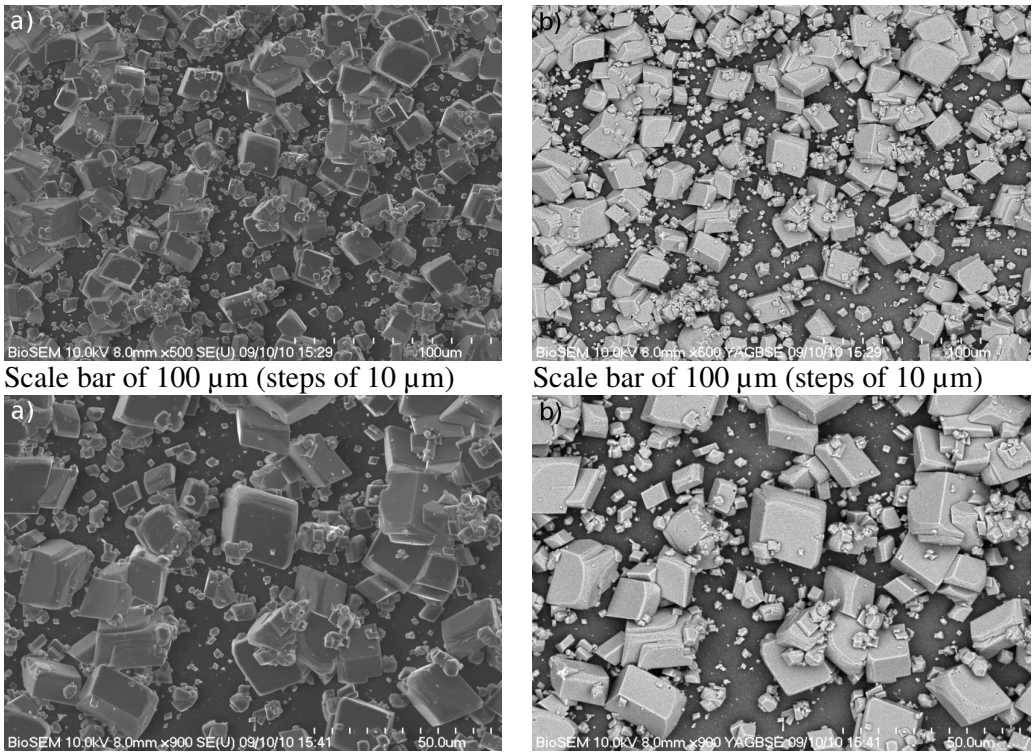

Scale bar of 100 µm (steps of 10 µm) Scale bar of 100 µm (steps of 10 µm)

Scale bar of 50 µm (steps of 5 µm) Scale bar of 50 µm (steps of 5 µm)

Figure 94. SEM image of membrane surface after an experiment with uranium (0.5 mg/L) and calcium (60 mg/L) solution (+ 20 mM NaCl and 1 mM $NaHCO_3$) and no applied pressure.

11.5.3 ToF-SIMS instrument settings

- Primary voltage: 25,000 or 25 KV
- Primary source: Bi_3^+
- Pulse width: 30 ns
- Total acquisition time/sample: 15 scans
- Analysis area: 400 x 400 µm.
- Charge compensation was applied in the form of an electron floodgun
- Pulsed Target current of ~1 pA used
- Samples were analysed below 1×10^{12} ion/cm^2, well below the primary ion dose density limit (avoids damage of the samples)
- Mode of operation used was "high current bunched", this provides high mass resolution spectra and images of ~1 µm.

11.5.4 Image results for all ions measured with ToF-SIMS

ToF-SIMS was performed for selected membranes after specific experiments performed with 50 mg/L uranium to ensure detection. Calcium concentrations were 60 mg/L and the background electrolyte (20 mM NaCl, 1 mM $NaHCO_3$) was used with all experiments, except the blanks where DIW was adjusted to the appropriate pH. Two pieces of the membrane were cut and analysed for each experiment. The image summaries are displayed in the figures given in the overview in Table 26.

Table 26. Overview of image summaries for positive and negative ions for relevant experiments.

Experiments	Positive ions	Negative ions
Blank, pH 6	Figure 95 and Figure 96	Figure 97
U, pH 6	Figure 98 and Figure 100	Figure 99 and Figure 101
U, pH 8.5	Figure 102 and Figure 104	Figure 103 and Figure 105
Blank, pH 10	Figure 106 and Figure 108	Figure 107 and Figure 109
U + Ca pH 10	Figure 110 and Figure 112	Figure 111 and Figure 113

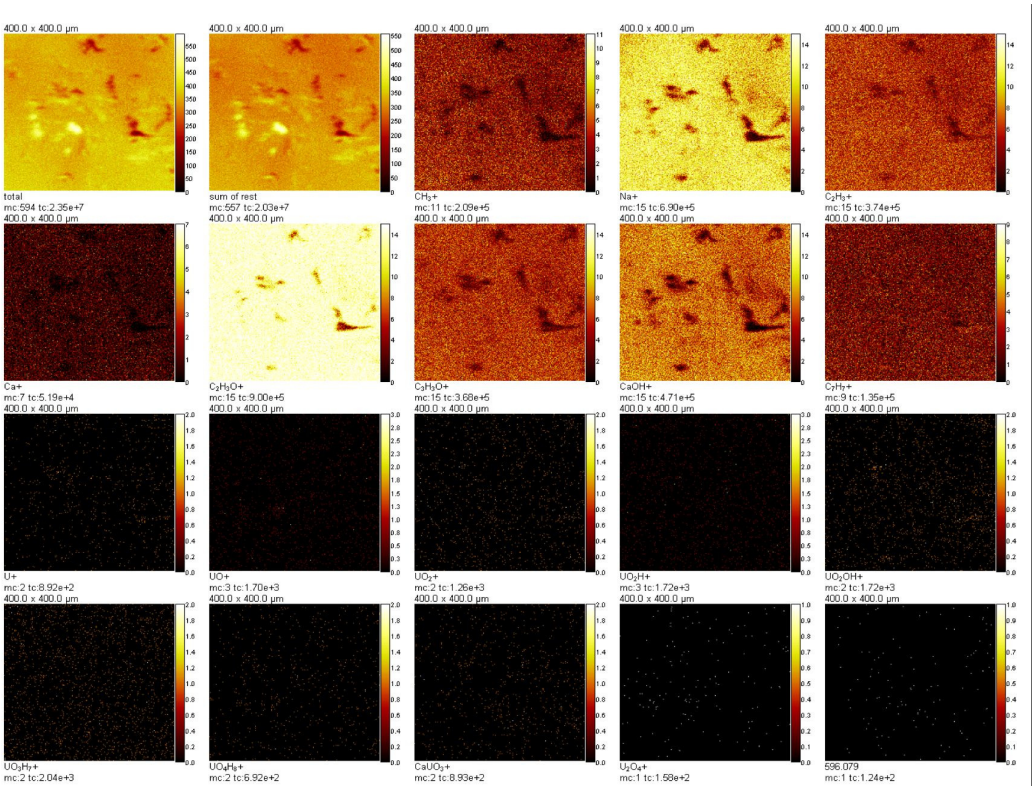

Figure 95. membrane blank at pH 6: image summary of positive ions (1st membrane piece).

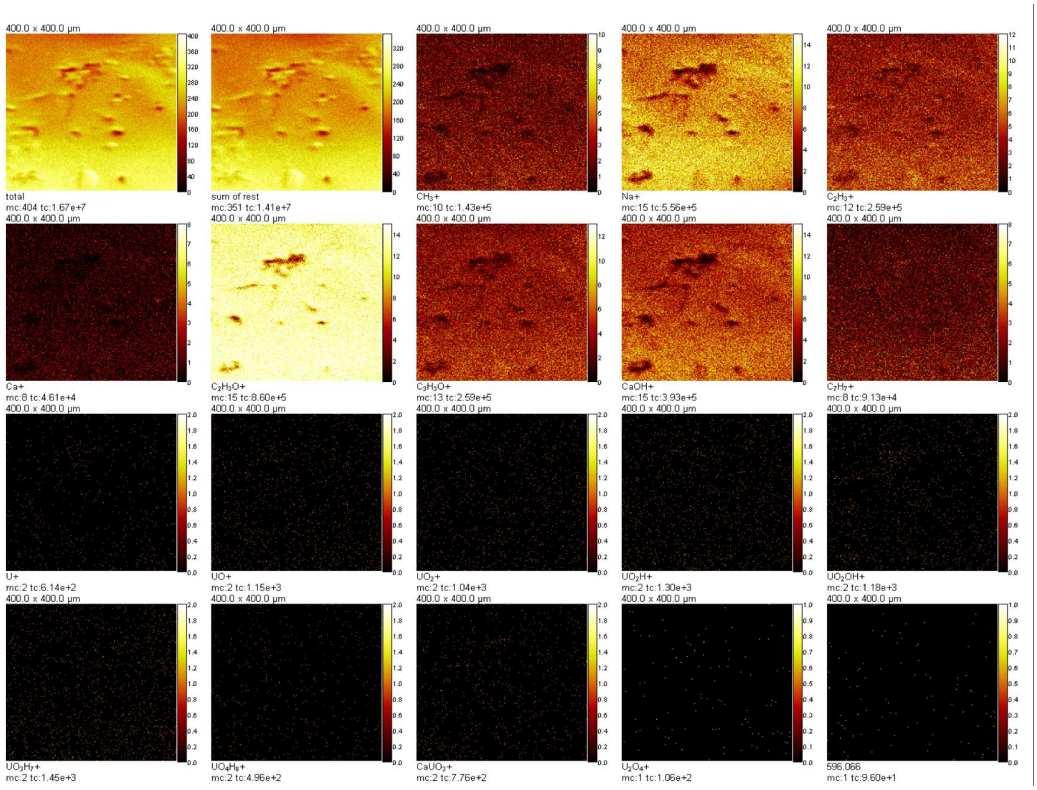

Figure 96. Membrane blank at pH 6: image summary of positive ions (2nd membrane piece)

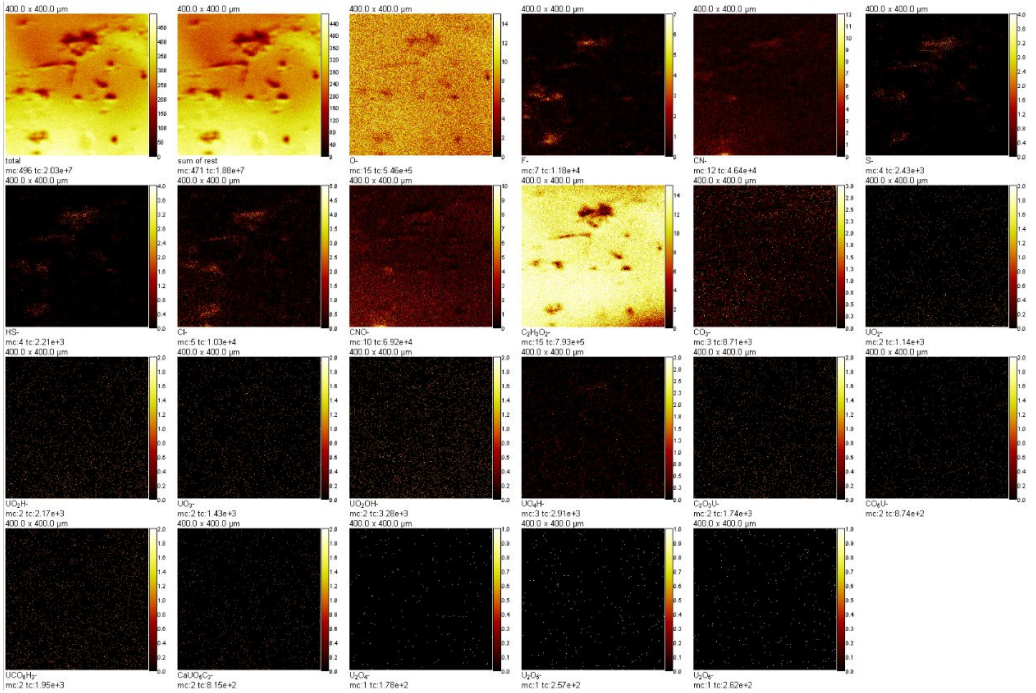

Figure 97. Membrane blank at pH 6: image summary of negative ions (2nd membrane piece)

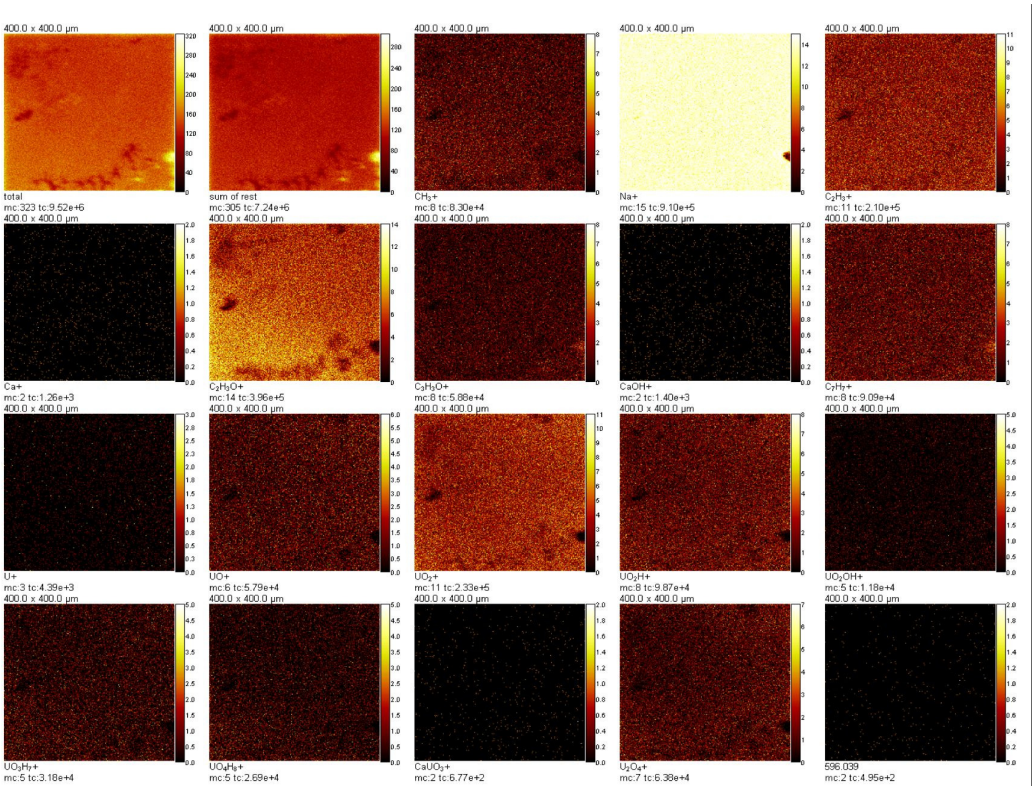

Figure 98. Membrane after uranium experiment at pH 6: image summary of positive ions (1st membrane piece)

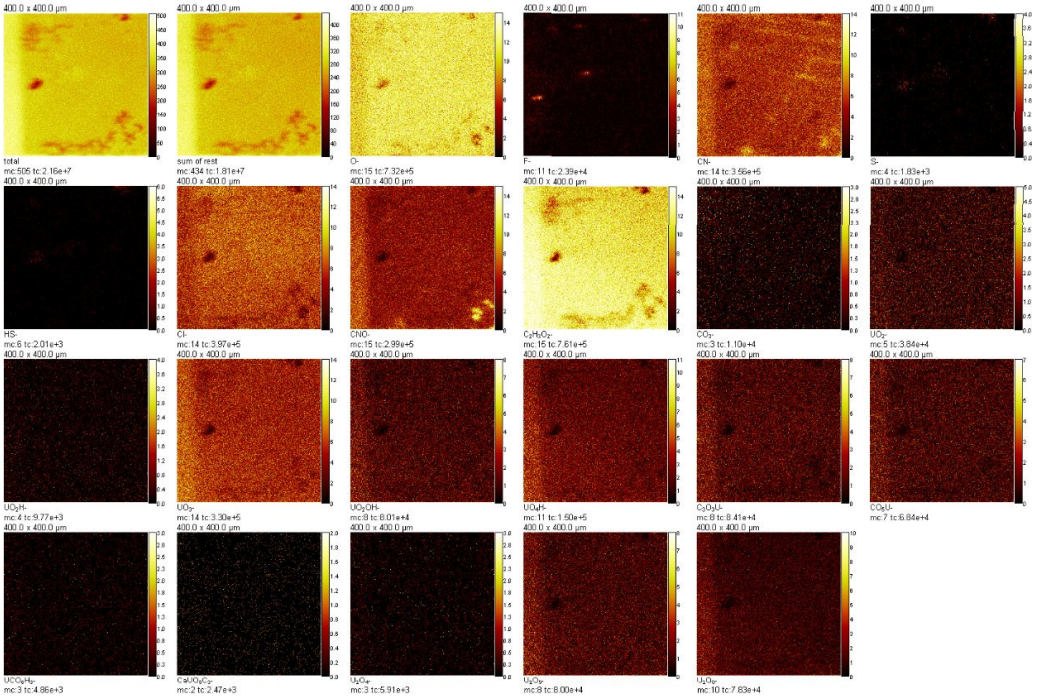

Figure 99. Membrane after uranium experiment at pH 6: image summary of negative ions (1st membrane piece)

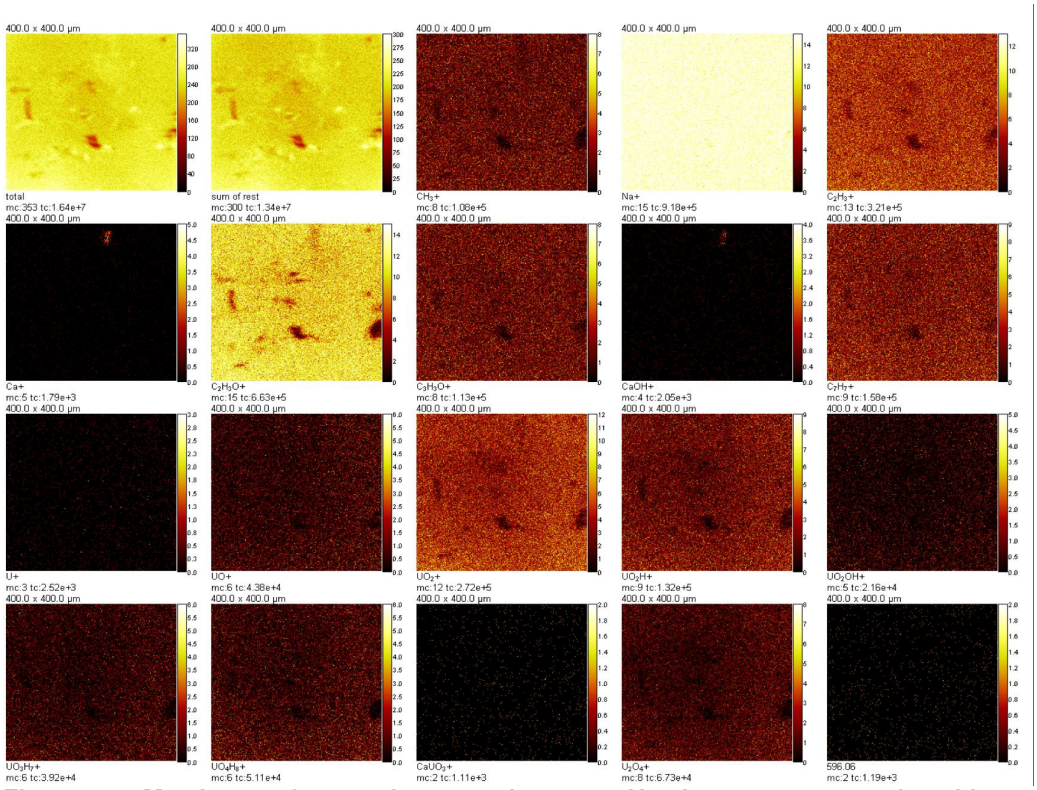

Figure 100. Membrane after uranium experiment at pH 6: image summary of positive ions (2nd membrane piece)

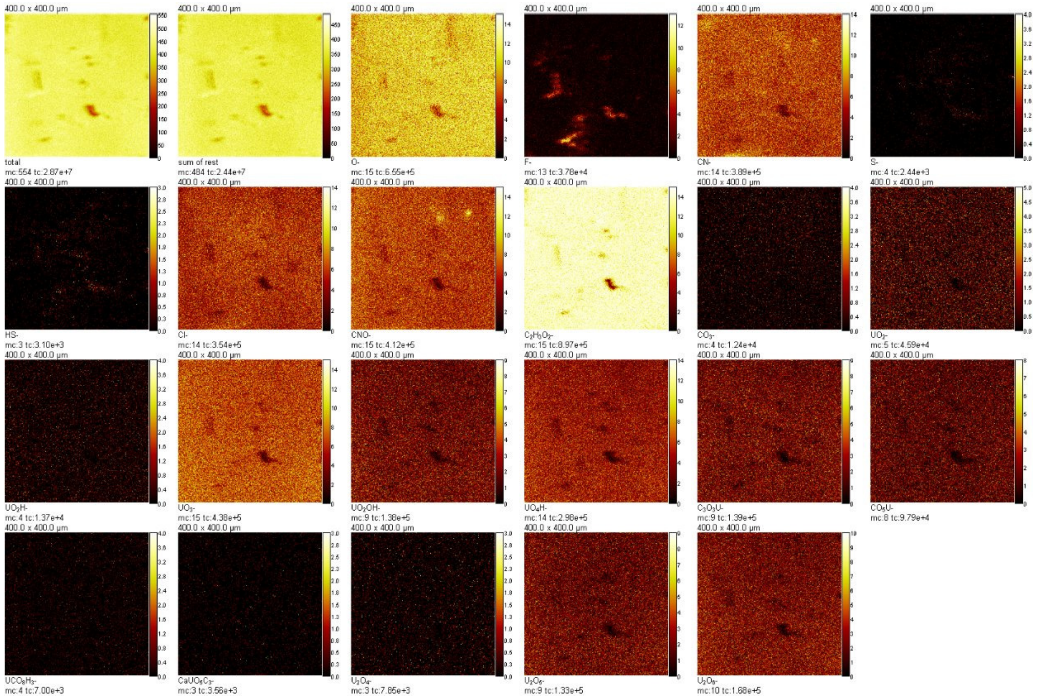

Figure 101. Membrane after uranium experiment at pH 6: image summary of negative ions (2nd membrane piece)

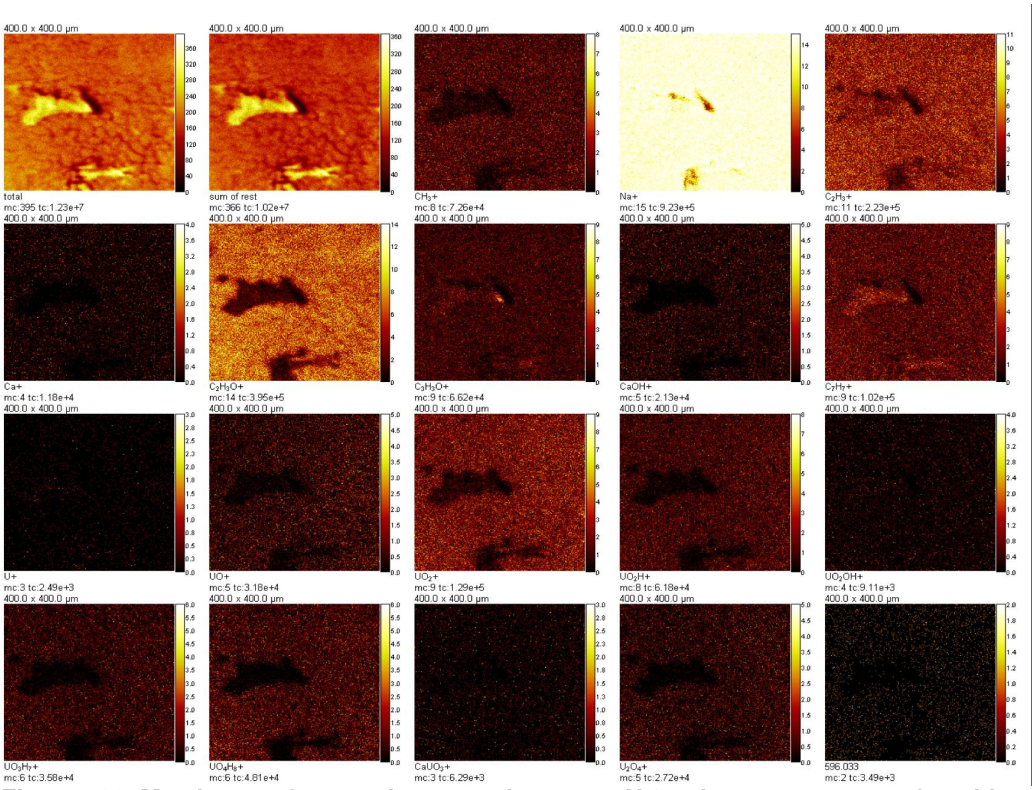

Figure 102. Membrane after uranium experiment at pH 8.5: image summary of positive ions (1st membrane piece)

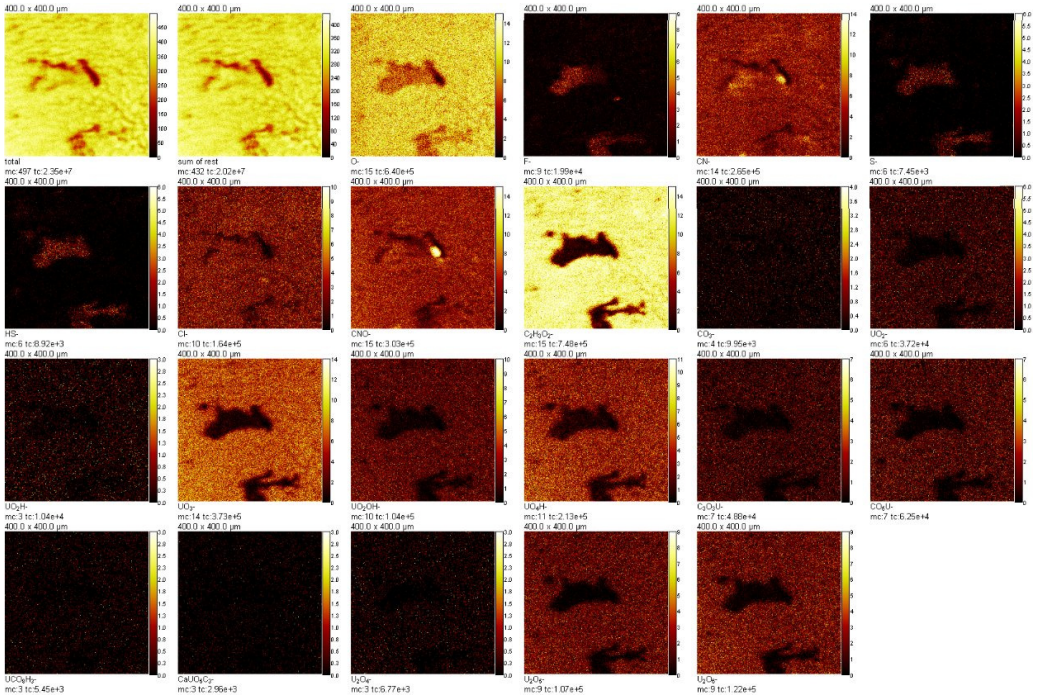

Figure 103. Membrane after uranium experiment at pH 8.5: image summary of negative ions (1st membrane piece)

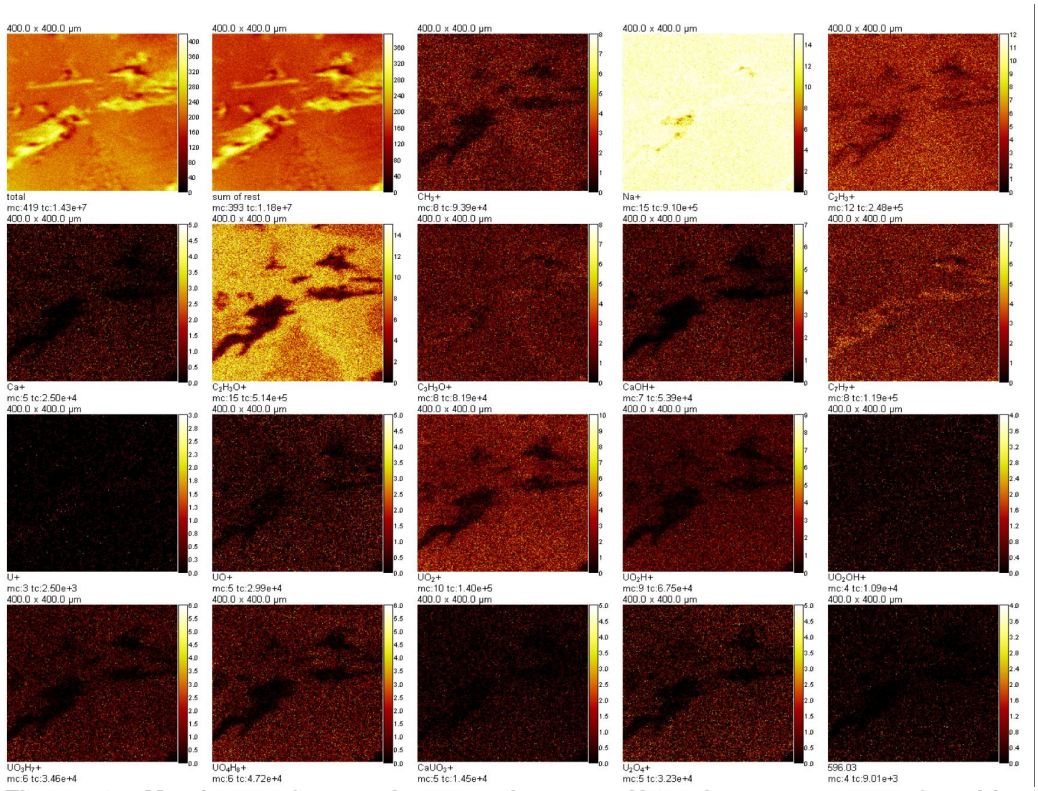

Figure 104. Membrane after uranium experiment at pH 8.5: image summary of positive ions (2nd membrane piece)

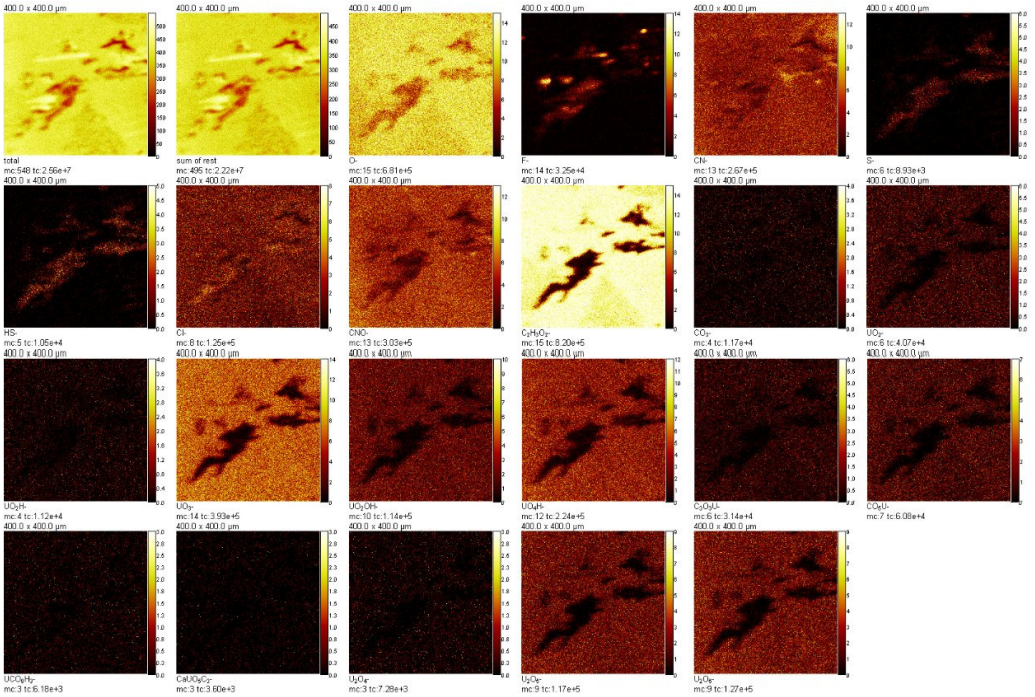

Figure 105. Membrane after uranium experiment at pH 8.5: image summary of negative ions (2nd membrane piece)

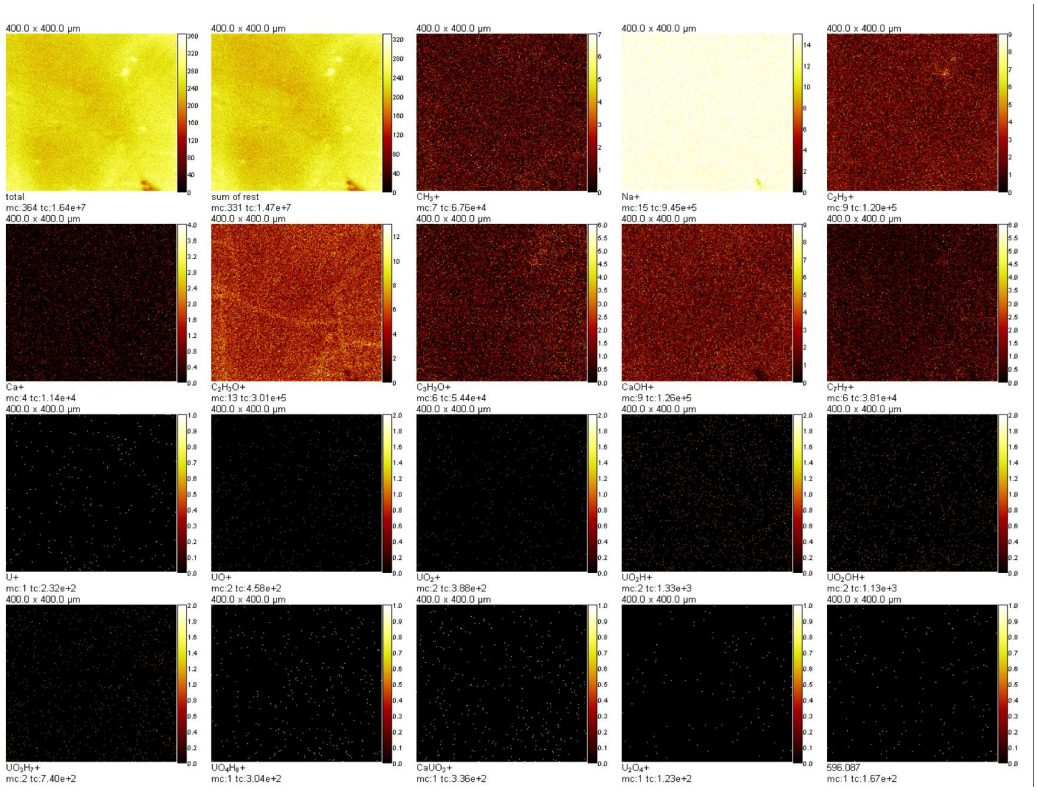

Figure 106. Membrane blank at pH 10: image summary of positive ions (1st membrane piece)

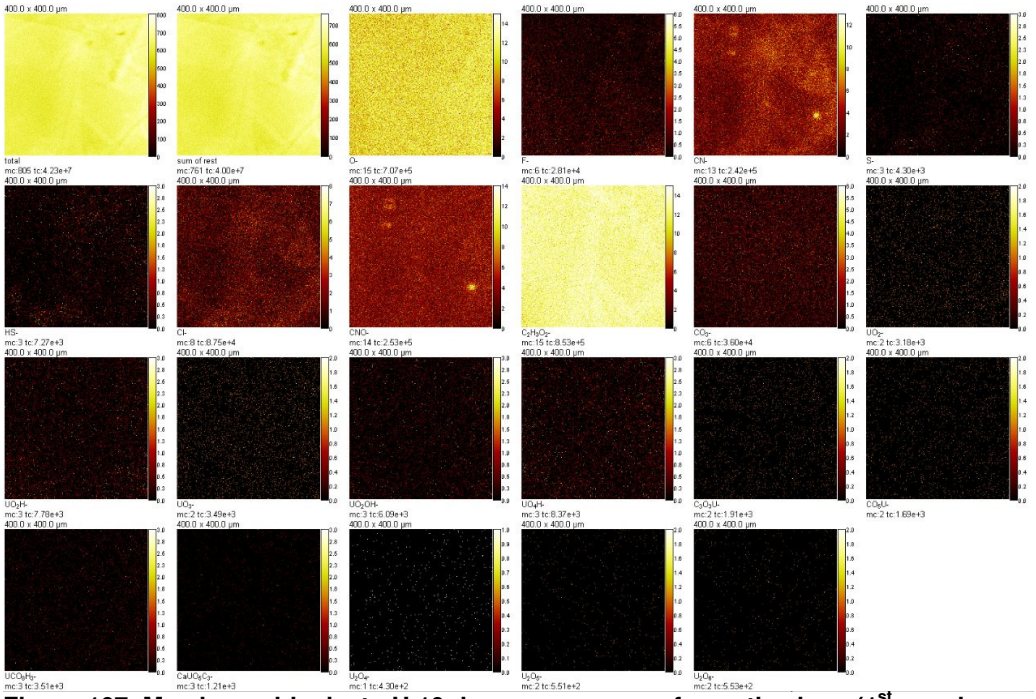

Figure 107. Membrane blank at pH 10: image summary of negative ions (1st membrane piece)

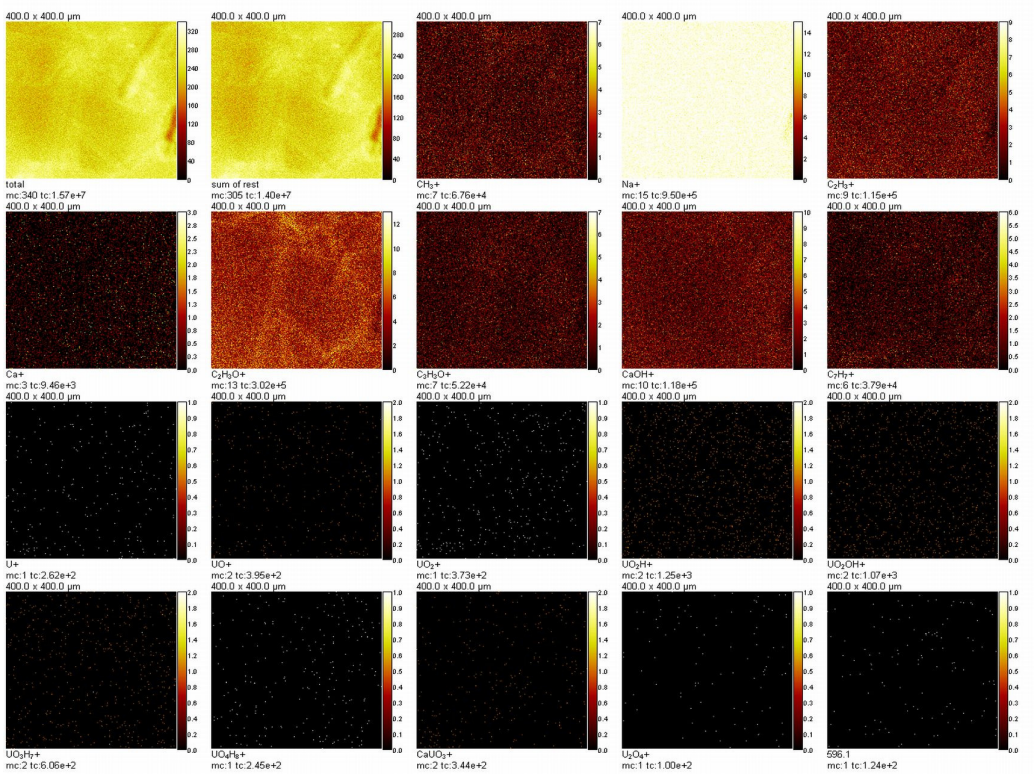

Figure 108. Membrane blank at pH 10: image summary of positive ions (2nd membrane piece)

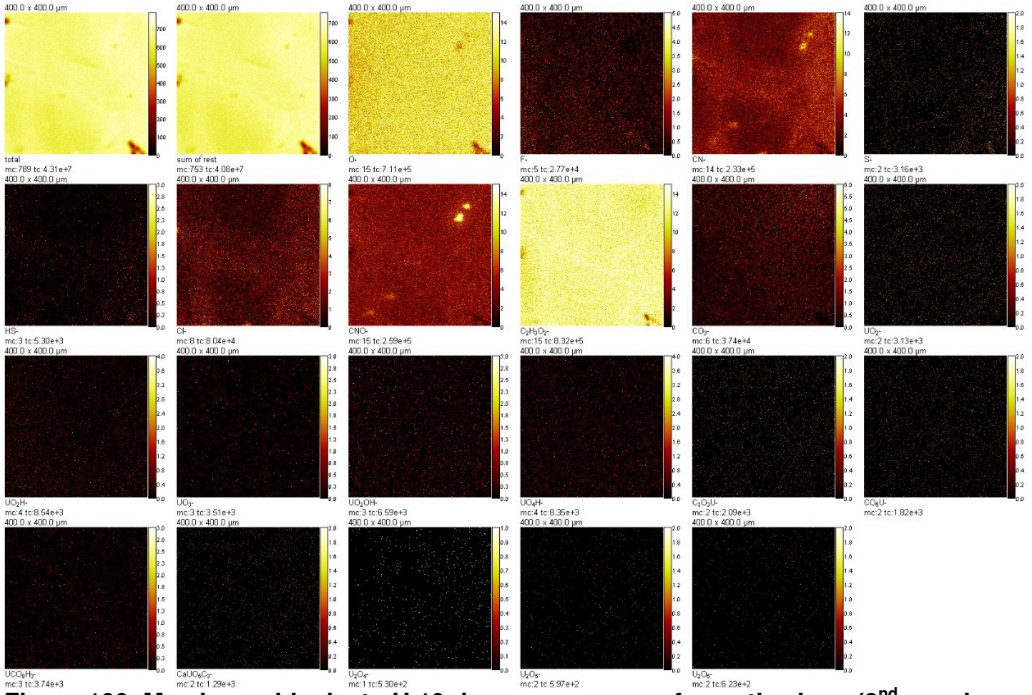

Figure 109. Membrane blank at pH 10: image summary of negative ions (2nd membrane piece)

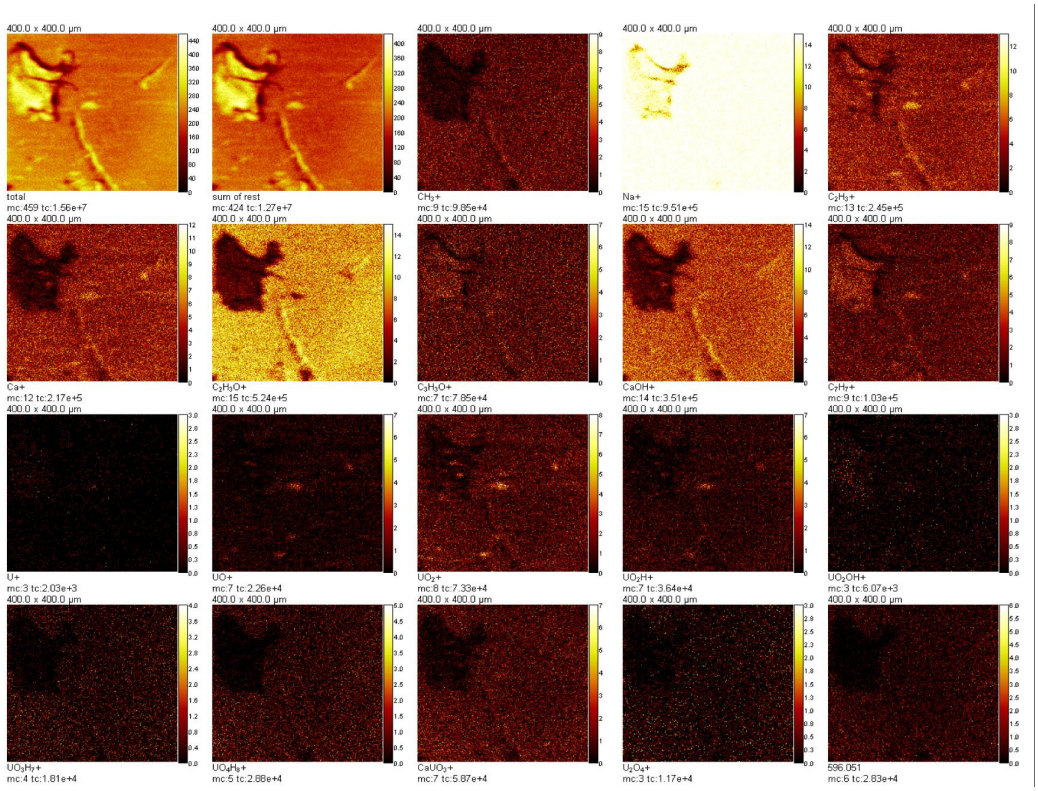

Figure 110. Membrane after uranium + calcium experiment at pH 10: image summary of positive ions (1st membrane piece)

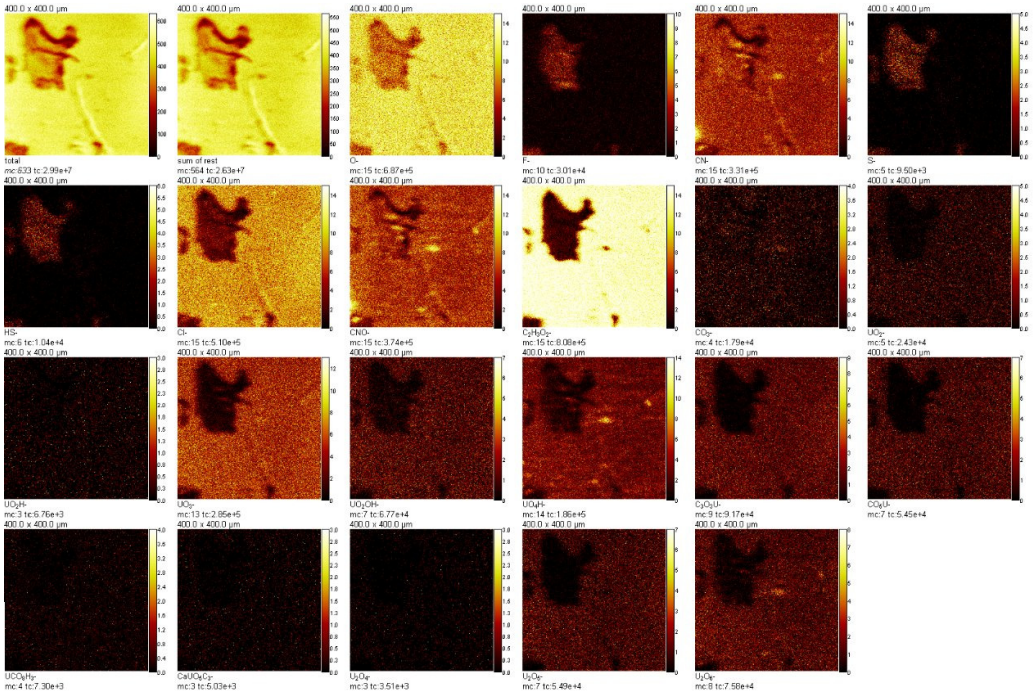

Figure 111. Membrane after uranium + calcium experiment at pH 10: image summary of negative ions (1st membrane piece)

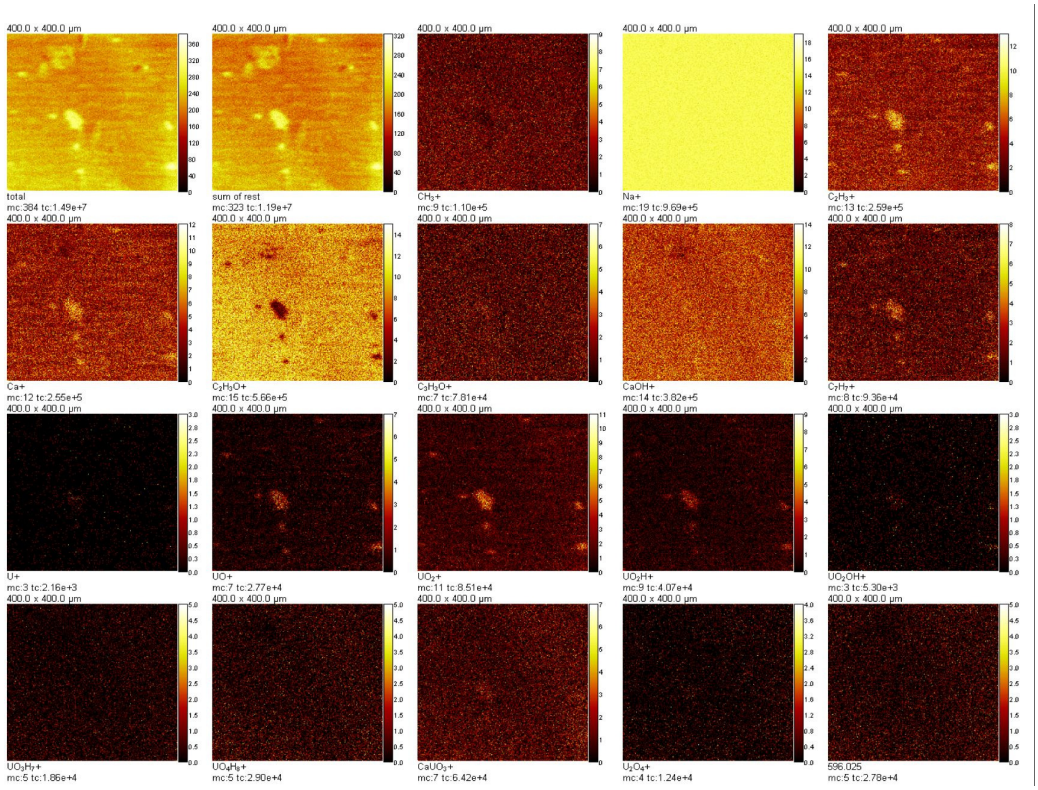

Figure 112. Membrane after uranium + calcium experiment at pH 10: image summary of positive ions (2nd membrane piece)

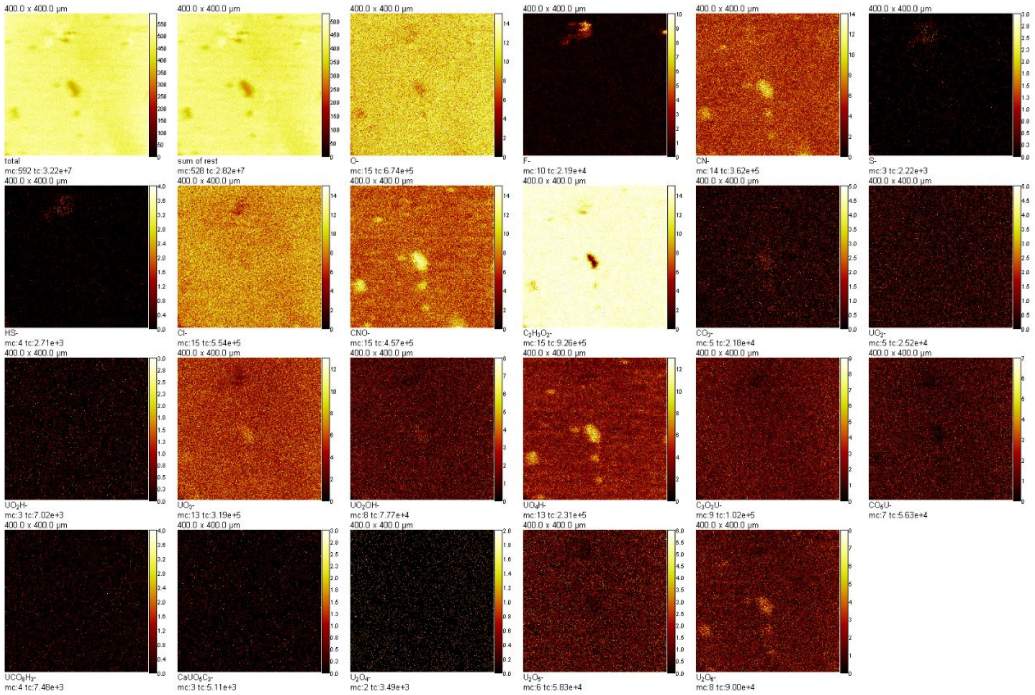

Figure 113. Membrane after uranium + calcium experiment at pH 10: image summary of negative ions (2nd membrane piece)

11.6 Appendix to Chapter 8

The speciation of boron for the Ghanaian was predicted using Visual Minteq 2.53, as described in section 3.1.8.